HEINRICH HEINE
UNIVERSITÄT DÜSSELDORF

Molecular remodeling of hepatic metabolism in different stages of fatty liver disease and their impact on hepatocyte secretome

Inaugural-Dissertation

zur Erlangung des Doktorgrades
der Mathematisch-Naturwissenschaftlichen Fakultät
der Heinrich-Heine-Universität Düsseldorf

vorgelegt von

Pia Fahlbusch
aus Solingen

Düsseldorf, Dezember 2018

aus dem Institut für Klinische Biochemie und Pathobiochemie
des Deutschen Diabetes-Zentrums
Leibniz-Zentrum für Diabetesforschung
an der Heinrich-Heine-Universität Düsseldorf

Gedruckt mit der Genehmigung der
Mathematisch-Naturwissenschaftlichen Fakultät der
Heinrich-Heine-Universität Düsseldorf

Berichterstatter:

1. Prof. Dr. Hadi Al-Hasani
2. Prof. Dr. Michael Feldbrügge

Tag der mündlichen Prüfung: 04.04.2019

"If you knew time as well as I do,"
said the hatter,
"you wouldn't talk about wasting it."

Lewis Carroll – Alice in Wonderland

Zusammenfassung

In der westlichen Zivilisation ist die exzessive Anhäufung von Lipiden in der Leber die häufigste Ursache einer chronischen Fettlebererkrankung. Eine erhöhte systemische Lipidbelastung bedingt durch eine unausgewogene Ernährung, eine erhöhte Lipolyse des Fettgewebes oder ein Ungleichgewicht des intrahepatischen Lipidstoffwechsels tragen zur Entwicklung einer Fettleber bei. Einzelne Aspekte der Pathogenese dieser Erkrankung sind Gegenstand zahlreicher Studien, jedoch ist das komplexe Zusammenspiel der Veränderungen im Leberstoffwechsel, ebenso wie die in Folge einer chronischen Fettlebererkrankung veränderten Sekretionsmuster auf Proteinebene nach wie vor unklar.

Das Ziel dieser Studie war die Charakterisierung verschiedener Stadien der Fettleber anhand von zwei verschiedenen Mausmodellen. Ein Modell (alb-SREBP-1c) weist eine genetisch-induzierte, lipogene Lipidakkumulation auf, während im zweiten Mausmodell (aP2-SREBP-1c) die Abwesenheit des Fettgewebes (generalisierte Lypodistropie) zu einer erhöhten systemischen, letzlich metabolischen Lipidbelastung und als Konsequenz zur ektopischen Akkumulation von Lipiden in der Leber führt.

In bioinformatischen Analysen des Transkriptoms wurde die differenzielle Expression der Lebergene jedes einzelnen Phänotyps in Zusammenhang zu den molekularen Veränderungen des Leberstoffwechsels bestimmt. Es zeigte sich, dass die deutlichsten Veränderungen dem Fett- und Kohlenhydratstoffwechsel sowie der Mitochondrienfunktion zuzuordnen sind. Ein direkter Vergleich differenziell exprimierter Gene spezifischer Stoffwechselwege zeigte allerdings, dass die Genexpressionsmuster für jeden untersuchten Fettleberphänotyp hochspezifisch sind. Die Ergebnisse der bioinformatischen Analysen konnten in *ex vivo* Studien mittels Enzymaktivitätsanalysen verifiziert werden. Dementsprechend stellte sich heraus, dass wenn auch die funktionelle Zuordnung differentieller Genexpression auf ähnliche Veränderungen im Leberstoffwechsel der beiden Fettleberphänotypen hinwies, die funktionellen Konsequenzen für jeden Leberphänotyp grundsätzlich verschieden waren. So zeigten die alb-SREBP-1c Mäuse bedingt durch die Transgen-vermittelte Überrepräsentation des Transkriptionsfaktors Sterol regulatory element-binding protein (SREBP)-1c eine gesteigerte *de novo* Lipidsynthese (DNL). Darüber hinaus konnte ein erhöhtes Potential der Mitochondrienfunktion sowie eine gesteigerte Glykolyserate ermittelt werden, was auf eine Adaption an die metabolische Belastung hindeutet. In den Hepatozyten aus den aP2-SREBP-1c Mäusen hingegen konnte nur eine leicht gesteigerte DNL ermittelt werden, wohingegen die mitochondriale β-Oxidation reduziert war. Ferner deuteten die Transkriptionsanalysen in diesem Phänotyp auf eine Verschiebung des Lipidmetabolismus zu einem gesteigerten Cholesterinstoffwechsel hin. Weitergehende Genexpressionsanalysen indizierten eine

grundlegende Veränderung des Lebertranskriptoms hin zu einem adipozyten-ähnlichen Transkriptom, welches insbesondere die Lagerung der Lipide forciert. Obwohl die Glukoneogenese in allen Modellen vergleichbar war, war die Glykogenbildung in dem metabolischen Modell reduziert. Zusammenfassend stellt das lipogene Mausmodell den Phänotyp einer leichten Lebersteatose dar, während der metabolische Phänotyp auf eine progressive Fettleber hinweist.

Bioinformatische Analysen des Sekretoms zeigten, dass sich der Stoffwechselstatus der Hepatozyten aus den verschiedenen Phänotypen dort wiederspiegelt. Im Einklang mit der Transkriptomanalyse wurde für jeden Phänotyp ein einzigartiges Muster sekretierter Proteine (Hepatokine) nicht nur im Vergleich zur Kontrollgruppe, sondern auch zwischen den beiden Fettlebermodellen identifiziert. Ein Topkandidat war Insulin-like growth factor-binding protein (IGFBP) 2, ein lösliches Bindungsprotein für den Wachstumsfaktor Insulin-like growth factor (IGF)-I. Die bioinformatische Aufarbeitung der Transkriptomdaten ergab, dass das IGF-I/IGFBP2 System als übergeordnetes Netzwerk den metabolischen vom lipogenen Leberphänotyp differenzieren kann. In Konsistenz damit wurde IGFBP2 im sekretierten Proteom der primären Hepatozyten des metabolischen Phänotyps gegenüber den übrigen Phänotypen als reduziert identifiziert. In e*x vivo* Experimenten konnte gezeigt werden, dass IGFBP2 keine unmittelbare Signalwirkung hatte, vielmehr die Signalwirkung von IGF-I moduliert. Weitergehende Analysen zeigten, dass die Expression und Sekretion von IGFBP2 unmittelbar an den Status der Fettleber gekoppelt ist. Demzufolge könnte IGFBP2 als Marker für das Fortschreiten der Fettleber dienen und den Status anzeigen, an dem die metabolischen Veränderungen für den Gesamtorganismus gravierend werden.

Die Analyse von Plasma aus einer Kohorte mit NAFLD-Patienten zeigte, dass die IGFBP2 Konzentrationen im Plasma negativ mit dem Status einer hepatischen Steatose korrelierten. Patienten, die einer bariatrischen Intervention unterzogen wurden, zeigten im 2-Jahres follow-up nicht nur eine Verringerung des Fettlebergrades, sondern in unmittelbarer Abhängigkeit des Steatosegrades auch eine Steigerung des IGFBP2 Plasmaspiegels.

Zusammenfassend zeigt diese Arbeit zum ersten Mal von der transkriptionellen über die funktionelle bis hin zur sekretierten Ebene des Leberstoffwechsels einen umfassenden Einblick in die Pathogenese der Fettleber. Die in dieser Arbeit dargestellten Daten deuten darauf hin, dass letztlich die evolutionäre Adaption des Organismus an Hungerperioden ein Fortschreiten der Fettlebererkrankung, mit einer gestörten DNL im Zentrum, bedingt. Einhergehend mit der Pathogenese der Fettleber konnten Veränderungen im Hepatozytensekretom ermittelt werden, wobei IGFBP2 ein vielversprechender Kandidat für die nicht-invasive Klassifizierung der Fettleber darstellen könnte.

Abstract

In the western civilization excessive hepatic lipid accumulation is the most common cause of chronic fatty liver disease. An increased systemic lipid load either by dietary intake or by increased adipose tissue lipolysis as well as an imbalance of intrahepatic lipid metabolism contribute to the development of fatty liver. Although single aspects of disease development and progression are subjected to numerous studies, the complex interplay of metabolic changes within the liver and the fatty liver associated changes in protein secretion patterns still remain unclear.

The objective of this study was to characterize different stages of fatty liver using two different mouse models. One model (alb-SREBP-1c) exhibited genetically induced lipogenic lipid accumulation while in the second model (aP2-SREBP-1c) hepatic steatosis was induced by absent adipose tissue (generalized lipodystrophy) which lead to increased systemic lipid load and consequently ectopic hepatic lipid accumulation.

In bioinformatic analyses of the transcriptome, the differential liver gene expression of each phenotype was set in relation to the molecular changes in hepatic metabolism. The most pronounced differences were annotated to lipid and carbohydrate metabolism as well as mitochondrial function. However, direct comparison of differentially expressed genes showed highly specific gene expression patterns for each fatty liver phenotype for identical pathways. The results from the bioinformatical analyses could be verified in *ex vivo* studies using enzyme activity-based assays. Thus, although functional annotation provided similar pathways of changed hepatic metabolism in the fatty liver transcriptomes functional consequences were fundamentally different. Thus, alb-SREBP-1c mice presented increased *de novo* lipogenesis (DNL) by transgene-mediated overrepresentation of the transcription factor sterol regulatory element-binding protein (SREBP)-1c. In addition, an increased mitochondrial potential as well as increased glycolysis could be determined, which indicated an adaption to metabolic stress. In hepatocytes from the aP2-SREBP-1c mice, however, only a slightly increased DNL was determined, while mitochondrial β-oxidation was decreased. Transcriptional analysis suggests a shift in lipid metabolism to increased cholesterol homeostasis in this phenotype. Transcriptome analyses also indicated fundamental changes in liver transcriptome towards an adipocyte-like transcriptome, which in particular forces the storage of lipids. Although gluconeogenesis was similar in all phenotypes, glycogen formation was reduced in the metabolic model. In summary, the lipogenic mouse model presents the phenotype of a mild hepatic steatosis while the metabolic phenotype indicates progressive fatty liver.

Bioinformatics analyses of the secretome showed that the metabolic status of hepatocytes from the different phenotypes is reflected there. In line with transcriptome analysis, a unique pattern of secreted proteins (hepatokines) was identified for each phenotype not only compared to control but also between the two fatty liver models. A top candidate was the insulin-like growth factor binding protein (IGFBP) 2, a soluble binding protein for the insulin-like growth factor (IGF)-I. Bioinformatical processing of the transcriptome data identified that the IGF-I/IGFBP2 system, as top score upstream regulatory network, can differentiate between the metabolic and the lipogenic liver phenotype. Consistent with this, IGFBP2 was reduced in the secreted proteome of the primary hepatocytes from the metabolic phenotypes compared to the other phenotypes. *Ex vivo* experiments identified IGFBP2 not to have an immediate signaling effect, but to modulate IGF-I signaling. Further analyses showed that expression and secretion of IGFBP2 to be directly linked to fatty liver status. Consequently, IGFBP2 could serve a marker for the gradual fatty liver progression and might indicate the status at which changes in liver metabolism severely impact the whole organism.

In humans, analyses of plasma from a cohort of NAFLD patients showed IGFBP2 levels to negatively correlate with hepatic steatosis status. In this cohort, two years follow-up post bariatric intervention showed increased IGFBP2 plasma levels in direct relation to a reduction of hepatic steatosis.

In conclusion, this thesis showed for the first time a comprehensive insight on the pathogenesis and progression of fatty liver from transcriptome, to functional, up to the secretory level of liver metabolism. The data obtained in this thesis suggest that the evolutionary adaptation of the organism to periods of hunger ultimately leads to the progression of fatty liver disease, with a disturbed DNL in the center. In conjunction with the pathogenesis of fatty liver, changes in hepatocyte secretion could be detected, with IGFBP2 being a promising candidate for the non-invasive classification of fatty liver.

Table of contents

1 Introduction

1.1 Nonalcoholic fatty liver disease (NAFLD)

Nonalcoholic fatty liver disease (NAFLD), the hepatic manifestation of metabolic diseases, turns into the major risk of chronic liver diseases and liver related morbidity and mortality worldwide (Loomba et al. 2013, Diehl and Day 2017, Estes et al. 2018). NAFLD is defined as the occurrence of steatosis without any secondary cause like alcohol abuse, certain medication, immune or genetic diseases, and represents the leading cause of chronic liver diseases today. The accumulation of lipid droplets is defined as hepatic steatosis if more than 5% of the hepatocytes on liver biopsy were affected (European Association for the Study of the Liver 2016). The global prevalence of NAFLD was estimated with 25% and metabolic comorbidities associated with NAFLD included hyperlipidemia (69%), obesity (51%), metabolic syndrome (42%) and type 2 diabetes (T2D, 22%) (Younossi et al. 2016). Furthermore, a more severe disease progression was observed in patients with primary diseases such as obesity, metabolic syndrome or T2D (Leite et al. 2009, Chalasani et al. 2012, Blachier et al. 2013, Younossi et al. 2016). However, NAFLD also occurs in non-obese metabolically healthy and insulin sensitive individuals indicating its pivotal role in the development of pathological metabolic conditions and comorbidities (Kim and Kim 2017).

The health burden of NAFLD is indicated as the beginning of a progressive aggravating process via non-alcoholic steatohepatitis (NASH) to end-stage liver diseases as cirrhosis and hepatocellular carcinomas (HCC, figure 1.1). NAFLD is currently the second most common cause of HCC in end-stage liver disease requiring liver transplantation (Wong et al. 2015). As a future perspective of the disease, the number of NAFLD patients were estimated to increase from today 83 million (2015) to more than 100 million within the next 15 years while NASH is even estimated to increase by more than 60% to 27 million patients. Further, the onset of decompensated alcohol-independent cirrhosis is expected to increase to 168% accounting for more than 100,000 cases and an increase in HCC by 137% within the next 15 years (Estes et al. 2018). Therefore, much attempt needs to be spend on the mechanisms of the disease progression, and the correct diagnosis of disease stage to optimize interventions.

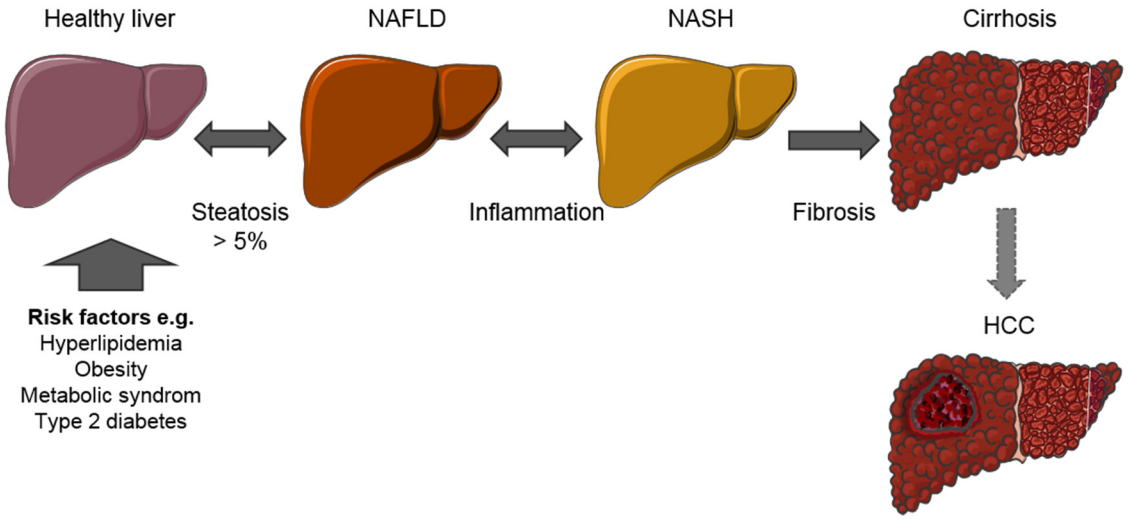

Figure 1.1: Spectrum of non-alcoholic fatty liver disease (NAFLD). Schematic progression of NAFLD from normal liver to end stage liver disease. NASH: non-alcoholic steatohepatitis; HCC: hepatocellular carcinoma.

1.1.1 Histopathology

In NAFLD steatosis is mild to moderate but degrees may vary. Overall, steatosis below 5% is not considered clinically significant. The gradual severity of NAFLD was defined in four steps, and the common definitions of the histological spectrum of NAFLD are listed in table 1.1. Type 1 and 2 describe simple steatosis in the absence or presence of hepatic inflammation while progressed disease is referred to type 3 and 4 which include hepatocellular ballooning, fibrosis, other NASH associated characteristics and cirrhosis (Kleiner and Makhlouf 2016). Moreover, NAFLD steatohepatitis is accompanied by a mild, unspecific inflammation with frequent lobular inflammation in contrast to chronic hepatitis or chronic cholestatic liver disease. Typical characteristics are dense steatosis at the central veins (especially in zones 2 and 3), and spared periportal areas in early stages of the disease, whereas microgranulomas and infiltrates of immune cells are widespread (Kleiner and Makhlouf 2016). In progressive NASH inflammation in the area of the portal vein and the duct are common, combined with clinically and diagnostically relevant hepatocellular zone 3 injury including hepatocellular ballooning, with or without Mallory-Denk Bodies (MDB). NAFLD is usually not accompanied by fibrosis, whereas in NASH fibrosis starts in the pericentral region or acinar zone 3 and can progress to bridging fibrosis and cirrhosis (Kleiner and Makhlouf 2016). Consequently, the fatty acid induced hepatocyte injury, inflammation, and fibrosis cooperatively drive steatosis towards NASH which can further progress to cirrhosis or ultimately lead to the development of HCC (Marrero et al 2002, Tiniakos et al. 2010, Sanyal et al. 2011). The understanding of the molecular alterations of the progression of the disease are therefore important to identify predictive biomarkers and therapeutic targets for intervention.

Table 1.1: Histological spectrum of non-alcoholic fatty liver disease (NAFLD).

Diagnosis	Type	Steatosis	Zone	Lobular inflammation	Portal inflammation	Hepatocellular ballooning
Simple steatosis	1	any degree	any pattern	+/-	+/-	-
Borderline NASH zone 1	2	any degree	zone 1 or acinar	+/-	+/-	-
Borderline NASH zone 3	3	any degree	zone 3	+	+/-	-
Definite NASH	4	any degree	zone 3	+	+/-	+

NASH: non-alcoholic steatohepatitis; +: present; -: absent

1.1.2 Diagnosis

NAFLD usually remains unnoticed for years as specific symptoms are absent. Most findings are incidental, based on liver function tests which assess non-specific hepatocellular damage by a group of blood tests. The best known are the liver enzymes alanine aminotransferase (ALT) and aspartate aminotransferase (AST) which are moderately elevated (1.5 – 2-fold) or even normal in patients with NAFLD usually with an AST/ALT ratio < 1. Further, alkaline phosphatase, gamma glutamyl transferase (gGT) or C-reactive protein (CRP) might also indicate impaired liver function (Attar and Thiel 2013). However, in mild conditions of fatty liver blood tests usually do not point towards impaired liver function as there are often no significant alterations. Although liver function tests can be used to identify patients with high risk of NAFLD, imaging techniques are necessary for exclusion diagnosis.

In non-invasive methodology, ultrasonography (US) represents the most common diagnostic procedure mainly because it represents a relatively inexpensive and widely available method. In severely obese patients or low grade hepatic steatosis (< 30%) the sensitivity of this method is limited, further, distinction between steatosis and steatohepatitis is not possible using US (Metha et al. 2008, Fierbinteanu-Braticevici et al. 2010, Petäjä and Yki-Järvinen 2016, Di Martino et al. 2017). Computed tomographic scanning (CT) can also be used for the assessment of NAFLD but this technique implies exposure of the patient to radiation. In practice, US has a high accuracy when liver fat exceeds 30%, but is markedly decreased in conditions of mild steatosis. However, the non-invasive reference standard is considered to be proton magnetic spectroscopy (^{1}H-MRS). In ^{1}H-MRS the assessment of hepatic steatosis can be sampled in large fractions of the organ with accurate and producible measurement of liver fat content as well as good correlation with liver histology (Metha et al. 2008, Fierbinteanu-Braticevici et al. 2010, Petäjä and Yki-Järvinen 2016, Di Martino et al. 2017). Unfortunately, ^{1}H-MRS as well as CT are not commonly available, according to high instrument costs and the need of highly specialized personnel. In addition,

a common limitation of non-invasive technologies is the inability to distinguish between NAFLD and more progressive forms of the disease (Saadeh et al. 2002), which still makes liver biopsy the gold standard for diagnosing and grading of NAFLD. Histological examination of hepatic tissue provides a classification of hepatic steatosis, hepatocellular injury, inflammation and fibrosis. In this context, the loss of staining for keratin 8 and 18 serve as useful molecular markers in diagnosis of hepatocellular ballooning (Guy et al. 2012). However, performance of liver biopsy is not reasonable for the majority of NAFLD patients as it is invasive and associated with procedure-related complications as well as high costs. Further, diagnosis using non-invasive methods is adequate in the majority of cases (Nalbantoglu and Brunt 2014, Castera 2018).

This lead to the development of surrogate indices combining several parameters of the patients' physiological and metabolic status for more appropriate non-invasive prediction of impaired liver function. Indices combine routinely available clinical and laboratory data like the calculation of the fatty liver index (FLI) according to Bedogni and colleagues (2006). The FLI includes patients' body mass index (BMI), waist circumference, triglyceride (TG) and gGT levels. The underlying algorithm computes an index between 0 and 100 where values < 30 can be used to rule out and ≥ 60 to rule in the occurrence of hepatic steatosis with good accuracy of detecting NAFLD, as proven in several studies (Bedogni et al. 2006, Gastaldelli et al. 2009, Kim et al. 2011). Another example is the NAFLD liver fat score, which was derived from a Finnish population and yielded high sensitivity (86%) and specificity (71%) for the prediction of liver fat content validated by MRS. This liver fat score incorporates the presence of metabolic syndrome and T2D, fasting serum insulin, AST and AST/ALT ratio in the calculation (Kotronen et al. 2009).

1.1.3 'Two hit' versus 'multiple hit' hypothesis

The underlying molecular mechanisms in fatty liver diseases have been extensively studied but cause or consequence of this disease and further the mechanisms leading to more progressive forms of NAFLD remain largely unknown. The molecular nature of the disease appears multifaceted as lipid homeostasis in the liver is a tightly regulated interplay between multiple metabolic pathways as well as inter-organ crosstalk. In 1998 Day and James proposed the so-called 'two hit' hypothesis with steatosis representing the initial event in fatty liver disease and the requirement of a second hit for further progression. The first hit represents the onset of the disease and was suggested to be caused by the increase of liver fat to a steatosis degree of > 5%. The 'second hit' was not clearly defined but was described as the beginning of histologic alterations mainly inflammation and lipid accumulation-dependent cellular alterations in regard to mitochondrial function or cellular stress processes. Present scientific knowledge underlines the improbability of a single

mechanism being responsible for the onset of the disease. It is rather supporting a hypothesis of multiple parallel hits due to metabolic alterations, not only limited to hepatic metabolism but rather systemic, as well as genetic and environmental components which determine the disease and its progression (Tilg and Moschen 2010, Buzzetti et al. 2016, Fang et al. 2018). The multiple hit model of the pathogenesis of NAFLD is based on the current state of knowledge on hepatic insulin resistance, increased *de novo* lipogenesis, alterations in lipid uptake, transport and oxidation in combination with increased inflammation, systemic and environmental triggers as well as genetic susceptibility which are introduced in the following.

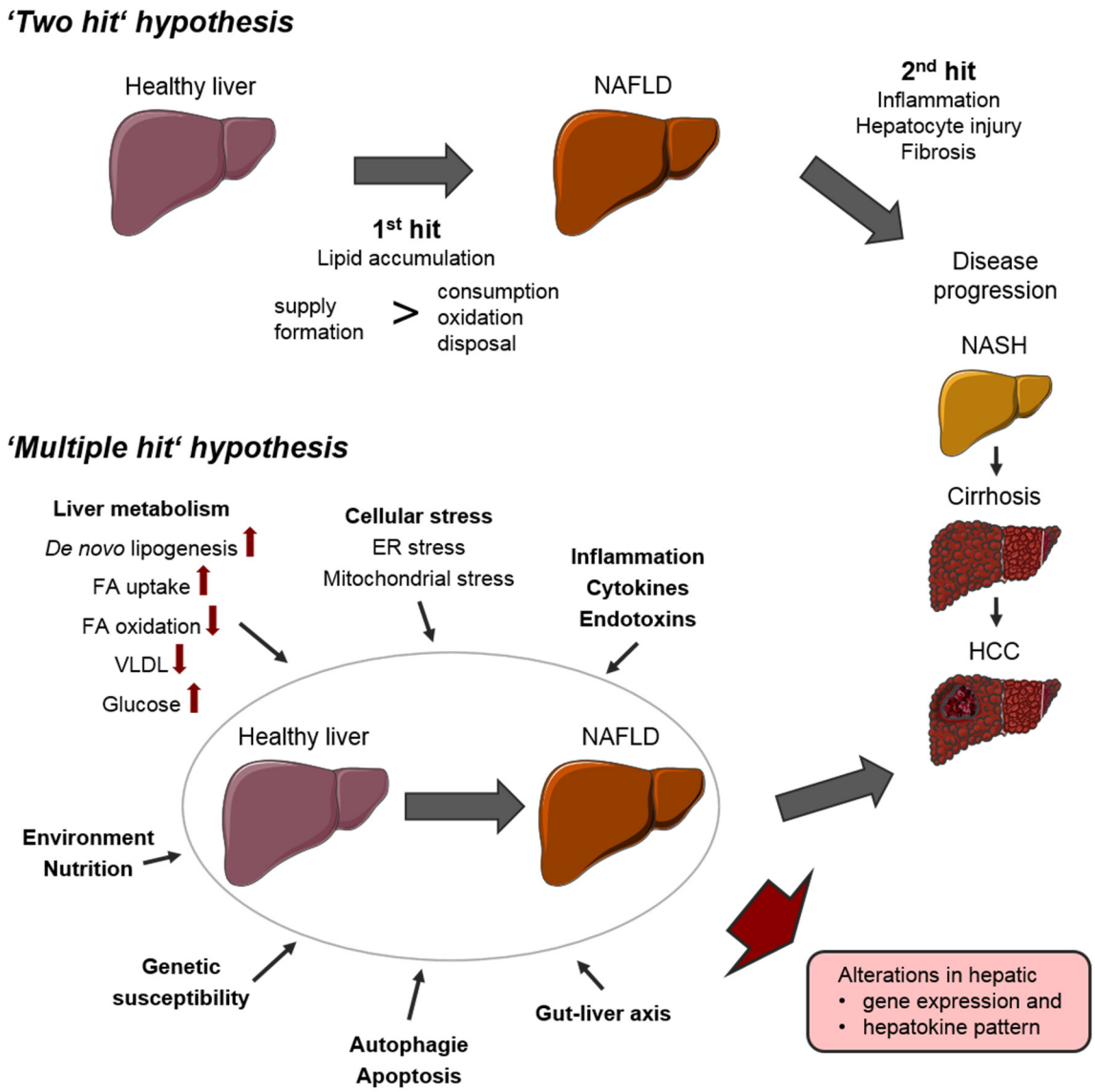

Figure 1.2: Hypotheses of NAFLD onset and progression: 'two hit' versus 'multiple hit' model. The 'two hit' hypothesis proposes non-alcoholic fatty liver disease (NAFLD) and its progression to be a disease of two successive hits. The first hit is the accumulation of lipids making the liver more prone to a second hit which leads to inflammation, hepatocyte injury and fibrosis. In contrast, the multiple hit model suggests a theory of cooperative interaction of multiple parallel hits in regard to hepatic metabolism as well as systemic, genetic and environmental factors which determine the disease and

its progression. NASH: non-alcoholic steatohepatitis; HCC: hepatocellular carcinoma; FA: fatty acid; VLDL: very low density lipoprotein; ER: endoplasmic reticulum.

1.2 Molecular mechanisms in NAFLD

In healthy conditions, the maintenance of hepatic lipid content is a balanced system of lipid synthesis, uptake, oxidation and release. Increased supply of fatty acids (FA) derived from dietary intake or due to increased adipose tissue lipolysis present in insulin resistant conditions leads to an imbalance of lipid homeostasis in the liver. The harmful effects of lipid accumulation in non-adipose tissues was taken into account by the concept of lipotoxicity (Unger et al. 2010). The current nutritional situation in developed countries and the evolutionary protective mechanism to store excess nutritional fuels in specialized organs to prevent toxic effects of lipids on non-adipose cells turns into an overall health bias. The imbalance of caloric intake and energy expenditure results in obesity and consequently to increased ectopic accumulation of excess lipids when the storage capacity of the adipose tissue begins to fail. In morbidly overweight conditions adipose tissue hyperplasia and the reduced ability of adipose tissue remodeling reduces the capacity to store fat. In parallel leptin secretion is reduced thus abolishing the hypothalamic release of satiety signals inducing a futile cycle. In addition, the adipose tissue becomes insulin-resistant which results in increased insulin-dependent activation of lipoprotein lipase and additional release of lipids by lipolysis. Overall, circulating lipids and also lipid flux into the peripheral organs increase mainly through the portal vein into the liver. The condition is aggravated with increased amounts of circulating FA derived from excess dietary uptake. Furthermore, transport of excess lipids leads to chronically increased circulating FA which can reach toxic levels in non-adipose tissues. Increased circulating lipids and metabolic changes in fatty acid metabolism and intracellular signal transduction are associated with peripheral insulin resistance in muscle and liver (Kusminski et al. 2009, Unger et al. 2010).

Persistent lipid accumulation in the liver leads to a vicious circle. One key metabolic alteration in NAFLD is the development of selective hepatic insulin resistance (Brown and Goldstein 2008, Softic et al. 2016). However, insulin resistance in lipid storage loss caused by lipotoxicity is systemic (Shimomura et al. 1999). Beside hepatic insulin resistance NAFLD is primary associated with alterations of metabolic rates triggered by impaired autophagy, endoplasmic reticulum (ER) stress and mitochondrial stress which in sum are also referred to as lipotoxicity (Malhi et al. 2008, Alkhouri et al. 2009). Increased *de novo* lipogenesis (DNL), impaired oxidation of FA as well as decreased lipid clearance (VLDL export) are liable to accumulation of excess lipids in hepatocytes. If the condition precedes it results in hepatic steatosis (Donnelly et al. 2005, Fabbrini et al. 2008, Postic and Girard 2008).

1.2.1 Hepatic lipid overflow

The accumulation of lipids in the liver is one of the key characteristics of NAFLD and it is suggested that the major proportion derives from circulating FA. In NAFLD patients with hypertriglyceridemia and hyperinsulinemia 15% of FA come from dietary intake, 26% from *de novo* lipogenesis and 60% from the circulating free FA (FFA) pool while 60 to 80% of FFAs in the circulation were identified to originate from the adipose tissue (Donnelly et al. 2005). Impaired inhibition of adipose tissue lipolysis associated with insulin resistance as present in obesity and other metabolic diseases is suggested to be causal for the dramatic increase of FFA released from the adipose tissue (Delarue and Magnan 2007).

Excess systemic availability of FA lead to increased uptake into the liver. The uptake of FA into hepatocytes involves lipoprotein lipase, a key enzyme in hydrolysis of circulating lipids and specific transport molecules, i.e. fatty acid transport proteins (FATP). In consequence, a liver-specific overexpression of lipoprotein lipase was found to be associated with hepatic steatosis in mice (Kim et al. 2001) and studies in knock-out mice of liver-specific FATP 2 and 5 showed a reduced uptake of FA and subsequent hepatic lipid accumulation (Doege et al. 2006, Falcon et al. 2010). Overexpression of FAT/CD36, a membrane glycoprotein fatty acid translocase involved in long chain FA transport, lead to increased hepatic lipid accumulation in mice even under standard chow diet (Koonen et al. 2007, Silverstein and Febbraio 2009). Further, the cytosolic fatty acid binding proteins (FABP) 1 and 5 direct FA transport to specific cell compartments for further processing and are highly expressed in the liver. In the absence of FABP5 murine hepatocytes were protected from hepatic lipid accumulation (Newberry et al. 2003, Makowski and Hotamisligil 2005).

Excess FA are incorporated into complex lipid droplets as triglycerides, phosphoglycerolipids, or cholesteryl esters for storage (Guo et al. 2009). Although lipid accumulation is described as hallmark of NAFLD, it is suggested to be an adaptive response. In studies overexpressing diacylglycerol acyltransferases (DGAT) which catalyzes the final step in triglyceride synthesis, hepatic steatosis was present, but animals were protected from systemic inflammation and insulin resistance (Monetti et al. 2007, Koliwad et al. 2010). Furthermore, in mice with inhibition of the isoform DGAT2, a decrease of hepatic lipid content was determined in combination to severe diet-induced NASH progression (Yamaguchi et al. 2007).

1.2.2 *De novo* Lipogenesis (DNL)

The proportion of hepatic lipids derived from intrahepatic DNL were found to account for 26% representing the second largest FA source in patients with NAFLD (Donnelley et al. 2005). In patients with NAFLD the rate of DNL was observed to be proportionally increased

with the amount of liver fat. The group classified with high liver fat content showed higher rates of lipid synthesis compared to the low liver fat group while adipose tissue derived FFA flux and production of very low density lipoprotein were not different between the groups (Diraison et al. 2003, Lambert et al. 2014). DNL comprises different steps including glycolysis for the conversion of glucose to acetyl-CoA, synthesis of FA followed by elongation and desaturation, and finally the formation of TG. The energy-dependent carboxylation of acetyl-CoA to malonyl-CoA is the rate limiting first step in DNL and catalyzed by acetyl-CoA carboxylase (ACC) (Munday 2002, Abu-Elheiga et al. 2005). Malonyl-CoA is then added to acetyl-CoA by fatty acid synthase (FAS). Monounsaturated FA are generated by elongation of FA catalyzed by long chain fatty acid synthase (ELOVL) 6 while stearoyl-CoA desaturase (SCD) 1 catalyzes desaturation. Monounsaturated FA provide the major source for TG synthesis (Miyazaki et al. 2001, Kawano and Cohen 2013, Sanders and Griffin 2016).

ACC is present with two isoforms in the cell, ACC1 is cytosolic and catalyzes malonyl-CoA while ACC2 is suggested to impair mitochondrial β-oxidation by modulation of local malonyl-CoA levels. Liver specific knock-out of ACC1 showed controversial results with one study reporting significantly decreased malonyl-CoA levels while in another mouse model ACC1 knock-out has no effects on DNL and malonyl-CoA levels in the cells (Mao et al. 2006). In both models increased ACC2 expression was observed and is suggested to compensate for ACC1 loss as dual inhibition of both isoforms shut down DNL (Harada et al. 2007).

TG synthesis is initiated by esterification of glycerol-3-phosphat from glycolysis with newly synthesized FA a process catalyzed by glycerol-3-phosphate acyltransferase (GPAT). 1-acylglycerol-3-phosphate acyltransferase (AGPAT) converts the resulting lysophosphatidic acids (LPA) to phosphatidic acids, which are further dephosphorylated to diglycerides (DG) by phosphatidic acid phosphorylase (PAP). Then, DGAT catalyzes acetylation from DG to TG (Kawano and Cohen 2013, Sanders and Griffin 2016). Lipids are incorporated in VLDL particles to mediate lipid clearance via release to be provided to peripheral organs. VLDL assembly comprises the partial lipidation of the liver specific apolipoprotein (apo) B100 to form VLDL precursors which are combined with large lipid droplets to mature VLDL particles (Perla et al. 2017). In NAFLD and obesity, the secretion rate of VLDL from the liver was found markedly increased while VLDL particle appear to be similar between the investigated groups (Fabbrini et al. 2008, Chan et al. 2010). Further, weight gain was found to increase VLDL export rate from the liver but fails to compensate for the accumulation of lipids (Fabbrini et al. 2016).

1.2.3 Fatty acid oxidation and mitochondrial function

In hepatic metabolism the breakdown of FA is the main source of energy production and to a minor degree to maintain the balance of intrahepatic lipids. It mainly takes place in the mitochondria and to lesser extend in peroxisomes and microsomes. Under normal conditions the primary site of medium and long chain FA oxidation are the mitochondria while very long chain FA (> 22 carbon atoms) can only be oxidized in peroxisomes, however, products of peroxisomal oxidation, including acetyl-CoA, are provided to the mitochondria for full oxidation (Wanders 2014, Lodhi and Semenkovich 2014).

FA are translocated to the mitochondria upon activation to fatty acyl-CoAs. Further conversion of fatty acyl-CoAs to fatty acyl-carnitines catalyzed by carnitine palmitoyl transferase (CPT) 1 occurs and the acyl-carnitines are transported across the inner mitochondrial membrane. CPT2 on the inner mitochondrial membrane converts acyl-carnitines back to acyl-CoAs. Further β-oxidation to acetyl-CoA and incorporation in the tricarboxylic acid (TCA) cycle for full oxidation takes place with subsequent ATP production within the electron transport chain (ETC) (McGarry and Foster 1980). Data remain controversial in human NAFLD patients while studies identified reduction in mitochondrial metabolism in patients with NAFLD and NASH (Cortez-Pinto et al. 1999, Schmid et al. 2011) as well as increased mitochondrial function (Sanyal et al. 2001, Sunny et al. 2011). In a mouse model of high fat diet induced fatty liver and hepatic steatosis impaired insulin-mediated suppression of TCA cycle and mitochondrial efficiency was observed which was associated with oxidative stress, inflammation and hepatocellular damage (Satapati et al. 2012).

1.2.4 Oxidative stress

In NAFLD hepatic lipotoxicity was further observed to be associated with an increase of reactive oxygen species (ROS) causing cellular oxidative stress. In several human studies enrolling also NAFLD and NASH patients oxidative stress markers including malondialdehyde or 3-nitrotyrosine, 4-hydroxy-2-noneal, 8-hydroxydeoxyguanosine and thiobarbituric acid-reacting substrate (TBARS) were found to be upregulated in liver tissue or plasma. In patients with NASH these markers were found even more elevated, suggesting a pivotal role of oxidative stress in disease progression (Sanyal et al. 2001, Chalasani et al. 2004, Seki et al. 2005, Madan et al. 2006, Yesilova et al. 2005, Bonnefont-Rousselot et al. 2006). Furthermore, in patients with NASH serum levels of oxidized low density lipoprotein (LDL) and increased serum lipid peroxidation showed an increased oxidative challenge compared to controls. Further, in these patients insulin resistance was independently associated with oxidized LDL serum levels (Chalasani et al. 2004). The elevation of ROS in fatty liver is presumably a result of increased FA β-oxidation in the

mitochondria and the resultant electron overflow in the ETC (Li et al. 2008, Vial et al. 2011, Ursini et al. 2016).

Excessive ROS production and insufficient antioxidant response is directly detrimental to cellular structures and favors apoptosis by the activation of stress sensitive pathways like nuclear factor κB, p38 mitogen-activated protein kinase (MAPK) and c-Jun N-terminal kinase (JNK) (Klaunig et al. 2010, Ursini et al. 2016). Increased expression and activity of the cytochrome P450 2E1 (CYP2E1) monooxygenase was also found to contribute to oxidative stress in hepatic lipotoxicity. CYP2E1 localized in the membrane of the ER is described as a significant source of oxidative intermediates and was shown to positively correlate with BMI and steatosis. Of note, it was also found to be increased in patients with NAFLD (Weltman et al. 1998, Chalasani et al. 2003, Videla et al. 2004, Orellana et al. 2006,). In animal models, FA-induced oxidative stress was observed to induce insulin resistance via JNK activation and subsequent increased ROS production from FA β-oxidation in the mitochondria e.g. in rat hepatocytes (Nakamura et al. 2009). NADPH oxidase 3 was identified to be a key molecule in palmitate-induced ROS generation in db/db mice and in an *in vitro* model of palmitate-treated hepatocellular HepG2 cells, and may be linked to saturated FA-induced insulin resistance mediated via JNK and p38 MAPK signaling (Gao et al. 2010).

1.2.5 Endoplasmic reticulum stress

An imbalance of energy expenditure and demand, as present in cells exposed to excess lipids, is known to induce cellular stress pathways. Toxic lipid concentrations were observed to induce ER stress in hepatocytes, defined as the response of the ER to the accumulation of unprocessed proteins (Wang et al. 2006, Wei et al. 2007, Lake et al. 2014). The type of FA is crucial for disease progression also in this process. Saturated FA were identified to exert higher lipotoxic potential also in triggering ER stress. Hepatoma cells treated with saturated FA induced ER stress response genes CCAAT/enhancer-binding protein homologous protein (CHOP), growth arrest and DNA damage (GADD) 34, and glucose-regulated protein (GPR) 78 which was accompanied with increased apoptosis. In contrast, cells treated with monounsaturated fatty acids abrogated the saturated FA-induced ER stress (Wei et al. 2006). In human hepatocellular cell line HepG2 palmitate induced ER stress and apoptosis identified by increased eukaryotic translation initiation factor (eIF) 2α phosphorylation, inositol-requiring enzyme (IRE) 1α and CHOP upregulation, which was not present in cells treated with the unsaturated FA oleate (Gu et al. 2010).

When lipid load exceeds ER protein folding capacity, a coordinated stress response cascade is activated to restore ER homeostasis, termed the unfolded protein response (UPR) (Ji and Kaplowitz 2006, Ron and Walter 2007, Todd et al. 2008). The UPR response

involves three major domains which collectively activate adaptive processes namely IRE1, protein kinase RNA-like ER kinase (PERK) and activating transcription factor (ATF) 6. These molecules mediate deceleration of protein synthesis, expression of ER chaperons and degradation of misfolded proteins to overcome the stress stimulus. When ER stress persists UPR is unable to restore ER function and associates with apoptosis (Wang et al. 2006, Cao et al. 2012). In human NAFLD and NASH there were equivocal findings regarding UPR activity in liver tissue but patients with liver disease showed consistent increase in phosphorylation of eIF2α compared to control group pointing towards increased PERK activation. Additionally, in NASH decreased spliced X-box binding protein (XBP) 1 mRNA was found as well as activation of JNK (Puri et al. 2008). XBP1 activated through IRE1 exerts a role in regulation of lipid homeostasis as well as inflammatory cascades including JNK (Ozcan et al. 2004, So et al. 2012). Activated JNK also interferes with insulin signaling cascade by negative regulation of the insulin receptor substrate (IRS) 1 and represents a key link to insulin resistance (Hirosumi et al. 2002, Ozcan et al. 2004, Li and Yu 2013).

1.2.6 Hepatic insulin signaling

Disruption of insulin signaling in the liver lead to severe hyperglycemia accompanied with peripheral insulin resistance (Michael et al. 2000) suggesting hepatic insulin resistance as central event contributing not only to development and progression of NAFLD, but also associated systemic pathological metabolic conditions. In hepatic steatosis lipid metabolites interfere with insulin signal transduction and cause insulin resistance characterized by insufficient cellular response to circulating insulin. Inadequate insulin-stimulated transport of glucose and insufficient suppression of endogenous glucose production are the two main consequences.

The molecular mechanism of insulin resistance is defined as the inability of insulin signaling cascade to regulate insulin mediated metabolic pathways for systemic glucose disposal (Schinner et al. 2005, Saini 2010). In healthy individuals insulin binds to the insulin receptor which activates its kinase activity and autophosphorylation of tyrosine residues. Tyrosine phosphorylation enables protein binding to intracellular receptor sites with consecutive protein phosphorylation. Most insulin mediated effects involve IRS phosphorylation after binding to the insulin receptor. Activation of IRS further recruits phosho-inositide-3 (PI3) kinases as key molecules in insulin signaling. PI3-kinases class 1a generate 3'-phosphoinositides to activate protein kinase B, also known as Akt which mediates several downstream effects of the insulin signaling cascade like glucose transport, glycogen synthesis, protein synthesis, lipogenesis and suppression of hepatic gluconeogenesis (Schinner et al. 2005, Saini 2010). In the liver, the most important function contributing to regulation of circulating glucose levels is insulin-mediated suppression of hepatic glucose

production. There are two key mechanisms well described to suppress hepatic glucose production. First the transcriptional inhibition of the gluconeogenic genes phosphoenolpyruvate carboxykinase (PEPCK) and the glucose-6-phosphatase (G6PC) catalytic subunit by Akt targeted transcriptional regulation through phosphorylation and thus inactivation of forkhead box, class O (FoxO)-family transcription factors (Hall et al. 2000, Schmoll et al. 2000). Second Akt-targeted inactivation of glycogen synthase kinase-3 (GSK3) and subsequent activation of glycogen synthesis (Sung et al. 1998, Summers et al. 1999). Impairment of this tightly regulated processes lead to restricted insulin action and consequently insulin resistance.

Insulin also promotes a pivotal role in regulation of DNL by activation of sterol regulatory element-binding protein (SREBP)-1c. This transcription factor regulates genes involved in the synthesis of fatty acids (Horton et al. 1998, Shimomura et al. 1999). It can be further activated by saturated fatty acids and the liver X receptor (LXR) alpha, (Chen et al. 2004). Overexpression of the transcriptional active domain of SREBP-1c leads to constantly active DNL in mouse liver associated with adiposity and hepatic insulin resistance (Knebel et al. 2012, Jelenik et al. 2017). In mice with liver-specific insulin receptor knock-out decreased SREBP-1c and consecutive target expression was observed (Biddinger et al. 2008a, Emanuelli et al. 2014). Insulin further promotes DNL by facilitating FFA uptake (Softic et al. 2012). Interestingly, there is selective insulin resistance in patients associated with conditions like obesity or NAFLD, where despite systemic insulin resistance, insulin is still able to stimulate DNL (Softic et al. 2016).

In high fat diet fed rats hepatic suppression of glucose production was diminished prior to the development of adiposity or muscle insulin resistance (Samuel et al. 2004). In this model insulin resistance was associated with accumulation of Diglycerides (DG) and the activation of protein kinase C (PKC) ε. Activation of PKCε was found to be addressed to a DG-binding domain which translocate the molecule to the plasma membrane where it inhibits the activity of the intracellular kinase domain of the insulin receptor and subsequent inhibition of insulin signaling cascade (Samuel et al. 2004, Dries et al. 2007, Samuel at al. 2007). Knock-down studies further promote a central role of PKCε as it protected rodents from lipid-induced hepatic insulin resistance though hepatic steatosis was present (Frangioudakis et al. 2009). In humans, DG and PKCε activation were identified as strongest predictors for hepatic insulin resistance in liver biopsies (Kumashiro et al. 2011, Magkos et al. 2012). Also for other lipid species like ceramides, accumulation was observed to impair insulin signaling by dephosphorylation of Akt2 including PKC isoform ξ (Teruel et al. 2001, Fox et al. 2007, Blouin et al. 2010). In contrast, mice deficient in mitochondrial acyl-CoA:glycerol-sn-3-phosphate acyltransferase (mtGPAT) which catalyzes the formation of LPA from fatty acyl-CoA and glycerol-3-phosphate showed markedly lower hepatic DG and TG concentrations

compared to the control group. In addition, these mice were protected from the development of insulin resistance and even improved insulin sensitivity compared to wild type phenotype (Neschen et al. 2005). Also lipid induced ER and oxidative stress drives insulin resistance in the liver as described above through JNK activation. Hepatic insulin resistance was also shown to be improved by suppression of JNK in the adipose tissue further implicating an important role of adipose tissue function in hepatic insulin resistance (Sabio et al. 2009, Zhang et al. 2011).

1.2.7. Inflammation and the gut-liver axis

Inflammatory processes trigger the progression from NAFLD to NASH. Increased FFA levels, lipotoxicity, insulin resistance and other factors (e.g. endotoxins from the intestines) increase the release of systemic cytokines or hepatokines. In addition to parenchymal hepatocytes the liver also consists of endothelial cells, hepatic stellar cells and Kupffer cells, in particular the latter are involved in the immune regulation of the liver and can release cytokines such as tumor necrosis factor (TNF) α, transforming growth factor (TGF) β, interleukin (IL)-1, IL-4, IL-6, IL-10, and IL-12. Mechanistically the activation of JNK activator protein 1 (JNK-AP-1) leads to MAPK mediated apoptosis. Further the activation of the transcription factor I kappa B kinase (IKK) NF-κB regulates inflammation (Hotamisligil 2006). In particular IL-6 and TNFα are thought to be responsible for the NASH progression (Klein et al. 2007) and a yet to be identified predictive cytokine pattern could act as an indicator of NASH progression and liver damage.

Another aspect of the inflammatory processes came into focus in NAFLD, i.e. the bidirectional intestine-liver axis. From the intestinal lumen nutrients and small molecules enter the liver via the portal vein circulation. Conversely, bile acids produced in the liver are released via the bile duct into the small intestine and regulate the digestion of dietary fats (Poeta et al. 2017). Increased bile acid levels affect the intestinal environment, directly due to membrane damage and thus altered membrane permeability. This can result in increased uptake of inflammatory bacterial endotoxins into the liver. Elevated bile acid levels may support the fermentation into short-chain fatty acids rather than the digestion of dietary lipids. Such short-chain fatty acids unrestricted enter cells as they are not subject to any directed or regulated transport processes. As an indirect effect, the activation of bile acids regulated transcription factors of the farnesyl X receptor (FXR) family can also take place in the liver, which can lead to a reduced hepatic choline metabolism and thus reduce the secretion of cholesterol (Doulberis et al. 2017). This aspect of NAFLD progression strongly depends on individual lifestyle and nutritional habits.

1.2.8. Genetic susceptibility and metabolic risk

As shown by many syndromes caused or associated to metabolic disturbances, NAFLD progression also depends on the interaction of genetic susceptibility and metabolic risk due to individual lifestyle. Genetic factors influencing the action and metabolic rates of central enzymes, trigger inflammation, substrate oxidation and interfere with cellular stress response are likely to aggravate the individuals susceptibility. Functional implicative molecules and key regulators of the metabolic pathways were identified, analyzed or verified in *in vitro* studies and laboratory animal models. The latter mainly target central genes for lipid metabolism, especially the transcription factor SREBP-1, i.e. SREBP-1a and 1c (Jump 2011, Knebel et al. 2012, Kotzka et al. 2012, Xu et al. 2013, Jelinek et al. 2017) or bare molecular constructs resulting in lipodystrophic phenotypes like the 'fat-free' A-ZIP mouse (Moitra et al. 1998) or the aP2-SREBP-1c mouse (Shimomura et al. 1998), resulting in fatty liver phenotypes. Moreover, naturally occurring models like the db/db and ob/ob mice, the polygenic NZO mice or Zucker-rat develop fatty liver phenotypes, probably on different etiologies including hyperphagia behavior (Kanuri and Bergheim 2013, Knebel et al. 2018a). In humans, genetic variability in genes involved in lipid metabolism were associated to the NAFLD risk and the number of candidates is emerging (Romeo et al. 2008, Speliotes et al. 2010).

Overall, despite the detailed molecular knowledge of the multiple single pathologies accompanied the pathogenesis of NAFLD still remains unknown. In regard to human studies one central open question is how the diverse molecular mechanisms interact and to which extend the metabolic susceptibility or predisposition of a patient accounts to the onset or progression of NAFLD. In this regard the main objective in the context of NAFLD will be the differentiation of processes due to certain genetic modifications of lipid metabolism from the aggravating changes caused by excess systemic lipids.

2 Aim of the study

Fatty liver is the leading cause of chronic liver disease in the western population. The close relation to metabolic dysfunctions also found in obesity, metabolic syndrome or T2D makes it difficult to identify the driving molecular mechanisms underlying NAFLD. In this study two different mouse models with either a genetic or a metabolic phenotype of fatty liver were investigated to gain further insight in the pathophysiology and progression of this disease. The first model represents intrahepatic induction of steatosis by genetically induced accumulation of lipids. Lipid synthesis is constitutively activated in hepatocytes of these animals by liver specific overexpression of the human transcription factor SREBP-1c, the master regulator of lipid synthesis. Physiology of this mouse model named alb-SREBP-1c was previously described and represents a suitable model for primary lipid accumulation in the liver and its systemic impact (Knebel at al. 2012). The second mouse model included in the study displays a phenotype of fatty liver caused by dramatic increase of systemic lipid load due to the absence of adipose tissue. Here, the lipodystrophic phenotype is based on adipose tissue specific overexpression of the human transcription factor SREBP-1c. In these animals the mechanism responsible for accumulation of lipids in the liver is certainly indirect as the transgene is not expressed in liver tissue and systemic lipid overflow in the circulation is caused by absent adipose tissue (Shimomura et al. 1998). Of note, both mouse models develop the fatty liver phenotype under standard chow diet. The genetic phenotype is further associated with selective hepatic while the lipodystrophic phenotype shows systemic insulin resistance (Jelenik et al. 2017).

Although the physiological conditions accompanied with fatty liver are well described the detailed molecular mechanisms underlying the pathogenesis of NAFLD still remain puzzling, especially how the diverse molecular mechanisms interact. Therefore the first aim of this study was to investigate whether these animal models represent suitable mouse models for the different stages of fatty liver. This was conducted by genetic and functional characterization of these animal models *in vivo* and *ex vivo* in regard to nodal points of carbohydrate and lipid metabolism. Thus the two different animal models allowed to distinguish between genetically and systemic induced hepatic lipid accumulation in the absence of dietary manipulation the study further aimed to identify regulators which promote the progression of fatty liver on molecular basis. In addition the interplay between genetic intracellular changes, secretion of hepatic molecules and its impact on cellular metabolism allowed the identification of potential biomarkers which might help to predict the presence of fatty liver. In subsequent experiments a selected biomarker should be identified and verified in the investigated animal models and further evaluated for its transferability to the human situation.

3 Material and Methods

3.1 Material

3.1.1 Chemicals, solutions and cell culture media

Standard laboratory chemicals and solutions were purchased from common vendors. Specific chemicals, solutions and cell culture media used in this study are listed in table 3.1.

Table 3.1: Chemicals, solutions and culture media.

Item	Vendor/ product code
(+)-Etomoxir, sodium salt hydrate, ≥98% (HPLC), powder	Merck KGaA , Darmstadt, Germany/ E1905
5x First Strand Buffer	Promega Corporation, Madison, USA/ M531A
Albumin Fraction V, fatty acid free	Carl Roth GmbH + Co. KG, Karlsruhe, Germany/ 0052.3
Antibiotic-Antimycotic (100 x)	Gibco™ Thermo Fischer Scientific Corporation, Massachusetts, USA/ 15240062
Antimycin A from Streptomyces sp.	Merck KGaA , Darmstadt, Germany/ A8674
Carbonyl cyanide 4-(trifluoromethoxy)phenylhydrazone (FCCP, ≥98% (TLC), powder)	Merck KGaA , Darmstadt, Germany/ C2920
Collagen I, rat tail	Advanced BioMatrix, Inc., California, USA/ 5056
Collagenase, Type IV	Worthington Biochemical Corporation, New Jersey, USA/ CLS-4 (Lot 46A16396)
cOmplete, Mini protease inhibitor cocktail tablets	Roche Diagnostics GmbH, Mannheim, Germany/ 04 693 124 001
Dexametasone, ≥98% (HPLC), powder	Merck KGaA , Darmstadt, Germany/ D1756
D-Glucose	AppliChem GmbH, Darmstadt, Germany/ A3617
Dulbecco's modified Eagle's medium (DMEM), low glucose, pyruvate, HEPES	Gibco™ Thermo Fischer Scientific Corporation, Massachusetts, USA/ 22320022
DMEM, without glucose, L-glutamine, phenol red, sodium pyruvate and sodium bicarbonate, powder, suitable for cell culture	Merck KGaA , Darmstadt, Germany/ D5030
DMEM/F-12, GlutaMAX™ Supplement	Gibco™ Thermo Fischer Scientific Corporation, Massachusetts, USA/ 31331028
DMEM/F-12, HEPES, no phenol red	Gibco™ Thermo Fischer Scientific Corporation, Massachusetts, USA/ 11039021
Dulbecco's Phosphate Buffered Saline (PBS), modified, without calcium chloride and magnesium chloride, powder, suitable for cell culture	Merck KGaA , Darmstadt, Germany/ D5652
Easycoll Separating Solution (Density 1.077 g/ml)	Biochrome GmbH, Berlin, Germany/ L6135
Fetal Calf Serum (FCS)	Biochrom GmbH, Berlin, Germany/ S0115
Formaldehyde solution, ACS reagent, 37 wt. % in H_2O, contains 10-15% methanol as stabilizer (to prevent polymerization)	Merck KGaA , Darmstadt, Germany/ 252549
GlutaMAX™-I (100x)	Gibco™ Thermo Fischer Scientific Corporation, Massachusetts, USA/ 35050061
Glycogen from rabbit liver, Type III	Merck KGaA , Darmstadt, Germany/ G8876

Table 3.1 continued.

Item	Vendor/ product code
4-(2-Hydroxyethyl)piperazine-1-ethanesulfonic acid (HEPES) Buffer Solution (1 M)	Gibco™ Thermo Fischer Scientific Corporation, Massachusetts, USA/ 15630056
Immobilon Western Chemiluminescence HRP Substrate	Merck KgaA, Darmstadt, Germany/ WBKLS0500
Insulin from porcine pancreas	Merck KGaA , Darmstadt, Germany/ I5523
L-Carnitine inner salt, synthetic, ≥98%	Merck KGaA , Darmstadt, Germany/ C0158
L-Glutamine	Merck KGaA , Darmstadt, Germany/ G8540
Minimum Essential Medium (MEM) Vitamin Solution (100x)	Gibco™ Thermo Fischer Scientific Corporation, Massachusetts, USA/ 11120037
MEM Non-Essential Amino Acids (NEAA, 100x)	Gibco™ Thermo Fischer Scientific Corporation, Massachusetts, USA/ 11140035
M-MLV reverse transcriptase, RNase (H-), point mutant	Promega Corporation, Madison, USA/ M3683
Nonidet® P (NP)-40 (Substitute) – Solution 10% peroxide-free	AppliChem GmbH, Darmstadt, Germany/ A2239
Oil-Red-O, certified by the Biological Stain Commission	Merck KGaA , Darmstadt, Germany/ O0625
Oleic acid, analytical standard	Merck KGaA , Darmstadt, Germany/ 75090
Oligomycin A, ≥95% (HPLC)	Merck KGaA , Darmstadt, Germany/ 75351
PhosSTOP phosphatase inhibitor cocktail tablets	Roche Diagnostics GmbH, Mannheim, Germany/ 04 906 845 001
Precision Plus Protein™ All Blue Prestained Protein Standards	Bio-Rad Laboratories GmbH, Munich, Germany/ 161-0373
QIAzol® Lysis Reagent	QIAGEN GmbH, Hilden, Germany/ 79306
qPCR MasterMix plus w/o UNG (2x)	Eurogentec Deutschland GmbH, Köln, Germany/ RT-QP2X-03-WOU+
Random Primers	Promega Corporation, Madison, USA/ C1181
Rotenone, ≥95%	Merck KGaA , Darmstadt, Germany/ R8875
Rotiphorese® Gel 30 30% acrylamide and bisacrylamide stock solution at a ratio of 37.5:1	Carl Roth GmbH + Co. KG, Karlsruhe, Germany/ 3029.1
Rotiszint® eco plus	Carl Roth GmbH + Co. KG, Karlsruhe, Germany/ 0016.3
Set of dATP, dCTP, dGTP, dTTP (dNTP nucleotide mix)	Promega Corporation, Madison, USA/ U1240
Sodium bicarbonate ($NaHCO_3$, 7.5%)	Gibco™ Thermo Fischer Scientific Corporation, Massachusetts, USA/ 25080094
Sodium lactate BioChemica	AppliChem GmbH, Darmstadt, Germany/ A1004
Sodium palmitate, ≥ 98.5%	Merck KGaA , Darmstadt, Germany/ P9767
Sodium pyruvate (100 mM), 100x	Gibco™ Thermo Fischer Scientific Corporation, Massachusetts, USA/ 11360-070

3.1.2 Radiolabeled solutions

Table 3.2: Radiolabeled solutions used for analysis.

Radiolabeled solution	Vendor/ product code
^{14}C-glucose, Glucose, D-[^{14}C(U)]	Perkin Elmer, Inc., Massechusetts, USA/ NEC042X250UC
^{14}C-acetate, Acetic Acid, Sodium Salt [1-^{14}C]	Perkin Elmer, Inc., Massechusetts, USA/ NEC084H001MC
^{14}C-palmitate, Palmitic Acid, [1-^{14}C]	Perkin Elmer, Inc., Massechusetts, USA/ NEC075H250UC
^{3}H-palmitate, Palmitic Acid [9,10-^{3}H(N)]	Perkin Elmer, Inc., Massechusetts, USA/ NET043025MC

3.1.3 Recombinant proteins

Table 3.3: Recombinant proteins used for cell culture experiments.

Recombinant protein	Source	Vendor/ product code
Recombinant Human IGF-I	E. coli	PeproTech Germany, Hamburg, Germany/ 100-11
Recombinant Human IGFBP-2	Mouse myeloma cell line	R&D Systems, Inc., Minneapolis, USA/ 674-B2

3.1.4 Buffer

Table 3.4: Buffer compositions.

Name	Composition
Easycoll working solution	10% (v/v) 10x PBS (Gibco 14200-067) 90% (v/v) Easycoll Separating Solution (Density 1.077 g/ml; Biochrome L6135)
Fatty acid uptake (FAU) transport buffer	2.5 µM BSA 5 µM palmitate – BSA (see section 3.9.1) 8.5 nM ^{3}H-palmitate
Fixation solution	10% (v/v) formaldehyde in dH_2O
Hanks' balanced salt solution (HBSS, isolation)	5.33 mM KCl 0.44 mM KH_2PO_4 0.34 mM Na_2HPO_4 138 mM NaCl 4.17 mM $NaHCO_3$ 5.56 mM Glucose 0.5 mM EGTA 25 mM HEPES
HBSS (secretome)	HBSS (Gibco 14175-053) +1.26 mM $CaCl_2$
Krebs-Ringer-HEPES (KRH)	136 mM NaCl 4.7 mM KCl 1.25 mM $MgSO_4$ 1.25 mM $CaCl_2$ 10 mM HEPES
Methyltransferase (MTase) assay 4 x reaction buffer	80 mM Tris, pH 8.0 200 mM NaCl 4 mM EDTA 12 mM $MgCl_2$ 0.4 mg/ml BSA 4 mM Dithiothreitol
NP-40 lysis buffer	1% (v/v) NP-40 in PBS
Oil-red-o stock solution	0.7 g (w/v) oil-red-o in 200 ml isopropanol, 0.2 µm filtered
Oil-red-o working solution	60% (v/v) oil-red-o stock solution in dH_2O, 0.2 µm filtered
PBS	9.6 g powder (w/v) (see table 3.1) add 1 l ddH_2O
Resolving gel buffer	1.5 M Tris-HCl (pH 8.8)
Radioimmunoprecipitation assay buffer (RIPA) lysis buffer	30 mM Tris-HCl (pH 7.5) 1 mM EDTA 150 mM NaCl 0.5% (v/v) Triton-X-100 0.5% (v/v) Sodium deoxycholate 1x cOmplete, protease inhibitor 1x PHOSstop, phosphatase inhibitor

Table 3.4 continued.

Name	Composition
Seahorse lysis buffer	10 mM Tris-HCl 10 mM $Na_2HPO4•2H_2O$ 10 mM $NaH_2PO_4•H_2O$ (pH 7.5) 130 mM NaCl 10 mM $Na_4P_2O_7•10H_2O$ 1% (v/v) Triton X-100
Stacking gel buffer	0.5 M Tris-HCl (pH 6.8)
Tris-buffered saline with Tween20 (TBS-T)	20 mM Tris (pH 7.5) 150 mM NaCl 0.1% (v/v) Tween® 20
Transfer buffer	25 mM Tris 192 mM glycine 20% (v/v) methanol in dH_2O
1x electrode running buffer	250 mM Tris 190 mM glycine 0.1% (v/v) SDS
5x Laemmli sample buffer	312.5 mM Tris-HCl (pH 6.8) 10% (v/v) SDS 50% (v/v) glycerol in dH_2O 500mM DTT 0.01% (v/v) bromphenol blue

3.1.5 Cell culture media supplementation

Table 3.5: Supplementation of cell culture media for hepatocyte isolation, culture maintenance and experiments.

Name	Medium base	Supplements
Collagenase medium	DMEM, low glucose	2x Antibiotic-Antimycotic mix 100 or 150 U/ml collagenase IV (specific activity 280 U/mg)
Fatty acid oxidation (FAO) assay medium	DMEM/F-12, GlutaMAX™ Supplement	+ 1.5 mM sodium pyruvate (final conc. 2 mM) 10 µM BSA Fraction V, fatty acid free 2x Antibiotic-Antimycotic mix 1 µM L-Carnitin 2.6 µM ^{14}C-palmitate
Glucose assay medium	DMEM w/o glucose, L-glutamine, phenol red, sodium pyruvate and sodium bicarbonate	2.5 mM L-Glutamine 15 mM HEPES 3.7 g/ml $NaHCO_3$ 1x Antibiotic-Antimycotic mix pH adjusted to 7.4 with NaOH
Glycogen assay glucose starvation medium	DMEM w/o glucose, L-glutamine, phenol red, sodium pyruvate and sodium bicarbonate	1x MEM-vitamin mix 1x MEM NEAA 2 mM GlutaMAX™-I 1 mM sodium pyruvate 0.24 % $NaHCO_3$ 1x Antibiotic-Antimycotic mix
Glycolysis stress assay medium	DMEM w/o glucose, L-glutamine, phenol red, sodium pyruvate and sodium bicarbonate	2 mM glutamine pH adjusted to 7.4 with NaOH

Table 3.5 continued.

Name	Medium base	Supplements
Isolation medium	DMEM, low glucose	10% (v/v) FCS + 1 mM sodium pyruvate (final conc. 2 mM) 0.1 µM porcine insulin 1 µM Dexamethasone 2x Antibiotic-Antimycotic mix
Mito stress assay medium	DMEM w/o glucose, L-glutamine, phenol red, sodium pyruvate and sodium bicarbonate	2 mM glutamine 1 mM sodium pyruvate 10 mM glucose pH adjusted to 7.4 with NaOH
Plating medium	DMEM/F-12, GlutaMAX™ Supplement	10% (v/v) FCS + 1.5 mM sodium pyruvate (final conc. 2 mM) 0.1 µM porcine insulin 1 µM Dexamethasone 2x Antibiotic-Antimycotic mix
Secretome medium	DMEM/F-12, HEPES, no phenol red	0.2% (v/v) BSA Fraction V + 1.5 mM sodium pyruvate (final conc. 2 mM) 2x Antibiotic-Antimycotic mix
Serum-free medium	DMEM/F-12, GlutaMAX™ Supplement	0.2% (v/v) BSA Fraction V + 1.5 mM sodium pyruvate (final conc. 2 mM) 2x Antibiotic-Antimycotic mix

3.1.6 Materials

3.1.6.1 Material and disposables

Standard laboratory material and disposables were purchased from common vendors. Specific material used in this study is listed in table 3.6.

Table 3.6: Material and disposables.

Material	Vendor/ product code
Amicon Ultra-4, PLBC Ultracel-PL membrane, 3 kDa	Merck KGaA, Darmstadt, Germany/ UFC800324
Cell culture plate, sterile, CELLSTAR®, TC-treated, 48-well	Greiner Bio One International GmbH, Frickenhausen, Germany/ 677180
Cell culture plate, sterile, flat bottom, TC-treated, 12 and 24-well	VWR International GmbH, Darmstadt, Germany/ 734-2324 and 734-2325
Cell Scraper, 2-Position Blade, 16 cm and 25 cm	Sarstedt AG & Co. KG, Nümbrecht, Germany/ 83.1832 and 83.1830
ClearLine® cell strainers, 70 µm	Kisker Biotech GmbH & Co. KG, Steinfurt, Germany/ 141379C
Corning® 96 Well White Polystyrene Microplate, clear flat bottom, white polystyrene (TC-Treated), individually wrapped, sterile, lid 96 well plates white	Merck KGaA , Darmstadt, Germany / CLS3610-48EA
Electrode paper (NOVABLOT)	GE Healthcare Bio-Sciences AB, Uppsala, Sweden/ 80-1106-19
Greiner CELLSTAR® dish, diameter × H 100 mm × 20 mm, vented	Merck KGaA , Darmstadt, Germany/ P7612
Immobilon®-P Transfer Membrane (PVDF membrane, nominal pore size 0.45 µm)	Merck KgaA, Darmstadt, Germany/ IPVH00010

Table 3.6 continued.

Material	Vendor/ product code
MicroAmp™ Fast Optical 96-Well Reaction Plate with Barcode, 0.1 mL	Applied Biosystems™, Thermo Fischer Scientific Corporation, Massachusetts, USA/ 4346906
MicroAmp™ Optical Adhesive Film	Applied Biosystems™/ Thermo Fischer Scientific Corporation, Massachusetts, USA/ 4311971
Sterican® cannula G 26/ø 0,45 x 25 mm	B. Braun Melsungen AG, Melsungen Germany/ 4657683
Surgical blades, sterile	VWR International GmbH, Darmstadt, Germany/ 233-0028
Thermo Scientific™ BioLite Cell Culture Treated Dishes, Diameter 60 mm	Thermo Fischer Scientific Corporation, Massachusetts, USA/ 130181
XF^{e}96 FluxPak with PS Cell Culture Microplates	Agilent Technologies, Inc., California, USA/ 102416-100

3.1.6.2 Reaction Kits

Table 3.7: Commercially acquired reaction kits for experimental analysis.

Kit	Vendor/ product code
RNA 6000 Nano Kit & Reagents	Agilent Technologies, Inc., California, USA/ 5067-1511
Bio-Plex Pro Mouse Cytokine 23-plex Assay	Bio-Rad Laboratories GmbH, Munich, Germany/ M60009RDPD
DNeasy® Blood & Tissue Kit	QIAGEN GmbH, Hilden, Germany/ 69506
EpiTect® PCR Control DNA Set	QIAGEN GmbH, Hilden, Germany/ 59695
EpiTect® Fast DNA Bisulfite Kit	QIAGEN GmbH, Hilden, Germany/ 59824
Glucose (GO) assay kit	Merck KGaA , Darmstadt, Germany/ GAGO-20
IGFBP2 Mouse SimpleStep ELISA® Kit	Abcam plc, Cambridge, UK/ ab207615
MTase-Glo™ Methyltransferase Assay	Promega Corporation, Madison, USA/ V7601
NAD/NADH-Glo™ Assay	Promega Corporation, Madison, USA/ G9071
Pierce™ BCA Protein Assay Kit	Thermo Fischer Scientific Corporation, Massachusetts, USA/ 23225
Precellys Lysing Kit, Tissue homogenizing CKMix	Bertin GmbH, Frankfurt am Main, Germany/ P000918-LYSK0-A
Proteome Profiler Mouse Cytokine Array Kit, Panel A	R&D Systems, Ltd., Minneapolis, USA/ ARY006
PyroMark Gold Q96 Reagents (5 x 96)	QIAGEN GmbH, Hilden, Germany/ 972812
PyroMark PCR Kit	QIAGEN GmbH, Hilden, Germany/ 978703 or 978705
Quantikine® ELISA Mouse IGFBP-3	R&D Systems, Inc., Minneapolis, USA/ MGB300
Quantikine® ELISA Mouse/Rat IGF-I	R&D Systems, Inc., Minneapolis, USA/ MG100
Quantikine® ELISA Human IGFBP-2	R&D Systems, Inc., Minneapolis, USA/ DGB200
RNeasy® Mini Kit (250)	QIAGEN GmbH, Hilden, Germany/ 74106
SIRT-Glo™ Assay System	Promega Corporation, Madison, USA/ G6450

3.1.7 Equipment

Table 3.8: Laboratory Equipment.*

Device	Manufacturer
AE31 Trinocular inverted microscope	Motic Deutschland GmbH, Wetzlar, Germany
Agilent Bioanalyzer 2100	Agilent Technologies, Inc., California, USA
Beckman beta spectrometer LS 6000LL/LS 6000IC	Beckman Coulter GmbH, Krefeld, Germany
Heraeus™ Multifuge™ X3	Thermo Fischer Scientific Corporation, Massachusetts, USA
iMark Microplate Reader	Bio-Rad Laboratories, GmbH, Munich, Germany
Mini PROTEAN® Tetra Cell	Bio-Rad Laboratories GmbH, Munich, Germany
Mini Trans-Blot® Cell	Bio-Rad Laboratories GmbH, Munich, Germany
Molecular Imager® VersaDoc™ MP 4000 system	Bio-Rad Laboratories GmbH, Munich, Germany
Multiplex Immunoassay Bioplex, Bio-Plex™ Protein Array System	Bio-Rad Laboratories GmbH, Munich, Germany
Bio-Plex™ 200 System	Bio-Rad Laboratories GmbH, Munich, Germany
NanoDrop 2000 Spectrophotometer	Thermo Fischer Scientific Corporation, Massachusetts, USA
Olympus IX70-S8F2	Olympus Optical Co., Ltd.
Power Pac Basic power supply	Bio-Rad Laboratories GmbH, Munich, Germany
Precellys Evolution	Bertin GmbH, Frankfurt am Main, Germany
PyroMark Q96 ID	Qiagen GmbH, Hilden, Germany
PyroMark Q96 Vacuum Workstation	Qiagen GmbH, Hilden, Germany
Seahorse XF^{e}96 Analyzer	Agilent Technologies, Inc., California, USA/ 102416-100
Applied Biosystems StepOnePlus™ Real-Time PCR System	Thermo Fischer Scientific Corporation, Massachusetts, USA
T100™ thermal cycler	Bio-Rad Laboratories GmbH, Munich, Germany
Table centrifuge 5471 R	Eppendorf Vertrieb Deutschland GmbH, Wesseling-Berzdorf, Germany
Tecan Infinite 200 reader	Tecan Austria GmbH, Grödig, Austria
Thermomixer comfort	Eppendorf Vertrieb Deutschland GmbH, Wesseling-Berzdorf, Germany
VersaDoc MP4000 Detection System	Bio-Rad Laboratories GmbH, Munich, Germany

* Standard laboratory equipment was not listed.

3.2 Animal models

Two different transgenic mouse models with a phenotype of fatty liver were used in this study. Animals with liver-specific overexpression of human transcription factor SREBP-1c (aa 2-436) named alb-SREBP-1c mice develop a fatty liver phenotype due to constitutively active hepatic lipid synthesis and were kindly provided for this project by Dr. Birgit Knebel and Dr. Jörg Kotzka (Knebel et al. 2012). The second model, i.e. aP2-SREBP-1c, has an adipose tissue-specific overexpression of the human SREBP-1c (aa 2-436) which leads to a lipodystrophic phenotype in these mice. As a consequence, ectopic fat accumulation

occurs and results in a phenotype of fatty liver (Shimomura et al. 1998). The aP2-SREBP-1c mice were purchased at Jackson laboratory and were backcrossed to C57Bl6 genetic background by mating aP2-SREBP-1c male mice with C57Bl6 females over > 20 generations. The backcrossed animals were also kindly provided for this study by Dr. Birgit Knebel and Dr. Jörg Kotzka. The C57Bl6 mice strain used for backcross served as control group in this study as it is the genetic background of both fatty liver mouse models.

All mice were housed in groups under standard conditions with a 12/12 hours (h) light/dark cycle. All animals received water as well as standard chow, normal-caloric diet *ad libitum*. Animal experiments were performed in accordance with 'principle of laboratory animal care' (NIH publication No. 85–23, revised 1996) and the current version of the German law on the protection of animals. All animal experiments were approved by the Animal Care Committee of the University Düsseldorf (approval number Az.84-02.04.2015.A424, 2015).

Data for physiological characterization (bodyweight, liver weight and liver total fatty acids) as well as serum parameters of liver function (triglycerides, cholesterol, free fatty acids, liver transaminases (ALT and AST) and glutamate dehydrogenase (GLDH)) for the three study groups were determined on a Hitachi 912 laboratory device (Roche, Mannheim, Germany).

3.2.1 Liver transcriptome analysis

3.2.1.1 RNA isolation from liver tissue

Mouse transcriptome was analyzed using total RNA isolated from liver tissue from the three mouse phenotypes C57Bl6, alb-SREBP-1c and aP2-SREBP-1c. Mouse livers were excised from animals and snap frozen in liquid nitrogen. Hepatic tissue was lysed in 1 ml QIAzol lysis reagent (table 3.1) and combined with the Precellys® Lysing Kit (table 3.7). Homogenization of liver tissue was performed with two cycles of 15 seconds (sec) at 5800 rounds per minute (rpm) in the Precellys® Evolution tissue homogenizer (table 3.8). 200 µl chloroform were then added to each sample, mixed and incubated for 5 minutes (min) at RT followed by 15 min centrifugation at maximal relative centrifugal force (rcf). Aqueous phase was then transferred to RNA isolation column and total RNA was isolated using the RNeasy kit (table 3.7) according to the manufacturers' protocol. RNA concentration was determined with the NanoDrop System (Thermo Fisher Scientific) via OD_{260} measurement. RNA quality was further analyzed by measurement of 18s and 28s rRNA using the Agilent Bioanalyzer 2100 (Agilent Technologies).

3.2.1.2 Affymetrix analysis

The analysis of liver transcriptome was performed from the DDZ core facility 'Genomics' headed by Dr. Birgit Knebel. The isolated hepatic RNA was analyzed using Affymetrix

GeneChip™ Mouse Gene 1.0 Array (Applied Biosystems™). The raw data received from the 'Genomics' department were analyzed for differences between groups using the Transcriptome Analysis Console software version 4.0 from Thermo Fischer Scientific.

3.2.2 Isolation of mouse primary hepatocytes

Isolation of primary hepatocytes was established for control animals, as well as the fatty liver models described above by adaption of the previously described procedure published from Akie and Cooper for the isolation of mouse primary hepatocytes (Akie and Cooper 2015). The isolation of primary hepatocytes from the different animal models was performed as follows: Animals were used from 18 to 24 weeks of age and sacrificed by CO_2 asphyxiation. The animals were disinfected with 70% ethanol before the abdominal cavity was opened to expose the liver. Further, the diaphragm was carefully opened to clamp the thoracic *inferior vena cava* (IVC) and intestines were carefully laid aside to expose the abdominal IVC. Blood from the animals was removed at this point via cardiocentesis to collect EDTA plasma. Peristaltic pump for HBSS isolation buffer (table 3.4) was started at low pump rate (approx. 0.2 - 0.5 ml/min) to remove any air from the attached tubes and needle. When the system was completely filled with HBSS isolation buffer the needle was carefully inserted into the abdominal IVC and hold in place. The *portal vein* was cut immediately after insertion of the needle and then pump rate was increased to 4.5 – 5 ml/min to start open perfusion. In aP2-SREBP-1c animals, the liver was perfused at higher pump rate (6 – 6.5 ml/min) due to increased organ size. Perfusion was performed up to 5 min until no blood was left in the organ. When the liver appeared yellowish or grey the peristaltic pump was changed to switch from HBSS to collagenase medium (table 3.5) to initiate digestion of liver tissue. Collagenase concentration was adjusted to the animal model prepared: C57Bl6 and alb-SREBP-1c livers were digested using 100 U/ml collagenase IV, while aP2-SREBP-1c livers were treated with 150 U/ml. Digestion was performed at a pump rate of 4 – 4.5 ml/min for C57Bl6 and alb-SREBP-1c or 5 – 5.5 ml/min for aP2-SREBP-1c liver tissue. Digestion was completed when the liver appeared reddish and enlarged (approx. 5 - 15 min depending on animal model). Afterwards, the digested liver tissue was removed from the dead animal and transferred to petri dish, where the gall bladder was carefully removed. The organ was then covered with 5 ml isolation medium (table 3.5) and scraped using a scalpel blade until the complete tissue was dissociated into the medium. The cell suspension was filtered through cell strainer units with 70µm pore size to remove any excess tissue and rinsed with additional 5 ml isolation medium.

The resulted liver homogenate was centrifuged at 50 rcf for 5 min at 4°C. Hepatocyte pellet was washed once with 10 ml plating medium (table 3.5) followed by additional centrifugation at 50 rcf for 5 min at 4°C. Then viable cells were separated from dead cells and debris with

density gradient centrifugation using a percoll gradient. Therefore, the cells were resuspended in 10 ml plating medium combined with 28 ml easycoll working solution (table 3.4). Centrifugation was performed at 50 rcf for 10 min at 4°C with low settings for acceleration and deceleration. Then cells were washed again in 10 ml plating medium as described above. The final cell pellet was again resuspended in 2 to 10 ml plating medium depending on pellet size, and cell count was assessed with trypan blue stained cells in a Neubauer hemocytometer. Cells were seeded in plating medium on rat tail collagen I (50 µg/ml diluted in 1x PBS) coated cell culture plates at assay dependent cell densities. Cells were let sit at least 3 h at 37°C, 5% CO_2 before any assay was started.

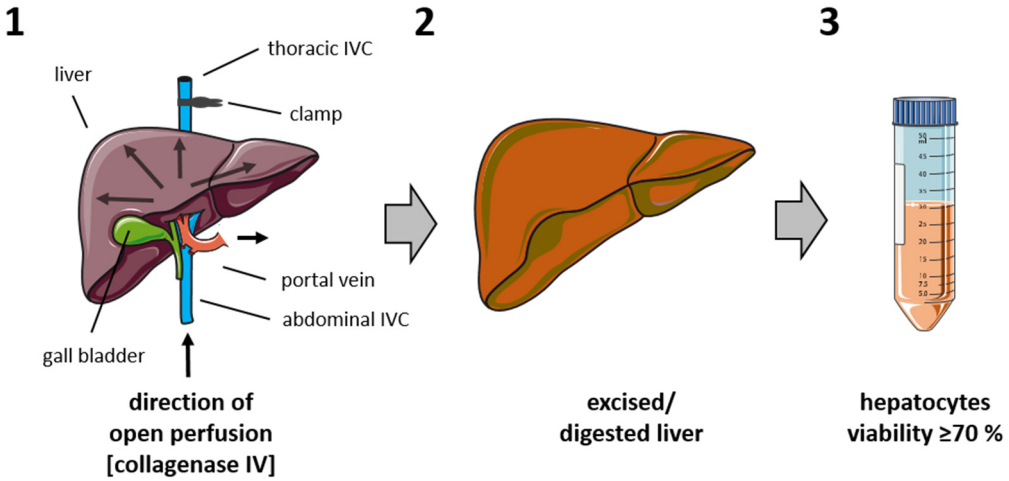

Figure 3.1: Schematic illustration of primary hepatocytes isolation procedure. 1 - Perfusion was directed from the abdominal *inferior vena cava* (IVC) through the liver and perfusate left the organ via the *portal vein*. 2 - Digested liver was excised from the mouse corpus and gall bladder was removed. 3 - Isolated hepatocytes were washed and separated from dead cells and debris prior to plating for cell culture experiments. Hepatocytes were seeded with at least 70 % viability.

3.3 Biochemical analysis of whole cell protein lysates

3.3.1 Cell treatment

Isolated hepatocytes from each phenotype were seeded with a density 250,000 cells/4 cm^2. The cells were let sit at least 3 h prior to medium change to serum-free medium (table 3.5) and incubated overnight at 37°C and 5% CO_2. At day 1 of culture cells were treated with 10 nM insulin or kept untreated for 10 min. Immediately at the end of incubation the cells were washed twice with ice cold 1x PBS and stored at -20°C until cells were lysed for total protein isolation.

3.3.2 Preparation of whole cell protein lysates

Isolation of whole cell protein was performed by adding 75 µl RIPA lysis buffer (table 3.4) to 250,000 cells. Cells were scraped from growth area and transferred to 1.5 ml reaction tubes. Further, the lysates were centrifuged at maximal rcf for 15 min to sediment any debris. The protein lysates were then transferred to fresh 1.5 ml reaction tubes and stored at -20°C.

3.3.3 Measurement of protein concentration in cell lysates

Determination of total protein concentration was performed using Pierce™ BCA Protein Assay Kit (table 3.7). First, cell lysates were diluted 1:5 with dH_2O to achieve protein concentrations within the standard curve of the assay. A serial dilution of BSA solution with known concentration was used to generate the standard curve which ranged from 2000 to 125 µg/ml BSA. For detection of protein concentration 10 µl of each standard and each diluted sample were transferred into clear 96 well microplates. BCA working reagent was prepared as instructed by the manufacturer and 200 µl were added to each well. The plates were mixed on a plate shaker and incubated 30 min at 37°C. The colorimetric reaction was measured at 562 nm using an iMark plate reader (BioRad). Standard and samples were measured in duplicates. Protein concentration was calculated using the linear equation of the BSA standard curve.

3.3.4 Western blot

Relative quantification of total protein abundance and phosphorylation of specific target proteins was assessed using western blot procedure. Separation of whole cell total protein lysates according to their molecular weight was performed with SDS-PAGE. For separation gels with 10% or 8% acrylamide/bisacrylamide resolving and 5% acrylamide/bisacrylamide stacking gel were prepared (table 3.9). Each sample was loaded on the gel with an amount of 10 µg total protein. Gels were placed in the BioRAD Mini Protean Tetra Cell system and filled with 1x electrode running buffer (table 3.4). Stacking of proteins was performed for 10 – 15 min at 90 V, followed by resolving of proteins at 130 V.

Table 3.9: Gel formulations for SDS-PAGE.

Acrylamide/ bisacrylamide concentration	Rotiphorese® Gel 30 [ml]	Stacking gel buffer [ml]	Resolving gel buffer [ml]	dH_2O [ml]
5%	1.7	2.5	-	5.7
8%	2.7	-	2.5	4.7
10%	3.3	-	2.5	4.1
10% SDS (w/v)		100 µl		
10% APS (w/v)		50 µl		
TEMED		20 µl		

In a second step the separated protein samples were transferred to PVDF membrane using the BioRad Trans Blot system. Transfer was conducted in 1x transfer buffer (table 3.4) for at least 2 h with 200 mA at 4°C. After successful transfer membrane was blocked with 5% non-fat dried milk powder dissolved in TBS-T (table 3.4) for at least 30 min at RT and gentle rocking. Incubation with first antibodies was performed overnight at 4°C and HRP-linked secondary antibody incubations for at least 90 min at RT and gentle rocking. Antibodies and their dilutions are given in table 3.10. Protein detection was performed with the VersaDoc™ 4000 MP detection system (BioRad Laboratories) using the Immobilon Western detection reagents (table 3.7). Analysis of protein was performed using the Image Lab software version 5.2 and normalization of protein abundance was calculated against GAPDH and in case of phosphorylated target proteins further normalized to the specific total protein amount.

Table 3.10: Antibodies used in western blot experiments for analysis of mouse primary hepatocyte protein lysates.

Target	Phosphorylation site	Size [kDa]	Species	Vendor/ product code
Akt	-	60	rabbit	Cell Signaling Technology, Inc./ #9272
GAPDH	-	37	rabbit	Cell Signaling Technology, Inc./ #2118
GSK3β	-	46	rabbit	Cell Signaling Technology, Inc./ #9315
IGFBP2	-	36	mouse	Santa Cruz Biotechnology, Inc./ sc-515134
Insulin receptor β	-	90	rabbit	Santa Cruz Biotechnology, Inc./ sc-711
IRS-1	-	160-185	rabbit	Merck KGaA/ #06-248
pAkt	Ser473	60	rabbit	Cell Signaling Technology, Inc./ #9271
pAkt	Thr308	60	rabbit	Cell Signaling Technology, Inc./ #9275
pGSK3β	Ser9	46	rabbit	Cell Signaling Technology, Inc./ #9323
anti-rabbit, HRP-linked	-	-	goat	Cell Signaling Technology, Inc./ #7074
anti-mouse, HRP-linked	-	-	horse	Cell Signaling Technology, Inc./ #7076

3.4 Gene expression analysis

3.4.1 Cell culture

Isolation of primary hepatocytes from each phenotype was performed as described in section 3.2.2. Cells were seeded at a density of 250,000 cells per 4 cm^2 growth area. After cells were let sit for at least 3 h plating medium was changed to serum-free medium (table 3.5) to serum starve the cells overnight. The next day, cells were washed twice with ice cold

1x PBS, which was completely removed and the cells were then stored at -20°C until isolation of total RNA.

3.4.2 Isolation of total RNA

The isolation of total RNA from mouse primary hepatocytes was performed using the RNeasy Kit (table 3.7) according to the protocol provided by the manufacturer: In brief, cell lysis was performed using 300 µl RLT lysis buffer to lyse 250,000 cells. Cells were scraped from cell culture plate and the resulting cell lysates were transferred to 1.5 ml reaction tube. One volume of 70% ethanol was added to the cell lysate and mixed gently by pipetting, prior to transfer to RNA isolation column. After centrifugation the flow through was discarded and the column was washed several times according to protocol. Finally, RNA was eluted in 30 µl nuclease-free water. The concentration of total RNA in each sample was measured with the NanoDrop System (Thermo Fisher Scientific Inc.) via OD_{260} measurement. RNA quality was analyzed with the Agilent Bioanalyzer 2100 (Agilent Technologies) by measurement of 18s and 28s rRNA.

3.4.3 Reverse transcription

For RNA expression analysis 1 µg total RNA per sample was transcribed into cDNA. The initial step of reverse transcription was the incubation of RNA with 0.25 µg Random Primers (table 3.1) at 60°C for 10 min to denature RNA secondary structure, followed by cool down on ice for at least one min to let Random Primers anneal. After short spin the samples were pre-heated to 42°C, as well as a cDNA mastermix composed of 1x first strand buffer, 0.5 mM dNTP nucleotide mix and 200 U M-MLV Reverse Transcriptase (table 3.1) per sample. After at least 2 min at 42°C the mastermix was added to the samples to perform cDNA synthesis for 90 min at 42°C. The final volume of one cDNA synthesis reaction was 25 µl.

3.4.4 Real-time PCR

In this study, the analysis of relative gene expression was performed using TaqMan Assays (Thermo Fisher Scientific Inc.) in real-time PCR experiments. For analysis 1.7 µl of each cDNA sample was added to a mastermix including 1x qPCR MasterMix Plus w/o UNG (table 3.1) and 1x TaqMan assay for the gene of interest (table 3.11). All samples were measured in triplicates. Real-time PCR was performed using a StepOnePlus device (Life technologies). The real-time PCR program started with an initial activation of the hotstart enzyme HotGoldStar for 10 min at 95°C and 40 consecutive cycles of 15 sec at 95°C to separate double strands followed by 60 sec at 60°C for primer and probe binding and elongation of amplicon by Taq polymerase. Data were calculated as exponential function of

the determined Ct values (eCt) and were normalized by dividing the target gene eCt by 18s eCt as previously described by Fu et al. 2005.

Table 3.11: TaqMan assays for analysis of relative gene expression.

Target gene	TaqMan® gene expression assay ID
Igf1	Mm00439560
Igfbp2	Mm00492632
Igfbp3	Mm01187817
CHOP	Mm01135937
BiP	Mm00517691
18S	4310893E

3.5 Histological staining of lipid droplets

3.5.1 Cell treatment

Cells were isolated from all three mouse phenotypes as described above (section 3.2.2) and seeded at 250,000 cells/4 cm^2 or 400,000 cells/10 cm^2. Cells were kept in plating medium until day one of culture. Cells were washed at least twice with warm 1x PBS until dead cells and debris were washed out. Thereafter primary hepatocytes were fixed in culture plates using fixation solution (table 3.4) and gently rocked for at least 10 min at RT. Fixed cells were stored at 4°C in fixation solution until staining.

3.5.2 Oil-red-O staining

Prior to staining, fixation solution was removed and cells were washed once with 60% isopropanol. The cells were dried completely under a fume hood before proceeding. Dried cultures were stained with 500 µl (4 cm^2) or 800 µl (10 cm^2) Oil-red-O working solution (table 3.4) and gently shook at RT for 10 min. Oil-red-O working solution was completely removed from the cells followed by at least 4 wash steps under running dH_2O. Cells were covered with dH_2O for documentation using an Olympus IX70-S8F2 microscope (table 3.8).

3.6 Secretome anaylsis

3.6.1 Cell treatment

Isolated primary hepatocytes from C57Bl6, alb-SREBP-1c and aP2-SREBP-1c mice were seeded in 20 or 60 cm^2 cell culture dishes at a density of 500,000 to 750,000 cells per cm^2 and let sit for at least 3 h after seeding. Medium was removed from culture and cells were washed twice with pre-warmed HBSS (table 3.4) prior to the addition of secretome medium (table 3.5) to the cultures. Cells were incubated for 24 h at 37°C and 5% CO_2. At the end of incubation the supernatant was collected and frozen at -20°C until further processing. The cells were washed twice with 1x PBS, scraped from growth area and transferred to 1.5 ml

reaction tubes. Cells were pelleted by short spin using a mini-centrifuge and remaining 1x PBS was removed by pipetting. Cell pellets were dry frozen at -20 °C until further use.

3.6.2 Supernatant preparation

Cell culture supernatants of primary hepatocyte cultures were processed to concentrate the proteins released from the cells to analyze differences in fatty liver hepatocyte secretome. The supernatants were thawed on ice and 10 ml of each sample was subjected to ultracentrifugation at 26,000 rcf for 45 min at 4°C to remove any particles and debris. Supernatant was concentrated using Amicon Ultra-4 columns (table 3.6) with a nominal molecular weight limit of 3 kDa. Concentration of each sample was performed with consecutive centrifugation of 10 ml culture supernatant at 4000 rpm at 4°C until sample volume was narrowed down to approximately 100 µl per sample. Determination of protein concentration was conducted by OD_{280} measurement using the NanoDrop System (Thermo Fisher Scientific Inc.).

3.6.3 Quality control of concentrated hepatocyte supernatants

The quality of concentrated proteins from hepatocyte culture supernatants was tested by separation of proteins according to their molecular weight. Samples were loaded to AnykD™ TGX™ precast midi protein gels (table 3.6) where 5 µg protein per sample was separated via electrophoresis. Band patterns of separated samples were visually examined for protein degradation.

3.6.4 Analysis of hepatocyte secretome

Concentrated culture supernatants were analyzed for differences in protein composition by the DDZ core facility ‘Proteome Analysis’ headed by Dr. Stefan Lehr. 10 µg of each sample was provided to Dr. Sonja Hartwig and Ulrike Kettel for sample preparation and mass spectrometry. Analysis of raw data received from the ‘Proteome Analysis’ department was performed with Proteome Discoverer version 2.2 (Thermo Fisher Scientific Inc.) and Spectronaut™ Pulsar X version 11.0.15 (Biognosys).

3.7 Cell culture based functional assays

3.7.1 Analysis of lipid metabolism

3.7.1.1 Cell treatment

Isolated mouse primary hepatocytes from each phenotype were seeded at day of isolation in 24-well cell culture plates (2 cm^2 growth area per well) with 90,000 cells/well (DNL) or

100,000 cells/well (FAU) or 48-well cell culture plates (growth area per well approx. 1 cm^2) with 30,000 cells/well (FAO). Serum-free medium (table 3.5) was supplemented with 10 nM recombinant IGF-I, 10 nM recombinant IGFBP2 or a combination of IGF-I and IGFBP2 proteins (table 3.3) each 10 nM. Supplemented media were pre-incubated 30 min at 37°C and 5% CO_2. For analysis of DNL an additional condition containing 100 nM Insulin and for FAO assay a condition of 40 µM etomoxir was added. After an at least 3 h rest of isolated hepatocytes cells were washed once with warm 1x PBS and medium was changed to serum-free medium without supplements or supplemented as described above. Cells were incubated for assay dependent periods before experiments were started.

3.7.1.2 *De novo* lipogenesis (DNL) assay

Primary mouse hepatocytes were analyzed for their ability to synthesize fatty acids using a method described by Akie and Cooper (2015) which quantifies DNL using radiolabeled substrate. The procedure from Akie and Cooper was adjusted as follows: After overnight incubation of the cells with or without recombinant proteins or insulin culture medium was supplemented with 10 µM cold acetate and 0.5 µCi ^{14}C-acetate per well. After an incubation time of 2 h the cells were washed once with 1x PBS followed by cell lysis with 120 µl/well 0.1 N HCl. Lipid extraction was conducted using 100 µl lysate. In a first step 500 µl of chloroform:methanol 2:1 (v/v) was added to the lysate thoroughly mixed by vortex and incubated 5 min at RT. Next, 250 µl of dH_2O were added to the homogenate which was again vortexed followed by a 5 min incubation at RT. Centrifugation of the homogenate was performed at 2,500 rcf for 10 min at RT to separate phases. The lower organic phase including cellular lipids was then removed and transferred to scintillation fluid to measure ^{14}C activity using the Beckman beta spectrometer LS 6000LL (Beckman Coulter).

3.7.1.3 Fatty acid uptake (FAU) assay

The ability of primary hepatocytes from different fatty liver phenotypes to take up fatty acids was measured providing radiolabeled ^{3}H-palmitate in culture medium for defined incubation time followed by quantification of ^{3}H activity in cell lysates. After overnight incubation with or without recombinant proteins culture medium was changed to serum-free medium supplemented with 1% BSA and further incubated for 2 h at 37°C and 5% CO_2. Prior to uptake assay cells were washed three times with KRH buffer (table 3.4) containing 0.1% BSA. Subsequently 500 µl KRH buffer containing 40 µM BSA was added per well and uptake assay was started with the addition of 500 µl FAU transport buffer (table 3.4). The uptake was stopped after 0, 5 and 15 min of incubation with three wash steps using KRH buffer supplemented with 0.1% BSA. Then, cells were lysed in 120 µl 0.1 N HCl per well. Cells were scraped from growth area and 80 µl of each lysate was added to scintillation

fluid to measure ^{3}H activity in the Beckman beta spectrometer LS 6000LL (Beckman Coulter).

3.7.1.4 Fatty acid β-oxidation (FAO) assay

For the analysis of fatty acid β-oxidation mouse primary hepatocytes were seeded only in every other row of the 48-well cell culture plate as described above (section 3.7.1.1). After 20 h of incubation with the respective conditions described in section 3.7.1.1 the assay was started. The wells of the culture plate where no cells were seeded were loaded with filter papers with a defined size of 4 cm^2. Filter papers were soaked with 50 µl 1 N NaOH and each well with cells was supplemented with 25 µl FAO assay medium (table 3.5) including ^{14}C-palmitate as substrate for fatty acid β-oxidation. The whole plates were placed in an oxidation chamber and further incubated for 4 h at 37°C and 5% CO_2. At the end of incubation one volume 1 M HCl was added to each well including hepatocytes to release $^{14}CO_2$. The oxidation chamber connects every well containing hepatocytes with an adjacent well which allowed the released $^{14}CO_2$ to be trapped in NaOH soaked filter papers. The reaction is further incubated at 37 °C at least overnight. Finally, filter papers with captured $^{14}CO_2$ were transferred to vials containing scintillation fluid. Prior to counting radioactivity with the Beckman beta spectrometer LS 6000LL (Beckman Coulter) the vials were pre-incubated in scintillation fluid for a minimum of 30 min to minimize background noise.

3.7.2 Analysis of glucose metabolism

3.7.2.1 Glucose production assay

3.7.2.1.1 Cell treatment

Cells were seeded at a density of 250,000 cells/4 cm^2 and after an at least 3 h rest the medium was changed to serum-free medium (table 3.5) for overnight serum starvation of the cells. The next day cells were washed twice with pre-warmed glucose production medium (table 3.5) which was also added to cells afterwards. Cells kept untreated were used as control condition, 10 nM porcine insulin was used to suppress glucose production and was added to the cells at assay start with a total incubation time of 5 h. After 1 h, 2 mM pyruvate and 2 mM lactate were added to stimulate glucose production for 4 h. At the end of the incubation period all conditions were stopped simultaneously and supernatant was collected. The supernatant was centrifuged at maximal rcf for 20 min at 4°C to remove any particles and debris.

3.7.2.1.2 Determination of glucose concentration

Glucose concentration in culture supernatant was measured using the Glucose Assay Kit (table 3.7) according to the manufacturers' manual. Volumes were down-scaled to measure the colorimetric reaction in 96-well plates. In brief, 100 µl of each blank (glucose production medium), sample or standard were mixed with 200 µl assay reagent (kit component). The reaction took place at 37°C for 30 min. Directly at the end of incubation the reaction was stopped with the addition of 200 µl 12 N H_2SO_4 to each sample. After the samples were carefully mixed all samples were measured in quadruplicates by pipetting 100 µl/well in a clear 96-well plate and absorbance was measured at 540 nm against blank reaction. Glucose concentration was quantified from glucose standard curve which ranged from 10 to 100 µg/ml glucose.

3.7.2.2 Glycogen synthesis assay

Glycogen synthesis was measured in mouse primary hepatocytes from all phenotypes cultured in the presence of radiolabeled ^{14}C (U)-glucose as substrate for glycogen synthesis. Cells were seeded at 250,000 cells/4 cm^2 and were let sit for at least 3 h after isolation (section 3.2.2). Medium was changed to serum-free medium and cultured overnight. Culture medium was then changed to glycogen assay glucose starvation medium (table 3.5) and incubated for 90 min at 37°C and 5% CO_2. The assay was started with an additional medium change to serum-free medium (table 3.5) containing 2 µCi/ml ^{14}C(U)-glucose with or without 100 nM porcine insulin and further incubation for 3 h at 37°C and 5% CO_2. At the end of incubation time the cells were washed twice with ice cold PBS and each well was incubated with 400 µl 1 M KOH for 5 min at RT followed by an overnight freeze at -20°C to lyse the cells. For precipitation of synthesized glycogen 180 µl of thawed cell lysate was transferred to 1.5 ml reaction tube and kept on ice. 57 µl 60% KOH (w/v) and 30 µl of glycogen (120 µg/ml) were added to lysate and incubated at 80°C for 20 min. The samples were cooled down on ice and 1 ml ice cold 100% ethanol was added to each sample to precipitate glycogen followed by centrifugation at 10,000 rpm for 20 min at 4°C. Glycogen pellet was washed once with 70% ethanol followed by a second centrifugation with same setting. Supernatant was removed and glycogen pellet was air-dried under a fume hood. Each Pellet was dissolved in 500 µl dH2O and 300 µl of each sample was transferred into scintillation fluid for counting radioactivity in the Beckman beta spectrometer LS 6000LL (Beckman Coulter).

3.7.2.3 Glycolysis rate assay

3.7.2.3.1 Glycolysis stress test

To analyze the rate of glycolysis primary hepatocytes from all phenotypes were seeded at a density of 10,000 cells/well in specific Seahorse 96-well culture plates coated with 50µg/ml rat tail I collagen diluted in 0.02 M acetic acid. Cells were let sit for at least 3 h. After one wash with warm 1x PBS (table 3.4) medium was changed to serum-free medium (table 3.5) and cells were serum starved overnight. At day of the assay, cells were washed twice with 200 µl glycolysis stress assay medium (table 3.5) per well and 180 µl of this medium was added to the cells for assay procedure. The cells were incubated at 37°C in a non-CO_2 incubator for 45 to 60 min. The plate was then loaded to the Seahorse XF^{e}96 Analyzer and the assay started with 3 cycles of 3 min mix and 3 min measure to assess basal extracellular acidification rate (ECAR). Then, glucose was injected into each well to produce a final concentration of 25 mM glucose in the medium. Subsequently, acidification of the extracellular medium was measured for 4 cycles of 3 min mix and 3 min measure. At the end of the assay medium was removed from the wells and 25 µl seahorse lysis buffer (table 3.4) was added per well. The plate was stored at -20°C until further processing.

3.7.2.3.2 Normalization of glycolysis stress test

The data obtained by the glycolysis stress test with the Seahorse XF^{e}96 Analyzer were normalized to total protein amount for each well. Isolation of total protein was performed using Seahorse lysis buffer (table 3.4) which was added to each well directly after the end of measurements as described above. Cells were lysed by freezing the plate for at least 1 h followed by thawing at RT and gentle rotation (600 rpm) for a minimum of 20 min. At least 4 freeze – thaw cycles were performed and progress of cell lysis was controlled visually under the microscope. Cell lysates were then subjected to determination of protein concentration using the Pierce™ BCA Protein Assay Kit (table 3.7). Lysates were applied undiluted to BCA assay and measured in duplicates as described in section 3.3.3. The detected glycolysis stress test measures were then normalized by the division of ECAR values with the total protein amount of each well.

3.7.2.3.3 Calculations

Table 3.12: Calculations of parameters identified with glycolysis stress test.

Parameter	Calculation
Non-glycolytic acidification	normalized last rate ECAR measurement before the injection of glucose
Rate of glycolysis	non-glycolytic acidification - normalized maximum rate ECAR measurement after glucose injection

3.7.3 Analysis of mitochondrial function

3.7.3.1 Mito stress test

Isolated mouse primary hepatocytes from all three phenotypes were seeded with 10,000 cells per well in a specific Seahorse 96-well culture plate coated with 50 µg/ml rat tail I collagen diluted in 0.02 M acetic acid. At least 3 h after seeding, medium was changed to serum-free medium after one wash with warm 1x PBS. Serum starvation of the cells was performed overnight. The assay was started with two washes using 200 µl mito stress assay medium (table 3.5) per well followed by the addition of 180 µl of this medium to each well. Cells were let sit 45 to 60 min at 37°C in a non-CO_2 incubator then loaded to the Seahorse XF^e96 Analyzer. The assay program was set as follows: Basal oxygen consumption rate (OCR) was measured for 3 cycles of 3 min mix followed by 3 min measure, for all other conditions OCR was measured for 4 cycles of 3 min mix followed by 3 min measure after each injection. First injection was oligomycin (final well concentration 1 µM) followed by injection of carbonyl cyanide 4-(trifluoromethoxy)phenylhydrazone (FCCP, final well concentration 0.5 µM) and a mixture of rotenone and antimycin A (final well concentration 0.5 µM each). After the assay run medium was discarded and cells were lysed with 25 µl seahorse lysis buffer (table 3.4) per well. Total protein amount was determined as described in section 3.7.2.3.2.

3.7.3.2 Normalization of mito stress test

Normalization of mito stress test was done dividing the measured OCR values by the total protein amount for each single well. Determination of total protein amount was performed as described in section 3.7.2.3.2.

3.7.3.3 Calculations

Table 3.13: Calculations for parameters of mitochondrial function analyzed with the mito stress test.

Parameter	Calculation
Non-mitochondrial respiration	minimum OCR after rotenone/antimycin A injection
Basal respiration	(last OCR before first injection) – (non-mitochondrial respiration)
Maximal respiration	(maximum OCR after FCCP injection) – (non-mitochondrial respiration)
Spare respiratory capacity	(maximal respiration) – (basal respiration)
ATP production	(last OCR before oliomycin injection) – (minimum OCR after oligomycin injection)
Proton leak	(minimum OCR after oligomycin injection) – (non-mitochondrial respiration)
Coupling efficiency (%)	(ATP production)/(basal respiration) * 100

3.7.4 Enzyme activity assays

3.7.4.1 Sample preparation

Analysis of enzyme activity was performed in whole cell lysates from primary hepatocytes which were cultured 24 h under serum-free conditions. Cells were pelleted and dry frozen at the end of incubation (see section 3.6.1). Depending on pellet size 250 – 500 µl NP-40 buffer (table 3.4) was added to each pellet and vortexed to lyse the cells. Homogenate was centrifuged at maximal rcf for 20 min at 4°C to remove any particles and debris. Protein lysates were then transferred to fresh tubes and protein concentration was determined using the BCA assay as described in section 3.3.3.

3.7.4.2 Bioluminescence-based assays

3.7.4.2.1 Sirtuins activity assay

The activity of NAD^+-dependent histone deacetylase class III enzymes, also known as sirtuins (SIRTs), was analyzed in whole cell protein lysates from isolated primary hepatocytes. Analysis was performed with the SIRT-Glo™ assay kit from Promega. The assay was performed using 5 µg total protein of each sample prepared in section 3.7.4.1 according to the kit instructions. Luminescence signals were measured using the Tecan Infinite 200 reader.

3.7.4.2.2 Methyltransferase assay

The MTase-Glo™ Methyltransferase assay from Promega was used to analyze the activity of methyltransferases present in whole cell lysates from primary hepatocytes. Protein samples processed as described in section 3.7.4.1 were used with 1 µg protein for each reaction and assayed according to the manufacturers' protocol. Luminescence was measured using the Tecan Infinite 200 reader.

3.8 Biochemical analysis of mouse EDTA plasma and cell culture supernatants

3.8.1 Collection of EDTA plasma

Blood was removed from C57Bl6, alb-SREBP-1c and aP2-SREBP-1c mice via cardiocentesis during isolation of primary hepatocytes as described in section 3.2.2. Whole blood was removed using needles, syringes and tubes which were rinsed with 0.01 M EDTA to prevent coagulation. Samples were inverted several times and centrifuged at 2,000 rcf

for 10 min at 4°C. Plasma was then removed and transferred to fresh tubes for further use. Samples were stored at -80°C.

3.8.2 Collection of primary hepatocyte culture supernatants

After isolation procedure (section 3.2.2) cells were seeded with 250,000 cells on culture plates with 4 cm^2 growth area. After cells were let sit for at least 3 h culture was washed once with pre-warmed PBS and serum-free medium (table 3.5) was added. Serum-starvation was performed overnight prior to collection of culture supernatant. The collected supernatant was centrifuged at maximum rcf for 20 min at 4°C to remove any particles and cell debris. The supernatant collected with this procedure was subjected to enzyme linked immunosorbent assays (ELISAs, section 3.8.3) and 23-plex cytokine analysis (section 3.8.4).

3.8.3 Enzyme-linked immunosorbent assays (ELISAs)

3.8.3.1 Mouse Igfbp2

The analysis of Igfbp2 in mouse serum and mouse primary hepatocyte culture supernatant was performed using the IGFBP2 Mouse SimpleStep ELISA® Kit from Abcam (table 3.7). EDTA-plasma from the different phenotypes investigated in this study was diluted 1:800 and cell culture supernatants were diluted 1:250 in the provided sample diluent. The ELISA assay was performed according to the manufacturers' instructions. This kit recognizes native and recombinant mouse Igfbp2 and shows neither cross-reactivity nor interference with mouse Igf-I, Igf-II, Igfbp6 and human IGFBP2. The manufacturer states the mean intra-assay coefficient of variation (CV) as 4.3% and the mean inter-assay CV as 4.9% for this assay. The minimal detectable dose of mouse Igfbp2 for this assay is 103.6 pg/ml.

3.8.3.2 Mouse Igfbp3

Mouse Igfbp3 was detected in mouse EDTA plasma and cell culture supernatant using the Mouse IGFBP-3 Quantikine® ELISA Kit from R&D Systems, Ltd (table 3.7). The assay was performed as prescribed in the manufacturers' protocol. Plasma samples were diluted 1:300 and cell culture supernatants were used without dilution. The provided mouse IGFBP-3 control sample was assayed as demanded and calculated concentration was within the given range of concentration verifying assay procedure. The assay recognizes natural and recombinant mouse Igfbp3 at full length or fragmented as well as Igfbp3 complexed with IGF-I, IGF-II, IGF-I/ALS and IGF-II/ALS. The manufacturer states that no significant cross-reactivity was observed for tested components of the IGF-system as well as human IGFBP3. The minimal detectable dose of mouse Igfbp3 is 7.95 pg/ml. Intra-assay CV

ranged from 4.0 to 5.6% and inter-assay CV ranged from 5.9 to 8.3% tested by the manufacturer.

3.8.3.3 Mouse Igf-I

The Mouse/Rat IGF-I Quantikine® ELISA Kit from R&D Systems, Ltd (table 3.7) was used to detect mouse Igf-I in EDTA plasma and cell culture supernatant from the animal models investigated in this study. Plasma samples were used at 500-fold dilution and cell culture supernatants were used at 10-fold dilution. The assay procedure was performed according to the manufacturers' manual. An IGF-I control sample was provided with the kit and the measured concentration met the range given by the manufacturer. Sensitivity of the assay is described as a minimal detectable dose of mouse/rat Igf-I with 3.5 pg/ml. The used kit is able to detect natural and recombinant mouse and rat Igf-I and shows no interference with several components of the mouse IGF-system as well as human IGF-I. Intra-assay CV ranged from 3.3 to 5.6% and inter-assay CV ranged from 4.3 to 9.1% tested by the manufacturer.

3.8.4 Plasma cytokine array

Mouse EDTA plasma was analyzed to identify differences in cytokine composition between the fatty liver phenotype investigated in this study. The Proteome Profiler Mouse Cytokine Array Kit, Panel A from R&D Systems was used for analysis. Each serum sample was analyzed on 4 membranes where cytokine antibodies were spotted in duplicates to analyze 40 different cytokines. Six animals per group were analyzed according to manufacturers' protocol. Chemiluminescent reaction was detected using the VersaDoc 4000 MP detection system (BioRad Laboratories) and quantified with Image Lab software.

3.8.5 Bio-Plex assay

Cell culture supernatants were investigated for differences in cytokine composition using the Bio-Plex Pro Mouse Cytokine 23-plex assay from Bio-Rad Laboratories. Cell culture supernatants were processed according to kit protocol with the use of 50 µl cell culture supernatant from each sample. Serum-free medium was used as reference sample. Fluorescence was measured using the Bio-Plex™ 200 System (table 3.8).

3.9 Treatment of primary hepatocytes with free fatty acids

3.9.1 Coupling of free fatty acids to BSA

Free fatty acids (FFAs) were conjugated to fatty acid-free BSA for use in cell culture experiments. Conjugation to BSA provides susceptibility of the specific FFA for the cells as

FFA are poorly soluble in aqueous media and have detergent-like properties. Coupling of palmitate or oleate to BSA was performed as follows: In a water bath 25 mM sodium palmitate or 20 mM oleate were dissolved in 0.1 M NaOH and warmed to 70°C until fatty acids were completely dissolved. In parallel DMEM, 1 g/l glucose with 10% fatty acid-free BSA (w/v) was prepared and warmed to 55°C in a second water bath. When all solutions were warmed to the specific temperature 25 mM palmitate or 20 mM oleate solution were added dropwise to DMEM, 1 g/l glucose with 10% BSA with a pre-heated pipet tip and gentle shaking of the medium. Conjugated fatty acids had a final concentration of 3.5 M palmitate or 5 mM oleate. The solutions were aliquoted and stored at -20°C until further use. Prior to use in cell culture experiments conjugated fatty acids were heated to 55°C until medium appeared clear and were then cooled down to 37°C.

3.9.2 Cell treatment

Isolated C57Bl6 mouse primary hepatocytes were seeded on culture plates with 4 cm^2 growth area per well at a density of 250,000 cells per well. After cells were let sit for at least 3 h medium was changed to serum-free medium (table 3.5) supplemented with 500 µM conjugated palmitate-BSA, oleate-BSA or BSA alone. Cells were incubated for 24 or 48 h. At the end of incubation period, culture supernatants were collected. Supernatant was centrifuged at maximal rcf for 20 min at 4°C to pellet any particles and debris. Supernatant was then transferred to fresh reaction tube and stored at -20°C. Supernatant was analyzed for Igfbp2, Igfbp3 and Igf-I content using enzyme linked immunosorbent assays (ELISAs) as described in section 3.8.3. Cells were washed twice with ice cold 1x PBS and stored at -20°C until RNA isolation and gene expression analysis was performed as described in section 3.4.

3.10 DNA methylation analysis

3.10.1 Sample preparation

Analysis of Igfbp2 DNA methylation was performed using DNA prepared from isolated primary hepatocytes from the different phenotypes analyzed in this study. Cells were isolated from liver tissue as described in section 3.2.2. The cells were not cultured prior to methylation analysis, cells were sampled directly after isolation from tissue to avoid changes of methylation pattern during culture. After cell count 500,000 viable hepatocytes were transferred into 1.5 ml reaction tubes and pelleted by short spin. Supernatant was removed and cell pellets were frozen dry at -20°C until total DNA was isolated.

3.10.2 DNA isolation

Isolation of total DNA from isolated primary hepatocytes was performed using the DNeasy® Blood & Tissue Kit from Qiagen (table 3.7). Isolation procedure was carried out according to the manufacturers' protocol. In brief, cell pellets were resuspended in 200 µl PBS and 20 µl proteinase K prior to the addition of 200 µl buffer AL to each sample. Samples were incubated for 20 min at 56°C. Then, 200 µl Ethanol (100%) was added to each sample, vortexed and loaded to DNeasy Mini spin columns. Washing of loaded DNA was performed as described in the provided protocol. DNA was eluted in 200 µl 10 mM Tris/HCl, pH 7.8 and DNA concentration was measured using the NanoDrop 2000 Spectrophotometer (Thermo Fisher Scientific Inc.) via OD_{260} measurement. Quality of isolated DNA was visually checked after separation by 1.5% agarose-gel electrophoresis.

3.10.3 Bisulfid conversion of isolated DNA

The EpiTect® Fast DNA Bisulfite Kit from Qiagen was used for DNA conversion of 1 µg isolated DNA from each sample. Samples were subjected to bisulfite conversion protocol provided by the manufacturer. Each sample was combined with 85 µl bisulfite solution and 35 µl DNA protect buffer and was incubated for two cycles with 5 min denaturation at 95°C and 10 min incubation at 60°C to perform DNA conversion. Further, the bisulfite converted DNA was purified using the cleanup protocol provided. For purification converted DNA samples were combined with 310 µl buffer BL and 250 µl ethanol (100%), pulse vortexed for 15 sec, and samples were then loaded to MinElute DNA spin columns. After several washing steps described in detail in the manufacturers' protocol bisulfite converted DNA was eluted from spin columns using 15 µl elution buffer. Concentration of purified DNA was measured with the NanoDrop 2000 Spectrophotometer (Thermo Fisher Scientific Inc.).

3.10.4 Pyrosequencing

3.10.4.1 Amplification of sequence to analyze

Methylation analysis was performed from Mus musculus chromosome 1 (clone RP23-38P22, complete sequence, ID: AC121498.12) position 2912. The exact sequence analyzed is given in table 3.14. Primer were designed using the PyroMark Assay Design Software (table 3.16) and are also listed in the table below.

Table 3.14: Sequences used for methylation analysis of Igfbp2 gene regulating sequence.

Sequence to analyze	YGGAATTGTT GGGGTT
Forward primer (biotinylated)	GAGTTTTTGGGAATAAAGATAAAAGAGT
Reverse primer	CCCCAAACAACATTTCTCTCT
Sequencing primer	AGATAAAAGAGTTAATAGTAAAGT

The sequence to analyze was amplified using the PyroMark PCR Kit from Qiagen (table 3.7). In addition to the bisulfite converted DNA samples from the different types of hepatocytes methylated and unmethylated control DNA was also amplified as assay controls provided in the EpiTect PCR Control DNA Set (table 3.7). In brief, 10 ng of bisulfite treated DNA from each sample and controls was combined with PyroMark PCR master mix, CoralLoad® concentrate and primers. The PCR program started with 15 min at 95°C for enzyme activation followed with 45 cycles of 30 sec denaturation at 94°C, 30 sec annealing at 56°C, 30 sec extension at 72°C and the program ended with 10 min of final extension. Quality of PCR products was visually controlled by separating 3 µl of each PCR reaction in 2% agarose-gel electrophoresis.

3.10.4.2 Methylation analysis

Analysis of DNA methylation was then performed using the PyroMark Q96 ID device from Qiagen (table 3.8). PyroMark Gold Q96 Reagents required for analysis (enzyme, substrate and nucleotides) were loaded to the device according to manufacturers' instructions. Further, the amplified bisulfite DNA samples were purified with the PyroMark Q96 Vacuum Workstation through sepharose beads which bound the biotinylated primer of the amplicons. The purified PCR products were processed according to the manufacturers' instructions before samples were mixed with reaction buffer and sequencing primer for pyrosequnecing with the PyroMark Q96 ID.

3.11 Human cohort

Obese men which had bariatric surgery including gastric banding or gastric bypass from the Obster study (Ruige et al. 2012, Bekaert et al. 2015) were included in analysis. The clinical study was validated by the Ethical Review Board of Ghent University Hospital (Clinical Registration no. NCT00740194 and B67020084018) in accordance with the Declaration of Helsinki. Patients gave written informed consent to participate in the study. Serum samples were collected after overnight fasting before (pre) and 2 years after (post) bariatric intervention. Patient characteristics were listed in table 3.15.

Table 3.15: Patients characteristics of obese men before (pre) and 2 years after (post) bariatric intervention from Obster study. Data are presented as mean ±SD. Differences between groups were analyzed using Wilcoxen test, *p*-values < 0.05 were considered as statistical significant. BMI: body mass index; HOMA-IR: homeostasis model assessment of insulin resistance; HDL: high density lipoprotein; LDL: low density lipoprotein; TG: triglycerides; gGT: gamma glutamyltransferase; AST: aspartate aminotransferase; ALT: alanine aminotransferase.

Variable	Pre	Post	*p*-value
n	15	15	
Age [years]	51,07 ± 11,76	53,33 ± 11,60	< 0.001
Body weight [kg]	142,53 ± 26,97	109,00 ± 25,70	< 0.001
BMI [kg/m^2]	44,14 ± 7,94	34,25 ± 7,95	< 0.001
Waist circumference [cm]	144,87 ± 20,30	117,20 ± 19,99	< 0.001
Fat [% body weight]	44,03 ± 9,52	35,65 ± 11,19	0.021
Glucose [mmol/l]	6,45 ± 1,63	5,45 ± 0,80	0.049
Insulin [pmol/l]	162,23 ± 87,05	86,93 ± 70,59	< 0.001
HOMA-IR	7,08 ± 4,38	3,13 ± 2,66	0.002
Adiponectin [µg/ml]	4,93 ± 2,44	10,56 ± 5,84	< 0.001
Cholesterol [mg/dl]	164,87 ± 30,39	167,93 ± 35,73	0.772
HDL [mg/dl]	42,43 ± 9,51	60,53 ± 13,94	< 0.001
LDL [mg/dl]	92,13 ± 25,91	86,73 ± 29,72	0.429
TG [mg/dl]	149,33 ± 81,60	103,87 ± 49,95	0.046
gGT [U/l]	44,67 ± 47,54	35,53 ± 33,30	0.4
AST [U/l]	41,73 ± 24,76	28,93 ± 14,75	0.03
ALT [U/l]	64,87 ± 52,15	31,47 ± 14,76	0.007

3.11.1 Determination of IGFBP2 serum concentration

IGFBP2 serum concentration was determined using the Human IGFBP-2 Quantikine® ELISA Kit from R&D Systems, Ltd (table 3.7). Serum samples from pre and post visits were assayed as described by the manufacturers' protocol. Dilution of serum was 50-fold. The ELISA was specific for human IGFBP2 and showed no cross-reactivity with other components from the IGF system as well as mouse Igfbp2 while inter-assay CV ranged from 3.6 to 5% and intra-assay CV from 4.5 to 7.6% as tested by the manufacturer.

3.11.2 Calculation of fatty liver index

The fatty liver index (FLI) was calculated as described in Bedogni et al. 2006 as predictor for the presence of fatty liver. The calculation of FLI includes body mass index (BMI) and waist circumference (WC) as well as triglyceride (TG) and gamma glutamyltransferase (gGT) serum concentration of the patient according to the following formula:

$$FLI = \frac{(e^{0.953*loge\,(TG)+0.139*BMI+0.718*loge\,(gGT)+0.053*(WC)-15.745})}{(1+e^{0.953*loge\,(TG)+0.139*BMI+0.718*loge\,(gGT)+0.053*(WC)-15.745})} * 100$$

3.12 Software

Table 3.16: Software for experimental set up and analysis of result data.

Type	Version	Provider
Bio-Plex Manager™	6.1	Bio-Rad Laboratories, Inc.
GraphPad Prism	7.04	GraphPad Software, Inc.
Image Lab™ Software	5.2	Bio-Rad Laboratories, Inc.
Ingenuity® Pathway Analysis	Summer 2018	Qiagen Bioinformatics
Microplate Manager® Software	6.1	Bio-Rad Laboratories, Inc.
NanoDrop 2000/2000c	1.6.198	Thermo Fischer Scientific Inc.
Proteome Discoverer™	2.2	Thermo Fischer Scientific Inc.
PyroMark Assay Design	2.0.1	Qiagen Bioinformatics
PyroMark Q96 ID Software	2.5	Qiagen Bioinformatics
Quantity One	4.6.7	Bio-Rad Laboratories, Inc.
Spectronaut™ Pulsar X	11.0.5	Biognosys AG
StepOne™ Software	2.3	Life Technologies Corporation
Tecan i-control	1.6.19.0	Tecan Austria GmbH
Transcriptome Analysis Console	4.0.1	Thermo Fischer Scientific Inc.
Wave	2.4.0.60	Agilent Technologies

3.13 Statistics

Analysis of data was performed using the GraphPad Prism 7 software (table 3:16) and all data were represented as mean ± standard deviation (SD) of at least 4 independent experiments per group. Statistical differences between two groups were calculated using an unpaired and two-tailed Mann-Whitney-U-test if not stated otherwise. *P*-values less than 0.05 were considered as statistically significant.

Transcriptome analysis was conducted using the Transcriptome Analysis Console 4.0.1 to identify statistical significant gene regulation in pairwise analysis of the investigated groups. Bioinformatic analysis was performed using *Ingenuity® Pathway Analysis*, release summer 2018.

Data dependent as well as independent analysis of secretome proteomics was performed using the Proteome Discoverer version 2.2 and Spectronaut™ Pulsar X software (version 11.0.5). Bioinformatic analysis was performed using *Ingenuity® Pathway Analysis*, release summer 2018.

4 Results

4.1 Characterization of mouse models with fatty liver phenotype

Investigation of fatty liver was performed using two different mouse models with overexpression of the transcriptional active N-terminal domain of human SREBP-1c, one of the master regulators of lipid metabolism. The first model, alb-SREBP-1c, expresses SREBP-1c in the liver which results in a mild hepatic steatosis (Knebel et al. 2012). This genetically initiated fatty liver model is characterized by increased liver-specific lipogenesis accompanied with hepatic insulin resistance (Jelenik et al. 2017). The second model, aP2-SREBP-1c, expresses SREBP-1c under control of the adipocyte specific aP2 promoter which results in a lipodystrophic phenotype (Shimomura et al. 1998). This model resembles a metabolically initiated fatty liver model, characterized by ectopic lipid accumulation which exhibits systemic insulin resistance (Jelenik et al. 2017). These mouse models provide insight in the pathological mechanisms underlying solely genetic or solely metabolic development of fatty liver phenotype.

4.1.1 Physiological characterization

The comparison of murine models with fatty liver phenotype to C57Bl6 control animals showed an increase in bodyweight in both fatty liver models. The bodyweight in alb-SREBP-1c mice was only moderately increased compared to C57Bl6 while a 23 to 31% higher bodyweight was measured in aP2-SREBP-1c animals compared to the control group (figure 4.1 A). Differences in bodyweight corresponded to liver weight in each group as depicted in figure 4.1 B. In male and female alb-SREBP-1c animals the mean liver weight was moderately increased or equal to C57Bl6 mice with liver weight accounting for approximately 5% of the bodyweight in both groups (figure 4.1 D). In contrast, in aP2-SREBP-1c animals the mean liver weight was significantly increased measured with 3.95 ± 0.87 g (male) or 2.49 ± 0.45 g (female) which made up for 8 or 10% of their bodyweight respectively (figure 4.1 B and D). Further total fatty acids (TFA) measured in liver tissue of the three model systems showed that lowest TFA were found in C57Bl6 animals (24.65 ± 4.01 mg (male) or 20.61 ± 2.21 mg (female) per g liver weight) which significantly increased in alb-SREBP-1c animals (75.8 ± 11.36 mg (male) and 48.34 ± 10.91 mg (female) per g liver weight) and were highest in aP2-SREBP-1c livers (196.86 ± 53.8 mg (male) or 113.25 ± 13.66 mg (female) per g liver weight, figure 4.1 C). These values corresponded with a 2-fold increase in alb-SREBP-1c and a 3-fold increase in aP2-SREBP-1c animals of average liver TFA per bodyweight compared to C57Bl6 livers (figure 4.1 E).

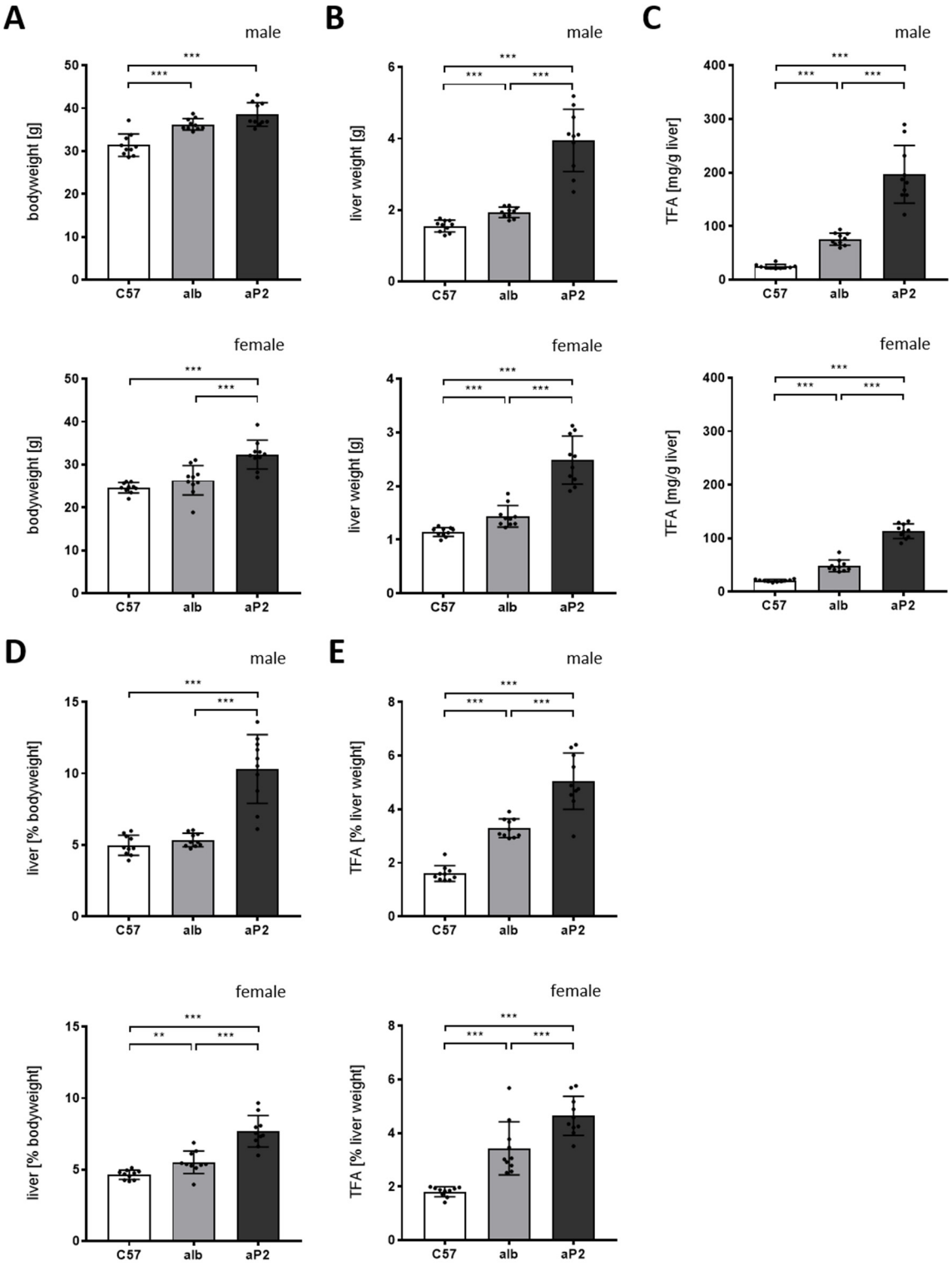

Figure 4.1: Physiological data of mouse models for the study of fatty liver. Bodyweight (A), liver weight (B) and liver total fatty acids (TFA, C) are shown for representative groups of C57Bl6 (C57), alb-SREBP-1c (alb) and aP2-SREBP-1c (aP2) mice. Male and female data were assessed separately. Liver weight and liver TFA were additionally calculated as percentage of bodyweight or liver weight (D, E). Data are represented as mean ±SD for 10 animals per group. Mann-Whitney-U test was used for analysis of statistical differences between two groups: ** $p < 0.01$, *** $p < 0.001$.

4.1.2 Serum parameters of liver function

Systemic lipid load was markedly increased in animals exhibiting the lipodystrophic phenotype reflected in 3-fold increased serum free fatty acids (FFA) compared to control animals (*p*-value < 0.001, figure 4.2 A). Also alb-SREBP-1c animals showed a significant increase in serum FFA compared to C57Bl6 (*p*-value < 0.001) but significantly lower compared to aP2-SREBP-1c. Measurement of serum parameters related to liver function like cholesterol and triglycerides as well as liver transaminases (ALT and AST) and glutamate dehydrogenase (GLDH) indicated impaired liver function in both fatty liver models. In aP2-SREBP-1c animals serum cholesterol and triglycerides were markedly increased compared to C57Bl6 control animals (figure 4.2 B and C). Independent from gender serum triglycerides were 3-fold higher in the serum of aP2-SREBP-1c animals compared to the control group ($p < 0.001$, figure 4.2 C). The alb-SREBP-1c group ranged between C57Bl6 and aP2-SREBP-1c with increased cholesterol and triglyceride levels compared to C57Bl6 but markedly lower serum concentrations as in aP2-SREBP-1c animals. Analysis of liver transaminases and glutamate dehydrogenase (GLDH) showed that compared to the C57Bl6 controls aP2-SREBP-1c animals had highest serum levels for all measured liver parameters, while alb-SREBP-1c mice showed intermediate values (figure 4.2 D, E and F). Alanine aminotransferase (ALT) was significantly increased in aP2-SREBP-1c animals compared to C57Bl6 in both genders. The circulating enzyme was 4-fold elevated in aP2-SREBP-1c animals while in alb-SREBP-1c mice ALT was approximately 1.5-fold increased (figure 4.2 D). The aspartate aminotransferase (AST) was also considerably higher in the aP2-SREBP-1c groups with 295.3 ± 90.01 U/l in male and 309.4 ± 45.72 U/l in female animals compared to 31.5 ± 10.69 U/l (male) and 103.3 ± 49.05 U/l (female) in C57Bl6 mice (figure 4.2 E). Alb-SREBP-1c serum AST was significantly lower compared to aP2-SREBP-1c but higher than C57Bl6 AST serum level ($p < 0.001$). Notably, circulating AST in females was 3-fold higher than in male littermates in C57Bl6 (male 31.5 ± 10.69 U/l vs. female 103.3 ± 49.05 U/l) as well as alb-SREBP-1c animals (male 66.6 ± 18.99 U/l vs. female 178.4 ± 44.87 U/l, figure 4.2 E), but there were no differences between genders in the aP2-group. Circulating GLDH levels again showed highest levels in aP2-SREBP-1c animals with 26.76 ± 8.58 U/l (male) and 27.36 ± 13.11 U/l (female) which was a 3- to 4-fold increase compared to C57Bl6 and approximately 2-fold higher compared to alb-SREBP-1c mice (figure 4.2 F).

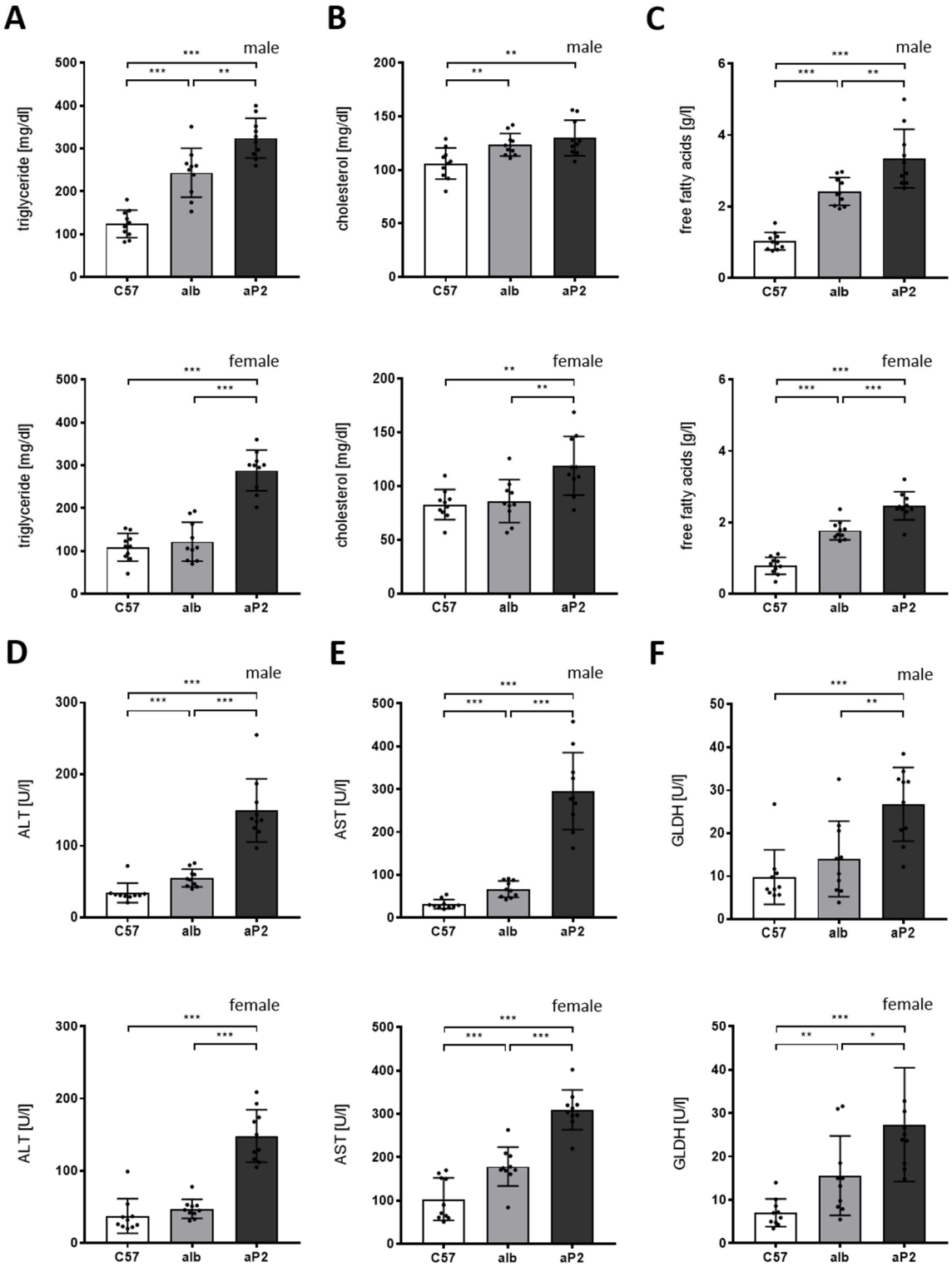

Figure 4.2: Serum parameters of liver function in mouse models for the study of fatty liver. Serum was analyzed for triglyceride (A), cholesterol (B), free fatty acid (C), liver transaminases ALT (D) and AST (E) and glutamate dehydrogenase (GLDH, F) concentration in representative groups of C57Bl6 (C57), alb-SREBP-1c (alb) and aP2-SREBP-1c (aP2) mice. Male and female data were assessed separately. Data are represented as mean ±SD for 10 animals per group. Mann-Whitney-U test was used for pairwise analysis of statistical differences between two groups: * $p < 0.05$, ** $p < 0.01$, *** $p < 0.001$.

4.2 Liver Transcriptome analysis in mouse models of fatty liver

In order to identify novel pathophysiological mechanisms involved in the fatty liver phenotype holistic liver transcriptomes were generated. Specifics of the genetic impact on the fatty liver phenotype were afterwards subtracted to determine the differences that are specific for the metabolic development of fatty liver in the aP2-SREBP-1c model. To clarify the mechanistically details in the holistic gene expression analyses metabolic verification was performed in primary hepatocytes of the animal models investigated.

4.2.1 General Transcriptome analyses

Liver tissue from C57Bl6, alb-SREBP-1c and aP2-SREBP-1c mice were subjected to transcriptome analysis to identify differential gene expression. An overview of the results from pairwise analysis was illustrated in table 4.1. The comparison of C57Bl6 to alb-SREBP-1c transcriptome revealed 306 genes differentially expressed whereby 272 of these differentially expressed genes were of unknown function. In alb-SREBP-1c 225 genes were up- and 81 genes were downregulated compared to C57Bl6. The comparisons with aP2-SREBP-1c transcriptome showed markedly higher numbers of differential gene expression in relation to C57Bl6 (3003 genes) or alb-SREBP-1c (4124 genes). Between C57Bl6 and aP2-SREBP-1c liver transcriptome 1290 genes were found to be up- and 1713 genes downregulated. Comparing both fatty liver models 1603 genes were up- and 2521 genes were downregulated in aP2-SREBP-1c liver tissue compared to alb-SREBP-1c representing the highest amount of differentially expressed genes while 23% of these regulated genes were of unknown function.

Table 4.1: General overview of differential gene expression in liver transcriptome. Amount of differentially expressed genes from pairwise analysis of C57Bl6, alb-SREBP-1c and aP2-SREBP-1c hepatic gene expression. Expressed transcripts with no known function or no annotation were listed as ‘Unknown’ and removed from further analyses.

Comparison	Regulated genes	Upregulated	Downregulated	Unknown
C57Bl6 vs. alb-SREBP-1c	306	225	81	272
C57Bl6 vs. aP2-SREBP-1c	3003	1290	1713	785
alb-SREBP-1c vs. aP2-SREBP-1c	4124	1603	2521	928

As illustrated in the Venn diagram in figure 4.3 97 genes were found differentially expressed in all three phenotypes. Analysis of C57Bl6 versus alb-SREBP-1c or aP2-SREBP-1c liver transcriptome showed an overlap of 44 genes, while 63 genes were uniquely regulated in C57Bl6 versus alb-SREBP-1c and 470 in C57Bl6 versus aP2-SREBP-1c. Highest number of regulated genes was found by analyzing alb-SREBP-1c versus aP2-SREBP-1c liver transcriptome with 1533 genes confined to the comparison of the two fatty liver models.

Further, 2392 differentially expressed genes were identified to be associated only with ectopic lipid accumulation in the liver.

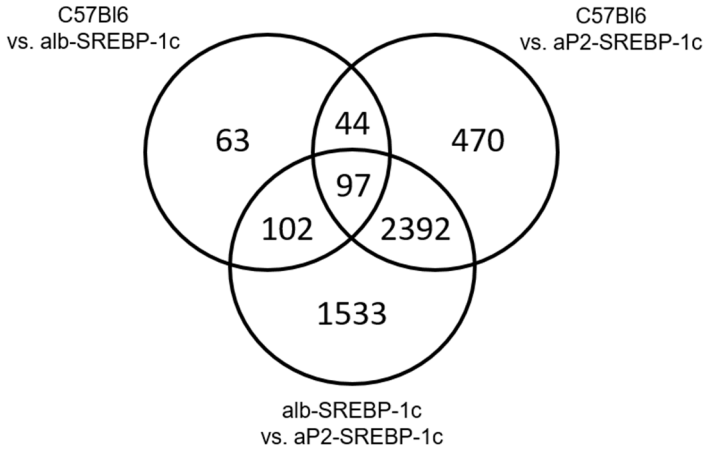

Figure 4.3: Venn analysis of liver transcriptome. Relations between C57Bl6, alb-SREBP-1c and aP2-SREBP-1c differential gene expression in liver tissue.

4.2.1.1 Genes differentially expressed in fatty liver

Analysis of transcriptome data was performed using pairwise comparison of two phenotypes at a time to assess differences in gene expression between each fatty liver model with C57Bl6 normal liver tissue and between the two different fatty liver models. In tables 4.2 to 4.4 the top 10 up- and downregulated genes were listed for each data set. In general, the analyzed data revealed that gene expression patterns between C57Bl6 and alb-SREBP-1c were less different than the comparison of C57Bl6 with aP2-SREBP-1c. C57Bl6 and alb-SREBP-1c liver tissue gene expression differed not more than 2 to 3-fold for most of the top ranking genes listed in table 4.2. The highest fold-changes were found for monooxygenase DBH-like 1 (*Moxd1*, *p*-value: 3.52 x 10^{-14}, fold-change: -7.77), lipocalin 2 (*Lcn2*, 1.92 x 10^{-10}, -5.39), serum amyloid A 1 (*Saa1*, 2.00 x 10^{-06}, -4.09) and cytochrome P450, family 4, subfamily a, polypeptide 14 (*Cyp4a14*, 7.07 x 10^{-09}, 3.91). In contrast, differential gene expression was found regulated with folds greater than 5 in the top 10 regulated hepatic genes in aP2-SREBP-1c versus control and cell death-inducing DNA fragmentation factor, alpha subunit-like effector A (*Cidea*, 1.22 x 10^{-10}, -42.05), mitochondrially encoded ATP synthase membrane subunit 6 (*Mt-atp6*, 1.69 x 10^{-08}, -35.07), hydroxy-delta-5-steroid dehydrogenase, 3 beta- and steroid delta-isomerase 4 (*Hsd3b4*, 2.61 x 10^{-11}, 7.93) and ribosomal protein L39 (*Rpl39*, 2.23 x 10^{-11}, 10.78) were identified with highest score fold-changes (table 4.3). The comparison of aP2-SREBP-1c with alb-SREBP-1c hepatic gene expression (table 4.4) revealed markedly differences in gene expression patterns between the two fatty liver models with top score fold-changes for *Mt-atp6* (6.93 x 10^{-09} -65.92), *Cidea* (3.59 x 10^{-11}, -17.97), *Hsd3b4* (1.25 x 10^{-12}, 20.84) and

Moxd1 (4.53 x 10^{-11}, 44.66). Expression of the top ranking regulated genes was also more than 5-fold different between alb-SREBP-1c and aP2-SREBP-1c.

Table 4.2: Analysis of regulated gene expression in fatty liver tissue. Top 10 up- or downregulated transcripts in the comparison of alb-SREBP-1c versus C57Bl6 hepatic gene expression. Differentially expressed genes with top score fold-changes and *p*-values are shown (cut-off values: > 1.5-fold regulation; *p*-value < 0.05, ANOVA). Gene ID as defined by Mouse Gene 1.0 Expression Array with annotation of gene ID according to IPA analyses ready molecules. FDR: false discovery rate.

Gene ID	Symbol	expression p-value	expression fold change	expression FDR (q-value)
upregulated in alb-SREBP-1c				
10362186	MOXD1	3.52E-14	-7.77	1.43E-11
10481627	LCN2	1.92E-10	-5.39	2.79E-08
10553274	SAA1	2.00E-06	-4.09	5.20E-05
10366346	PHLDA1	1.31E-08	-3.4	1.70E-05
10603208	MID1	1.56E-08	-3.09	1.90E-05
10505451	Orm1 (incl. others)	8.94E-08	-3.07	5.00E-06
10573578	WDR83OS	7.92E-10	-2.69	6.00E-06
10402428	SERPINA12	1.00E-06	-2.54	3.60E-05
10523128	Ppbp	1.29E-07	-2.52	6.20E-05
10421648	SLC25A30	2.56E-07	-2.49	1.10E-05
downregulated in alb-SREBP-1c				
10565811	RPS3	1.44E-09	2.06	1.65E-07
10512487	RMRP	1.88E-14	2.09	8.35E-12
10583312	TAF1D	1.48E-07	2.16	7.00E-06
10522368	NIPAL1	1.62E-07	2.28	8.00E-06
10465831	5730408K05Rik	1.00E-13	2.76	3.59E-11
10431697	ABCD2	2.09E-08	2.82	2.00E-06
10507163	CYP4A11	2.22E-16	2.85	1.65E-13
10551197	CYP2B6	1.87E-12	3.91	4.73E-10
10454731	CDC23	1.10E-06	4.04	2.88E-04
10515187	Cyp4a14	7.07E-09	11.68	1.10E-05

Table 4.3: Analysis of regulated gene expression in fatty liver tissue. Top 10 up- or downregulated transcripts in the comparison of aP2-SREBP-1c versus C57Bl6 hepatic gene expression. Differentially expressed genes with top score fold-changes and *p*-values are shown (cut-off values: > 1.5-fold regulation; *p*-value < 0.05, ANOVA). Gene ID as defined by Mouse Gene 1.0 Expression Array with annotation of gene ID according to IPA analyses ready molecules. FDR: false discovery rate.

Gene ID	Symbol	expression p-value	expression fold change	expression FDR (q-value)
upregulated in aP2-SREBP-1c				
10456392	CIDEA	1.22E-10	-42.05	1.16E-07
10598085	MT-ATP6	1.69E-08	-35.07	2.00E-06
10501494	AMY2B	2.25E-14	-19.04	3.15E-12
10470316	RPL7A	9.11E-09	-17.86	2.00E-06
10598087	MT-ND6	5.82E-08	-15.86	5.00E-06
10566205	Usp17la (incl. others)	1.61E-07	-9.42	1.00E-05
10413012	FUT11	6.96E-08	-9.06	1.00E-06
10523901	RPL5	1.11E-16	-8.9	3.69E-14
10544523	RNY1	5.55E-16	-8.36	1.40E-13
10497463	CPB1	1.71E-12	-7.6	1.19E-10
downregulated in aP2-SREBP-1c				
10495252	ROMO1	1.56E-11	5.21	7.11E-08
10364696	ATP5D	1.79E-10	5.3	1.48E-07

Table 4.3 continued.

Gene ID	Symbol	expression p-value	expression fold change	expression FDR (q-value)
downregulated in aP2-SREBP-1c				
10559233	MRPL23	4.09E-09	5.37	1.00E-06
10362186	MOXD1	4.00E-06	5.74	3.60E-05
10593219	NNMT	2.38E-14	6.01	3.31E-12
10445251	ADGRF1	9.57E-12	7.12	4.96E-10
10434643	PSMB3	5.02E-10	7.23	2.80E-07
10373610	OR2AP1	3.33E-16	7.93	9.27E-14
10427266	RPL39	2.23E-11	10.78	7.11E-08
10500545	Hsd3b4 (incl. others)	2.61E-11	12.56	7.11E-08

Table 4.4: Analysis of regulated gene expression in fatty liver tissue. Top 10 up- or downregulated transcripts in the comparison of alb-SREBP-1c versus aP2-SREBP-1c hepatic gene expression. Differentially expressed genes with top score fold-changes and *p*-values are shown (cut-off values: > 1.5-fold regulation; *p*-value < 0.05, ANOVA). Gene ID as defined by Mouse Gene 1.0 Expression Array with annotation of gene ID according to IPA analyses ready molecules. FDR: false discovery rate.

Gene ID	Symbol	expression p-value	expression fold change	expression FDR (q-value)
upregulated in aP2-SREBP-1c				
10598085	MT-ATP6	6.93E-09	-65.92	5.21E-07
10456392	CIDEA	3.59E-11	-41.52	1.70E-08
10598087	MT-ND6	1.44E-15	-23.68	1.60E-13
10501494	AMY2B	2.02E-14	-17.97	1.58E-12
10470316	RPL7A	4.24E-10	-17.53	8.60E-08
10515187	Cyp4a14	3.41E-11	-13.57	1.70E-08
10523901	RPL5	1.29E-12	-11.72	6.11E-09
10544523	RNY1	2.93E-09	-9.97	2.90E-07
10566205	Usp17la (incl. others)	4.06E-08	-9.53	2.00E-06
10431697	ABCD2	2.59E-07	-8.84	7.00E-06
downregulated in aP2-SREBP-1c				
10364696	ATP5D	6.10E-12	5.9	7.07E-09
10543067	ASNS	3.43E-14	6.09	2.49E-12
10445251	ADGRF1	2.63E-12	6.19	1.12E-10
10430778	PHF5A	6.08E-12	6.5	7.07E-09
10352439	SUSD4	3.25E-09	6.59	3.10E-07
10495252	ROMO1	1.42E-11	7.31	1.03E-08
10434643	PSMB3	9.64E-13	7.73	6.11E-09
10427266	RPL39	8.48E-12	13.22	8.12E-09
10500545	Hsd3b4 (incl. others)	1.25E-12	20.84	6.11E-09
10362186	MOXD1	4.53E-11	44.66	2.08E-08

4.2.1.2 Bioinformatics based annotation of differential gene expression in fatty liver

Ingenuity® Pathway Analysis (IPA) of differential gene expression revealed that in comparison of C57Bl6 with each of the fatty liver models the transcriptional regulators hepatic nuclear factor 4, alpha (HNF4A, C57Bl6 vs. alb-SREBP-1c: *p*-value 2.70 x 10^{-30}, C57Bl6 vs. aP2-SREBP-1c: *p*-value 9.90 x 10^{-39}), RPTOR independent companion of mTOR, complex 2 (RICTOR, C57Bl6 vs. alb-SREBP-1c: 3.28 x 10^{-28}, C57Bl6 vs. aP2-SREBP-1c: 6.16 x 10^{-31}) and peroxisome proliferator activated receptor alpha (PPARA,

C57Bl6 vs. alb-SREBP-1c: 3.92 x 10^{-16}, C57Bl6 vs. aP2-SREBP-1c: 2.40 x 10^{-27}) were most likely the top three key molecules causing regulated gene expression between C57Bl6 and the SREBP-1c models (table 4.5). These factors were found to be described as regulators of high numbers of molecules differentially expressed between C57Bl6 and alb-SREBP-1c or aP2-SREBP-1c (HNF4A: 555/462 molecules, RICTOR: 123/108 molecules, PPARA: 144/140 molecules). In contrast, these transcription regulators were predicted to only regulate a markedly smaller number of molecules when comparing alb-SREBP-1c with aP2-SREBP-1c hepatic gene expression (HNF4A: alb-SREBP-1c vs. aP2-SREBP-1c: 3.71 x 10^{-06}/ 49 molecules, RICTOR: alb-SREBP-1c vs. aP2-SREBP-1c: 4.83 x 10^{-06}/ 14 molecules, PPARA: alb-SREBP-1c vs. aP2-SREBP-1c: 6.08 x 10^{-13}/ 28 molecules). Further, as expected sterol regulatory binding protein 1 gene (SREBF-1, C57Bl6 vs. alb-SREBP-1c: 1.77 x 10^{-07}, C57Bl6 vs. aP2-SREBP-1c: 4.78 x 10^{-09}, alb-SREBP-1c vs. aP2-SREBP-1c: 1.15 x 10^{-05}) and SREBF-2 (C57Bl6 vs. alb-SREBP-1c: 1.39 x 10^{-10}, C57Bl6 vs. aP2-SREBP-1c: 1.71 x 10^{-09}, alb-SREBP-1c vs. aP2-SREBP-1c: 3.28 x 10^{-06}) and also the gene encoding for SREBP cleavage activating protein (SCAP, C57Bl6 vs. alb-SREBP-1c: 4.88 x 10^{-09}, C57Bl6 vs. aP2-SREBP-1c: 1.51 x 10^{-07}, alb-SREBP-1c vs. aP2-SREBP-1c: 2.41 x 10^{-07}) were found to be in the top score lists of all comparisons applied as key regulators of genes related to glucose and lipid metabolism in the liver. The SREBFs were found to most likely affect 30 to 76 genes in the comparisons of C57Bl6 with either alb-SREBP-1c or aP2-SREBP-1c. When both fatty liver models were compared 8 to 13 genes were found to be regulated annotated to SREBFs regulation. The proto-oncogenes myelocytomatosis oncogene (MYC, C57Bl6 vs. alb-SREBP-1c: 5.32 x 10^{-11}, C57Bl6 vs. aP2-SREBP-1c: 1.26 x 10^{-08}, alb-SREBP-1c vs. aP2-SREBP-1c: 9.44 x 10^{-03}) and v-myc avian myelocytomatosis viral related oncogene, neuroblastoma derived (MYCN, C57Bl6 vs. alb-SREBP-1c: 4.80 x 10^{-12}, C57Bl6 vs. aP2-SREBP-1c: 4.18 x 10^{-11}) were also found to be potential upstream regulators. Also the solute carrier family members SLC13A1 (C57Bl6 vs. alb-SREBP-1c: 2.10 x 10^{-07}, C57Bl6 vs. aP2-SREBP-1c: 6.11 x 10^{-10}, alb-SREBP-1c vs. aP2-SREBP-1c: 1.85 x 10^{-06}) and SLC25A13 (C57Bl6 vs. alb-SREBP-1c: 2.12 x 10^{-08}, C57Bl6 vs. aP2-SREBP-1c: 2.32 x 10^{-09}, alb-SREBP-1c vs. aP2-SREBP-1c: 2.09 x 10^{-09}) were found to possibly affect differential gene expression in all comparisons. The insulin induced gene (INSIG) 1 (alb-SREBP-1c vs. aP2-SREBP-1c: 2.64 x 10^{-05}) and INSIG2 (alb-SREBP-1c vs. aP2-SREBP-1c: 2.64 x 10^{-05}) involved in regulation of cholesterol synthesis were in the list of top score regulators restricted to analysis of alb-SREBP-1c versus aP2-SREBP-1c.

Functional annotation of differential gene expression listed in table 4.6 showed that in comparison of alb-SREBP-1c with C57Bl6 regulated gene expression was mostly annotated to fatty acid metabolism including synthesis, conversion and oxidation of lipids (Oxidation

of lipid: *p*-value 3.01 x 10^{-07}, Conversion of lipid: 8.90 x 10^{-07}, Concentration of lipid: 1.40 x 10^{-05}, Oxidation of fatty acid: 2.10 x 10^{-05}, Reduction of lipid: 3.06 x 10^{-05}, Elongation of fatty acid: 1.71 x 10^{-04}, Synthesis of lipid: 1.94 x 10^{-04}, Conversion of fatty acid: 2.24 x 10^{-04}). The number of differentially expressed molecules was relatively low (12–25 molecules) compared to 47 to 233 molecules annotated to the same pathways when analyzed for C57Bl6 versus aP2-SREBP-1c (Oxidation of lipid: 1.99 x 10^{-08}, Concentration of lipid: 1.95 x 10^{-15}, Oxidation of fatty acid: 8.55 x 10^{-06}, Reduction of lipid: 1.12 x 10^{-03}, Elongation of fatty acid: 4.88 x 10^{-04}, Synthesis of lipid: 1.94 x 10^{-04}) or alb-SREBP-1c versus aP2-SREBP-1c (Oxidation of lipid: 2.02 x 10^{-07}, Concentration of lipid: 3.27 x 10^{-12}, Oxidation of fatty acid: 9.54 x 10^{-06}, Reduction of lipid: 9.78 x 10^{-05}, Elongation of fatty acid: 2.46 x 10^{-05}, Synthesis of lipid: 7.86 x 10^{-08}). For example, oxidation of lipids was analyzed to involve 15 differentially expressed genes identified between C57Bl6 and alb-SREBP-1c liver transcriptome while 64 and 77 differentially expressed molecules were annotated to lipid oxidation when aP2-SREBP-1c was compared either C57Bl6 or alb-SREBP-1c. Further, some of the annotated functions to differential gene expression between C57Bl6 and alb-SREBP-1c like N-glycosylation of proteins (C57Bl6 vs. alb-SREBP-1c: 1.05 x 10^{-4}) or accumulation of glutamine (C57Bl6 vs. alb-SREBP-1c: 1.33 x 10^{-04}) were not detected in comparisons involving aP2-SREBP-1c. In contrast, when C57Bl6 gene expression was compared to aP2-SREBP-1c many tumor or cancer related diseases and functions like cell death (C57Bl6 vs. aP2-SREBP-1c: 4.54 x 10^{-20}, alb-SREBP-1c vs. aP2-SREBP-1c: 1.52 x 10^{-17}) and necrosis (C57Bl6 vs. aP2-SREBP-1c: 1.83 x 10^{-19}, alb-SREBP-1c vs. aP2-SREBP-1c: 2.82 x 10^{-16}) were included in the top score list of functional annotation besides differential gene expression related to fatty acid metabolism (Fatty acid metabolism: alb-SREBP-1c vs. aP2-SREBP-1c: 4.75 x 10^{-12}, Homeostasis of Lipid: alb-SREBP-1c vs. aP2-SREBP-1c: 1.69 x 10^{-10}). In analysis of alb-SREBP-1c versus aP2-SREBP-1c cancer related functions and diseases had to be omitted to identify metabolism related changes between the two fatty liver models. Nevertheless, cell death and necrosis processes were included in the top 25 list of mechanisms assigned to regulated gene expression in the fatty liver models. Further, differential gene expression was related to pathways like triacylglycerol (alb-SREBP-1c vs. aP2-SREBP-1c: 3.06 x 10^{-10}), cholesterol (alb-SREBP-1c vs. aP2-SREBP-1c: 4.61 x 10^{-11}) and sterol metabolism (alb-SREBP-1c vs. aP2-SREBP-1c: 5.91 x 10^{-10}) among the top 25 regulated functions when alb-SREBP-1c and aP2-SREBP-1c were compared. Infectious (Viral infection: C57Bl6 vs. aP2-SREBP-1c: 1.12 x 10^{-14}, alb-SREBP-1c vs. aP2-SREBP-1c: 1.84 x 10^{-12}, Infection of cells: C57Bl6 vs. aP2-SREBP-1c: 1.01 x 10^{-10}, alb-SREBP-1c vs. aP2-SREBP-1c: 5.58 x 10^{-12}, Infection by RNA virus: C57Bl6 vs. aP2-SREBP-1c: 1.16 x 10^{-11}, alb-SREBP-1c vs. aP2-SREBP-1c: 4.68 x 10^{-10}) and translational processes (Translation: C57Bl6 vs. aP2-SREBP-1c: 2.37 x 10^{-11},

alb-SREBP-1c vs. aP2-SREBP-1c: 3.65 x 10^{-12}, Translation of protein: C57Bl6 vs. aP2-SREBP-1c: 6.47 x 10^{-10},alb-SREBP-1c vs. aP2-SREBP-1c: 1.03 x 10^{-10}) were included in the top lists of both comparisons including aP2-SREBP-1c either to C57Bl6 or alb-SREBP-1c. Notably, diseases and functions annotated to differential gene expression between aP2-SREBP-1c and C57Bl6 or alb-SREBP-1c included more than 100 differentially expressed genes annotated to the top 25 identified diseases and functions and were mostly not detectable in the comparison of C57Bl6 with alb-SREBP-1c. These results support the observation that aP2-SREBP-1c animals display severe differences in liver function compared to C57Bl6 while differences between alb-SREBP-1c and C57Bl6 display a rather mild phenotype of impaired hepatic metabolism at least on transcriptional level.

Table 4.5: Analysis of upstream regulators of differential gene expression in fatty liver tissue. Ingenuity® pathway analysis (IPA) of differentially expressed upstream regulator genes in liver tissue of C57Bl6, alb-SREBP-1c and aP2-SREBP-1c. 25 top score upstream regulators are shown for comparison of C57Bl6 vs. alb-SREBP-1c, C57Bl6 vs. aP2-SREBP-1c and alb-SREBP-1c vs. aP2-SREBP-1c. Data were ranked separately according to *p*-value output for enrichment of category molecules for each data set analyzed using IPA software. Upstream regulators identified in the indicated comparisons were also analyzed for any other comparison. nd: not determined.

		C57Bl6 vs. alb-SREBP-1c					
Regulator	**Type**	**C57Bl6 vs. alb-SREBP-1c**		C57Bl6 vs. aP2-SREBP-1c		alb-SREBP-1c vs. aP2-SREBP-1c	
		p-value	molecules (n)	*p*-value	molecules (n)	*p*-value	molecules (n)
HNF4A	transcription regulator	2.70E-30	555	9.90E-39	462	3.71E-06	49
RICTOR	transcription regulator	3.28E-28	123	6.16E-31	108	4.83E-06	14
PPARA	ligand-dependent nuclear receptor	3.92E-16	144	2.40E-27	140	6.08E-13	28
RORC	ligand-dependent nuclear receptor	1.86E-13	66	8.72E-16	59	6.53E-13	18
ACOX1	enzyme	5.48E-13	62	1.49E-17	59	7.01E-05	9
NFE2L2	transcription regulator	4.00E-12	129	2.00E-09	96	3.62E-06	18
MYCN	transcription regulator	4.80E-12	96	4.18E-11	76	nd	
RORA	ligand-dependent nuclear receptor	1.12E-11	73	1.51E-16	69	2.74E-14	21
MYC	transcription regulator	5.32E-11	264	1.26E-08	195	9.44E-03	22
SREBF2	transcription regulator	1.39E-10	37	1.71E-09	30	3.28E-06	8
POR	enzyme	1.75E-10	67	6.37E-11	56	8.16E-11	17
SCAP	enzyme	4.88E-09	28	1.51E-07	22	2.41E-07	8
ATP7B	transporter	6.87E-09	23	nd		7.19E-06	6
GPD1	enzyme	1.03E-08	40	1.20E-09	35	nd	
SLC25A13	transporter	2.12E-08	40	2.32E-09	35	2.09E-09	12
SMARCB1	transcription regulator	8.38E-08	58	2.83E-07	46	1.76E-02	6
FOLR1	transporter	1.23E-07	38	9.16E-06	28	nd	
SREBF1	transcription regulator	1.77E-07	76	4.78E-09	65	1.15E-05	13
SLC13A1	transporter	2.10E-07	37	6.11E-10	35	1.85E-06	9
PEX5L	ion channel	2.44E-07	11	4.45E-04	7	4.67E-04	3
POLG	enzyme	2.88E-07	16	2.12E-10	17	nd	
HNF1A	transcription regulator	4.14E-07	119	2.99E-07	94	3.28E-03	13
INSR	kinase	5.48E-07	101	1.83E-06	78	1.42E-02	10
KDM5A	transcription regulator	6.56E-07	46	nd		nd	
XBP1	transcription regulator	8.75E-07	65	2.66E-05	48	2.56E-04	10

Table 4.5 continued.

		C57Bl6 vs. aP2-SREBP-1c					
Regulator	**Type**	C57Bl6 vs. alb-SREBP-1c		**C57Bl6 vs. aP2-SREBP-1c**		alb-SREBP-1c vs. aP2-SREBP-1c	
		p-value	molecules (n)	*p*-value	molecules (n)	*p*-value	molecules (n)
HNF4A	transcription regulator	2.70E-30	555	9.90E-39	462	3.71E-06	49
RICTOR	transcription regulator	3.28E-28	123	6.16E-31	108	4.83E-06	14
PPARA	ligand-dependent nuclear receptor	3.92E-16	144	2.40E-27	140	6.08E-13	28
ACOX1	enzyme	5.48E-13	62	1.49E-17	59	7.01E-05	9
RORA	ligand-dependent nuclear receptor	1.12E-11	73	1.51E-16	69	2.74E-14	21
RORC	ligand-dependent nuclear receptor	1.86E-13	66	8.72E-16	59	6.53E-13	18
MYCN	transcription regulator	nd		4.18E-11	76	nd	
POR	enzyme	1.75E-10	67	6.37E-11	56	8.16E-11	17
POLG	enzyme	2.88E-07	16	2.12E-10	17	nd	
SLC13A1	transporter	2.10E-07	37	6.11E-10	35	1.85E-06	9
GPD1	enzyme	1.03E-08	40	1.20E-09	35	nd	
NR1I2	ligand-dependent nuclear receptor	3.70E-04	43	1.28E-09	47	9.12E-05	9
SREBF2	transcription regulator	1.39E-10	37	1.71E-09	30	3.28E-06	8
NFE2L2	transcription regulator	4.00E-12	129	2.00E-09	96	3.62E-06	18
MAP4K4	kinase	6.66E-05	38	2.07E-09	40	nd	
SLC25A13	transporter	2.12E-08	40	2.32E-09	35	2.09E-09	12
SREBF1	transcription regulator	1.77E-07	76	4.78E-09	65	1.15E-05	13
ATP7B	transporter	6.87E-09	23	6.62E-09	20	7.19E-06	6
LEP	growth factor	4.26E-05	108	1.08E-08	97	9.18E-04	14
MYC	transcription regulator	5.32E-11	264	1.26E-08	195	9.44E-03	22
ELOVL5	enzyme	7.96E-05	14	2.87E-08	16	4.68E-03	3
CYP27A1	enzyme	8.54E-04	10	6.91E-08	13	1.75E-03	3
FGF19	growth factor	5.79E-05	30	7.40E-08	30	3.84E-03	5
SCAP	other	4.88E-09	28	1.51E-07	22	2.41E-07	8
LONP1	peptidase	1.74E-06	28	1.86E-07	25	nd	

Table 4.5 continued.

		alb-SREBP-1c vs. aP2-SREBP-1c					
Regulator	**Type**	C57Bl6 vs. alb-SREBP-1c		C57Bl6 vs. aP2-SREBP-1c		**alb-SREBP-1c vs. aP2-SREBP-1c**	
		p-value	molecules (n)	*p*-value	*p*-value	molecules (n)	*p*-value
RORA	ligand-dependent nuclear receptor	1.12E-11	73	1.51E-16	69	2.74E-14	21
PPARA	ligand-dependent nuclear receptor	3.92E-16	144	2.40E-27	140	6.08E-13	28
RORC	ligand-dependent nuclear receptor	1.86E-13	66	nd		6.53E-13	18
POR	enzyme	1.75E-10	67	6.37E-11	56	8.16E-11	17
GPD1	enzyme	nd		nd		1.63E-09	12
SLC25A13	transporter	2.12E-08	40	2.32E-09	35	2.09E-09	12
AHR	ligand-dependent nuclear receptor	2.18E-03	80	nd		4.00E-08	19
NR1I3	ligand-dependent nuclear receptor	1.11E-05	36	nd		4.76E-08	11
SCAP	enzyme	4.88E-09	28	1.51E-07	22	2.41E-07	8
NKX2-1	transcription regulator	nd		nd		3.00E-07	13
SLC13A1	transporter	2.10E-07	37	6.11E-10	35	1.85E-06	9
SREBF2	transcription regulator	1.39E-10	37	1.71E-09	30	3.28E-06	8
NFE2L2	transcription regulator	4.00E-12	129	2.00E-09	96	3.62E-06	18
HNF4A	transcription regulator	2.70E-30	555	9.90E-39	462	3.71E-06	49
RICTOR	transcription regulator	nd		6.16E-31	108	4.83E-06	14
ATP7B	transporter	6.87E-09	23	nd		7.19E-06	6
CFTR	ion channel	1.31E-02	23	6.91E-06	26	7.81E-06	8
ZBTB16	other	nd		nd		8.14E-06	10
SREBF1	transcription regulator	1.77E-07	76	4.78E-09	65	1.15E-05	13
STAT6	transcription regulator	3.70E-03	69	1.00E-02	51	1.46E-05	14
INSIG2	other	3.25E-05	10	1.85E-04	8	2.64E-05	4
INSIG1	other	9.07E-04	31	1.94E-06	31	3.56E-05	8
TERC	other	4.01E-05	16	4.54E-04	12	4.64E-05	5
ACOX1	enzyme	5.48E-13	62	1.49E-17	59	7.01E-05	9
HRG	other	nd		2.43E-01	4	8.95E-05	4

Table 4.6: Top 25 diseases and function annotation of differentially expressed hepatic genes. Knowledge based analysis of liver transcriptome data from pairwise analysis of C57Bl6 vs. alb-SREBP-1c, C57Bl6 vs. aP2-SREBP-1c and alb-SREBP-1c vs. aP2-SREBP-1c. Top 25 diseases and function annotated to differential gene expression were listed according to the *p*-value for enrichment of category molecules in each data set analyzed and pathways identified in the indicated comparisons were also given for any other comparison. Cancer related diseases and functions were omitted from analysis of alb-SREBP-1c vs. aP2-SREBP-1c. nd: not detected.

	C57Bl6 vs. alb-SREBP-1c					
Diseases or function	**C57Bl6 vs. alb-SREBP-1c**		C57Bl6 vs. aP2-SREBP-1c		aP2-SREBP-1c vs. alb-SREBP-1c	
	p-value	molecules (n)	*p*-value	molecules (n)	*p*-value	molecules (n)
Oxidation of lipid	3.01E-07	15	1.99E-08	64	2.02E-07	77
Metabolism of terpenoid	3.19E-07	18	3.54E-07	80	2.20E-08	106
Conversion of lipid	8.90E-07	12	nd		nd	
Concentration of lipid	1.40E-05	31	1.95E-15	238	3.27E-12	292
Synthesis of terpenoid	1.48E-05	15	6.44E-07	76	1.12E-05	92
Steroid metabolism	1.66E-05	14	4.37E-07	70	1.72E-07	90
Oxidation of fatty acid	2.10E-05	11	8.55E-06	47	9.54E-06	59
Reduction of lipid	3.06E-05	5	1.12E-03	11	9.78E-05	15
Metabolism of sterol	9.74E-05	8	5.08E-06	34	9.11E-08	46
N-glycosylation of protein	1.05E-04	5	nd		nd	
Hepatic steatosis	1.09E-04	14	4.48E-09	86	1.26E-06	100
Accumulation of farnesyl pyrophosphate	1.33E-04	2	nd		nd	
Accumulation of glutamine	1.33E-04	2	nd		nd	
Initiation of growth of hepatocellular carcinoma	1.33E-04	2	nd		2.96E-02	2
Oxidation of vitamin A	1.33E-04	2	nd		nd	
Size of liver tissue	1.33E-04	2	4.93E-01	2	nd	
Quantity of steroid	1.49E-04	19	1.69E-09	131	4.79E-09	166
Metabolism of vitamin	1.61E-04	7	nd		8.51E-04	8
Conversion of dihydrotestosterone	1.71E-04	3	nd		nd	
Elongation of fatty acid	1.71E-04	3	4.88E-04	6	2.46E-05	8
Synthesis of lipid	1.94E-04	25	1.05E-11	195	7.86E-08	233
Conversion of fatty acid	2.24E-04	5	nd		nd	
Hydroxylation of lipid	2.84E-04	4	9.81E-06	13	1.31E-03	12
Conversion of acyl-coenzyme A	3.09E-04	3	nd		nd	
Quantity of retinyl ester	3.09E-04	3	nd		nd	

Table 4.6 continued.

	C57Bl6 vs. aP2-SREBP-1c					
Diseases or Functions Annotation	C57Bl6 vs. alb-SREBP-1c		**C57Bl6 vs. aP2-SREBP-1c**		aP2-SREBP-1c vs. alb-SREBP-1c	
	p-value	molecules (n)	*p*-value	molecules (n)	*p*-value	molecules (n)
Cell death of osteosarcoma cells	nd		7.75E-30	71	1.03E-19	69
Enzymopathy	nd		1.82E-20	109	8.35E-13	115
Cell death	nd		4.54E-20	804	1.52E-17	1051
Metabolism of protein	nd		9.98E-20	288	1.87E-16	356
Necrosis	nd		1.83E-19	648	2.82E-16	836
Concentration of lipid	1.40E-05	31	1.95E-15	238	3.27E-12	292
Fatty acid metabolism	nd		3.09E-15	180	4.75E-12	217
Viral Infection	nd		1.12E-14	401	1.84E-12	513
Necrosis of malignant tumor	nd		9.90E-14	119	5.78E-08	130
Cell death of cancer cells	nd		1.49E-13	118	1.29E-07	128
Cell death of tumor cell lines	nd		2.76E-13	383	1.84E-12	498
Necrosis of tumor	nd		2.93E-13	138	4.63E-07	151
Concentration of triacylglycerol	nd		4.62E-13	106	3.06E-10	124
Cell death of tumor cells	nd		2.21E-12	133	2.16E-06	145
Synthesis of protein	nd		2.26E-12	135	8.90E-12	169
Concentration of acylglycerol	nd		6.59E-12	110	8.94E-09	128
Morphology of liver	nd		8.27E-12	105	6.74E-13	135
Synthesis of lipid	1.94E-04	25	1.05E-11	195	7.86E-08	233
Infection by RNA virus	nd		1.16E-11	241	4.68E-10	305
Homeostasis of lipid	nd		2.24E-11	66	1.69E-10	79
Translation	nd		2.37E-11	85	3.65E-12	108
Expression of protein	nd		4.04E-11	101	7.38E-10	123
Infection of cells	nd		1.01E-10	207	5.58E-12	274
Mitochondrial disorder	nd		1.44E-10	56	5.33E-06	57
Expression of mRNA	nd		1.47E-10	77	7.53E-09	91

Table 4.6 continued.

	alb-SREBP-1c vs. aP2-SREBP-1c					
Diseases or Functions Annotation	C57Bl6 vs. alb-SREBP-1c		C57Bl6 vs. aP2-SREBP-1c		**aP2-SREBP-1c vs. alb-SREBP-1c**	
	p-value	molecules (n)	*p*-value	molecules (n)	*p*-value	molecules (n)
Cell death of osteosarcoma cells	nd		7.75E-30	71	1.03E-19	69
Cell death	nd		4.54E-20	804	1.52E-17	1051
Metabolism of protein	nd		9.98E-20	288	1.87E-16	356
Necrosis	nd		1.83E-19	648	2.82E-16	836
Morphology of liver	nd		8.27E-12	105	6.74E-13	135
Enzymopathy	nd		1.82E-20	109	8.35E-13	115
Viral Infection	nd		1.12E-14	401	1.84E-12	513
Cell death of tumor cell lines	nd		2.76E-13	383	1.84E-12	498
Transport of protein	nd		3.54E-07	80	2.12E-12	118
Concentration of lipid	nd		1.95E-15	238	3.27E-12	292
Translation	nd		2.37E-11	85	3.65E-12	108
Fatty acid metabolism	nd		3.09E-15	180	4.75E-12	217
Infection of cells	nd		1.01E-10	207	5.58E-12	274
Synthesis of protein	nd		2.26E-12	135	8.90E-12	169
Transport of molecule	nd		2.66E-07	366	2.35E-11	516
Concentration of cholesterol	nd		6.48E-10	91	4.61E-11	118
Nonhematologic malignant neoplasm	nd		3.74E-07	2180	5.22E-11	3031
Translation of protein	nd		6.47E-10	79	1.03E-10	101
Homeostasis of lipid	5.24E-03	8	2.24E-11	66	1.69E-10	79
Replication of RNA virus	nd		1.28E-09	134	1.81E-10	175
Replication of Influenza A virus	nd		3.16E-10	85	2.06E-10	107
Concentration of triacylglycerol	nd		4.62E-13	106	3.06E-10	124
Infection by RNA virus	nd		1.16E-11	241	4.68E-10	305
Concentration of sterol	nd		8.18E-10	94	5.91E-10	119
Expression of protein	nd		4.04E-11	101	7.38E-10	123

4.3 Physiological verification of differential gene expression in fatty liver

4.3.1 Differential gene expression annotated to lipid and carbohydrate metabolism

The analysis of differential gene expression between the three study groups revealed that the top 25 downstream effects were mostly related to lipid metabolism as listed in table 4.6. In figure 4.4 differences in hepatic gene expression were further analyzed based on enrichment of pathways associated to lipid and carbohydrate metabolism as central metabolic nodes of fatty liver disease. The comparison of C57Bl6 versus the alb-SREBP-1c model showed significant but small differences in gene expression related to lipid and carbohydrate metabolism compared to the comparisons involving the aP2-SREBP-1c model. When aP2-SREBP-1c liver transcriptome was compared to either C57Bl6 or alb-SREBP-1c approximately 500 genes known to be related to lipid metabolism were found differentially expressed while only 60 genes had regulated expression between C57Bl6 and alb-SREBP-1c (figure 4.4 B). A similar result achieved the analysis of genes related to carbohydrate metabolism with approximately 300 genes affected when groups were compared to aP2-SREBP-1c hepatic gene expression and only 14 genes differentially expressed between C57Bl6 and alb-SREBP-1c (figure 4.4 B). These findings were also reflected when relation to metabolic diseases was analyzed where aP2-SREBP-1c comparisons showed a 8- to 10-fold higher number of genes to be differentially expressed compared to the C57Bl6 versus alb-SREBP-1c analysis. In the following *ex vivo* analysis was performed in primary hepatocytes isolated from the different murine models to verify whether the observed genetic changes were related to cellular function.

A

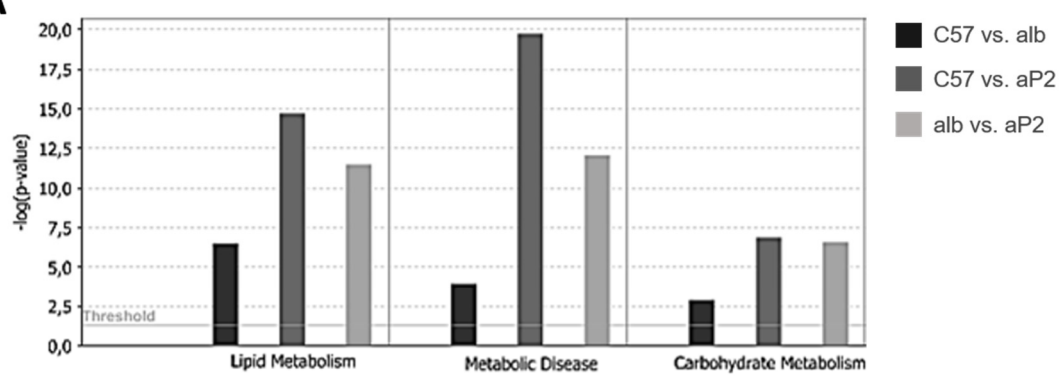

B

Category	C57 vs. alb		C57 vs. aP2		alb vs. aP2	
	p-value	n	*p*-value	n	*p*-value	n
Lipid metabolism	3.01E-07-1.88E-02	60	1.95E-15-2.18E-03	447	3.27E-12-3.25E-03	539
Metabolic disease	1.09E-04-1.56E-02	63	1.82E-20-2.33E-03	477	8.35E-13-3.16E-03	609
Carbohydrate metabolism	1.30E-03-1.26E-02	14	1.31E-07-2.30E-03	272	2.65E-07-2.53E-03	333

Figure 4.4: Analysis of differential hepatic gene expression related to lipid and carbohydrate metabolism. (A) Differences in hepatic gene expression between C57Bl6, alb-SREBP-1c and aP2-SREBP-1c were analyzed with IPA for enrichment based on –log(p-value) of pathways of lipid and carbohydrate metabolism as well as metabolic diseases. (B) Associated top *p*-values and differentially expressed molecules annotated to the analyzed pathways for each comparison.

4.3.2 Primary hepatocytes display fatty liver phenotype

Functional investigation of hepatic metabolism was performed using metabolically active primary hepatocytes from the exact phenotypes used for transcriptome analysis. Characterization of primary hepatocytes was conducted by morphological appearance observed with phase contrast microscopy and showed that the cells mostly form the characteristic hexagonal shape and were binucleated (figure 4.5 A). In phase contrast microscopy there seem to be no differences between primary hepatocytes from C57Bl6 and alb-SREBP-1c culture. Cultured hepatocytes from aP2-SREBP-1c liver tissue appear to have a more dense structure of cytoplasm and in some cells nuclei are only partly or even not visible. Visualization of lipids was performed using oil-red-o dye which unspecifically stained neutral triglycerides, lipids and some lipoproteins (figure 4.5 B). In cells isolated from C57Bl6 livers staining was less intense with a lower number of stained droplets compared to the cells from the two fatty liver models. In alb-SREBP-1c primary hepatocytes oil-red-o stained droplets could be found at higher density compared to C57Bl6. Droplets were equally distributed and uniformly sized throughout the cells. In contrast, stained lipid droplets in cells isolated from aP2-SREBP-1c livers appeared more irregular in size and distribution. Compared to alb-SREBP-1c there seem to be quantitatively less stained droplets but with markedly increased size in aP2-SREBP-1c primary hepatocytes. In sum, primary hepatocytes isolated from the three study groups showed that not only the fatty liver

phenotype but also specific differences between the fatty liver models were present in culture providing a convenient model system to study cellular function *ex vivo*.

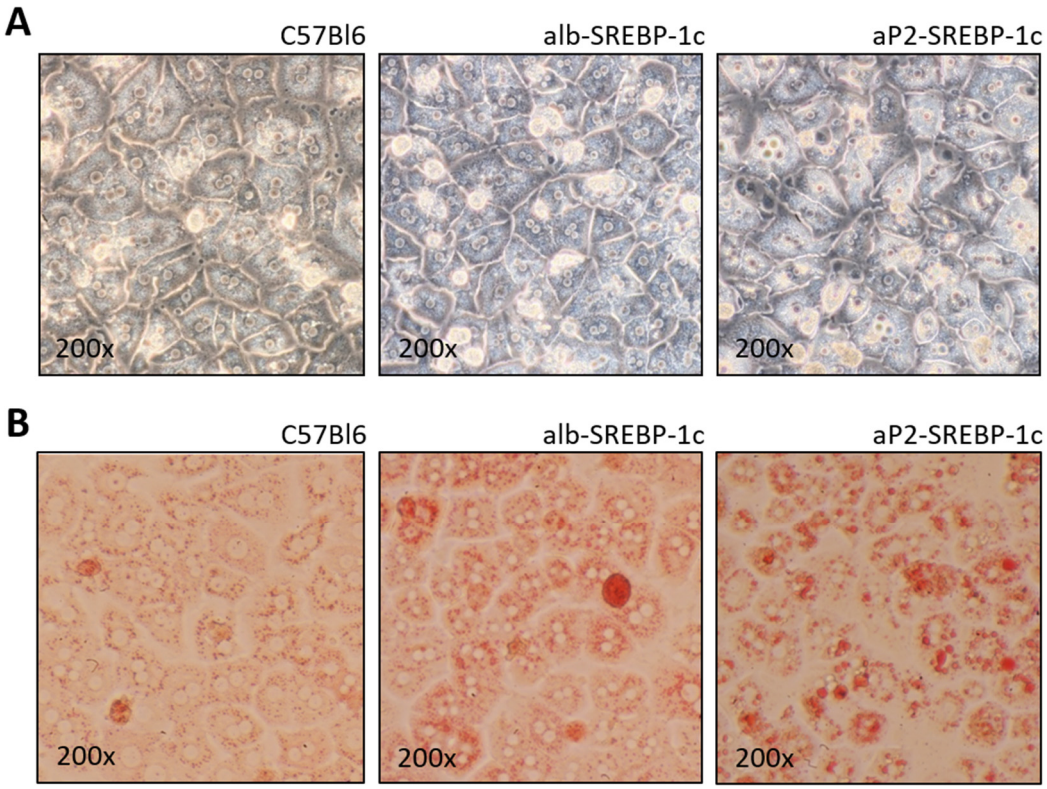

Figure 4.5: Mouse primary hepatocytes for functional analysis of fatty liver. (A) Microscopic images under phase contrast after overnight culture of C57Bl6, alb-SREBP-1c and aP2-SREBP-1c primary hepatocytes. (B) Lipid droplets were stained with oil-red-o in primary hepatocytes after overnight culture and light microscopic images were recorded. Magnification: 200x.

4.3.2.1 Fatty acid metabolism in primary hepatocytes from fatty liver

Assessment of differences in hepatic lipid metabolism was conducted in primary hepatocytes isolated from the different model systems and was focused on *de novo* lipogenesis (DNL), fatty acid uptake and mitochondrial β-oxidation to gain further insight in phenotype related changes.

Differences in the ability of primary hepatocytes from the different liver phenotypes to produce fatty acids from acetyl-CoA were investigated by providing the cells radiolabeled acetate as substrate for lipogenesis. Afterwards, lipids were extracted from whole cell lysates to measure radioactivity which was proportional to the rate of DNL during the assay. DNL in the different phenotypes was analyzed at basal level and after stimulation of the cells with 100 nM insulin as described in detail in section 3.7.1.2. In figure 4.6 A and B basal and insulin-stimulated DNL was depicted for the three different phenotypes investigated. Hepatocytes isolated from alb-SREBP-1c animals had the highest level of DNL at basal as

well as insulin-stimulated conditions counting for 651.9 ± 101.7 and 941.8 ± 101.7 CPM respectively. DNL was significantly lower in C57Bl6 (338.1 ± 69.7 CPM, insulin-stimulated 556.8 ± 62.3 CPM), and also aP2-SREBP-1c hepatocytes (508.3 ± 105.6 CPM, insulin-stimulated 726.6 ± 105.6 CPM) compared to alb-SREBP-1c. When aP2-SREBP-1c primary hepatocytes were compared to C57Bl6, DNL was significantly increased by 50% in the fatty liver cells. Insulin stimulation lead to a significant increase of DNL in all phenotypes compared to their respective basal condition ($p<0.001$, not shown). As expected, alb-SREBP-1c primary hepatocytes showed highest rate of DNL due to genetic interference of this pathway in the liver of these animals. Interestingly, the rate of DNL compared to control hepatocytes was significantly higher in aP2-SREBP-1c although these cells already exhibit a massive lipid load.

Assessment of the ability to take up fatty acids was investigated providing radiolabeled palmitate in culture medium of primary hepatocytes from the different phenotypes to measure uptaken radiolabeled palmitate after 0, 5 and 15 min of incubation (figure 4.6 C). Over the whole incubation timecourse palmitate uptake was measured with a statistical significant increase compared to time point 0 within each group. 15 min incubation showed significantly higher uptake of palmitate in alb-SREBP-1c (1592.95 ± 105.76 CPM) compared to C57Bl6 (1370.65 ± 78.47 CPM) and aP2-SREBP-1c (1324.13 ± 289.68 CPM) hepatocytes but overall there seem to be no differences in fatty acid uptake between the compared phenotypes.

Oxidation of fatty acids was also measured providing the cells radiolabeled palmitate which was catabolized to CO_2 through the ETC in the mitochondria of primary hepatocytes. Activity of released radiolabeled CO_2 was counted which corresponded to the rate of fatty acid oxidation in the cells analyzed. The results showed that mitochondrial β-oxidation was not different between C57Bl6 (3774.18 ± 518.58 CPM) and alb-SREBP-1c (3596.93 ± 628.11 CPM) primary hepatocytes but showed a 60% decrease in cells derived from aP2-SREBP-1c livers (1557.18 ± 351.38 CPM, $p<0.001$), (figure 4.6 D). Cells treated with etomoxir served as control experiment as it blocked the transport of fatty acids into the mitochondria and allowed measurement of CO_2 production from sources other than mitochondrial β-oxidation during the assay. In etomoxir treated hepatocytes radiolabeled CO_2 activity was significantly decreased in each phenotype compared to the respective untreated condition but showed no differences in non-β-oxidation CO_2 production between the three phenotypes. Hence the oxidation of lipids was not different between control animals and the genetic model of fatty liver but showed severe impairment of mitochondrial β-oxidation in cells derived from lipodystrophic animals.

SIRT activity was measured in cell lysates from primary hepatocytes using a chemiluminescence-based assay which measured deacetylation of a specific acetylated,

luminogenic peptide substrate by SIRT activity. Deacetylation lead to emission of a luminescence signal which allowed relative quantification of SIRT activity. Investigation of SIRT activity showed that there was a 2-fold increase in alb-SREBP-1c compared to C57Bl6 cell lysates but without statistical significance (figure 4.6 E). AP2-SREBP-1c lysates were measured with the highest SIRT activity which was significantly different from C57Bl6 but not from alb-SREBP-1c. SIRT activity was found opposed to the direction of mitochondrial β-oxidation.

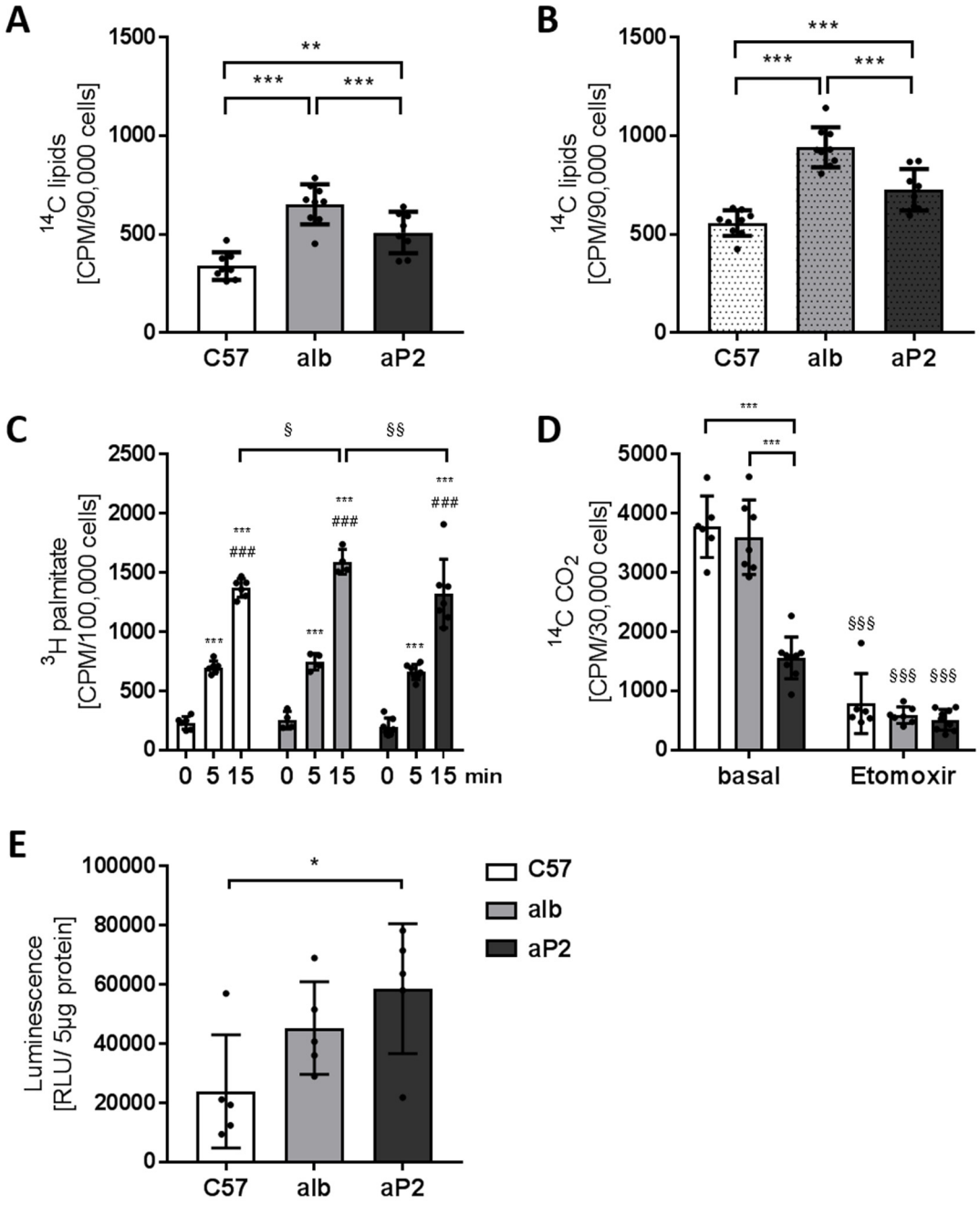

Figure 4.6: Functional analysis of lipid metabolism in primary hepatocytes from fatty liver. (A, B) Cells were provided radiolabeled acetate as substrate for DNL. DNL was measured as activity of metabolized acetate in the (A) absence or (B) presence of 100 nM insulin. (C) Fatty acid uptake was measured as the activity of uptaken radiolabeled palmitate into the cells after 0, 5 and 15 min of

incubation. (D) Fatty acid β-oxidation was analyzed as activity of oxidized radiolabeled palmitate to CO_2 in the absence (basal) or presence of etomoxir. (E) Activity of sirtuin activity was assessed as the measure of chemiluminescence signal intensity of substrate deacetylation by sirtuins. Bar graphs represent the mean ±SD of 4 to 9 independent experiments. Differences between two groups were calculated using Mann-Whitney-U test. * or § $p < 0.05$ as indicated, ** or §§ $p < 0.01$ as indicated, *** $p < 0.001$ vs. t0 or as indicated, §§§ $p < 0.001$ vs. basal. C57: C57Bl6, alb: alb-SREBP-1c, aP2: aP2-SREBP-1c, RLU: relative luminescence units.

4.3.2.2 Carbohydrate metabolism in primary hepatocytes from fatty liver

Glucose metabolism was investigated with regard to breakdown and production of glucose to picture changes in glucose related pathways within fatty liver. First, glycolytic capacity of primary hepatocytes isolated from different fatty liver phenotypes was investigated using a glycolysis stress assay. The analysis started with three basal ECAR measurements of glucose starved hepatocyte culture followed by four measurements of ECAR after glucose concentration was increased to 25 mM. Figure 4.7 A shows the ECAR profile of the three investigated phenotypes during the assay. In alb-SREBP-1c cells ECAR increased 2-fold after injection of glucose from 1.55 ± 0.51 mpH/min/µg protein at basal level to a maximal ECAR of 3.25 ± 0.74 mpH/min/µg protein. In contrast, in C57Bl6 and aP2-SREBP-1c glucose injection only had a modest effect on ECAR increase of approximately 30%. Extracellular acidification was lowest in aP2-SREBP-1c ranging from 0.93 ± 0.05 mpH/min/µg protein to 1.24 ± 0.09 mpH/min/µg protein and C57Bl6 ECAR levels ranged from 1.23 ± 0.13 mpH/min/µg protein to 1.59 ± 0.13 mpH/min/µg protein representing the intermediate group. Basal ECAR levels were markedly different between all groups but only reached statistical significance between C57Bl6 and aP2-SREBP-1c basal ECAR level. ECAR after induction of glycolytic stress was calculated as significantly different between all of the tested groups.

The calculated glycolysis rate (figure 4.7 B) was significantly higher in alb-SREBP-1c culture compared to C57Bl6 as well as aP2-SREBP-1c, while there was no statistical significant difference between C57Bl6 and aP2-SREBP-1c. Non-glycolytic acidification (figure 4.7 C) was significantly lower in aP2-SREBP-1c (0.93 ± 0.05 mpH/min/µg protein) compared to C57Bl6 (1.22 ± 0.13 mpH/min/µg protein). Furthermore, there was markedly increased non-glycolytic acidification in alb-SREBP-1c culture (1.75 ±0.15 mpH/min/µg protein) compared to C57Bl6 and aP2-SREBP-1c. The results indicate a markedly higher glycolytic potential in alb-SREBP-1c hepatocytes as in C57Bl6 or aP2-SREBP-1c while there was no markedly difference between control and aP2-SREBP-1c.

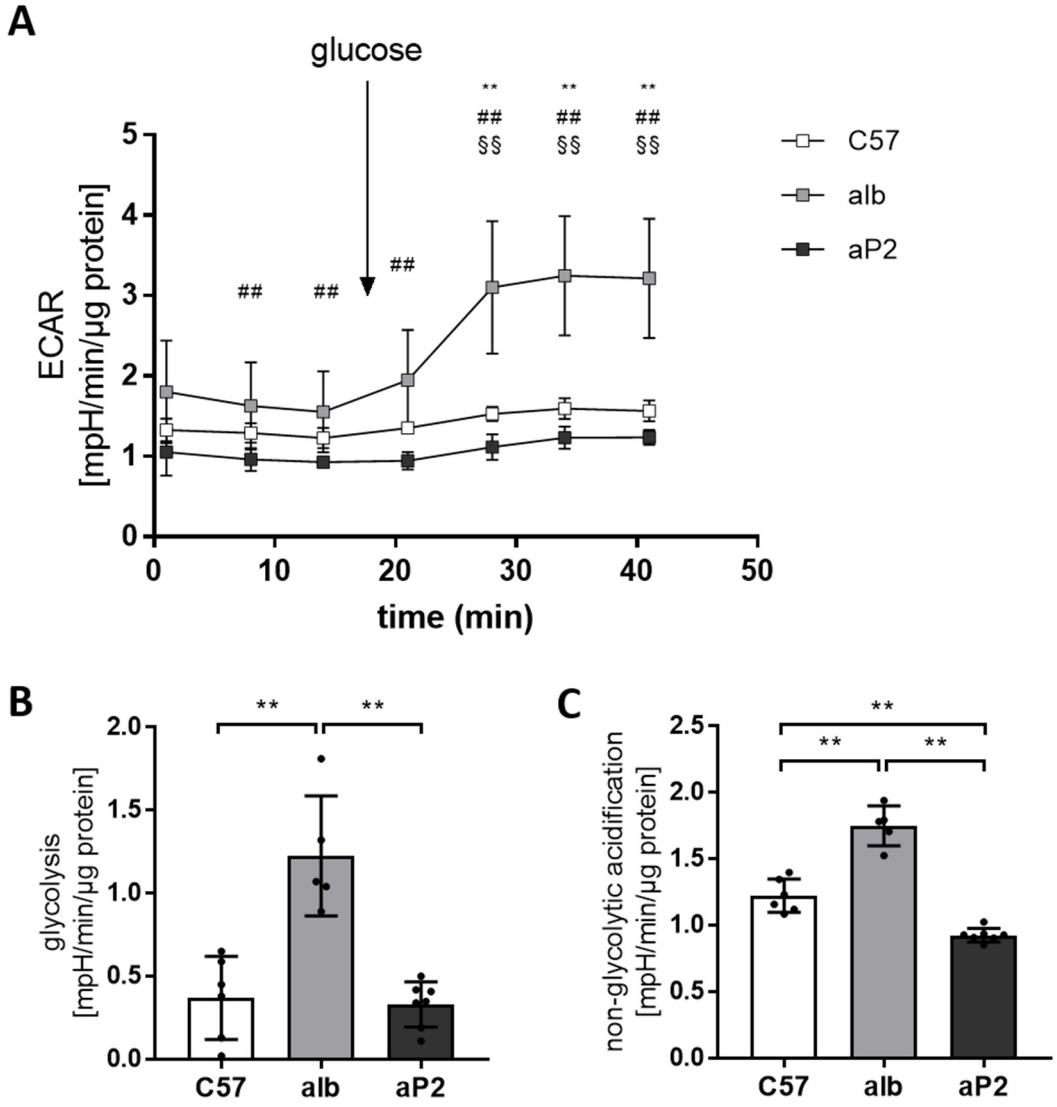

Figure 4.7: Glycolysis in primary hepatocytes from fatty liver. (A) Profile of glycolysis stress test performed with an extracellular flux analyzer. Extracellular acidification rate (ECAR) was measured at basal level and after acute injection of glucose (final concentration 25 mM) for each phenotype analyzed. (B) Rate of glycolysis and (C) non-glycolytic acidification were calculated. All measurements were normalized to total protein concentration. Glycolysis profiles and bar graphs represent the mean ±SD of 5 to 7 independent experiments Differences between two groups were calculated using Mann-Whitney-U test. ** $p < 0.01$ C57 vs. alb or as indicated, ## $p < 0.01$ C57 vs. aP2, §§ $p < 0.01$ alb vs. aP2. C57: C57Bl6, alb: alb-SREBP-1c, aP2: aP2-SREBP-1c.

Glycogen synthesis was investigated in primary hepatocytes isolated from different mouse phenotypes of fatty liver using radiolabeled glucose in the presence or absence of insulin. Basal glycogen synthesis without addition of insulin was depicted in figure 4.8 A. The amount of ^{14}C-labeled glycogen was significantly lower in aP2-SREBP-1c hepatocytes (264.9 ± 27.12 CPM) compared to C57Bl6 (369.3 ± 38.56 CPM, $p<0.05$). In alb-SREBP-1c glycogen was not calculated as significantly different from C57Bl6 or aP2-SREBP-1c but with 336.5 ± 39.38 CPM it was 27% higher than ^{14}C-glycogen amount in aP2-SREBP-1c

culture. Insulin-stimulated glycogen synthesis was significantly increased in each phenotype compared to the respective basal condition (figure 4.8 A versus B, $p < 0.05$ comparison not shown). Insulin increased glycogen synthesis in C57Bl6 and aP2-SREBP-1c by approximately 45% and in alb-SREBP-1c by 22% compared to the respective basal glycogen synthesis (figure 4.8 B). Also the insulin-stimulated glycogen synthesis was lowest in aP2-SREBP-1c culture with 381.5 ± 27.12 CPM and increased to 409.1 ± 39.38 CPM in alb-SREBP-1c which was not calculated as significantly different. In contrast, both fatty liver phenotypes had significantly lower glycogen synthesis in the insulin-stimulated condition compared to C57Bl6 (523.5 ± 38.56 CPM, $p<0.05$).

In all three liver phenotypes, incubation with pyruvate and lactate increased the amount of glucose in culture medium significantly compared to basal condition where no substrates were provided (figure 4.8 C). Basal glucose production was significantly lower in aP2-SREBP-1c hepatocyte culture (56.64 ± 14.5 µg/ml) compared to alb-SREBP-1c (71.82 ± 5.93 µg/ml; $p<0.05$) but basal glucose production was not significantly different between C57Bl6 compared to either SREBP-1c cultures. In pyruvate/lactate stimulated cultures equal amounts of glucose were measured in all three phenotypes which ranged between 83.5 ± 6.73 µg/ml in aP2-SREBP-1c and 92.82 ± 5.98 µg/ml in C57Bl6. Incubation of primary hepatocytes with 10 nM insulin resulted in significantly lower glucose concentrations as in pyruvate/lactate treated cells but there were no differences in glucose concentration to the respective basal cultures in all phenotypes. Glucose production assessed in this experiment revealed that there were no differences between primary hepatocytes from C57Bl6 and alb-SREBP-1c, while basal glucose production was reduced in aP2-SREBP-1c primary hepatocyte culture.

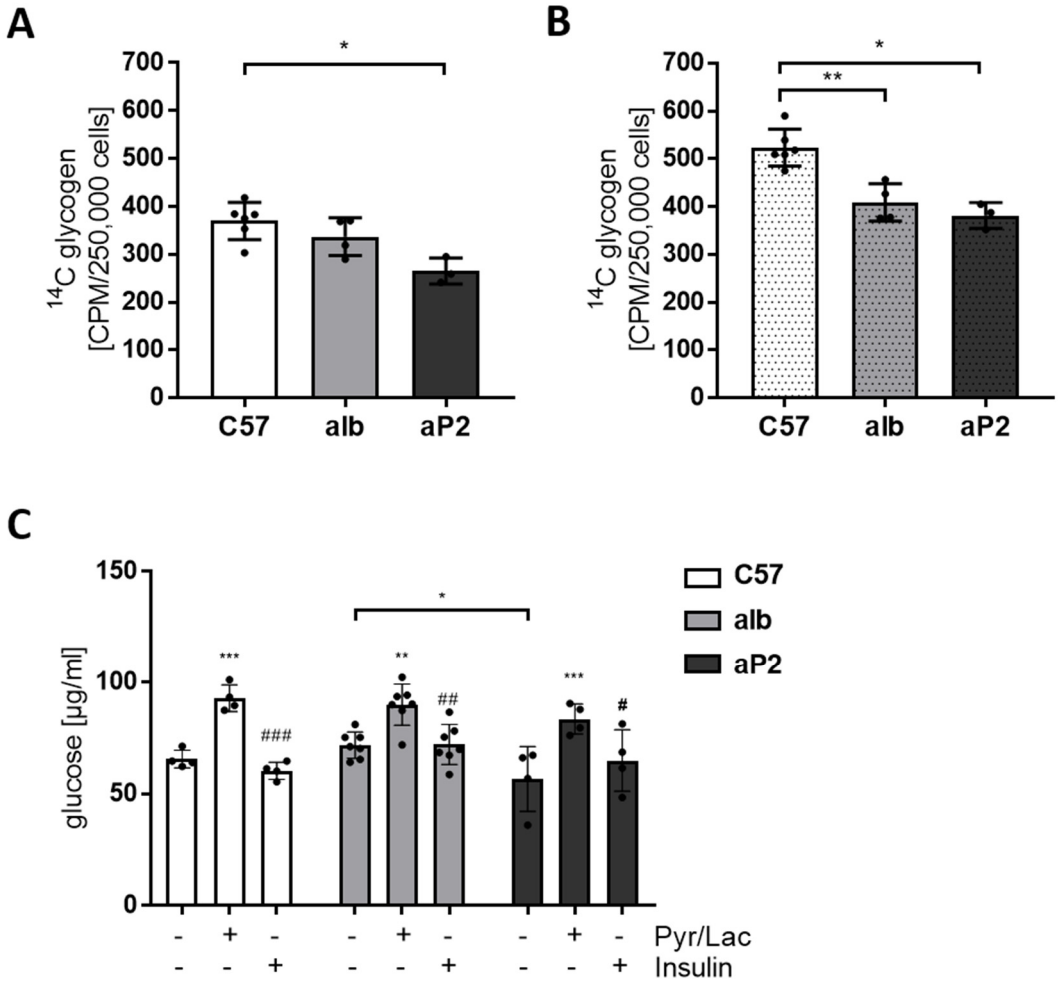

Figure 4.8: Glycogen production and gluconeogenesis in primary hepatocytes from fatty liver. (A, B) Cells were provided radiolabeled glucose to measure glycogen synthesis as activity of incorporated glucose during glycogen synthesis in (A) absence or (B) presence of 100 nM insulin. (C) Gluconeogenesis was measured as glucose produced by primary hepatocytes in culture in the presence or absence of 2 mM pyruvate/ 2 mM lactate or 10 nM insulin. Glucose was measured in supernatants after 5 h of culture in glucose-free medium. Bar graphs represent the mean ±SD of 3 to 7 independent experiments. Differences between two groups were calculated using Mann-Whitney-U test (A, B) or (C) 2-way ANOVA. * $p < 0.05$ as indicated, ** $p < 0.01$ vs. untreated or as indicated, *** $p < 0.001$ vs. untreated, # $p < 0.05$ vs. Pyr/Lac, ## $p < 0.01$ vs. Pyr/Lac, ### $p < 0.001$ vs. Pyr/Lac. C57: C57Bl6, alb: alb-SREBP-1c, aP2: aP2-SREBP-1c.

4.3.3 Gene expression differences related to mitochondrial function

Mitochondrial dysfunction was identified to be among the top 25 downstream effects listed in table 4.6 caused by differential gene expression in C57Bl6 versus alb-SREBP-1c and aP2-SREBP-1c. Detailed analysis of pathway enrichment which point to altered mitochondrial function namely energy production, small molecule biochemistry and free radical scavenging showed markedly changes in gene expression when the fatty liver models were compared to each other or to C57Bl6 (figure 4.9). Regulation of gene expression was similar for each comparison when energy production and free radical

scavenging were investigated. Differences in gene expression annotated to small molecule biochemistry showed markedly higher transcriptional regulation in comparisons involving aP2-SREBP-1c hepatic gene expression. Comparisons including aP2-SREBP-1c model also resulted in high numbers of differentially expressed genes related to the analyzed pathways while noticeable fewer gene numbers were identified with changed expression when alb-SREBP-1c was compared to C57Bl6. Hence, mitochondrial function was assessed with regard to mitochondrial potential and energy production to identify functional differences in fatty liver hepatocytes.

A

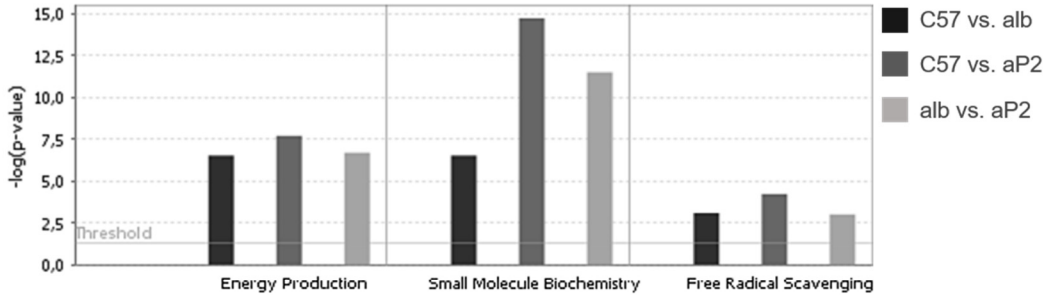

B

Category	C57 vs. alb		C57 vs. aP2		alb 1c vs. aP2	
	p-value	n	*p*-value	n	*p*-value	n
Energy production	3.01E-07-1.15E-02	15	1.99E-08-2.03E-03	138	2.02E-07-2.32E-03	158
Small molecule biochemistry	3.01E-07-1.88E-02	70	1.95E-15-2.18E-03	558	3.27E-12-3.25E-03	657
Free radical scavenging	7.83E-04-7.83E-04	2	5.79E-05-2.04E-04	118	9.51E-04-1.93E-03	147

Figure 4.9: Analysis of differential hepatic gene expression related to mitochondrial function. (A) Differences in hepatic gene expression between C57Bl6, alb-SREBP-1c and aP2-SREBP-1c were analyzed with IPA for enrichment based on –log(p-value) of pathways of mitochondrial function grouped in energy production, small molecule biochemistry and free radical scavenging. (B) Associated top *p*-values and differentially expressed molecules annotated to the analyzed pathways for each comparison.

4.3.3.1 Mitochondrial function and energy metabolism in primary hepatocytes from fatty liver

Mitochondrial function was analyzed using a mitochondrial (mito) stress test in an extracellular flux analyzer. The profiles of mito stress assay OCR for each of the investigated groups were shown in figure 4.10 A. All groups showed the characteristic response to the subsequent injections of inhibitors. Oligomycin decreased OCR in all phenotypes compared to basal respiration while uncoupling of the mitochondrial membrane by FCCP injection rapidly increased OCR levels before mitochondrial respiration was shut down after rotenone and antimycin A injection. Significantly different mitochondrial

performance over the whole assay was found between alb-SREBP-1c hepatocytes compared to the two other groups (figur4.10 A). There were no differences between C57Bl6 and aP2-SREBP-1c mitochondrial profile. Calculation of the key parameters of mitochondrial function showed that basal respiration was highest in alb-SREBP-1c (11.88 ± 2.87 pmol/min/µg protein) compared to C57Bl6 (7.12 ± 1.88 pmol/min/µg protein) and aP2-SREBP-1c hepatocytes (5.46 ± 1.83 pmol/min/µg protein). Lowest basal respiration was observed in aP2-SREBP-1c hepatocytes which showed no statistical significance compared to C57Bl6 (figure 4.10 B). Maximal respiration was significantly different between all groups with highest level of OCR in alb-SREBP-1c of 24.46 ± 3.88 pmol/min/µg protein and lowest in aP2-SREBP-1c culture accounting for 7.51 ± 2.0 pmol/min/µg protein (figure 4.10 C). Spare respiratory capacity was 3-fold increased in alb-SREBP-1c compared to C57Bl6 or aP2-SREBP-1 while the two last mentioned groups showed no differences, if compared directly (figure 4.10 D). Parameters calculated for proton leak and coupling efficiency of the analyzed primary culture were not different between the groups. ATP production was similar in C57Bl6 (5.17 ± 1.23 pmol/min/µg protein) and aP2-SREBP-1c (4.34 ± 0.56 pmol/min/µg protein) but was markedly increased in alb-SREBP-1c (9.15 ± 1.16 pmol/min/µg protein).

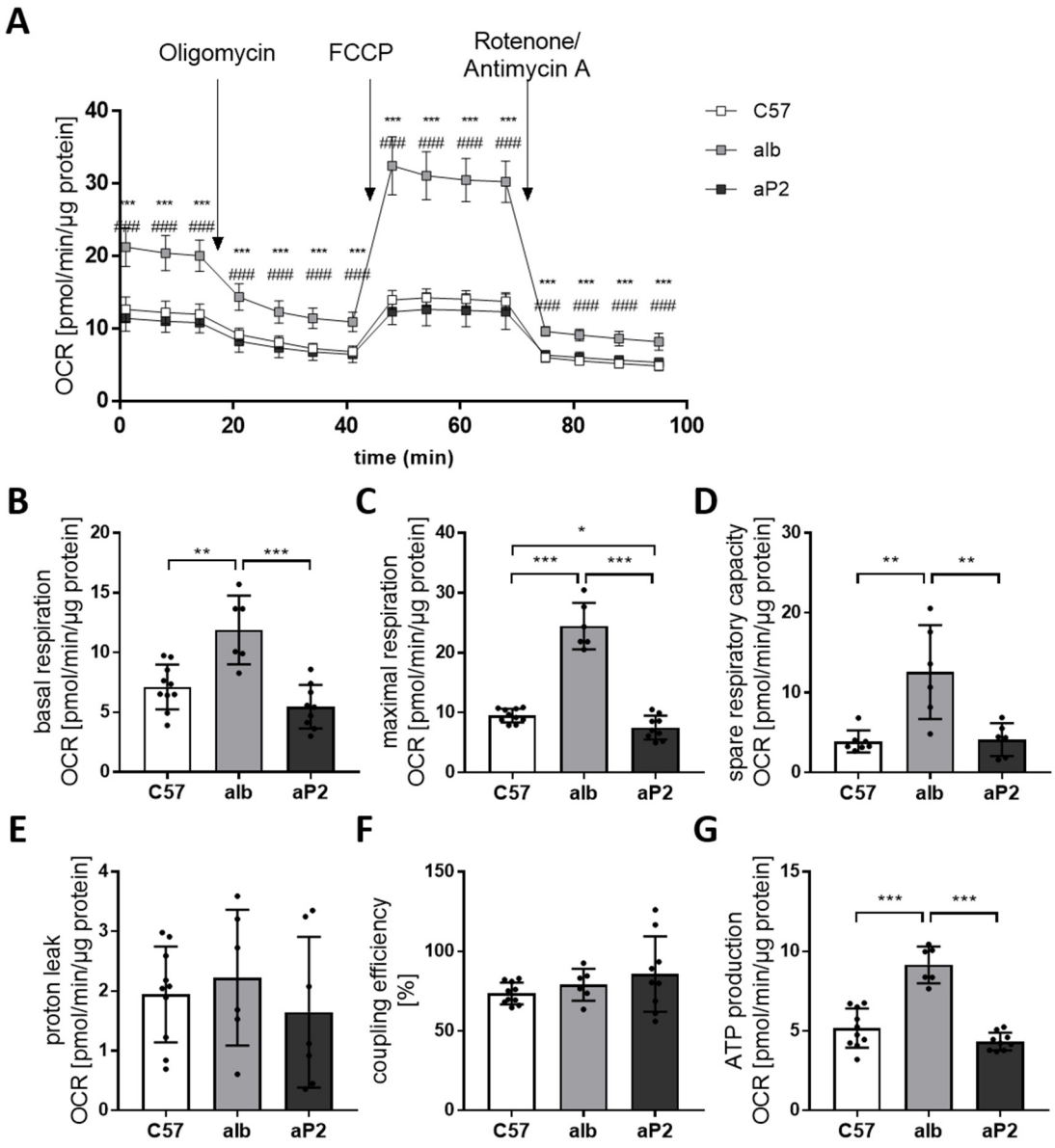

Figure 4.10: Mitochondrial function in primary hepatocytes from fatty liver. (A) Mitochondrial stress test was performed in primary hepatocytes by serial injection of inhibitors of the electron transport chain and concurrent measurement of oxygen consumption rate (OCR) of primary hepatocytes in an extracellular flux analyzer. OCR profiles for mitochondrial performances are shown for each phenotype. Based on OCR measured during mito stress assay (B) basal and (C) maximal respiration, (D) spare respiratory capacity, (E) proton leak, (F) coupling efficiency and (G) ATP production were calculated. All measurements were normalized to total protein concentration. Mito stress profiles and bar graphs represent the mean ±SD of 6 to 9 independent experiments Differences between two groups were calculated using Mann-Whitney-U test. * $p < 0.05$ as indicated, ** $p < 0.01$ as indicated, *** $p < 0.001$ C57 vs. alb or as indicated, ### $p < 0.001$ aP2 vs. alb. C57: C57Bl6, alb: alb-SREBP-1c, aP2: aP2-SREBP-1c.

4.3.4 Gene expression differences in growth regulation, cell maintenance and cell-to-cell signaling

Detailed analysis of gene expression changes between the three study groups revealed significant differences in liver transcriptome in mechanisms related to cell growth and maintenance as well as signal transduction. Genes differentially expressed related to endocrine function and disease, connective tissue function and cell-to-cell signaling were grouped and analyzed in detail for differences between the comparisons applied to transcriptome data (figure 4.11). Several genes were found differentially expressed in comparisons including aP2-SREBP-1c liver transcriptome while the comparison of C57Bl6 versus alb-SREBP-1c also showed significant differences in cell signaling and maintenance processes but included markedly less differentially expressed genes. Whether differential gene expression was also manifested in cellular function was exemplarily analyzed in primary hepatocytes from the three study groups for relevant targets of the insulin signaling cascade.

A

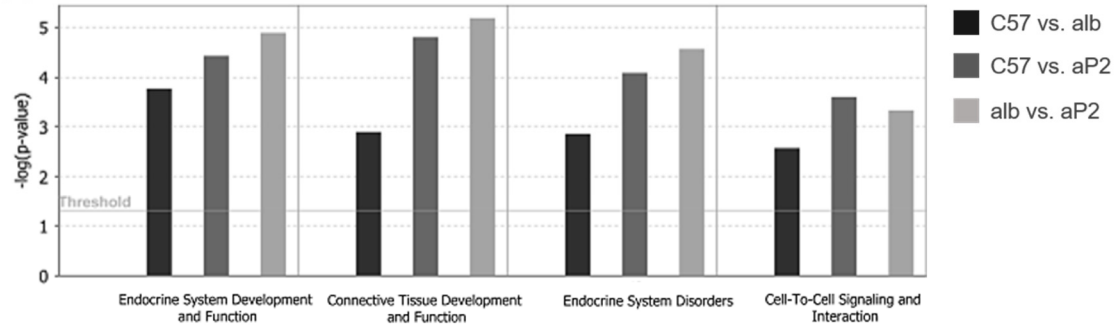

B

Category	C57 vs. alb *p*-value	n	C57 vs. aP2 *p*-value	n	alb vs. aP2 *p*-value	n
Endocrine system development and function	1.71E-04-1.15E-02	11	3.74E-05-2.04E-03	111	1.29E-05-2.32E-03	134
Connective tissue development and function	1.25E-03-1.60E-02	30	1.59E-05-1.99E-03	201	6.56E-06-2.90E-03	300
Endocrine system disorders	1.37E-03-1.56E-02	35	8.21E-05-2.33E-03	169	2.74E-05-3.16E-03	252
Cell-to-cell signaling and interaction	2.64E-03-1.62E-02	33	2.50E-04-2.18E-03	127	4.65E-04-2.29E-03	40

Figure 4.11: Analysis of differential hepatic gene expression related to cell maintenance, development and cell-to-cell signaling. (A) Differences in hepatic gene expression between C57Bl6, alb-SREBP-1c and aP2-SREBP-1c were analyzed with IPA for enrichment based on –log(p-value) of pathways of endocrine system as well as connective tissue development and function, endocrine system disorders, and cell-to-cell signaling and interaction. (B) Associated top *p*-values and differentially expressed molecules annotated to the analyzed pathways for each comparison.

4.3.4.1 Insulin signaling cascade in primary hepatocytes from fatty liver

Based on transcriptome data insulin resistance, alterations in insulin signaling, as well as the participation of central insulin signaling components in the nodal alterations deduced from gene expression analyses. Therefore, primary hepatocytes isolated from the different fatty liver phenotypes were analyzed for differences in insulin signaling cascade. Whole cell lysates from untreated and insulin stimulated hepatocytes were investigated for the abundance of insulin receptor β (IRβ), insulin receptor substrate 1 (IRS-1) and insulin-mediated phosphorylation of the downstream targets protein kinase B (Akt), and glycogen synthase kinase 3β (GSK3β). The abundance of IRβ, IRS-1 and Akt was unchanged between C57Bl6 and aP2-SREBP-1c while in alb-SREBP-1c cell lysates the abundance of these three targets was significantly increased compared to both C57Bl6 and aP2-SREBP-1c (Figure 4.12 A to C). Insulin-stimulated phosphorylation of Akt a downstream target of insulin receptor signaling, showed that in all investigated phenotypes 10 nM Insulin was able to increase phosphorylation significantly compared to basal phosphorylation without insulin-stimulation. This was the case for both investigated phosphorylation sites at serine (Ser) 473 and threonine (Thr) 308 (figure 4.12 D and E). In aP2-SREBP-1c primary hepatocytes insulin-stimulated phosphorylation of Akt Ser 473 was 40% and Akt Thr 308 was 50% reduced compared to C57Bl6 and alb-SREBP-1c insulin effect. The abundance of GSK3β was not different between the investigated groups (figure 4.12 F). Investigation of GSK3β as a downstream target of Akt showed that there were no differences on insulin-mediated phosphorylation at Ser 9 between all phenotypes while insulin was able to significantly increase GSK3β Ser 9 phosphorylation compared to each respective basal condition (figure 4.12 G). Basal phosphorylation of GSK3β Ser9 was significantly reduced in aP2-SREBP-1c cell lysates compared to C57Bl6.

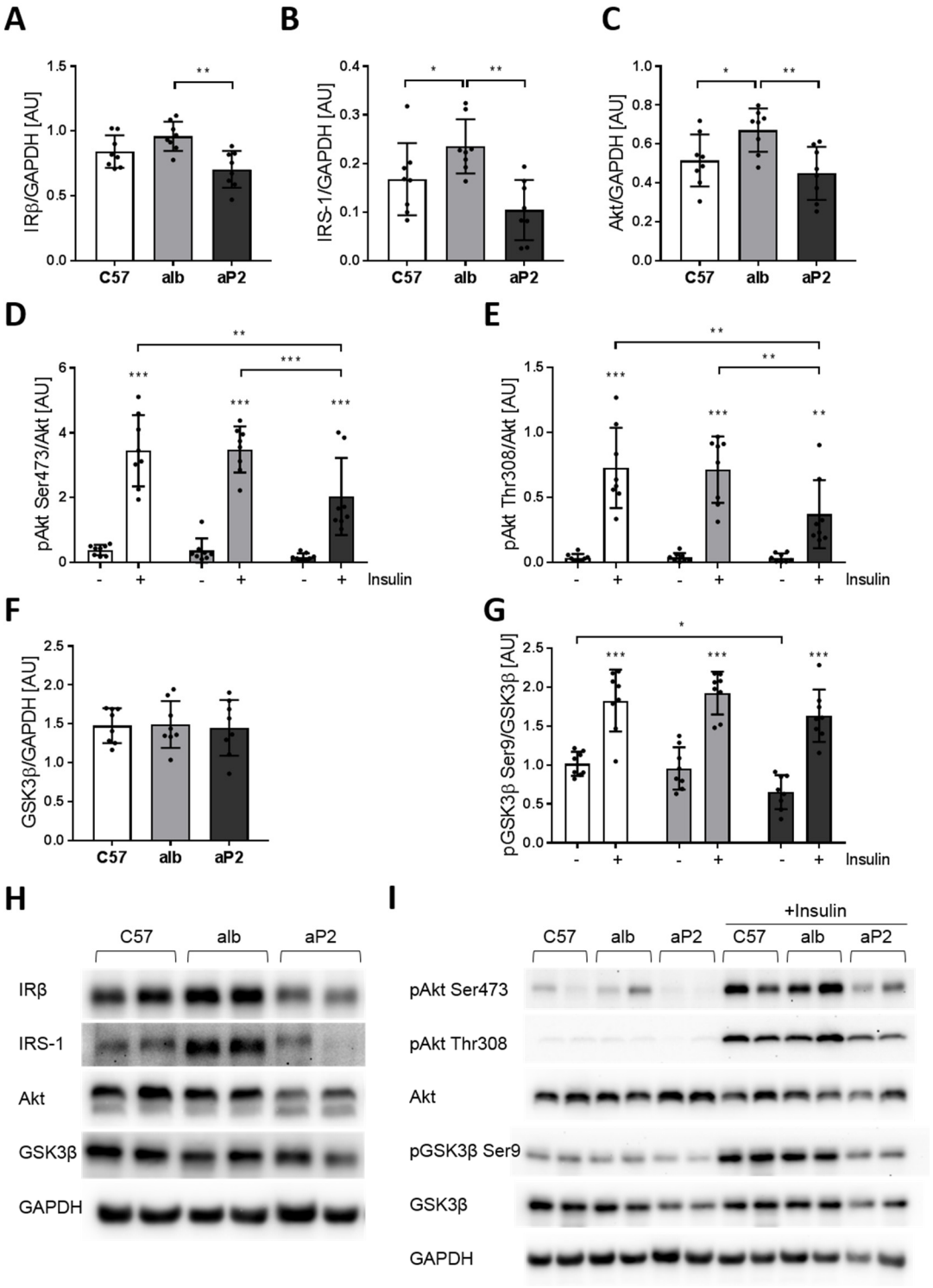

Figure 4.12: Analysis of the insulin signaling cascade in hepatocytes derived from fatty liver. Primary hepatocytes isolated from C57Bl6 (C57), alb-SREBP-1c (alb) and aP2-SREBP-1c (aP2) livers were cultured overnight in serum free medium and kept untreated or stimulated with 10 nM insulin for 10 min. Abundance of Insulin receptor β (IRβ, A), insulin receptor substrate-1 (IRS-1, B), protein kinase b (Akt, C), glycogen synthase kinase 3β (GSK3β, F) and insulin-stimulated phosphorylation of Akt Ser 473 (D), Akt Thr 308 (E) and GSK3β Ser 9 (G) were detected. Bar graphs represent the mean ±SD of 8 independent experiments. Representative western blot pictures for each target are shown in H and I. Mann-Whitney-U test was used for pairwise analysis of total protein abundance, 2-way ANOVA followed by multiple comparison was used to calculate statistical differences of phosphorylation experiments: * $p < 0.05$, ** $p < 0.01$, *** $p < 0.001$.

4.3.5 Gene expression differences in cell-to-cell communication in immune response

Hepatic gene expression analyzed in liver tissue derived from the three different model systems was investigated for changes in cellular immune response processes. Figure 4.13 showed significant differences in gene expression related to inflammatory and immunological diseases in all analyzed data sets. Differential gene expression involved more than 300 molecules when aP2-SREBP-1c was compared to C57Bl6 hepatic gene expression. Markedly lower amounts of genes were found deregulated when both fatty liver models were compared and less than 50 genes showed differential gene expression between C57Bl6 and alb-SREBP-1c. Further, immune cell trafficking was included in immune response analysis and showed that there were significant differences between C57Bl6 and either alb-SREBP-1c or aP2-SREBP-1c but there were no genes found to be differentially expressed in comparison of both fatty liver models. AP2-SREBP-1c showed 3-fold higher amounts of differentially expressed genes as alb-SREBP-1c compared to C57Bl6. Functional verification of cell-to-cell communication in immune response was conducted by measurement of cytokines released from primary hepatocytes and their concentration in the circulation in the different fatty liver models systems.

A

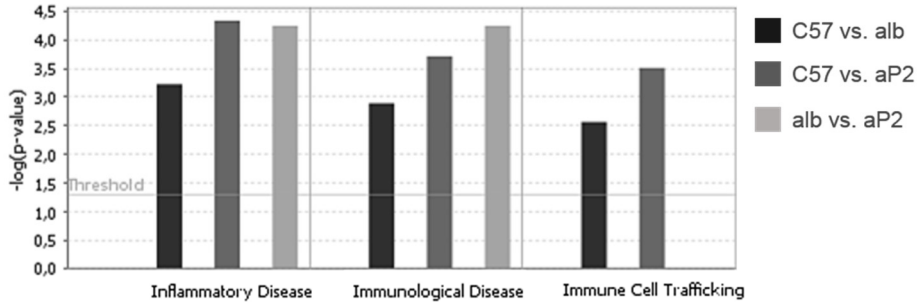

B

	C57 vs. alb		C57 vs. aP2		alb vs. aP2	
Category	*p*-value	n	*p*-value	n	*p*-value	n
Inflammatory Disease	5.98E-04-1.32E-02	43	4.69E-05-1.96E-03	368	5.79E-05-2.90E-03	103
Immunological Disease	1.28E-03-1.74E-02	42	1.94E-04-1.91E-03	321	5.79E-05-2.90E-03	101
Immune Cell Trafficking	2.71E-03-1.68E-02	25	3.10E-04-1.56E-03	74	n.d.	

Figure 4.13: Analysis of differential hepatic gene expression related to immune response. (A) Differences in hepatic gene expression between C57Bl6, alb-SREBP-1c and aP2-SREBP-1c were analyzed with IPA for enrichment based on –log(p-value) of pathways of inflammatory and immunological diseases and immune cell trafficking. (B) Associated top *p*-values and differentially expressed molecules annotated to the analyzed pathways for each comparison.

4.3.5.1 Physiological verification of gene expression alterations in primary hepatocytes of inflammation and cell-to-cell communication

4.3.5.1.1 Cytokine release from primary hepatocytes from fatty liver

Based on transcriptome data, several cytokines were found to be differentially regulated on gene expression level. To determine whether cytokine release from primary hepatocytes of the different models were also changed, Bio-Plex technology was used. Proteins released from the different phenotypes of primary hepatocytes into cell culture supernatant were analyzed for a set of 23 cytokines. Of these 18 were found to be secreted from C57Bl6, alb-SREBP-1c and aP2-SREBP-1c primary hepatocytes (figure 4.14). The most abundant cytokines were keratinocyte chemoattractant (KC)/CXCL1 and monocyte chemoattractant protein (MCP) 1/CCL2, (figure 4.14 M and N). In animals with normal liver phenotype release of KC/CXCL1 and MCP-1/CCL2 was roughly 3000 pg/ml. MCP-1/CCL2 abundance was significantly lower in both fatty liver phenotypes (alb-SREBP-1c: 1354.6 ± 934.7 pg/ml, aP2-SREBP-1c: 1986.9 ± 776.6 pg/ml) as well as KC/CXCL1 (alb-SREBP-1c: 1710 ± 780.6 pg/ml, aP2-SREBP-1c: 2153 ± 1156 pg/ml) but was calculated with statistical significance only for the amount of KC/CXCL1 in alb-SREBP-1c versus C57Bl6 supernatant (MCP-1/CCL2: 3326.3 ± 1247 pg/ml, KC/CXCL1: 2845.8 ± 910.7 pg/ml). Several interleukins (IL) were also found markedly reduced in the supernatant from fatty liver hepatocyte culture compared to C57Bl6 like IL-6, IL-10 or IL-12(p70). Further, mean interferon (IFN) γ and tumor necrosis factor (TNF) α secretion was found to be lowest from aP2-SREBP-1c hepatocytes (IFNγ: 10.8 ± 6.6 pg/ml, TNFα: 80 ± 28.31 pg/ml) (figure 4.14 K and R), but could not reach statistical significance compared to C57Bl6 (IFNγ: 14.73 ± 7.03 pg/ml, TNFα: 142.5 ± 56.26 pg/ml) or alb-SREBP-1c (IFNγ: 19.61 ± 14.86 pg/ml, TNFα: 117.5 ± 70.58 pg/ml). Macrophage inflammatory protein (MIP)-1a/CCL3 and -1b/CCL4 were also found secreted in lower amounts in primary hepatocyte culture supernatants from fatty liver compared to C57Bl6 supernatant with a reduction of 80% for MIP-1a/CCL3 and 50% for MIP-1b/CCL4 (figure 4.14 O and P). Abundance of these cytokines was similar between alb-SREBP-1c and aP2-SREBP-1c. IL-2, IL-3, IL-13 and IL-17 as well as G-CSF were not differentially secreted between the three phenotypes.

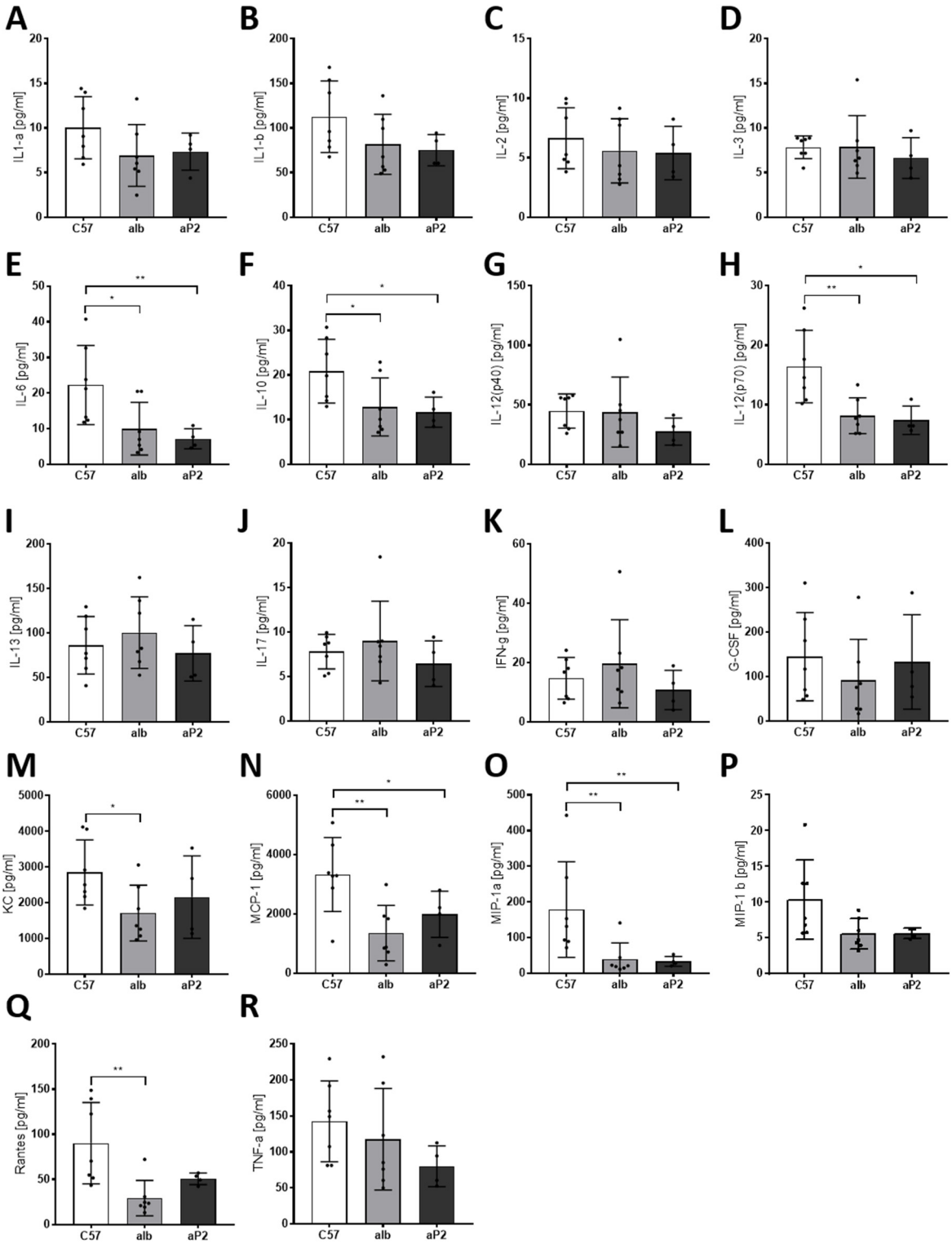

Figure 4.14: Cytokines released from primary hepatocytes in culture. Analysis of cytokine secretion from primary hepatocyte cultures of C57Bl6 (C57), alb-SREBP-1c (alb) and aP2-SREBP-1 (aP2) animals. Cells were incubated overnight in serum-free culture, supernatant was collected and processed for 23plex cytokine analysis. Bar graphs represent the mean ±SD of 4 to 7 independent experiments for each group. Differences between two groups were calculated using Mann-Whitney-U test. * $p < 0.05$ or ** $p < 0.01$ as indicated.

4.3.5.1.2 Serum cytokine composition in murine models of fatty liver

To determine whether the differences in hepatocellular secretion of cytokines also interfere with the systemic cytokine pattern, mouse serum was analyzed using an array of 40 different cytokines to identify differences in circulating cytokine composition between fatty liver mouse models and control animals. The cytokines with the highest abundance in the sera of all phenotypes were found to be soluble intercellular adhesion molecule-1 (sICAM/CD54), macrophage colony-stimulating factor (M-CSF)-1, complement component C5a (C5a) and tissue inhibitor of metalloproteinases (Timp)-1 (table 4.7). sICAM/CD54 had the highest abundance in sera from aP2-SREBP-1c mice with a pixel density of 107 ± 3.74 which was significantly different from the other two groups while the amount between C57Bl6 (pixel density 89 ± 4.03) and alb-SREBP-1c (pixel density 87 ± 2.6) was similar. In contrast, M-CSF serum level had 10% increase in both fatty liver mouse models compared to C57Bl6 samples but remained unchanged between alb-SREBP-1c and aP2-SREBP-1c. C57Bl6 serum contained the lowest abundance of C5a with a pixel density of 57 ± 2.31, intermediate values were found in alb-SREBP-1c animals (pixel density 68 ± 2.03) and highest C5a was measured in aP2-SREBP-1c (pixel density 89 ± 3.08). Differences between all groups were calculated with statistical significance (p<0.001). Timp-1 abundance in serum was not different between C57Bl6 and alb-SREBP-1c serum but showed a nearly 3-fold increase in aP2-SREBP-1c serum. Further factors known to be related to liver dysfunction and disease such as IFNγ showed similar abundance between C57Bl6 and alb-SREBP-1c sera (pixel density approx. 5) but showed a significant increase of up to 100% in comparison to aP2-SREBP-1c serum (pixel density 9.24 ± 1.07). MCP1/CCL2 and IL-6 showed highest amounts in alb-SREBP-1c animals with pixel intensities of 3.13 ± 0.09 (MCP-1) and 1.98 ± 0.06 (IL-6), significantly lower levels were found in the serum of aP2-SREBP-1c animals (pixel densities: MCP1 2.93 ± 0.11, IL-6 1.59 ± 0.17) and showed lowest abundance in C57Bl6 (pixel densities: MCP-1 2.03 ± 0.1, IL-6 0.82 ± 0.05) serum. TNFα was 2-fold increased in aP2-SREBP-1c animals compared to the two remaining groups but there was no significant difference between C57Bl6 and alb-SREBP-1c serum concentration of this cytokine.

Table 4.7: Serum cytokine analysis in mouse models for the study of fatty liver. Serum of C57Bl6, alb-SREBP-1c and aP2-SREBP-1c mice was analyzed for differences in cytokine abundance with the Proteome Profiler™ Array panel A from R&D Systems. Data are represented as mean ±SD from 6 animals per group. Statistical differences between all groups were analyzed using one-way ANOVA. Differences between two groups were analyzed using Mann-Whitney-U test; * $p < 0.05$ and ** $p < 0.01$ vs. C57Bl6, # $p < 0.05$ and ## $p < 0.01$ vs. alb-SREBP-1c.

Cytokine	C57Bl6 [pixel density]	alb-SREBP-1c [pixel density]	aP2-SREBP-1c [pixel density]	ANOVA p-value
sICAM-1/CD54	89.489 ± 4.026	87.053 ± 2.594	107.393 ± 3.737$^{**,\#\#}$	< 0.001
M-CSF	61.177 ± 2.535	66.269 ± 1.975**	68.742 ± 2.369**	< 0.001
C5a	56.664 ± 2.306	67.691 ± 2.031**	89.172 ± 3.076$^{**,\#\#}$	< 0.001
Timp-1	13.177 ± 0.613	13.520 ± 0.405	35.438 ± 1.273$^{**,\#\#}$	< 0.001
JE	12.209 ± 0.624	7.562 ± 0.440**	13.866 ± 0.556$^{**,\#\#}$	< 0.001
TREM-1	7.591 ± 0.510	6.309 ± 0.311**	7.027 ± 0.245$^{\#\#}$	< 0.001
KC	7.422 ± 0.274	6.445 ± 0.418**	10.362 ± 0.593$^{**,\#\#}$	< 0.001
IFN-γ	4.633 ± 0.507	4.985 ± 0.608	9.238 ± 1.065$^{**,\#\#}$	< 0.001
IL-13	4.069 ± 0.248	4.618 ± 0.359*	6.789 ± 0.331$^{**,\#\#}$	< 0.001
IL-16	3.962 ± 0.172	4.570 ± 0.136**	12.904 ± 0.570$^{**,\#\#}$	< 0.001
G-CSF	3.819 ± 0.181	4.304 ± 0.182**	4.846 ± 0.167$^{**,\#\#}$	< 0.001
MIP-2	3.266 ± 0.187	3.258 ± 0.118	4.994 ± 0.283$^{**,\#\#}$	< 0.001
IL1-a	3.166 ± 0.178	4.279 ± 0.147**	4.068 ± 0.162**	< 0.001
IL-4	2.870 ± 0.111	3.328 ± 0.117**	6.129 ± 0.248$^{**,\#\#}$	< 0.001
IL-1ra	2.257 ± 0.086	2.805 ± 0.110**	2.996 ± 0.165$^{**,\#}$	< 0.001
IL-2	2.253 ± 0.227	2.900 ± 0.309**	2.405 ± 0.167$^{\#\#}$	< 0.001
CCL1/TCA-3	2.241 ± 0.133	2.771 ± 0.083**	5.028 ± 0.182$^{**,\#\#}$	< 0.001
IP-10	2.229 ± 0.117	2.349 ± 0.124	5.708 ± 0.523$^{**,\#\#}$	< 0.001
MIG	2.168 ± 0.111	2.724 ± 0.101**	6.551 ± 0.258$^{**,\#\#}$	< 0.001
IL-17	2.102 ± 0.115	2.288 ± 0.093*	3.350 ± 0.281$^{**,\#\#}$	< 0.001
IL-7	2.093 ± 0.095	2.121 ± 0.070	4.807 ± 0.226$^{**,\#\#}$	< 0.001
MCP-1	2.032 ± 0.101	3.125 ± 0.094**	2.934 ± 0.109$^{**,\#}$	< 0.001
TNF-α	1.999 ± 0.074	2.093 ± 0.147	4.108 ± 0.141$^{**,\#\#}$	< 0.001
IL-23	1.933 ± 0.091	2.419 ± 0.075**	2.445 ± 0.140**	< 0.001
I-TAC	1.906 ± 0.081	1.983 ± 0.067	4.559 ± 0.164$^{**,\#\#}$	< 0.001
IL-27	1.723 ± 0.182	1.884 ± 0.256	2.920 ± 0.133$^{**,\#\#}$	< 0.001
Rantes	1.646 ± 0.107	2.132 ± 0.067**	2.945 ± 0.150$^{**,\#\#}$	< 0.001
CXCL13/BCA-1	1.560 ± 0.266	2.384 ± 0.303**	3.899 ± 0.627$^{**,\#\#}$	< 0.001
IL1- b	1.559 ± 0.067	1.725 ± 0.053**	2.441 ± 0.159$^{**,\#\#}$	< 0.001
MIP-1a	1.232 ± 0.072	1.601 ± 0.053**	3.110 ± 0.169$^{**,\#\#}$	< 0.001
IL-3	1.150 ± 0.126	1.642 ± 0.130**	3.494 ± 0.262$^{**,\#\#}$	< 0.001
Tarc	0.924 ± 0.166	1.452 ± 0.127**	1.915 ± 0.293$^{**,\#\#}$	< 0.001
IL-6	0.817 ± 0.052	1.983 ± 0.062**	1.590 ± 0.166$^{**,\#\#}$	< 0.001
SDF-1	0.637 ± 0.066	1.929 ± 0.170**	1.009 ± 0.062$^{**,\#\#}$	< 0.001
MIP-1b	0.611 ± 0.024	1.112 ± 0.041**	1.849 ± 0.064$^{**,\#\#}$	< 0.001
GM-CSF	0.603 ± 0.025	1.056 ± 0.057**	1.664 ± 0.072$^{**,\#\#}$	< 0.001
IL-5	0.431 ± 0.050	0.857 ± 0.108**	1.062 ± 0.058$^{**,\#\#}$	< 0.001
Eotaxin	0.424 ± 0.124	0.940 ± 0.239**	1.790 ± 0.226$^{**,\#\#}$	< 0.001
IL-12-p70	0.403 ± 0.118	0.766 ± 0.180**	1.546 ± 0.163$^{**,\#\#}$	< 0.001
IL-10	0.389 ± 0.056	0.849 ± 0.115**	1.284 ± 0.078$^{**,\#\#}$	< 0.001

4.4 Transcriptome analyses indicate genetic causes for fatty liver

The transcriptome analyses indicated differential gene regulation that can be confirmed by the observed physiological alterations in the primary hepatocytes of the models investigated. The differences in gene regulation can be mainly summarized in alterations in canonical pathways related to mitochondrial function, hepatic glucose and lipid metabolism for all comparisons analyzed. In table 4.8 the top canonical pathways identified by the enrichment of differentially expressed molecules for each comparison annotated to specific metabolic processes were listed. Mitochondrial dysfunction (C57Bl6 vs. alb-SREBP-1c: *p*-value 1.58 x 10^{-04}, C57Bl6 vs. aP2-SREBP-1c: 1.00 x 10^{-16}, alb-SREBP-1c vs. aP2-SREBP-1c: 3.31 x 10^{-10}) including SIRT signaling pathway (C57Bl6 vs. alb-SREBP-1c: 1.35 x 10^{-04}, C57Bl6 vs. aP2-SREBP-1c: 5.01 x 10^{-17}, alb-SREBP-1c vs. aP2-SREBP-1c: 6.31 x 10^{-12}) and oxidative phosphorylation (C57Bl6 vs. alb-SREBP-1c: 1.58 x 10^{-03}, C57Bl6 vs. aP2-SREBP-1c: 5.01 x 10^{-13}, alb-SREBP-1c vs. aP2-SREBP-1c: 2.19 x 10^{-07}) belonged to the top 10 canonical pathways identified with differential transcripts in all phenotypes. The number of deregulated genes from these pathways were found to be markedly higher in aP2-SREBP-1c liver tissue as there were only few genes affected when C57Bl6 and alb-SREBP-1c hepatic gene expression was compared. In alb-SREBP-1c versus C57Bl6 several functions regarding cholesterol metabolism like the super-pathway of cholesterol biosynthesis (*p*-value 2.82 x 10^{-04}) and cholesterol biosynthesis I to III (9.55 x 10^{-03} each) were found to be most likely affected by differential gene expression included in the top score list. EIF signaling known to be involved in insulin-induced ER stress was top score affected canonical pathway in differential gene expression when aP2-SREBP-1c was compared to the remaining models (C57Bl6 vs. aP2-SREBP-1c: 1.58 x 10^{-17}, alb-SREBP-1c vs. aP2-SREBP-1c: 3.98 x 10^{-15}). Further, pathways involved in hepatic lipid and glucose metabolism like mTOR signaling (C57Bl6 vs. aP2-SREBP-1c: 2.14 x 10^{-08}, alb-SREBP-1c vs. aP2-SREBP-1c: 1.91 x 10^{-08}), PPARα/RXRα (C57Bl6 vs. aP2-SREBP-1c: 3.09 x 10^{-03}, alb-SREBP-1c vs. aP2-SREBP-1c: 1.62 x 10^{-05}) or FXR/RXR activation (C57Bl6 vs. aP2-SREBP-1c: 7.41 x 10^{-06}, alb-SREBP-1c vs. aP2-SREBP-1c: 7.94 x 10^{-06}) were found to be potentially affected by large numbers of differentially regulated genes in aP2-SREBP-1c versus C57Bl6 or alb-SREBP-1c.

Table 4.8: Functional annotation of differentially expressed genes in fatty liver. Knowledge based analysis of differentially expressed genes in liver of C57Bl6, alb-SREBP-1c and aP2-SREBP-1c. Regulated pathways are shown individually for comparison of C57Bl6 vs. alb-SREBP-1c, C57Bl6 vs. aP2-SREBP-1c and alb-SREBP-1c vs. aP2-SREBP-1c which were scored according to *p*-value output for enrichment of canonical pathway molecules in the data set analyzed using IPA software. Amount of molecules differentially expressed for each pathway identified are given for each data comparison. n: number of molecules, nd: not determined.

C57Bl6 vs. alb-SREBP-1c						
Canonical Pathway	**C57Bl6 vs. alb-SREBP-1c**		C57Bl6 vs. aP2-SREBP-1c		alb-SREBP-1c vs. aP2-SREBP-1c	
	p-value	n	*p*-value	n	*p*-value	n
Sirtuin Signaling Pathway	1.35E-04	12	5.01E-17	89	6.31E-12	97
Mitochondrial Dysfunction	1.58E-04	9	1.00E-16	63	3.31E-10	63
Tryptophan Degradation III (Eukaryotic)	1.82E-04	4	4.79E-04	10	7.41E-05	13
Superpathway of Cholesterol Biosynthesis	2.82E-04	4	5.25E-03	9	1.32E-03	12
Glutaryl-CoA Degradation	7.59E-04	3	9.55E-03	6	2.63E-03	8
Oxidative Phosphorylation	1.58E-03	6	5.01E-13	43	2.19E-07	41
Dolichyl-diphosphooligosaccharide Biosynthesis	6.76E-03	2	3.80E-02	4	2.75E-02	5
Retinoate Biosynthesis I	6.92E-03	3	4.17E-01	5	3.66E-01	7
Pregnenolone Biosynthesis	8.13E-03	2	5.13E-02	4	3.41E-01	3
Complement System	8.91E-03	3	3.39E-02	7	4.27E-02	11
Heparan Sulfate Biosynthesis (Late Stages)	9.12E-03	4	1.65E-01	12	2.30E-01	15
Cholesterol Biosynthesis I	9.55E-03	2	6.76E-02	4	1.48E-02	6
Cholesterol Biosynthesis II (via 24, 25-dihydrolanosterol)	9.55E-03	2	6.76E-02	4	1.48E-02	6
Cholesterol Biosynthesis III (via Desmosterol)	9.55E-03	2	6.76E-02	4	1.48E-02	6
Mevalonate Pathway I	9.55E-03	2	6.76E-02	4	5.75E-02	5
Thyroid Hormone Metabolism II (via Conjugation and/or Degradation)	9.55E-03	3	1.00	4	1.00	6
2-amino-3-carboxymuconate Semialdehyde Degradation to Glutaryl-CoA	1.15E-02	1	1.24E-01	1	1.72E-01	1
Acetyl-CoA Biosynthesis III (from Citrate)	1.15E-02	1	1.24E-01	1	1.72E-01	1
Asparagine Biosynthesis I	1.15E-02	1	1.24E-01	1	1.72E-01	1
Glutamine Biosynthesis I	1.15E-02	1	nd		nd	
C57Bl6 vs. aP2-SREBP-1c						
Canonical Pathway	C57Bl6 vs. alb-SREBP-1c		**C57Bl6 vs. aP2-SREBP-1c**		alb-SREBP-1c vs. aP2-SREBP-1c	
	p-value	n	*p*-value	n	*p*-value	n
EIF2 Signaling	1.13E-01	5	1.58E-17	76	3.98E-15	87
Sirtuin Signaling Pathway	1.35E-04	12	5.01E-17	89	6.31E-12	97
Regulation of eIF4 and p70S6K Signaling	2.72E-01	3	1.23E-10	50	2.51E-11	62

Table 4.8 continued.

C57Bl6 vs. aP2-SREBP-1c						
Canonical Pathway	C57Bl6 vs. alb-SREBP-1c		**C57Bl6 vs. aP2-SREBP-1c**		alb-SREBP-1c vs. aP2-SREBP-1c	
	p-value	n	*p*-value	n	*p*-value	n
Mitochondrial Dysfunction	1.58E-04	9	1.00E-16	63	3.31E-10	63
mTOR Signaling	4.09E-01	3	2.14E-08	54	1.91E-08	67
Protein Ubiquitination Pathway	3.47E-02	7	2.29E-06	60	1.20E-07	80
Oxidative Phosphorylation	1.58E-03	6	5.01E-13	43	2.19E-07	41
Hypoxia Signaling in the Cardiovascular System	5.82E-01	1	2.04E-02	16	7.41E-07	31
FXR/RXR Activation	4.28E-01	2	7.41E-06	34	7.94E-06	42
PPARα/RXRα Activation	1.00	2	3.09E-03	39	1.62E-05	57
Cancer Drug Resistance By Drug Efflux	4.34E-01	1	1.48E-02	12	2.29E-05	21
Bile Acid Biosynthesis, Neutral Pathway	nd		3.09E-06	9	4.79E-05	9
Estrogen Receptor Signaling	4.36E-01	2	3.80E-03	27	6.92E-05	40
Tryptophan Degradation III (Eukaryotic)	1.82E-04	4	4.79E-04	10	7.41E-05	13
NRF2-mediated Oxidative Stress Response	3.82E-01	3	1.62E-04	42	1.07E-04	54
Thyroid Cancer Signaling	3.72E-01	1	7.94E-03	11	1.55E-04	17
Non-Small Cell Lung Cancer Signaling	5.92E-01	1	2.57E-02	16	3.16E-04	26
Glycine Betaine Degradation	nd		4.90E-04	6	3.24E-04	7
PXR/RXR Activation	1.73E-01	2	1.58E-06	23	3.24E-04	23
PEDF Signaling	nd		4.37E-03	20	4.68E-04	28
alb-SREBP-1c vs. aP2-SREBP-1c						
Canonical Pathway	C57Bl6 vs. alb-SREBP-1c		C57Bl6 vs. aP2-SREBP-1c		**alb-SREBP-1c vs. aP2-SREBP-1c**	
	p-value	n	*p*-value	n	*p*-value	n
EIF2 Signaling	1.13E-01	5	1.58E-17	76	3.98E-15	87
Sirtuin Signaling Pathway	1.35E-04	12	5.01E-17	89	6.31E-12	97
Mitochondrial Dysfunction	1.58E-04	9	1.00E-16	63	3.31E-10	63
Oxidative Phosphorylation	1.58E-03	6	5.01E-13	43	2.19E-07	41
Regulation of eIF4 and p70S6K Signaling	2.72E-01	3	1.23E-10	50	2.51E-11	62
mTOR Signaling	4.09E-01	3	2.14E-08	54	1.91E-08	50
LPS/IL-1 Mediated Inhibition of RXR Function	1.35E-02	7	9.12E-07	53	1.78E-02	50
PXR/RXR Activation	1.73E-01	2	1.58E-06	23	3.24E-04	23
Estrogen Biosynthesis	3.72E-01	1	1.95E-06	19	5.50E-04	18
Protein Ubiquitination Pathway	3.47E-02	7	2.29E-06	60	1.20E-07	80
Bile Acid Biosynthesis, Neutral Pathway	nd		3.09E-06	9	4.79E-05	9
FXR/RXR Activation	4.28E-01	2	7.41E-06	34	7.94E-06	42
Retinol Biosynthesis	3.78E-01	1	1.45E-05	16	2.34E-03	15
Stearate Biosynthesis I	1.41E-02	3	4.07E-05	16	1.29E-02	14
LXR/RXR Activation	1.32E-02	5	1.38E-04	30	3.72E-03	33
NRF2-mediated Oxidative Stress Response	3.82E-01	3	1.62E-04	42	1.07E-04	54

Table 4.8 continued.

alb-SREBP-1c vs. aP2-SREBP-1c						
Canonical Pathway	C57Bl6 vs. alb-SREBP-1c		C57Bl6 vs. aP2-SREBP-1c		**alb-SREBP-1c vs. aP2-SREBP-1c**	
	p-value	n	*p*-value	n	*p*-value	n
Ethanol Degradation II	3.34E-01	1	1.66E-04	13	3.89E-03	13
Triacylglycerol Degradation	1.17E-01	2	3.02E-04	16	8.71E-02	13
Tryptophan Degradation III	1.82E-04	4	4.79E-04	10	7.41E-05	13
Glycine Betaine Degradation	nd		4.90E-04	6	3.24E-04	7

However, in order to specify differential gene expression to either the genetic (alb-SREBP-1c) or the metabolic (aP2-SREBP-1c) fatty liver model, detailed analysis was applied to identify potential genetic causes for the development of fatty liver. In comparison of C57Bl6 versus alb-SREBP-1c 63 genes were identified to be differentially expressed solely for this comparison (figure 4.15). The differential regulated genes in the data sets responsible for the annotation to the specific canonical pathways were indicated as so-called leading genes (figure 4.15, table 4.9). Bioinformatical analysis identified several pathways to be regulated in the alb-SREBP-1c liver compared to C57Bl6 but it remains debatable whether this causes significant changes in cell metabolism as not more than 3 molecules per pathway were affected. In contrast, the overlap between the analysis of aP2-SREBP-1c to C57Bl6 and alb-SREBP-1c revealed the highest number of regulated genes with 2392 molecules identified (figure 4.15 (6)). Genes identified within this overlap represent genes differentially expressed specific for the metabolic phenotype of fatty liver and mostly annotated to metabolic function. The list of pathways affected by the aP2-SREBP-1c phenotype included among others the sirtuin signaling pathway (-log(*p*-value) 11.300), mitochondrial dysfunction (11.400), oxidative stress response (3.910) or oxidative phosphorylation (9.210) all identified with numerous leading genes affected (table 4.9). Genes differentially expressed restricted to the comparison aP2-SREBP-1c versus C57Bl6 (figure 4.15 (3)) and aP2-SREBP-1c versus alb-SREBP-1c (figure 4.15 (7)) were analyzed to be annotated to similar pathways like glucocorticoid receptor signaling (Venn pos. (3): -log(*p*-value) 0.345, Venn pos. (7): 1.330), mTOR signaling (Venn pos. (3): 1.830, Venn pos. (7): 1.420) or protein ubiquination pathway (Venn pos. (3): 0.661, Venn pos. (7): 2.850) but each comparison included a different set of genes of the nominated pathways to be differentially expressed between the respective phenotypes. These data underline markedly differences not only between metabolic development of fatty liver in the aP2-SREBP-1c model and C57Bl6 normal liver tissue but also between the two different fatty liver models.

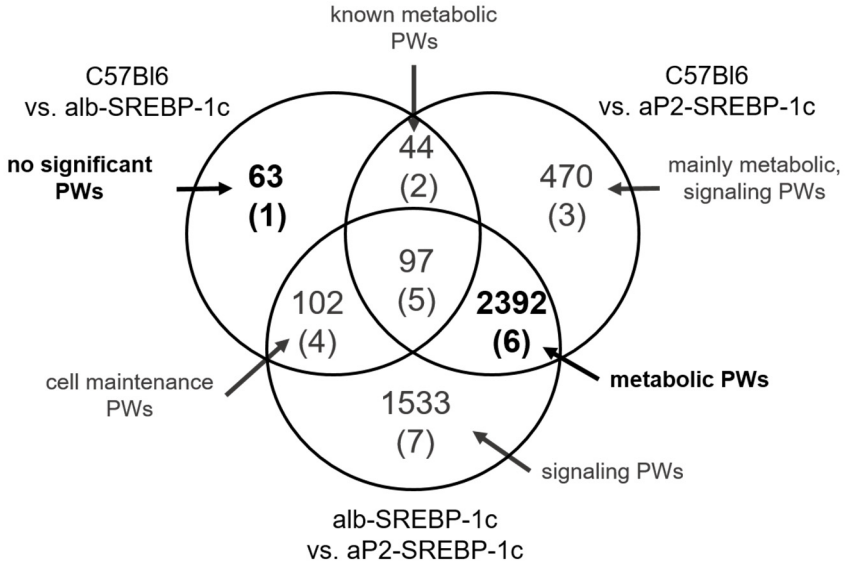

Figure 4.15: Analysis of hepatic transcriptome for changes specific to each fatty liver phenotype. Venn analysis of genes differentially expressed among all investigated groups and annotation to primarily affected pathways (also refer to table 4.9).

Table 4.9: Analysis of pathways annotated to differential gene expression found unique or overlapped in comparison of all study groups. Ingenuity pathway analysis was applied to genes differentially expressed between C57Bl6, alb-SREBP-1c and aP2-SREBP-1c and grouped according to unique or overlapped regulated expression for each comparison. Leading genes for pathways found related to differential gene expression were assigned to Venn analysis depicted in figure 4.15. n: number of leading genes involved in the respective pathway.

Venn Position (fig. 4.15)	Leading Genes (n)	% leading genes of total list of genes	Ingenuity Canonical Pathways	-log(p-value)	ratio	n
1	25	39.86	Aldosterone Signaling in Epithelial Cells	2.050	0.018	3
			Systemic Lupus Erythematosus Signaling	1.670	0.013	3
			Protein Ubiquitination Pathway	1.530	0.011	3
			Neuroinflammation Signaling Pathway	1.350	0.010	3
			Role of Macrophages, Fibroblasts and Endothelial Cells in Rheumatoid Arthritis	1.320	0.009	3
			Molecular Mechanisms of Cancer	1.100	0.008	3
			Complement System	2.400	0.054	2
			TR/RXR Activation	1.590	0.020	2
			Synaptic Long Term Potentiation	1.390	0.016	2
			Role of Tissue Factor in Cancer	1.360	0.015	2
			Phagosome Formation	1.360	0.015	2
			Adipogenesis pathway	1.340	0.015	2
			GNRH Signaling	1.150	0.012	2
			Role of NFAT in Regulation of the Immune Response	1.070	0.010	2
			Thrombin Signaling	1.000	0.010	2
			CREB Signaling in Neurons	0.975	0.009	2
			G-Protein Coupled Receptor Signaling	0.794	0.007	2
			Axonal Guidance Signaling	0.490	0.004	2
			Glutamine Biosynthesis I	2.600	1.000	1
			Thyronamine and Iodothyronamine Metabolism	2.120	0.333	1
2	24	54.54	Mitochondrial Dysfunction	5.050	0.029	5
			Protein Ubiquitination Pathway	2.020	0.011	3
			Sirtuin Signaling Pathway	1.900	0.010	3
			LPS/IL-1 Mediated Inhibition of RXR Function	2.230	0.014	3
			Oxidative Phosphorylation	3.100	0.028	3
			Systemic Lupus Erythematosus Signaling	1.240	0.009	2
			MIF Regulation of Innate Immunity	2.630	0.047	2
			T Helper Cell Differentiation	2.180	0.027	2

Table 4.9 continued.

Venn Position (fig. 4.15)	Leading Genes (n)	% leading genes of total list of genes	Ingenuity Canonical Pathways	-log(p-value)	ratio	n
2			MIF-mediated Glucocorticoid Regulation	2.810	0.057	2
			Nicotine Degradation II	2.280	0.031	2
			Stearate Biosynthesis I (Animals)	2.610	0.046	2
			Acetone Degradation I (to Methylglyoxal)	2.940	0.067	2
			TR/RXR Activation	0.822	0.010	1
			Triacylglycerol Degradation	1.070	0.019	1
			Melatonin Signaling	0.947	0.014	1
			Ephrin B Signaling	0.941	0.014	1
			GM-CSF Signaling	0.909	0.013	1
			LXR/RXR Activation	0.738	0.008	1
			Ephrin Receptor Signaling	0.588	0.006	1
			PPARα/RXRα Activation	0.573	0.005	1
3	171	36.38	Sirtuin Signaling Pathway	2.500	0.045	13
			LPS/IL-1 Mediated Inhibition of RXR Function	3.050	0.054	12
			Molecular Mechanisms of Cancer	0.714	0.025	10
			Xenobiotic Metabolism Signaling	1.310	0.034	10
			mTOR Signaling	1.830	0.044	9
			Colorectal Cancer Metastasis Signaling	1.000	0.032	8
			Protein Ubiquitination Pathway	0.661	0.026	7
			RAR Activation	1.200	0.037	7
			Glucocorticoid Receptor Signaling	0.345	0.020	7
			Mitochondrial Dysfunction	1.400	0.041	7
			EIF2 Signaling	0.894	0.031	7
			Neuroinflammation Signaling Pathway	0.291	0.019	6
			G-Protein Coupled Receptor Signaling	0.378	0.021	6
			Axonal Guidance Signaling	0.000	0.013	6
			RhoGDI Signaling	0.959	0.034	6
			Granulocyte Adhesion and Diapedesis	0.926	0.033	6
			Osteoarthritis Pathway	0.703	0.028	6
			cAMP-mediated signaling	0.610	0.026	6
			Cardiac Hypertrophy Signaling	0.544	0.025	6
			Protein Kinase A Signaling	0.000	0.015	6

Table 4.9 continued.

Venn Position (fig. 4.15)	Leading Genes (n)	% leading genes of total list of genes	Ingenuity Canonical Pathways	-log(p-value)	ratio	n
4	37	36.27	Actin Cytoskeleton Signaling	2.600	0.022	5
			Integrin Signaling	1.930	0.018	4
			Axonal Guidance Signaling	0.555	0.007	3
			Sirtuin Signaling Pathway	0.946	0.010	3
			Clathrin-mediated Endocytosis Signaling	1.290	0.015	3
			EIF2 Signaling	1.200	0.013	3
			Serotonin Degradation	2.430	0.039	3
			VEGF Signaling	2.010	0.028	3
			Role of Macrophages, Fibroblasts and Endothelial Cells in Rheumatoid Arthritis	0.433	0.006	2
			Retinoate Biosynthesis I	2.080	0.059	2
			Thyroid Hormone Metabolism II (via Conjugation and/or Degradation)	1.890	0.047	2
			Unfolded protein response	1.670	0.036	2
			Amyotrophic Lateral Sclerosis Signaling	1.130	0.018	2
			LXR/RXR Activation	1.070	0.017	2
			Glioblastoma Multiforme Signaling	0.834	0.012	2
			Acute Phase Response Signaling	0.802	0.011	2
			Ephrin Receptor Signaling	0.791	0.011	2
			Granulocyte Adhesion and Diapedesis	0.783	0.011	2
			RAR Activation	0.751	0.011	2
			Agranulocyte Adhesion and Diapedesis	0.740	0.010	2
5	29	29.89	Sirtuin Signaling Pathway	2.590	0.017	5
			Androgen Biosynthesis	1.350	0.071	1
			Glucocorticoid Biosynthesis	1.420	0.083	1
			Mineralocorticoid Biosynthesis	1.460	0.091	1
			Superpathway of Cholesterol Biosynthesis	4.000	0.107	3
			Tryptophan Degradation III (Eukaryotic)	2.530	0.080	2
			NRF2-mediated Oxidative Stress Response	0.868	0.010	2
			Xenobiotic Metabolism Signaling	0.605	0.007	2
			Protein Kinase A Signaling	0.428	0.005	2
			LPS/IL-1 Mediated Inhibition of RXR Function	0.792	0.009	2
			Mitochondrial Dysfunction	0.975	0.012	2

Table 4.9 continued.

Venn Position (fig. 4.15)	Leading Genes (n)	% leading genes of total list of genes	Ingenuity Canonical Pathways	-log(p-value)	ratio	n
5			EIF2 Signaling	0.777	0.009	2
			Cholesterol Biosynthesis I	3.100	0.154	2
			Cholesterol Biosynthesis II (via 24,25-dihydrolanosterol)	3.100	0.154	2
			Dolichyl-diphosphooligosaccharide Biosynthesis	3.250	0.182	2
			Cholesterol Biosynthesis III (via Desmosterol)	3.100	0.154	2
			Insulin Receptor Signaling	1.090	0.014	2
			Aldosterone Signaling in Epithelial Cells	0.376	0.006	1
			Protein Ubiquitination Pathway	0.238	0.004	1
			Glutaryl-CoA Degradation	1.300	0.063	1
6	876	36.85	Sirtuin Signaling Pathway	11.300	0.236	69
			EIF2 Signaling	16.700	0.300	68
			Axonal Guidance Signaling	0.702	0.112	51
			Protein Ubiquitination Pathway	4.900	0.185	49
			Mitochondrial Dysfunction	11.400	0.287	49
			Protein Kinase A Signaling	0.689	0.112	47
			Molecular Mechanisms of Cancer	0.874	0.117	46
			Regulation of eIF4 and p70S6K Signaling	10.500	0.282	46
			mTOR Signaling	6.510	0.217	45
			Xenobiotic Metabolism Signaling	1.970	0.142	42
			Glucocorticoid Receptor Signaling	0.906	0.119	41
			Role of Macrophages, Fibroblasts and Endothelial Cells in Rheumatoid Arthritis	0.868	0.119	40
			NRF2-mediated Oxidative Stress Response	3.910	0.186	37
			PPARα/RXRα Activation	2.870	0.172	36
			LPS/IL-1 Mediated Inhibition of RXR Function	2.680	0.162	36
			Breast Cancer Regulation by Stathmin1	2.260	0.156	35
			Neuroinflammation Signaling Pathway	0.532	0.109	34
			Cardiac Hypertrophy Signaling	1.280	0.133	34
			Phospholipase C Signaling	1.220	0.131	34
			Oxidative Phosphorylation	9.210	0.312	34

Table 4.9 continued.

Venn Position (fig. 4.15)	Leading Genes (n)	% leading genes of total list of genes	Ingenuity Canonical Pathways	-log(p-value)	ratio	n
7	439	28.63	Protein Ubiquitination Pathway	2.850	0.113	30
			Glucocorticoid Receptor Signaling	1.330	0.087	30
			Axonal Guidance Signaling	0.000	0.057	26
			Protein Kinase A Signaling	0.000	0.062	25
			Molecular Mechanisms of Cancer	0.000	0.061	24
			Role of Macrophages, Fibroblasts and Endothelial Cells in Rheumatoid Arthritis	0.000	0.063	22
			PPARα/RXRα Activation	2.470	0.118	22
			Clathrin-mediated Endocytosis Signaling	1.670	0.101	21
			ERK/MAPK Signaling	1.730	0.103	21
			G-Protein Coupled Receptor Signaling	0.486	0.071	20
			Huntington's Disease Signaling	0.786	0.080	20
			Sirtuin Signaling Pathway	0.415	0.069	20
			mTOR Signaling	1.420	0.097	20
			Osteoarthritis Pathway	1.110	0.090	19
			Cardiac Hypertrophy Signaling	0.727	0.079	19
			cAMP-mediated signaling	0.713	0.079	18
			Actin Cytoskeleton Signaling	0.659	0.077	18
			IL-8 Signaling	1.040	0.089	18
			ILK Signaling	1.140	0.091	18
			AMPK Signaling	0.857	0.083	18

As described above the most differentially regulated pathway genes were identified in the transcriptome of aP2-SREBP-1c liver tissue compared to either C57Bl6 or to the genetic fatty liver model alb-SREBP-1c. When these genes were annotated to biological functions highest significance levels for differential gene expression versus aP2-SREBP-1c were found annotated to lipid metabolism (*p*-values 8.98 x 10^{-16} – 3.26 x 10^{-3}), small molecule biochemistry (8.98 x 10^{-16} – 3.26 x 10^{-3}) and molecular transport (3.83 x 10^{-12} – 3.04 x 10^{-3}) including large sets of regulated genes (table 4.10). These pathways were also found regulated in the comparison of C57Bl6 versus alb-SREBP-1c but with markedly lower numbers of genes found to be regulated and subsequent lower statistical significance. Further, several molecules annotated to processes like differential gene expression (5.95 x 10^{-11} – 3.26 x 10^{-03}), cell signaling (5.66 x 10^{-06} – 1.59 x 10^{-03}), protein degradation (5.3 x 10^{-10} – 1.94 x 10^{-03}) or post-translational modification (8.98 x 10^{-08} – 2.24 x 10^{-03}) were identified to be uniquely regulated in comparisons including aP2-SREBP-1c.

However there are many examples that cooperative genes were either regulated to control or to the genetic model in aP2-SREBP-1c liver tissue a picture of fine regulation and interaction of genetic cause and metabolic interaction can be assigned to the investigation of fatty liver transcriptome. Figure 4.16 showed exemplarily the hierarchical cluster of diseases and biological functions with regard to lipid metabolism based on differential gene expression in the comparison of C57Bl6, alb-SREBP-1c and aP2-SREBP-1c. Pathways like concentration, oxidation, or conversion of lipids were annotated to differential gene expression in most comparisons applied to the data set, while lipidation of proteins or removal and clearance of lipids were restricted to differential gene expression between both fatty liver models. In contrast, several pathways including accumulation of lipids, morphology of lipid droplets or disorder of lipid metabolism were identified to be restricted to differential gene expression in aP2-SREBP-1c liver. Detailed illustrations of differential gene expression within the SCAP activation network, activation of bile acid biosynthesis or super-pathway of cholesterol metabolism were shown in figure 4.17 as examples for affected pathways of lipid metabolism and the interactive regulation within the three phenotypes. The SCAP activation network (figure 4.17 A) showed a small set of hepatic genes, namely trefoil factor (TFF) 3, methylsterol monoxygenase (MSMO) 1, isopentenyl-diphosphate delta isomerase (IDI) 1, farnesyl diphosphate farnesyl transferase (FDFT) 1 and ATP citrate lyase (ACLY) to be differentially regulated in all phenotypes. Interestingly MSMO1, IDI1 and FDFT1 were downregulated in alb-SREBP-1c while these genes were upregulated in aP2-SREBP-1c liver tissue. Except from these genes differentially expressed molecules belonging to the SCAP network were only found in aP2-SREBP-1c phenotype including ELOVL6, pyruvate dehydrogenase kinase (PDK) 1, SREBF2 or cytochrome b5 type A (CYB5A). Genes associated with activation of bile acid synthesis (figure 4.17 B) were

found to be differentially regulated restricted to the aP2-SREBP-1c phenotype while differences in NADP+ were found restricted to alb-SREBP-1c liver phenotype. The super-pathway of cholesterol metabolism (figure 4.17 C) also included MSMO1, IDI1 and FDFT1 regulated gene expression found in all phenotypes. Further differences in liver transcriptome related to cholesterol metabolism were found in several comparisons applied indicating that changes in this pathway were not unique to one phenotype.

Table 4.10: Analysis of regulated gene expression related to biological function. Bioinformatical analysis of genes differentially expressed related to aP2-SREBP-1c (aP2) liver phenotype (Venn position 6, figure 4.15, table 4.9) were compared to differential gene expression found in C57Bl6 (C57) vs. alb-SREBP-1c (alb) hepatic transcriptome. Analysis was restricted to annotation to biological function for differentially expressed genes in ingenuity pathway analysis. n: number of molecules

Category	*p*-value C57 vs alb	n	*p*-value C57 or alb vs. aP2 (Venn pos. 6)	n
Energy Production	3,01E-07-1,15E-02	15	1,53E-06-2,32E-03	97
Lipid Metabolism	3,01E-07-1,88E-02	60	8,98E-16-3,26E-03	340
Small Molecule Biochemistry	3,01E-07-1,88E-02	70	8,98E-16-3,26E-03	414
Vitamin and Mineral Metabolism	3,19E-07-1,15E-02	24	8,05E-06-6,37E-04	86
Molecular Transport	1,4E-05-1,78E-02	44	3,83E-12-3,04E-03	451
Post-Translational Modification	1,05E-04-1,26E-02	8	5,66E-06-1,94E-03	153
Gastrointestinal Disease	1,09E-04-1,56E-02	56	4,29E-08-3,26E-03	1664
Hepatic System Disease	1,09E-04-1,15E-02	25	4,29E-08-2,95E-03	142
Metabolic Disease	1,09E-04-1,56E-02	63	8,51E-18-3,26E-03	265
Organismal Injury and Abnormalities	1,09E-04-1,82E-02	137	8,9E-24-3,26E-03	1887
Amino Acid Metabolism	1,33E-04-1,43E-02	5	1,74E-07-3,26E-03	47
Cancer	1,33E-04-1,61E-02	41	8,9E-24-3,26E-03	1842
Digestive System Development and Function	1,33E-04-1,37E-02	10	1,01E-12-2,81E-03	158
Hepatic System Development and Function	1,33E-04-1,15E-02	3	1,01E-12-2,81E-03	113
Organ Morphology	1,33E-04-1,74E-02	16	1,01E-12-3,26E-03	204
Organismal Development	1,33E-04-1,37E-02	31	1,01E-12-3,11E-03	351
Tissue Morphology	1,33E-04-1,74E-02	46	1,11E-04-3,11E-03	282
Endocrine System Development and Function	1,71E-04-1,15E-02	11	2,32E-04-2,32E-03	84
Nucleic Acid Metabolism	3,09E-04-1,15E-02	12	5,55E-06-7,29E-04	93
Drug Metabolism	3,95E-04-1,15E-02	10	7,29E-04-3,26E-03	5
Cellular Function and Maintenance	5,01E-04-1,62E-02	36	2,61E-06-3,26E-03	152
Infectious Diseases	5,98E-04-1,15E-02	21	6,11E-13-3,26E-03	326
Inflammatory Disease	5,98E-04-1,32E-02	43	3,29E-04-3,26E-03	239
Respiratory Disease	5,98E-04-1,15E-02	10	2,11E-05-1,39E-04	53
Connective Tissue Disorders	7,34E-04-1,32E-02	49	3,82E-04-3,26E-03	202
Skeletal and Muscular Disorders	7,34E-04-1,78E-02	59	2,44E-06-3,26E-03	322
Cell Morphology	7,83E-04-1,58E-02	15	1,66E-05-2,81E-03	178
Free Radical Scavenging	7,83E-04-7,83E-04	2	1,98E-05-3,04E-03	115

Table 4.10 continued.

Category	*p*-value C57 vs alb	n	*p*-value C57 or alb vs. aP2 (Venn pos. 6)	n
Developmental Disorder	1,03E-03-1,15E-02	47	5,22E-08-3,26E-03	146
Hereditary Disorder	1,03E-03-1,78E-02	65	5,22E-08-3,26E-03	133
Cell Cycle	1,14E-03-1,8E-02	18	3,27E-04-3,26E-03	81
Connective Tissue Development and Function	1,25E-03-1,6E-02	30	2,39E-04-2,42E-03	241
Cellular Development	1,28E-03-1,44E-02	15	3,27E-04-3,26E-03	352
Cellular Growth and Proliferation	1,28E-03-1,32E-02	29	4,22E-04-3,26E-03	344
Hematological Disease	1,28E-03-1,61E-02	26	4,45E-05-2,64E-03	132
Immunological Disease	1,28E-03-1,74E-02	42	1,71E-03-3,26E-03	265
Tumor Morphology	1,28E-03-1,15E-02	8	8,9E-24-2,11E-08	108
Carbohydrate Metabolism	1,3E-03-1,26E-02	14	1,43E-06-3,26E-03	213
Endocrine System Disorders	1,37E-03-1,56E-02	35	2,36E-04-3,26E-03	100
Cell Death and Survival	1,93E-03-1,84E-02	24	8,9E-24-3,26E-03	716
Hematological System Development and Function	2,09E-03-1,84E-02	43	9,22E-04-2,25E-03	116
Neurological Disease	2,48E-03-1,89E-02	47	2,44E-06-3,26E-03	305
Renal and Urological Disease	2,5E-03-1,15E-02	22	1,63E-08-3,26E-03	76
Cellular Movement	2,6E-03-1,65E-02	31	1,08E-03-1,8E-03	22
Cell-To-Cell Signaling and Interaction	2,64E-03-1,62E-02	33	4,46E-05-3,26E-03	99
Inflammatory Response	2,64E-03-1,69E-02	56	3,29E-04-3,26E-03	287
Cellular Assembly and Organization	2,68E-03-1,15E-02	15	2,61E-06-3,26E-03	93
Embryonic Development	2,68E-03-1,15E-02	13	1,39E-04-3,11E-03	175
Skeletal and Muscular System Development and Function	2,68E-03-1,15E-02	6	1,53E-03-1,53E-03	12
Immune Cell Trafficking	2,71E-03-1,69E-02	25	2,25E-03-2,25E-03	58
Cell-mediated Immune Response	3,72E-03-1,65E-02	6	nd	
Cardiovascular System Development and Function	3,97E-03-1,15E-02	9	nd	
Ophthalmic Disease	3,97E-03-1,15E-02	10	3,89E-04-3,89E-04	4
Visual System Development and Function	3,97E-03-3,97E-03	4	1,08E-03-1,08E-03	4
Reproductive System Disease	4,18E-03-1,53E-02	23	9,12E-05-3,26E-03	58
Organismal Functions	4,36E-03-1,15E-02	10	4,17E-04-4,17E-04	12
Tissue Development	4,52E-03-1,69E-02	20	1,39E-04-2,79E-03	125
Cardiovascular Disease	4,89E-03-1,82E-02	30	1,66E-04-6,01E-04	89
Cellular Compromise	5,61E-03-1,8E-02	12	1,11E-04-1,34E-03	115
Nervous System Development and Function	8,82E-03-1,15E-02	10	3,81E-04-2,64E-03	33
Hematopoiesis	9,03E-03-1,42E-02	12		
Protein Trafficking	9,03E-03-9,03E-03	6	5,22E-09-1,28E-04	119
Organ Development	1,1E-02-1,15E-02	7	6,36E-06-3,26E-03	96
Respiratory System Development and Function	1,1E-02-1,26E-02	3	5,63E-04-2,79E-03	51
Lymphoid Tissue Structure and Development	1,13E-02-1,74E-02	27	1,53E-03-1,53E-03	70
Antimicrobial Response	1,15E-02-1,15E-02	1	2,38E-03-3,26E-03	39

Table 4.10 continued.

Category	*p*-value C57 vs alb	n	*p*-value C57 or alb vs. aP2 (Venn pos. 6)	n
DNA Replication, Recombination, and Repair	1,15E-02-1,15E-02	1	3,47E-04-3,12E-03	136
Dermatological Diseases and Conditions	1,15E-02-1,26E-02	3	2,75E-05-2,66E-03	177
Hair and Skin Development and Function	1,15E-02-1,15E-02	1	8,79E-04-2,55E-03	10
Humoral Immune Response	1,15E-02-1,15E-02	1	nd	
Nutritional Disease	1,15E-02-1,57E-02	15	1,49E-03-1,49E-03	48
Protein Synthesis	1,15E-02-1,15E-02	1	3,2E-20-3,26E-03	393
Psychological Disorders	1,15E-02-1,78E-02	22	1,43E-04-3,26E-03	154
Reproductive System Development and Function	1,15E-02-1,39E-02	8	4,22E-04-1,71E-03	29
Organismal Survival	1,81E-02-1,81E-02	56	7,59E-05-7,61E-05	423
Gene Expression	nd		5,95E-11-3,26E-03	389
Cell Signaling	nd		5,66E-06-1,59E-03	41
RNA Post-Transcriptional Modification	nd		8,98E-08-2,24E-03	75
Protein Degradation	nd		5,3E-10-1,94E-03	139
RNA Trafficking	nd		3,26E-03-3,26E-03	3
Renal and Urological System Development and Function	nd		1,05E-04-3,26E-03	92
Auditory Disease	nd		1,08E-03-1,08E-03	4

Figure 4.16: Phenotype specific differential gene expression in fatty liver lipid metabolism. Data for differential gene expression in the comparisons C57Bl6 vs. alb-SREBP-1c, C57Bl6 vs. aP2-SREBP-1c, and alb-SREBP-1c vs. aP2-SREBP-1c were processed in Venn analyses to identify regulation specific transcripts as indicated in Figure 4.15. All sections (1-7) of figure 4.15 were used for core analyses (IPA) and compared for functional specifics. Data were screened for functional downstream actions on lipid metabolism and presented as hierarchical cluster based on *p*-value of enrichment. Numbering according to figure 4.15 Venn diagram sections: 1 - (1) specific for the comparison C57Bl6 vs. alb-SREBP-1c; 2 - (2) intersection C57Bl6 vs. alb-SREBP-1c or aP2-SREBP-1c: *p*-values according to C57Bl6 vs. alb-SREBP-1c; 3 - (2) intersection C57Bl6 vs. alb-SREBP-1c or aP2-SREBP-1c: *p*-values according to C57Bl6 vs aP2-SREBP-1c; 4 - (3) specific for the comparison C57Bl6 vs aP2-SREBP-1c; 5 - (4) intersection alb-SREBP-1c vs. C57Bl6 or aP2-SREBP-1c: *p*-values according to C57Bl6 vs. alb-SREBP-1c; 6 - (4) intersection alb-SREBP-1c vs. C57Bl6 or aP2-SREBP-1c: *p*-values according to alb-SREBP-1c vs. aP2-SREBP-1c; 7 - (5) common transcripts, *p*-values according to C57Bl6 vs. alb-SREBP-1c; 8 - (5) common transcripts, *p*-values according to C57Bl6 vs. aP2-SREBP-1c; 9 - (5) common transcripts, *p*-values according to alb-SREBP-1c vs. aP2-SREBP-1c; 10 - (6) intersection C57Bl6 or alb-SREBP-1c vs. aP2-SREBP-1c: *p*-values according to C57Bl6 vs. aP2-SREBP-1c; 11 - (6) intersection C57Bl6 or alb-SREBP-1c vs. aP2-SREBP-1c: *p*-values according to alb-SREBP-1c vs. aP2-SREBP-1c; 12 - (7) specific for the comparison alb-SREBP-1c vs. aP2-SREBP-1c

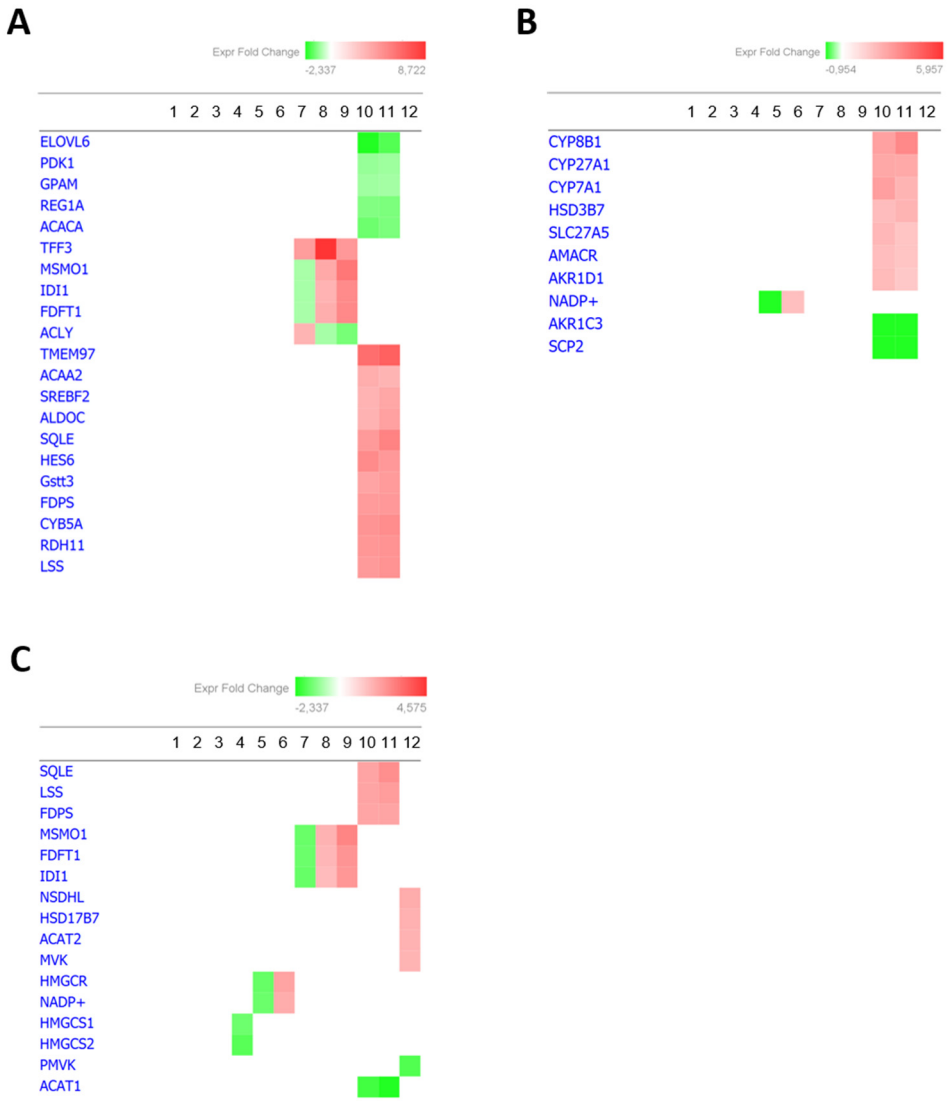

Figure 4.17: Phenotype specific differential gene expression in fatty liver SREBP cleavage activating protein (SCAP) interacting networks, bile acid biosynthesis and super-pathway of cholesterol biosynthesis. Data for differential gene expression in the comparisons C57Bl6 vs. alb-SREBP-1c, C57Bl6 vs. aP2-SREBP-1c, and alb-SREBP-1c vs. aP2-SREBP-1c were processed in Venn analyses to identify regulation specifics as indicated in figure 4.15. All sections (1-7) of figure 4.15 were used for core analyses (IPA) and compared for functional specifics. Exemplified hierarchical clusters are given for (A) SCAP interacting networks, (B) activation of bile acid synthesis, or (C) super-pathway of cholesterol synthesis. Color code: red - increase in condition 1, green - decrease in condition 1 based on measured expression differences. Numbering according to Figure 4.15 Venn diagram sections: 1 - (1) specific for the comparison C57Bl6 vs. alb-SREBP-1c; 2 - (2) intersection C57Bl6 vs. alb-SREBP-1c or aP2-SREBP-1c: *p*-values according to C57Bl6 vs. alb-SREBP-1c; 3 - (2) intersection C57Bl6 vs. alb-SREBP-1c or aP2-SREBP-1c: *p*-values according to C57Bl6 vs aP2-SREBP-1c; 4 - (3) specific for the comparison C57Bl6 vs aP2-SREBP-1c; 5 - (4) intersection alb-SREBP-1c vs. C57Bl6 or aP2-SREBP-1c: *p*-values according to C57Bl6 vs. alb-SREBP-1c; 6 - (4) intersection alb-SREBP-1c vs. C57Bl6 or aP2-SREBP-1c: *p*-values according to alb-SREBP-1c vs. aP2-SREBP-1c; 7 - (5) common transcripts, *p*-values according to C57Bl6 vs. alb-SREBP-1c; 8 - (5) common transcripts, *p*-values according to C57Bl6 vs. aP2-SREBP-1c; 9 - (5) common transcripts, *p*-values according to alb-SREBP-1c vs. aP2-SREBP-1c; 10 - (6) intersection C57Bl6 or alb-SREBP-1c vs. aP2-SREBP-1c: *p*-values according to C57Bl6 vs. aP2-SREBP-1c; 11 - (6) intersection C57Bl6 or alb-SREBP-1c vs. aP2-SREBP-1c: *p*-values according to alb-SREBP-1c vs. aP2-SREBP-1c; 12 - (7) specific for the comparison alb-SREBP-1c vs. aP2-SREBP-1c

4.5 Hepatokine patterns of primary hepatocytes differ according to fatty liver progression

Transcriptome analysis of liver tissue from the genetic and lipodystrophic model compared to normal liver tissue revealed that genetic changes were specific for each fatty liver phenotype. Consistent with analysis of differences in hepatic gene expression was the equivalent or even improved function of primary hepatocytes in *ex vivo* analysis of the alb-SREBP-1c model which exhibited a mild phenotype of fatty liver due to genetic manipulation by the well-known regulator of lipid metabolism. In contrast, the metabolic phenotype, which developed fatty liver due to ectopic accumulation without genetic manipulation of the liver was identified to display significantly impaired function of lipid and glucose breakdown as well as insulin signaling and energy production. In order to find predictors of pathological hepatic steatosis the secretome of primary hepatocytes was analyzed.

4.5.1 Interrelations due to differential gene expression

Subsequent regulator effect analysis (table 4.11) from knowledge-based database summarized the potential networks identified to be affected with hepatic differential gene expression. The most consistent regulation of genes was found for inflammatory responses when C57Bl6 versus alb-SREBP-1c hepatic gene expression was compared. Several cytokines or genes described to be involved in immune response like chemokine (C-X-C motif) ligand (CXCL) 10, KC/CXCL1, LCN2, CD59, CD74 or MYC regulated via myeloid differentiation primary response gene (MYD) 88, IL1B, IL27 or colony stimulating factor (CSF) were identified as top score networks directionally consistent with knowledge database. Differential gene expression between C57Bl6 and aP2-SREB-1c showed high consistency scores for regulator networks downstream from transcription factor (TF) EB (consistency score 6.718), SIRT6 (5.578), insulin receptor (INSR, 2.593) or mitogen-activated protein kinase (MAPK) 9 (2.593) annotated to organ degeneration and impaired lipid metabolism. Further genes involved in glucose metabolism were consistently regulated with literature like fibroblast growth factor (FGF) 21, ketohexokinase (KHK), glucose-6-phosphatase (G6PC) or pyruvate kinase liver and red blood cell (PKLR) within the MLX interacting protein-like (MLXIPL/ChREBP) network (-13.416). Within the top score network, effects between alb-SREBP-1c and aP2-SREBP-1c were based on differentially expressed genes of cholesterol metabolism, inflammatory response or fatty acid metabolism which included the regulators EIF4E (8.598), FOXO1 (8.598), SIRT6 (7.483), NK2 homeobox (NKX2) 3 (-14) or interferon regulatory factor (IRF) 7 (-23.085). However, in comparison of the two fatty liver models the top score regulator network between alb-SREBP-1c and aP2-SREBP-1c was insulin-like growth factor (IGFBP) 2 annotated among others to insulin sensitivity and carbohydrate synthesis (10.436).

The IGFPB2 protein itself is specifically less present in aP2-SREBP-1c mice, as well as genes that were classified from the knowledge based information available for analyses as involved in IGFBP2 signaling (figure 4.18). Those were either less present in aP2-SREBP-1c mice compared to controls or alb-SREBP-1c mice like signaling molecules AKT1, signal transducer and activator of transcription (STAT) 3 or growth factor receptors like GHR or EGFR, whereas e.g. lipid elongase ELOVL6 was more abundant in aP2-SREBP-1c (figure 4.18). If further molecules are considered together that were either experimentally detected or predicted to interact with IGFBP2 with high probability, the comparisons show the clearly different regulation of the IGFBP2 network in the datasets (figure 4.19).

The transcriptome analysis revealed that in comparison of different fatty liver models next to metabolic pathways, intracellular signaling pathways were affected, that directly depend on the activation and abundance of endocrine acting signaling molecules, e.g. derived from the IGF system. It is therefore reliable, that secreted hepatokines from the diseased cell models might show specific secretion profiles to manifest or counteract the metabolic state.

Table 4.11: Summary of top score regulator effect networks from transcriptome analysis of C57Bl6, alb-SREBP-1c and aP2-SREBP-1c liver tissue. Data sets were analyzed with knowledge based Ingenuity® Pathway Analysis (IPA) software to identify most consistent networks of regulated gene expression found in comparison of C57Bl6 vs. alb-SREBP-1c or aP2-SREBP-1c as well as alb-SREBP-1c vs. aP2-SREBP-1c.

C57Bl6 vs. alb-SREBP-1c			
Regulators	Target Molecules in Dataset	Diseases & Functions	Consistency Score
CSF2, CSF3, EPO, IL1B, MYD88, TNF	C3AR1, CD59, CD74, CXCL10, CXCL13, Ear2 (includes others), F2R, LCN2, LY96, MYC, RNASE2, SAA1, SNAP23, SPP1, UCP2, USP2	Endocytosis by eukaryotic cells, Homing of leukocytes, Internalization of cells, Phagocytosis of cells, Quantity of metal ion, Response of myeloid leukocytes	17.5
IL27, MYD88	CD74, CISH, CXCL10, MYC, RORC, SAA1, SPP1	Activation of blood cells, Hepatocellular carcinoma, Phagocytosis of cells	4.536
AKT1	CD74, CISH, CXCL10, LCN2, SPP1	Activation of blood cells	-4.919
TP53	CD59, F2R, FOXO3, GNA14, MYC, SPP1	Quantity of metal ion	-11.023
CSF2	CD74, CKS1B, CXCL10, F2R, LY96, MYC, SNAP23, SPP1	Organismal death	-14.496
C57Bl6 vs. aP2-SREBP-1c			
Regulators	Target Molecules in Dataset	Diseases & Functions	Consistency Score
TFEB	ARSB, ATP6V0C, CDH1, CLCN7, CTSA, MCOLN1, NAGLU, PSAP	Degeneration of central nervous system, Organ Degeneration, Organismal death, Size of body	6.718
26s Proteasome, SIRT6, TFEB	AKT1, ATG7, CLCN7, EGFR, FASN, G6PC, HSD3B1, IRS2, LSS, MAP1LC3B, NAGLU, PPARGC1A, PSAP, SOD2, SQSTM1, SREBF2, TOP2A	Biosynthesis of nucleoside triphosphate, Biosynthesis of purine ribonucleotide, Degeneration of nervous system, Disorder of lipid metabolism, Synthesis of terpenoid	5.578
INSR, MAPK9, PCGEM1	ACLY, BAK1, FASN, FDFT1, FDPS, IDI1, IFITM2, IFNA4, IFNB1, LEPR, LSS, MDM2, MMP9, PLA1A, RPS16, SCP2, SQLE, SREBF2	Metabolism of membrane lipid derivative, Replication of Influenza A virus	2.593
MYC	CASP8, EGR1, GFER, MMP9, Mt2, NFATC3, STAT3	Regeneration of liver	1.89
IFNA2, SUMO3	AGT, FAS, GOT1, HLA-A, IRS1, LYN, PLSCR1, XBP1	Metabolism of phosphatidic acid, Synthesis of carbohydrate, Synthesis of phospholipid	1.768
MLXIPL	FGF21, G6PC, KHK, PKLR, SLC2A2	Metabolism of carbohydrate	-13.416
SYVN1	IFITM2, PTPRJ, RPL18, ZC3HAV1	Infection of embryonic cell lines	-14
Akt	ATG7, CDH1, CXCL12, EGFR, FAS, HES1, LCN2, MDM2, MMP9, NR0B2, PCK1	Infection of tumor cell lines	-16.885
PEBP1	ACACA, ACLY, ELOVL6, FASN, PRKAR2B	Fatty acid metabolism	-20.125
ESR1	ARSG, EGFR, ERBB3, SP4	Quantity of Purkinje cells	-22

Table 4.11 continued.

alb-SREBP-1c vs. aP2-SREBP-1c			
Regulators	Target Molecules in Dataset	Diseases & Functions	Consistency Score
IGFBP2	AKT1, ARRB2, EFEMP1, EGFR, FN1, GHR, ITGA5, MYC, NUP210, STAT3	Anemia, Cell viability of tumor cell lines, Expression of RNA, Insulin sensitivity, Synthesis of carbohydrate, Transcription, Viral Infection	10.436
TFEB	ARSB, CLCN7, CTSA, MCOLN1, NAGLU, PSAP, TPP1	Ataxia, Autophagy, Degeneration of cells, Degeneration of central nervous system, Organ Degeneration, Size of body, Tremor	9.071
ATF4, CYP3A, EIF4E, FOXO1, HRAS, IFNA2, LGR4, NR0B2	ABCA1, ABCB11, AKT1, AMACR, APOM, ATXN1, CANX, CD36, CNP, CTSS, CTSV, CYP27A1, CYP7A1, CYP7B1, CYP8B1, EP300, HIF1A, HNF1A, IL22, IRF9, LPL, MAVS, NPC1, PLTP, PPARGC1A, PRNP, PSEN1, RHOA, S1PR3, SLC1A2, SOD1, SOD2, STAT3, TBP, TP53, TSPO, XBP1, ZPR1	Cholesterol transport, Degeneration of nervous system, Efflux of sterol, Flux of cholesterol, Synthesis of bile acid	8.598
SIRT6	AKT1, ALG12, ELOVL6, FABP6, G6PC, HMGCR, IRS2, LSS, MAPK3, PIGC, PPARGC1A, RPL6, SOD2, SREBF2	Cell viability, Dysglycemia, Insulin sensitivity, Metabolism of cholesterol, Organismal death, Synthesis of lipid	7.483
MUC1, NR0B2	ABCA1, ABCB11, ACACA, ACLY, AGT, APOM, CCND2, CD36, CDH1, CDKN1B, CEL, CYP7A1, CYP7B1, CYP8B1, EGLN3, EGR1, G6PC, HIF1A, HMGCR, HNF1A, HNF4A, MYC, PCK1, PPARGC1A, SOD1, SOD2	Biosynthesis of nucleoside triphosphate, Biosynthesis of purine ribonucleotide, Growth Failure, Hepatic steatosis, Synthesis of lipid, Transactivation	5.883
MAPK1	ATP1B1, CCNB1, PML, SAMHD1, TP53	Metabolism of nucleoside triphosphate	-13.416
NKX2-3	CD36, FAR2, GHR, MMP7, MYD88, PHGDH, PLA1A, PLD1, PLSCR1	Fatty acid metabolism	-14
SYVN1	IFITM2, PTPRJ, RPL18, ZC3HAV1	Infection of kidney cell lines	-14
IRF7	DDX58, IFNA4, IFNB1, IRF5, IRF9, Irgm1, ITGAX, Mx1/Mx2, S100A8, USP18	Inflammation of organ	-23.085
TRIM24	DDX58, FBN1, Igtp, IRF7, IRF9, MOV10, OASL, PARP12, SOCS2, SPP1, TAP1	Replication of RNA virus	-44.925

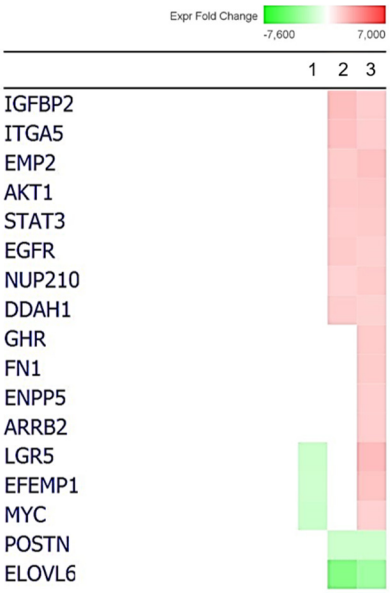

Figure 4.18: Hierarchical cluster of IGFBP2 interacting genes. Genes with differential gene expression (1.5-fold, *p*-value < 0.05) were used for IPA core analyses. Genes in the IGFBP2 network (Ingenuity knowledge database) were analyzed for differential expression in the comparisons (1) C57Bl6 vs. alb-SREBP-1c, (2) C57Bl6 vs. aP2-SREBP-1c and (3) alb-SREBP-1c and aP2-SREBP-1c and presented as heatmap. Color code: red - increase in condition 1, green - decrease in condition 1 based on measured expression differences.

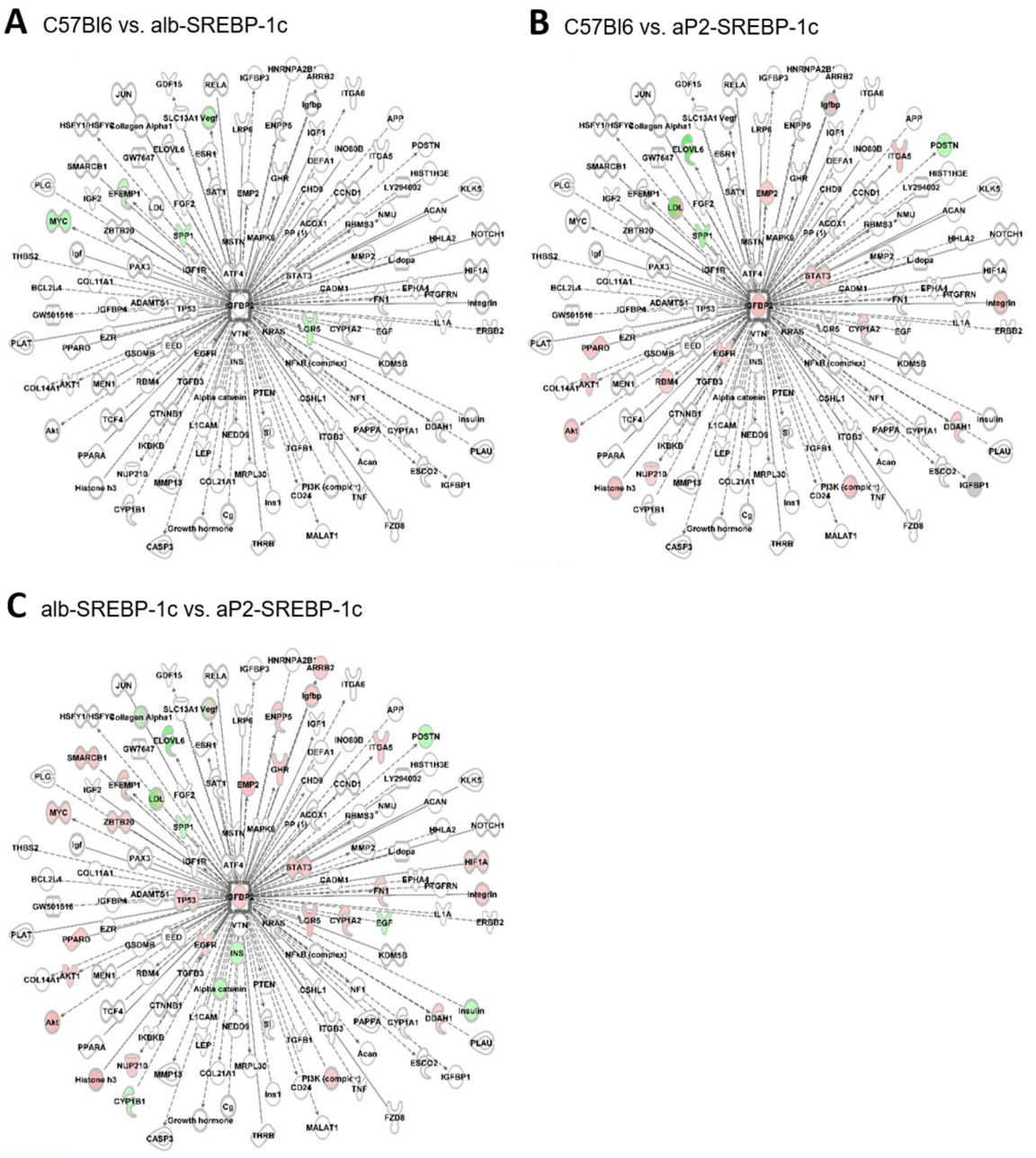

Figure 4.19: Differential regulation of IGFBP2-centered genes in the comparisons C57Bl6 vs. alb-SREBP-1c, C57Bl6 vs. aP2-SREBP-1c, and alb-SREBP-1c vs. aP2-SREBP-1c. Genes with differential gene expression (1.5-fold, p-value < 0.05) were used for IPA core analyses. Genes in the IGFBP2 network with differential expression in the comparisons (A) C57Bl6 vs. alb-SREBP-1c, (B) C57Bl6 vs. aP2-SREBP-1c, and (C) alb-SREBP-1c vs. aP2-SREBP-1c are highlighted. Color code: red - increase in condition 1, green - decrease in condition 1 based on measured expression differences. Solid lines indicate experimental proven interactions, whereas dotted lines indicate a highly predicted interaction (Ingenuity knowledge database).

4.5.2 Analysis of hepatokines by secretome analyses

Analysis of hepatokines was investigated in supernatants of primary hepatocyte culture. Primary hepatocytes were isolated from liver tissue of each model organism and cultured for 24 h in serum-free medium. Then, secretome was analyzed in mass spectrometry to identify proteins differentially secreted between hepatocytes from normal liver tissue (C57Bl6) and from fatty liver (alb-SREBP-1c/aP2-SREBP-1c). Top 10 differentially increased or decreased secreted proteins from pairwise analysis of the investigated phenotypes were listed in tables 4.12 to 4.14.

Consistent with the idea that alterations in lipid transporting mechanisms are one potential cause of hepatic lipid accumulation independent the pathogenesis, proteins involved in lipid transport were differentially secreted. Even within the top 10 regulated differential secreted proteins, apolipoproteins and fatty acid binding proteins were present. In detail, the apolipoproteins (Apo) A2 (fold change -1.729), ApoA5 (-1.505), ApoC3 (-1.718), ApoC4 (-1.633) and ApoF (-1.597) were increased in alb-SREBP-1c compared to controls. The comparison C57Bl6 versus aP2-SREBP-1c indicated decreased ApoA1 (1.528), ApoC1 (1.91) ApoM (1.599) and FABP5 (2.235) and increased ApoA4 (-1.622) as well as the fatty acid binding proteins FABP2 (-1.5) and FABP4 (-1.667). The comparison of the fatty liver models showed an increase in ApoA4 (-1.958) and FABP4 (-2.239) in aP2-SREBP-1c animals whereas ApoA1 (1.794), ApoA2 (1.714), ApoC1 (2.553), ApoC4 (2.085), lipocalin like ApoM (1.952) and the structural similar PON-1 (1.726), as well as FABP5 (2.031) were increased in alb-SREBP-1c animals indicating specific alterations in lipoprotein particles and thus transport.

In comparison of C57Bl6 with alb-SREBP-1c several keratins (Krt) like 16 (-4.91), 17 (-2.91), 19 (-7.58) were found increased in supernatants of alb-SREBP-1c hepatocytes. Further acetyl-coenzyme A synthetase (Acss2, -4.82) a major enzyme in fatty acid metabolism was found to be secreted at higher levels in alb-SREBP-1c compared to C57Bl6 hepatocytes. Decreased release of proteins related to mitochondrial function like subunits of ATP synthase subunit gamma (Atp5f1c, 5.46) or NADH dehydrogenase iron-sulfur protein 8 (Ndufs8, 3.66) were found in alb-SREBP-1c compared to C57Bl6. Also 26S proteasome regulatory subunit 6B (Psmc4, 2.73) and signal recognition particle 14kDa protein (Srp14, 4.58) were among the top score secreted hepatokines at decreased amounts from alb-SREBP-1c hepatocytes. Analysis of differential secretion between C57Bl6 and aP2-SREBP-1c also included Krt 16 (-6.06) and 19 (-5.77) in the list of top upregulated proteins in the supernatant of aP2-SREBP-1c. In this comparison several components related to fatty acid metabolism were found to be secreted in higher amounts from aP2-SREBP-1c like acyl-coenzyme A thioesterase (Acot) 3 (-4.31) and 4 (-4.81),

Acss2 (-4.53) or phospholipid transfer protein (Pltp, -4.30). Also in this comparison, proteins related to mitochondrial function were included in the top list of differentially secreted proteins namely Atp5f1c (3.64) and Ndufs8 (4.37). Further IGFBP2 (2.25) was released in 2-fold decreased amounts from aP2-SREBP-1c hepatocytes compared to C57Bl6. IGFBP2 was also found as one of the top five proteins with decreased amounts in supernatants of aP2-SREBP-1c hepatocytes when compared to alb-SREBP-1c (3.19). In comparison of alb-SREBP-1c to aP2-SREBP-1c similar proteins were found in the top upregulated protein lists when compared to the analysis of aP2-SREBP-1c versus C57Bl6 including Acot 1 (-3.44) and 3 (-3.44) and Ndufs5 (-3.66). Further, among the top downregulated hepatokines from aP2-SREBP-1c dereased secretion was identified for different fibrinogen chains (Fga (2.82), Fgb (3.65) and Fgg (3.79)) compared to alb-SREBP-1c.

Table 4.12: Top ranking hepatokines differentially secreted from primary hepatocytes in the comparison of C57Bl6 vs. alb-SREBP-1c. Proteins with top score fold-changes and *p*-values for increased or decreased concentration in primary hepatocyte culture supernatant are shown (cut-off values: > 1.5-fold regulation; *p*-value < 0.05, ANOVA). ID as defined by UniProt with annotation of genes according to IPA analyses ready molecules. *q*-value calculated from false discovery rate (FDR) analysis.

ID	Protein Descriptions	Fold Change	FDR (*q*-value)	UniProt ID	Genes	Peptides identified (n)
increased secretion from alb-SREBP-1c						
P19001	Keratin, type I cytoskeletal 19	-7.58	5,04E-01	P19001	Krt19	1
Q78PG9	Coiled-coil domain-containing protein 25	-7.00	3,16E-01	Q78PG9	Ccdc25	2
Q9Z2K1	Keratin, type I cytoskeletal 16	-4.91	1,96E-01	Q9Z2K1	Krt16	5
Q9QXG4	Acetyl-coenzyme A synthetase, cytoplasmic	-4.82	1,83E-01	Q9QXG4	Acss2	11
P97765	WW domain-binding protein 2;Isoform 2 of WW domain-binding protein 2	-3.67	2,93E-01	P97765;P97765-2	Wbp2	1
Q8VII3	Cystatin-14	-3.40	8,41E-02	Q8VII3	Cst14	1
Q6ZQ06	Centrosomal protein of 162 kDa	-3.20	3,16E-02	Q6ZQ06	Cep162	2
Q921E6	Polycomb protein EED;Isoform 2 of Polycomb protein EED;Isoform 3 of Polycomb protein EED	-3.16	9,65E-02	Q921E6;Q921E6-2;Q921E6-3	Eed	1
Q9QWL7	Keratin, type I cytoskeletal 17	-2.91	1,68E-01	Q9QWL7	Krt17	6
Q9QVP9	Protein-tyrosine kinase 2-beta	-2.81	1,18E-02	Q9QVP9	Ptk2b	1
decreased secretion from alb-SREBP-1c						
Q8R2U6	Diphosphoinositol polyphosphate phosphohydrolase 2	2.53	1,96E-01	Q8R2U6	Nudt4	1
Q8VCU1	Isoform 2 of Carboxylesterase 3B	2.58	1,83E-01	Q8VCU1-2	Ces3b	1
Q9DAW9	Calponin-3	2.64	2,93E-01	Q9DAW9	Cnn3	1
Q3UZV7	UPF0577 protein KIAA1324-like homolog;Isoform 2 of UPF0577 protein KIAA1324-like homolog;Isoform 4 of UPF0577 protein KIAA1324-like homolog;Isoform 6 of UPF0577 protein KIAA1324-like homolog;Isoform 7 of UPF0577 protein KIAA1324-like homolog	2.67	8,41E-02	Q3UZV7;Q3UZV7-2;Q3UZV7-4;Q3UZV7-6;Q3UZV7-7	NaN	1
P54775	26S proteasome regulatory subunit 6B	2.73	3,16E-02	P54775	Psmc4	7
Q8WUR0	Protein C19orf12 homolog	2.74	9,65E-02	Q8WUR0	NaN	1
Q9CQ48	NudC domain-containing protein 2	3.40	1,68E-01	Q9CQ48	Nudcd2	1

Table 4.12 continued.

ID	Protein Descriptions	Fold Change	FDR (*q*-value)	UniProt ID	Genes	Peptides identified (n)
			decreased secretion from alb-SREBP-1c			
Q8K3J1	NADH dehydrogenase [ubiquinone] iron-sulfur protein 8, mitochondrial	3.66	1,18E-02	Q8K3J1	Ndufs8	1
P16254	Signal recognition particle 14 kDa protein	4.58	2,40E-01	P16254	Srp14	3
Q91VR2	ATP synthase subunit gamma, mitochondrial	5.46	3,81E-01	Q91VR2	Atp5f1c	1

Table 4.13: Top ranking hepatokines differentially secreted from primary hepatocytes in the comparison of C57Bl6 vs. aP2-SREBP-1c. Proteins with top score fold-changes and *p*-values for increased or decreased concentration in primary hepatocyte culture supernatant are shown (cut-off values: > 1.5-fold regulation; *p*-value < 0.05, ANOVA). ID as defined by UniProt with annotation of genes according to IPA analyses ready molecules. *q*-value calculated from false discovery rate (FDR) analysis.

ID	Protein Descriptions	Fold Change	FDR (*q*-value)	UniProt ID	Genes	Peptides identified (n)
			increased secretion from aP2-SREBP-1c			
O89051	Integral membrane protein 2B	-77.66	5,40E-01	O89051	Itm2b	1
Q19LI2	Alpha-1B-glycoprotein	-6.11	2,38E-01	Q19LI2	A1bg	10
Q9Z2K1	Keratin, type I cytoskeletal 16	-6.06	5,43E-02	Q9Z2K1	Krt16	5
Q6P5D4	Centrosomal protein of 135 kDa	-6.04	4,41E-01	Q6P5D4	Cep135	1
P19001	Keratin, type I cytoskeletal 19	-5.77	3,67E-01	P19001	Krt19	1
O35403	Amine sulfotransferase	-4.88	4,28E-01	O35403	Sult3a1	8
Q8BWN8	Acyl-coenzyme A thioesterase 4	-4.81	2,64E-02	Q8BWN8	Acot4	3
Q9QXG4	Acetyl-coenzyme A synthetase, cytoplasmic	-4.53	3,51E-01	Q9QXG4	Acss2	11
Q9QYR7	Acyl-coenzyme A thioesterase 3	-4.31	4,93E-05	Q9QYR7	Acot3	16
P55065	Phospholipid transfer protein	-4.30	5,10E-03	P55065	Pltp	4
			decreased secretion from aP2-SREBP-1c			
Q00493	Carboxypeptidase E	2.97	9,62E-02	Q00493	Cpe	4
B5X0G2	Major urinary protein 17	3.01	1,09E-08	B5X0G2	Mup17	3
Q3UZZ6	Sulfotransferase 1 family member D1	3.13	2,25E-03	Q3UZZ6	Sult1d1	19
Q91VR2	ATP synthase subunit gamma, mitochondrial	3.64	2,01E-01	Q91VR2	Atp5f1c	1
Q8VCU1	Isoform 2 of Carboxylesterase 3B	3.69	3,40E-01	Q8VCU1-2	Ces3b	1
Q8R519	2-amino-3-carboxymuconate-6-semialdehyde decarboxylase	3.72	3,13E-05	Q8R519	Acmsd	3
P11588	Major urinary protein 1	3.82	2,14E-02	P11588	Mup1	2

Table 4.13 continued.

ID	Protein Descriptions	Fold Change	FDR (*q*-value)	UniProt ID	Genes	Peptides identified (n)
decreased secretion from aP2-SREBP-1c						
P16254	Signal recognition particle 14 kDa protein	3.95	1,71E-01	P16254	Srp14	3
Q8K3J1	NADH dehydrogenase [ubiquinone] iron-sulfur protein 8, mitochondrial	4.37	4,10E-01	Q8K3J1	Ndufs8	1
O35114	Lysosome membrane protein 2	8.46	3,18E-01	O35114	Scarb2	3

Table 4.14: Top ranking hepatokines differentially secreted from primary hepatocytes in the comparison of alb-SREBP-1c vs. aP2-SREBP-1c. Proteins with top score fold-changes and *p*-values for increased or decreased concentration in primary hepatocyte culture supernatant are shown (cut-off values: > 1.5-fold regulation; *p*-value < 0.05, ANOVA). ID as defined by UniProt with annotation of genes according to IPA analyses ready molecules. *q*-value calculated from false discovery rate (FDR) analysis.

ID	Protein Descriptions	Fold Change	FDR (*q*-value)	UniProt ID	Genes	Peptides identified (n)
increased secretion from aP2-SREBP-1c						
O89051	Integral membrane protein 2B	-39.00	5,05E-01	O89051	Itm2b	1
Q99LS3	Phosphoserine phosphatase	-4.84	4,33E-01	Q99LS3	Psph	1
Q19LI2	Alpha-1B-glycoprotein	-4.56	4,10E-01	Q19LI2	A1bg	10
Q9EQY0	Serine/threonine-protein kinase/endoribonuclease IRE1;Isoform 2 of Serine/threonine-protein kinase/endoribonuclease IRE1	-4.48	3,55E-01	Q9EQY0;Q9EQY0-2	Ern1	1
Q99LY9	NADH dehydrogenase [ubiquinone] iron-sulfur protein 5	-3.66	6,06E-02	Q99LY9	Ndufs5	5
Q3UZV7	UPF0577 protein KIAA1324-like homolog;Isoform 2 of UPF0577 protein KIAA1324-like homolog;Isoform 4 of UPF0577 protein KIAA1324-like homolog;Isoform 6 of UPF0577 protein KIAA1324-like homolog;Isoform 7 of UPF0577 protein KIAA1324-like homolog	-3.59	1,13E-01	Q3UZV7;Q3UZV7-2;Q3UZV7-4;Q3UZV7-6;Q3UZV7-7	NaN	1
Q9QYR7	Acyl-coenzyme A thioesterase 3	-3.44	2,33E-05	Q9QYR7	Acot3	16
O55137	Acyl-coenzyme A thioesterase 1	-3.44	6,78E-02	O55137	Acot1	7

Table 4.14 continued.

ID	Protein Descriptions	Fold Change	FDR (*q*-value)	UniProt ID	Genes	Peptides identified (n)
increased secretion from aP2-SREBP-1c						
P16045	Galectin-1	-3.30	1,72E-08	P16045	Lgals1	5
Q99KP3	Lambda-crystallin homolog	-3.04	1,62E-04	Q99KP3	Cryl1	4
decreased secretion from aP2-SREBP-1c						
Q00493	Carboxypeptidase E	2.82	1,45E-01	Q00493	Cpe	4
E9PV24	Fibrinogen alpha chain	2.82	3,37E-01	E9PV24	Fga	26
Q9JLC3	Methionine-R-sulfoxide reductase B1	2.83	1,66E-01	Q9JLC3	Msrb1	1
Q91WG8	Bifunctional UDP-N-acetylglucosamine 2-epimerase/N-acetylmannosamine kinase	3.14	3,74E-02	Q91WG8	Gne	4
Q8R519	2-amino-3-carboxymuconate-6-semialdehyde decarboxylase	3.19	2,43E-03	Q8R519	Acmsd	3
P47877	Insulin-like growth factor-binding protein 2	3.19	4,29E-01	P47877	Igfbp2	13
Q8K0E8	Fibrinogen beta chain	3.65	3,76E-20	Q8K0E8	Fgb	25
Q8VCM7	Fibrinogen gamma chain	3.79	7,17E-10	Q8VCM7	Fgg	16
B5X0G2	Major urinary protein 17	3.85	3,30E-13	B5X0G2	Mup17	3
P11588	Major urinary protein 1	3.96	6,74E-04	P11588	Mup1	2

4.5.3 Analysis of potential biomarkers for fatty liver

Proteins identified to be differentially expressed between C57Bl6, alb-SREBP-1c and aP2-SREBP-1c were analyzed for the identification of potential biomarkers of fatty liver using the IPA biomarker analysis tool. Additionally proteins assigned as potential biomarkers were further processed using the comparison routine to elucidate biomarkers unique for each data set. Potential biomarkers for the analysis C57Bl6 versus alb-SREBP-1c were listed in table 4.15. Molecules with top ranking fold-changes of downregulated secretion from alb-SREBP-1c hepatocytes were ATP synthase F1 subunit γ (ATP5F1C, fold change 5.462), signal recognition particle 14 (SRP14, 4.583), NADH ubiquinone oxidoreductase core subunit S8 (NDUFS8, 3.66) and NudC domain-containing (NUDCD) 2 (3.4) which was also identified to be unique for the comparison between C57Bl6 and alb-SREBP-1c. NDUFS8 (4.368) and SRP14 (3.945) were also found to be included in top score list of decreased protein secretion between aP2-SREBP-1c versus C57Bl6 (table 4.16). Biomarkers found to be unique in regulation between C57Bl6 and aP2-SREBP-1c with highest fold-changes were major urinary protein 1 (Mup1, 3.819) and aminocarboxymuconate semialdehyde decarboxylase (ACSMD, 3.716). Also among proteins found with a 2-fold decrease in supernatants of aP2-SREBP-1c hepatocytes and assigned as potential biomarker were IGFBP2 (2.25), fatty acid binding protein (FABP) 5 (2.235) and insulin receptor related receptor (INSRR, 2.186). In comparison of both fatty liver models major urinary protein (Mup) 1 (3.962) and aminocarboxymuconate semialdehyde decarboxylase (ACSMD, 3.191) were also identified as potential biomarkers with decreased secretion in aP2-SREBP-1c (table 4.17). Further the amount of the potential biomarker IGFBP2 (3.194) was 3-fold decreased in aP2-SREBP-1c culture supernatant compared to alb-SREBP-1c. Angiogenin (ANG, 2.117) was identified as unique potential biomarker with the highest fold-change for the comparison alb-SREBP-1c against aP2-SREBP-1c. Biomarkers identified with increased secretion from alb-SREBP-1c compared to C57Bl6 included Krt 16 (-4.913), 17 (-2.906) and 19 (-7.584), as well as ACSS2 (-4.822). Krt 16 (-6.062), 17 (-3.574) and 19 (-5.767) were also found with upregulated secretion in aP2-SREBP-1c compared to C57Bl6. In the last mentioned comparison the two top score biomarkers with upregulated secretion were integral membrane protein 2B (ITM2B, -77.662) and alpha-1-B glycoprotein (A1BG, -6.112) which were also top ranking upregulated biomarkers in aP2-SREBP-1c culture supernatant (ITM2B: -39.002, A1BG: -4.555) when compared to alb-SREBP-1c. In the comparison of alb-SREBP-1c with aP2-SREBP-1c S100 calcium binding protein A13 (S100A13, 1.947) was the biomarker identified as unique for the comparison with the highest fold-change between these two groups.

Potential biomarkers with differences in secretion from pairwise analysis of C57Bl6, alb-SREBP-1c and aP2-SREBP-1c were further subjected to knowledge-based analysis of upstream regulators and functional annotation of the differentially expressed proteins listed in tables 4.18 and 4.19. In comparison of C57Bl6 with alb-SREBP-1c secretome the top score upstream regulators were identified mainly as transcriptional regulators like HNF4A (*p*-value 1.14×10^{-08}), SREBF1 (1.28×10^{-05}), aryl hydrocarbon receptor nuclear translocator (ARNT: 1.51×10^{-05}) or upstream transcription factor (USF) 1 (2.20×10^{-05}) (table 4.18) with concentrated annotated function in dysregulated lipid metabolism (table 4.19). When potential biomarkers regulated in aP2-SREBP-1c versus C57Bl6 were investigated upstream regulation included several ligand dependent nuclear receptor, enzymes and cytokines like PPAR (2.30×10^{-26}), acyl-Coenzyme A oxidase (ACOX) 1 (1.76×10^{-16}) or IL-4 (1.34×10^{-07}) beside transcriptional regulators MYC (7.14×10^{-10}) or HNF1A (7.83×10^{-08}). Functional analysis resulted in several deregulated proteins annotated to lipid metabolism or hepatic steatosis. Differential potential biomarker secretion between the two fatty liver models alb-SREBP-1c and aP2-SREBP-1c evaluated dysregulation of lipid metabolism as one major functional annotation as well as involvement in amino acid metabolism and vascular dysfunctions. Upstream regulators assigned to this comparison were several transmembrane receptors like insulin-like growth factor I receptor (IGF1R: 5.74×10^{-07}) or leucine-rich repeat-containing G protein-coupled receptor (LGR) 4 (1.66×10^{-04}), transporter proteins like hemoglobin, beta adult major chain (Hbb-b1: 9.79×10^{-06}) or ATP binding cassette subfamily B (ABCB) 7 (9.12×10^{-05}) as well as several peptidases and kinases.

Table 4.15: Biomarkers identified in primary hepatocyte secretome. Differentially secreted proteins from the comparison of C57Bl6 vs. alb-SREBP-1c were analyzed with the biomarker routine of IPA. Potential biomarkers are listed with fold changes and *q*-values indicated. Data of biomarker analysis were further processed using the comparison routine to identify unique biomarker for the comparison C57Bl6 vs. alb-SREBP-1c, not present in the comparison C57Bl6 vs. aP2-SREBP-1c or alb-SREBP-1c vs. aP2-SREBP-1c. Biomarkers specific for the comparison of C57Bl6 vs. alb-SREBP-1c secretome are underlined.

Symbol	Entrez Gene Name	Location	Family	UniProt Accession	FDR (*q*-value)	Fold Change	Blood	Plasma/ Serum	Urine
ATP5F1C	ATP synthase F1 subunit gamma	Cytoplasm	transporter	Q91VR2	3,37E-01	5,462			
SRP14	signal recognition particle 14	Cytoplasm	other	P16254	1,21E-01	4,583			
NDUFS8	NADH:ubiquinone oxidoreductase core subunit S8	Cytoplasm	enzyme	Q8K3J1	3,59E-01	3,660			
NUDCD2	NudC domain containing 2	Cytoplasm	other	Q9CQ48	1,40E-01	3,400			
C19orf12	chromosome 19 open reading frame 12	Cytoplasm	other	Q8WUR0	2,01E-01	2,740			
PSMC4	proteasome 26S subunit, ATPase 4	Nucleus	peptidase	P54775	2,91E-02	2,727			
KIAA1324L	KIAA1324 like	Other	other	Q3UZV7	1,54E-01	2,675			
CNN3	calponin 3	Cytoplasm	other	Q9DAW9	6,54E-02	2,644			
CES3	carboxylesterase 3	Cytoplasm	enzyme	Q8VCU1	2,74E-01	2,584			
NUDT4	nudix hydrolase 4	Cytoplasm	phosphatase	Q8R2U6	2,90E-01	2,527			
PTK2B	protein tyrosine kinase 2 beta	Cytoplasm	kinase	Q9QVP9	1,18E-02	-2,814	x	x	
KRT17	keratin 17	Cytoplasm	other	Q9QWL7	1,68E-01	-2,906	x	x	x
EED	embryonic ectoderm development	Nucleus	transcription regulator	Q921E6	9,65E-02	-3,165	x		
CEP162	centrosomal protein 162	Nucleus	other	Q6ZQ06	3,16E-02	-3,195	x	x	
8030411F24Rik	RIKEN cDNA 8030411F24 gene	Other	other	Q8VII3	8,41E-02	-3,396			
WBP2	WW domain binding protein 2	Cytoplasm	transcription regulator	P97765	2,93E-01	-3,669			
ACSS2	acyl-CoA synthetase short chain family member 2	Cytoplasm	enzyme	Q9QXG4	1,83E-01	-4,822			

Table 4.15 continued.

Symbol	Entrez Gene Name	Location	Family	UniProt Accession	FDR (*q*-value)	Fold Change	Blood	Plasma/ Serum	Urine
KRT16	keratin 16	Cytoplasm	other	Q9Z2K1	1,96E-01	-4,913	x	x	
CCDC25	coiled-coil domain containing 25	Cytoplasm	other	Q78PG9	3,16E-01	-7,003			
KRT19	keratin 19	Cytoplasm	other	P19001	5,04E-01	-7,584	x	x	

Table 4.16: Biomarkers identified in primary hepatocyte secretome. Differentially secreted proteins from the comparison of C57Bl6 vs. aP2-SREBP-1c were analyzed with the biomarker routine of IPA. Potential biomarkers are listed and fold changes and *q*-values indicated. Data of biomarker analysis were further processed using the comparison routine to identify unique biomarker for the comparison C57Bl6 vs. aP2-SREBP-1c, not present in the comparison C57Bl6 vs. alb-SREBP-1c or alb-SREBP-1c vs. aP2-SREBP-1c. Biomarkers specific for the comparison of C57Bl6 vs. aP2-SREBP-1c secretome are underlined.

Symbol	Entrez Gene Name	Location	Family	UniProt Accession	FDR (*q*-value)	Fold Change	Blood	Plasma/ Serum	Urine
SCARB2	scavenger receptor class B member 2	Plasma Membrane	other	O35114	3,18E-01	8,462			x
NDUFS8	NADH:ubiquinone oxidoreductase core subunit S8	Cytoplasm	enzyme	Q8K3J1	4,10E-01	4,368			
SRP14	signal recognition particle 14	Cytoplasm	other	P16254	1,71E-01	3,945			
Mup1 (incl. others)	major urinary protein 1	Extracellular Space	other	P11588	2,14E-02	3,819			
ACMSD	aminocarboxymuconate semialdehyde decarboxylase	Cytoplasm	enzyme	Q8R519	3,13E-05	3,716	x		
CES3	carboxylesterase 3	Cytoplasm	enzyme	Q8VCU1	3,40E-01	3,691			
ATP5F1C	ATP synthase F1 subunit gamma	Cytoplasm	transporter	Q91VR2	2,01E-01	3,638			
Sult1d1	sulfotransferase family 1D, member 1	Cytoplasm	enzyme	Q3UZZ6	2,25E-03	3,134			
CPE	carboxypeptidase E	Cytoplasm	peptidase	Q00493	9,62E-02	2,972	x		x

Table 4.16 continued.

Symbol	Entrez Gene Name	Location	Family	UniProt Accession	FDR (*q*-value)	Fold Change	Blood	Plasma/ Serum	Urine
GNE	glucosamine (UDP-N-acetyl)-2-epimerase/N-acetylmannosamine kinase	Cytoplasm	kinase	Q91WG8	1,41E-01	2,815			
PLTP	phospholipid transfer protein	Extracellular Space	enzyme	P55065	5,10E-03	-4,296	x	x	
ACOT1	acyl-CoA thioesterase 1	Cytoplasm	enzyme	Q9QYR7	4,93E-05	-4,312			
ACSS2	acyl-CoA synthetase short chain family member 2	Cytoplasm	enzyme	Q9QXG4	3,51E-01	-4,529			
ACOT4	acyl-CoA thioesterase 4	Cytoplasm	enzyme	Q8BWN8	2,64E-02	-4,812			
Sult3a1/Sult3a 2	sulfotransferase family 3A, member 1	Cytoplasm	enzyme	O35403	4,28E-01	-4,881			
KRT19	keratin 19	Cytoplasm	other	P19001	3,67E-01	-5,767	x	x	
CEP135	centrosomal protein 135	Cytoplasm	other	Q6P5D4	4,41E-01	-6,042	x	x	
KRT16	keratin 16	Cytoplasm	other	Q9Z2K1	5,43E-02	-6,062	x	x	
A1BG	alpha-1-B glycoprotein	Extracellular Space	other	Q19LI2	2,38E-01	-6,112	x	x	X
ITM2B	integral membrane protein 2B	Plasma Membrane	other	O89051	5,40E-01	-77,662	x		x

Table 4.17: Biomarkers identified in primary hepatocyte secretome. Differentially secreted proteins from the comparison of alb-SREBP-1c vs. aP2-SREBP-1c were analyzed with the biomarker routine of IPA. Potential biomarkers are listed and fold changes and *q*-values indicated. Data of biomarker analysis were further processed using the comparison routine to identify unique biomarker for the comparison alb-SREBP-1c vs. aP2-SREBP-1c, not present in the comparison C57Bl6 vs. alb-SREBP-1c or C57Bl6 vs. aP2-SREBP-1c. Biomarkers specific for the comparison of alb-SREBP-1c vs. aP2-SREBP-1c secretome are underlined.

Symbol	Entrez Gene Name	Location	Family	UniProt Accession	FDR (*q*-value)	Fold Change	Blood	Plasma/ Serum	Urine
Mup1 (includes others)	major urinary protein 1	Extracellular Space	other	P11588	6,74E-04	3,962			
FGG	fibrinogen gamma chain	Extracellular Space	other	Q8VCM7	7,17E-10	3,788	x	x	x

Table 4.17 continued.

Symbol	Entrez Gene Name	Location	Family	UniProt Accession	FDR (*q*-value)	Fold Change	Blood	Plasma/ Serum	Urine
FGB	fibrinogen beta chain	Extracellular Space	other	Q8K0E8	3,76E-20	3,651	x	x	x
IGFBP2	insulin like growth factor binding protein 2	Extracellular Space	other	P47877	4,29E-01	3,194	x	x	x
ACMSD	aminocarboxymuconate semialdehyde decarboxylase	Cytoplasm	enzyme	Q8R519	2,43E-03	3,191	x		
GNE	glucosamine (UDP-N-acetyl)-2-epimerase/N-acetylmannosamine kinase	Cytoplasm	kinase	Q91WG8	3,74E-02	3,136			
MSRB1	methionine sulfoxide reductase B1	Nucleus	enzyme	Q9JLC3	1,66E-01	2,830			
FGA	fibrinogen alpha chain	Extracellular Space	other	E9PV24	3,37E-01	2,822	x	x	x
CPE	carboxypeptidase E	Cytoplasm	peptidase	Q00493	1,45E-01	2,817	x		X
8030411F24Rik	RIKEN cDNA 8030411F24 gene	Other	other	Q8VII3	2,03E-01	2,783			
CRYL1	crystallin lambda 1	Cytoplasm	enzyme	Q99KP3	1,62E-04	-3,039			x
LGALS1	galectin 1	Extracellular Space	other	P16045	1,72E-08	-3,298	x		x
ACOT1	acyl-CoA thioesterase 1	Cytoplasm	enzyme	Q9QYR7	2,33E-05	-3,437			
Acot1	acyl-CoA thioesterase 1	Cytoplasm	enzyme	O55137	6,78E-02	-3,437			
KIAA1324L	KIAA1324 like	Other	other	Q3UZV7	1,13E-01	-3,594			
Ndufs5	NADH dehydrogenase (ubiquinone) Fe-S protein 5	Cytoplasm	other	Q99LY9	6,06E-02	-3,664			
ERN1	endoplasmic reticulum to nucleus signaling 1	Cytoplasm	kinase	Q9EQY0	3,55E-01	-4,475	x	x	
A1BG	alpha-1-B glycoprotein	Extracellular Space	other	Q19LI2	4,10E-01	-4,555	x	x	x
PSPH	phosphoserine phosphatase	Cytoplasm	phosphatase	Q99LS3	4,33E-01	-4,845			
ITM2B	integral membrane protein 2B	Plasma Membrane	other	O89051	5,05E-01	-39,002	x		x

Table 4.18: Upstream regulators of differentially secreted potential biomarkers for fatty liver. Data of differential secreted proteins (cut-off values: > 1.5-fold regulation; *p*-value < 0.05, ANOVA) were subjected to biomarker analyses (IPA) and further processed using the comparison routine to identify unique biomarker for each comparison. Unique differential regulated proteins assigned as potential biomarker were then subjected to the IPA core analyses module to identify upstream regulatory networks.

C57Bl6 vs. alb-SREBP-1c			
Upstream Regulator	**Molecule Type**	***p*-value**	**Target molecules in dataset**
HNF4A	transcription regulator	1.14E-08	AKR1B1, AKR1C4, APOA2, Apoc3, COASY, DHRS4, DUSP3, EPHX1, GCKR, GFER, HSD11B1, HSPA4L, IGFBP1, KRT8, LBP, MSRB1, Mt1, MUTYH, PCYT1A, RANGAP1, RNASE4, RPL18, SERPINA3, SERPINE1, SNX3, UGT1A6, UGT2A3, UMPS, YKT6
SREBF1	transcription regulator	1.28E-05	AACS, APOA2, APOA5, MVD, PCYT1A, RBP1, SERPINA3, SERPINE1
ARNT	transcription regulator	1.51E-05	AKT2, ANGPTL4, RANGAP1, SERPINE1, TUBA4A, UGT1A6
USF1	transcription regulator	2.20E-05	APOA2, APOA5, IGFBP1, Mt1, SERPINE1
TP53	transcription regulator	2.45E-05	AKR1B1, Atp5k, CYR61, DHFR, EPHX1, HDLBP, HSPA4L, KRT8, LYZ, MSRB1, MVD, PDCD6IP, PRPSAP1, RANGAP1, RNASE4, SERPINA3, SERPINE1, TGM2, UMPS
NR3C1	ligand-dependent nuclear receptor	3.37E-05	AKT2, ANGPTL4, APOA2, CYR61, HSD11B1, IGFBP1, MSRB1, Mt1, NMT1, SDS, SERPINE1, TUBA4A
SP2	transcription regulator	3.53E-05	DHFR, PCYT1A, SERPINE1
MYC	transcription regulator	5.00E-05	CSE1L, CTNNA1, DHFR, GAMT, GFER, HNRNPH1, LGMN, LYZ, Mt1, PTBP1, RBP1, RPL5, RPS15A, SERPINE1, UGT1A6
Ins1	other	6.43E-05	ANGPTL4, APOA5, Apoc3, DHFR, IGFBP1, Mt1, SERPINE1, UMPS
CEBPA	transcription regulator	1.19E-04	AKR1B1, Apoc3, APOC4, CA2, CTNNA1, DHFR, EPHX1, HSD11B1, SERPINE1
USF2	transcription regulator	1.38E-04	APOA2, APOA5, IGFBP1, SERPINE1
HNF1A	transcription regulator	1.41E-04	AKR1C4, APOA2, GCKR, HSD11B1, IGFBP1, LBP, RNASE4, SERPINE1, UGT2A3
SOX4	transcription regulator	1.62E-04	CTNNA1, Hbb-b1, KYNU, LYZ, Mt1, RNASE4
ELF3	transcription regulator	2.71E-04	ANGPTL4, KRT8, LYZ
SND1	enzyme	2.71E-04	ANGPTL4, DHFR, KYNU
ARNT2	transcription regulator	2.96E-04	AKR1B1, ANGPTL4, APOA5, APOC4, MTPN, UGT1A6
SREBF2	transcription regulator	3.11E-04	AACS, APOA2, MVD, PCYT1A
SIM1	transcription regulator	3.37E-04	AKR1B1, ANGPTL4, APOA5, APOC4, MTPN, UGT1A6
QKI	other	3.91E-04	HNRNPF, HNRNPH1
TNF	cytokine	4.44E-04	AKR1B1, ANGPTL4, APOC4, BLVRA, CA2, CYR61, HSD11B1, IGFBP1, KRT8, KYNU, LBP, Mt1, PCYT1A, RBP1, RNASE4, SERPINA3, SERPINE1, TGM2
PDGF BB	complex	4.90E-04	CYR61, LBP, Mt1, RBP1, SERPINA3, SERPINE1, TGM2
AFF4	transcription regulator	6.66E-04	HNRNPH1, PTBP1
CDKN2B	transcription regulator	6.66E-04	DHFR, SERPINE1
KDM1A	enzyme	6.82E-04	Hbb-b1, HSD11B1, KRT8, SERPINE1
GNA15	enzyme	8.02E-04	LBP, Mt1, RBP1, SERPINA3

Table 4.18 continued.

C57Bl6 vs. alb-SREBP-1c			
Upstream Regulator	**Molecule Type**	***p*-value**	**Target molecules in dataset**
LEPR	transmembrane receptor	8.33E-04	ANGPTL4, APOA2, GCKR, LGMN, SERPINE1
AHR	ligand-dependent nuclear receptor	8.49E-04	DHFR, IGFBP1, LBP, Mt1, RBP1, SERPINE1, UGT1A6
F2R	g-protein coupled receptor	8.67E-04	CYR61, IGFBP1, KRT8, TGM2
ZNF106	other	1.00E-03	Hbb-b1, LYZ, SERPINA3
MKNK1	kinase	1.01E-03	CYR61, HSPA4L, PTBP1, RNH1
F2	peptidase	1.02E-03	AKR1B1, ANGPTL4, CLIC1, CYR61, RNH1, SERPINE1
RXRA	ligand-dependent nuclear receptor	1.04E-03	APOA2, APOA5, Apoc3, EPHX1, IGFBP1, RBP1
Brd4	kinase	1.07E-03	Hbb-b1, HNRNPH1, PTBP1
INHA	growth factor	1.12E-03	CYR61, EPHX1, KRT8, SERPINE1
TP73	transcription regulator	1.23E-03	ANGPTL4, CYR61, DHFR, LYZ, MUTYH, SERPINA3, SERPINE1
TGFBR2	kinase	1.38E-03	ANGPTL4, HSD11B1, KRT8, OSTF1, SERPINE1
NR3C2	ligand-dependent nuclear receptor	1.58E-03	MSRB1, SERPINA3, SERPINE1, TUBA4A
HNF1B	transcription regulator	1.74E-03	AKR1C4, CA2, IGFBP1, RNASE4
C57Bl6 vs. aP2-SREBP-1c			
Upstream Regulator	**Molecule Type**	***p*-value**	**Target molecules in dataset**
PPARA	ligand-dependent nuclear receptor	2.30E-26	ACAA1, Acaa1b, ACADVL, Acot1, ACOT2, ACOX1, APCS, APOA1, APOA4, APOM, C2, C8A, CPS1, ECI1, FABP2, FABP4, FABP5, FASN, GLUL, GSTK1, GSTP1, HADH, HIST1H1C, HSD17B4, IGFBP2, LIFR, Mup1 (includes others), NSDHL, Orm1 (includes others), PKLR, S100A9, SELENBP1, SRM, SULT2A1
ACOX1	enzyme	1.76E-16	ACAA1, ACADVL, ACOT2, ACOX1, APCS, CRAT, Cyp2d9 (includes others), EGFR, FABP2, FABP4, FASN, GSTP1, IGFBP2, Mup1 (includes others), Orm1 (includes others), SELENBP1, SERPINA1
MYC	transcription regulator	7.14E-10	CASP8, CAST, Cdc42, CLUH, EIF2S2, EIF3D, EIF3G, FABP2, FABP4, FABP5, FASN, GLUL, HNRNPU, ITM2B, LGALS1, LIMA1, NARS, NME1, PA2G4, PFAS, PKLR, RPS19, SCPEP1, SERPINA1, SRM, THBS1, UBE2I, VARS
NR1I2	ligand-dependent nuclear receptor	8.30E-10	ACOX1, APOA4, Apoc1, Cyp2d9 (includes others), ENTPD5, FASN, GLUL, GSTA5, GSTP1, Mup1 (includes others), SULT2A1, TCN2
RORC	ligand-dependent nuclear receptor	8.94E-10	ACOT2, APOA4, CYP2E1, GSTA5, GSTP1, HPGD, Mup1 (includes others), NSDHL, S100A9, SELENBP1, SULT2A1, Sult3a1/Sult3a2
RORA	ligand-dependent nuclear receptor	8.96E-10	ACOT2, APOA4, CYP2E1, FASN, GSTA5, GSTP1, HPGD, Mup1 (includes others), NSDHL, S100A9, SELENBP1, SULT2A1, Sult3a1/Sult3a2

Table 4.18 continued.

C57Bl6 vs. aP2-SREBP-1c			
Upstream Regulator	**Molecule Type**	***p*-value**	**Target molecules in dataset**
RXRA	ligand-dependent nuclear receptor	4.21E-09	Acot1, ACOX1, APOA1, APOM, FABP2, FABP4, FABP5, FASN, HSD17B4, NME1, Orm1 (includes others), PKLR, SULT2A1, THRSP
TP53	transcription regulator	9.63E-09	ACADVL, APOA1, C2, CASP8, Cdc42, CLPP, CLUH, COMT, Cox5b, CTGF, EGFR, FABP4, FAM3C, FASN, GLUL, GSTP1, H2AFY, HADH, IGFBP2, LIMA1, LMAN2, MAP2K1, MYH9, NARS, NEDD8, NME1, PA2G4, SCPEP1, TCN2, THBS1, TUBB, TUBB3
PPARD	ligand-dependent nuclear receptor	2.87E-08	ACAA1, ACADVL, ACOX1, APOA1, APOA4, FABP4, FASN, FBP1, GSTA5, IGFBP2, PKLR, THBS1
Ins1	other	3.37E-08	Acot1, APOA1, CRAT, Cyp2d9 (includes others), CYP2E1, ECI1, FABP4, FASN, GSTP1, HSD17B4, IGFBP2, LIFR, PKLR, THRSP
INSR	kinase	3.58E-08	ACADVL, ACOT2, C2, Cox5b, CRAT, CTGF, ECI1, FABP4, FASN, FBP1, HSD17B4, IDH3A, LGALS1, NSDHL, PKLR
NR1I3	ligand-dependent nuclear receptor	3.70E-08	ACOX1, APCS, APOA1, GSTA5, GSTP1, HSD17B4, PPP6R3, SULT2A1, THRSP
HNF1A	transcription regulator	7.83E-08	APCS, APOM, C2, C8A, C8B, COQ7, CYP2E1, ENPEP, FBP1, GBE1, GLUL, ITM2B, PCNP, PKLR, SERPINA1, UROD
IL4	cytokine	1.34E-07	ACOX1, APRT, CD14, Cdc42, CLUH, CTGF, CYP2E1, EIF3G, FABP4, FASN, GBE1, H1F0, Hist1h1e, HPGD, LGALS1, LIFR, LMAN2, MAP2K1, MYH9, S100A9, SRM, VARS
PPARGC1A	transcription regulator	1.34E-07	ACADVL, ACOX1, APOA4, Cox5b, EGFR, FABP4, FASN, IDH3A, LIFR, NSDHL, SIRT3, SULT2A1
PNPLA2	enzyme	1.90E-07	ACADVL, Acot1, ACOT2, ACOX1, FASN, GSTK1
GPD1	enzyme	2.87E-07	ACOT2, APOA4, C8A, EGFR, GSTA5, LIFR, Mup1 (includes others), TTC39C
SLC25A13	transporter	3.39E-07	ACOT2, APOA4, C8A, EGFR, GSTA5, LIFR, Mup1 (includes others), TTC39C
CEBPA	transcription regulator	3.48E-07	APOA4, CD14, CPS1, FABP4, FASN, GSTP1, HPGD, LGALS1, Mup1 (includes others), Orm1 (includes others), S100A9, SMPDL3A, SULT2A1, THBS1, UBE2I
LEP	growth factor	3.58E-07	ACADVL, ACOX1, APOA1, APOA4, APOM, CD14, CPS1, Cyp2d9 (includes others), CYP2E1, FABP4, FASN, IGFBP2, LIFR, THBS1, THRSP
KLF15	transcription regulator	5.56E-07	ACADVL, Acot1, ACOX1, CTGF, FABP5, FASN
Esrra	transcription regulator	6.76E-07	ACOX1, APOA4, Cox5b, CRAT, FABP2, FBP1, IDH3A, SIRT3
NR1H3	ligand-dependent nuclear receptor	8.38E-07	ACOX1, APCS, APOA1, Apoc1, APOM, FASN, FBP1, PKLR
NFE2L2	transcription regulator	1.16E-06	APCS, APOA4, CLPP, COQ7, CTGF, EIF3G, ENTPD5, FABP4, GBE1, GSTA5, GSTP1, NARS, TCN2, THRSP
CFTR	ion channel	1.73E-06	ACAA1, Acaa1b, Cyp2d9 (includes others), FABP2, HADH, HPGD, HSD17B4
FGF19	growth factor	2.04E-06	Cyp2d9 (includes others), FABP5, FASN, FBP1, PKLR, SERPINA1, THRSP
LEPR	transmembrane receptor	2.47E-06	ACOX1, APOA1, APOA4, CASP8, Cdc42, CYP2E1, EIF3A, FASN, Mup1 (includes others)
EHHADH	enzyme	2.81E-06	ACAA1, ACOT2, ACOX1, FASN
POR	enzyme	4.57E-06	ACADVL, Acot1, APOA4, ECI1, ENTPD5, FABP2, GSTA5, LGALS1, NSDHL

Table 4.18 continued.

C57Bl6 vs. aP2-SREBP-1c			
Upstream Regulator	**Molecule Type**	***p*-value**	**Target molecules in dataset**
TNF	cytokine	6.45E-06	ACADVL, ACOX1, APCS, APOA1, BCL2L13, CASP8, CD14, CTGF, CYP2E1, EGFR, ENTPD5, FABP4, FABP5, FASN, GSTP1, HEXA, HPGD, IGFBP2, LIFR, MYH9, NME1, Orm1 (includes others), S100A9, SIRT3, SMPDL3A, SND1, SULT2A1, THBS1, THRSP
FASN	enzyme	1.01E-05	Acaa1b, ACOX1, Apoc1, FASN, PKLR
alb-SREBP-1c vs. aP2-SREBP-1c			
Upstream Regulator	**Molecule Type**	***p*-value**	**Target molecules in dataset**
PPARA	ligand-dependent nuclear receptor	6.21E-09	ACADS, ALDH2, CAT, CPT2, CROT, CTH, ECH1, LECT2, MLYCD, PON1, SARDH, TPP1
INSR	kinase	1.23E-08	ACADS, ALDH2, ATP5F1D, CPT2, ETFA, ETFB, ETFDH, ligp1, MMP12, NDUFB4, NDUFV2
IGF1R	transmembrane receptor	5.74E-07	ACADS, ATP5F1D, CLU, CPT2, FTH1, MAPK14, NDUFB4, NDUFV2
DYSF	other	4.29E-06	CXCL10, FN1, FTL, MMP12, S100A13
NFE2L2	transcription regulator	4.53E-06	ANG, CAT, CXCL10, FN1, FTH1, FTL, OAT, S100A13, SHMT2
Growth hormone	group	4.64E-06	CAT, CLU, CROT, CTH, FN1, FTH1, PON1
Hbb-b2	other	6.65E-06	CXCL10, FN1, FTH1, FTL
Hbb-b1	transporter	9.79E-06	CXCL10, FN1, FTH1, FTL
SREBF1	transcription regulator	1.02E-05	ACADS, AGMAT, CXCL10, FN1, MLYCD, OAT, S100A13
FTMT	enzyme	2.75E-05	FTH1, FTL
TFAM	transcription regulator	2.98E-05	ACADS, CPT2, ECH1
LONP1	peptidase	4.94E-05	ACADS, ATP5F1D, ETFB, GPT2
PLAU	peptidase	5.25E-05	ANG, FN1, MMP12, PON1
ABCB7	transporter	9.12E-05	FTH1, FTL
cytokine	group	1.02E-04	ANG, CLU, EFNA1, MMP12, PON1
RXRA	ligand-dependent nuclear receptor	1.51E-04	CAT, CPT2, CXCL10, FTL, MLYCD, TPP1
LGR4	transmembrane receptor	1.66E-04	CXCL10, LECT2, OAT
NR2F1	ligand-dependent nuclear receptor	1.80E-04	ALDH2, CPT2, VTN
PDX1	transcription regulator	1.86E-04	CAT, CPT2, CROT, ECH1, EFNA1
PRKAA1	kinase	2.30E-04	CAT, FN1, MLYCD, OAT
VEGFA	growth factor	2.46E-04	ALDH2, CXCL10, ETFA, FN1, MMP12, SHMT2
IL4	cytokine	2.82E-04	ALDH2, CAT, CTSC, CXCL10, FN1, GCAT, ligp1, MMP12, MTDH, PLEC

Table 4.18 continued.

alb-SREBP-1c vs. aP2-SREBP-1c			
Upstream Regulator	**Molecule Type**	***p*-value**	**Target molecules in dataset**
KLF15	transcription regulator	3.29E-04	ACADS, CPT2, MLYCD
GH1	growth factor	3.46E-04	CLU, FN1, RPL6, SHMT2
PI3K (family)	group	3.71E-04	CAT, CXCL10, FTH1, MMP12
ANG	enzyme	4.06E-04	ANG, CXCL10
FTH1	enzyme	4.06E-04	FTH1, FTL
IREB2	translation regulator	4.06E-04	FTH1, FTL
Irp	group	4.06E-04	FTH1, FTL
MTOR	kinase	4.10E-04	CPT2, EFNA1, ETFA, FN1, MLYCD, Mug1/Mug2
PPARD	ligand-dependent nuclear receptor	4.75E-04	ALDH2, CPT2, ECH1, FN1, MLYCD

Table 4.19: Potential disease or function annotation of potential biomarkers for fatty liver. Data of differential secreted proteins (cut-off values: > 1.5-fold regulation; *p*-value < 0.05, ANOVA) were subjected to biomarker analyses (IPA) and further processed using the comparison routine to identify unique biomarker for each comparison. Unique differential regulated proteins assigned as potential biomarker were then subjected to the IPA core analyses module to identify downstream interaction networks.

C57Bl6 vs. alb-SREBP-1c			
Categories	**Disease or Function**	***p*-value**	**Molecules**
Lipid Metabolism, Small Molecule Biochemistry	Homeostasis of lipid	4.60E-08	GCKR,Mt1,APOA5,APOA2,RBP1,HSD11B1,APOC4,ANGPTL4,AKT2,Apoc3
Lipid Metabolism, Small Molecule Biochemistry	Homeostasis of triacylglycerol	1.84E-07	GCKR,APOA5,APOC4,ANGPTL4,Apoc3
Protein Synthesis	Quantity of hdl cholesterol in blood	4.96E-07	Anp32b,APOA2,HSD11B1,ANGPTL4,TGM2,Apoc3
Lipid Metabolism, Molecular Transport, Small Molecule Biochemistry	Transport of steroid	1.01E-06	PCYT1A,APOA5,APOA2,EPHX1,APOF,APOC4,AKR1C4,Apoc3

Table 4.19 continued.

C57Bl6 vs. alb-SREBP-1c			
Categories	**Disease or Function**	***p*-value**	**Molecules**
Lipid Metabolism, Molecular Transport, Small Molecule Biochemistry	Concentration of triacylglycerol	1.67E-06	AKR1B1,GCKR,PCYT1A,APOA5,APOA2,HSD11B1,SERPINE1,APOC4,ANGPTL4,AKT2,Apoc3
Connective Tissue Development and Function, Tissue Morphology	Quantity of connective tissue	1.89E-06	Mt1,LGMN,Hbb-b1,ANGPTL4,AKT2,Apoc3,IGFBP1,DHFR,GAMT,APOA2,ASPA,HSD11B1,SERPINE1,GFER,TGM2
Lipid Metabolism, Molecular Transport, Small Molecule Biochemistry	Flux of lipid	2.43E-06	PCYT1A,APOA5,APOA2,APOF,HSD11B1,APOC4,Apoc3
Lipid Metabolism, Molecular Transport, Small Molecule Biochemistry	Transport of lipid	3.82E-06	PCYT1A,APOA5,APOA2,EPHX1,APOF,LBP,APOC4,AKR1C4,Apoc3
Lipid Metabolism, Molecular Transport, Small Molecule Biochemistry	Concentration of cholesterol	5.43E-06	Anp32b,PCYT1A,APOA5,APOA2,HSD11B1,SERPINE1,GFER,ANGPTL4,TGM2,Apoc3
Lipid Metabolism, Molecular Transport, Small Molecule Biochemistry	Concentration of lipid	7.51E-06	GCKR,AKR1B1,RBP1,LBP,ANGPTL4,AKT2,Apoc3,Anp32b,PCYT1A,APOA5,APOA2,HSD11B1,SERPINE1,APOC4,GFER,TGM2,PDCD6IP
Endocrine System Disorders, Metabolic Disease	Insulin resistance	8.61E-06	GCKR,PCYT1A,APOA2,LBP,HSD11B1,SERPINE1,AKT2,TGM2,CA2,Apoc3
Lipid Metabolism, Molecular Transport, Small Molecule Biochemistry	Efflux of cholesterol	1.11E-05	PCYT1A,APOA5,APOA2,APOF,APOC4,Apoc3
Metabolic Disease	Disorder of lipid metabolism	1.16E-05	PCYT1A,APOA5,APOA2,LBP,HSD11B1,SERPINE1,ANGPTL4,AKT2,Apoc3
Connective Tissue Development and Function, Tissue Morphology	Quantity of adipose tissue	1.53E-05	Mt1,GAMT,APOA2,ASPA,HSD11B1,SERPINE1,ANGPTL4,AKT2,Apoc3

Table 4.19 continued.

C57Bl6 vs. alb-SREBP-1c			
Categories	**Disease or Function**	***p*-value**	**Molecules**
Hematological Disease, Metabolic Disease	Dyslipidemia	2.56E-05	APOA5,APOA2,LBP,HSD11B1,SERPINE1,ANGPTL4,Apoc3
Lipid Metabolism, Small Molecule Biochemistry, Vitamin and Mineral Metabolism	Metabolism of terpenoid	2.60E-05	RBP1,APOA2,APOF,ASPA,HSD11B1,DHRS4,AKR1C4,AACS,Apoc3
Lipid Metabolism, Molecular Transport, Small Molecule Biochemistry	Clearance of lipid	3.50E-05	APOA5,HSD11B1,ANGPTL4,Apoc3
Cancer, Gastrointestinal Disease, Organismal Injury and Abnormalities	Metastatic gastric adenocarcinoma	4.19E-05	UMPS,CYR61,DHFR,TUBA4A
Cell Morphology, Embryonic Development	Morphology of embryonic cell lines	4.96E-05	PTBP1,OXSR1,SERPINE1,AKT2
Lipid Metabolism, Small Molecule Biochemistry, Vitamin and Mineral Metabolism	Steroid metabolism	5.16E-05	APOA2,APOF,ASPA,HSD11B1,DHRS4,AKR1C4,AACS,Apoc3
Cancer, Organismal Injury and Abnormalities, Renal and Urological Disease	Hyperplasia of renal tubule	5.24E-05	LGMN,HSD11B1
Lipid Metabolism, Molecular Transport, Small Molecule Biochemistry	Clearance of triacylglycerol	5.62E-05	APOA5,ANGPTL4,Apoc3
Lipid Metabolism, Small Molecule Biochemistry	Metabolism of acylglycerol	5.93E-05	APOA5,APOA2,EPHX1,APOF,HSD11B1,Apoc3
Lipid Metabolism, Small Molecule Biochemistry	Catabolism of acylglycerol	6.66E-05	APOA5,APOA2,Apoc3

Table 4.19 continued.

C57Bl6 vs. alb-SREBP-1c			
Categories	**Disease or Function**	***p*-value**	**Molecules**
Lipid Metabolism, Molecular Transport, Small Molecule Biochemistry	Quantity of steroid	7.42E-05	Anp32b,PCYT1A,APOA5,APOA2,HSD11B1,SERPINE1,GFER,ANGPTL4,AKT2,TGM2,Apoc3
Cancer, Gastrointestinal Disease, Organismal Injury and Abnormalities	Metastatic gastrointestinal carcinoma	8.57E-05	CSE1L,UMPS,CYR61,DHFR,TUBA4A
Renal and Urological System Development and Function	Morphology of urinary system	8.90E-05	IGFBP1,AKR1B1,Mt1,Anp32b,LGMN,HSPA4L,HSD11B1,SERPINE1,ANGPTL4
Gastrointestinal Disease	Abnormal absorption of mineral in intestine	1.05E-04	KRT8,Mt1
Lipid Metabolism, Small Molecule Biochemistry	Metabolism of triacylglycerol	1.07E-04	APOA5,APOA2,APOF,HSD11B1,Apoc3
Molecular Transport	Transport of molecule	1.41E-04	SNX3,KRT8,GCKR,Mt1,RBP1,Hbb-b1,APOF,LBP,AKR1C4,AKT2,TNPO1,CLIC1,Apoc3,CA2,RANGAP1,PCYT1A,APOA5,APOA2,NUDT4,EPHX1,HSD11B1,APOC4
Cardiovascular Disease, Hematological Disease, Metabolic Disease	Hypertriglyceridemia	1.45E-04	APOA5,APOA2,ANGPTL4,Apoc3
C57Bl6 vs. aP2-SREBP-1c			
Categories	**Disease or Function**	***p*-value**	**Molecules**
Energy Production, Lipid Metabolism, Small Molecule Biochemistry	Beta-oxidation of fatty acid	1.17E-11	PEBP1,ECI1,ACADVL,ACOX1,HSD17B4,FASN,HADH,CYP2E1,ACAA1,BDH2,FABP2
Lipid Metabolism, Small Molecule Biochemistry	Fatty acid metabolism	6.79E-11	APOA4,NPC2,FASN,CYP2E1,MAP2K1,APOM,ACOX1,FABP5,Acot1,FABP2,EGFR,ACADVL,HPGD,FABP4,CD14,S100A9,CRAT,ACAA1,THRSP,APCS,ACOT1,HSD17B4,APOA1,ACOT2,SUCLG2,CASP8
Lipid Metabolism, Molecular Transport, Small Molecule Biochemistry	Concentration of lipid	8.73E-11	APOA4,HINT1,COMT,GNE,KLKB1,NPC2,FASN,CYP2E1,MAP2K1,Apoc1,APOM,FABP5,FABP2,ENTPD5,EGFR,HPGD,FABP4,H2AFY,CD14,S100A9,HADH,GSTK1,ECI1,THRSP,SIRT3,HSD17B4,APOA1,CPE,SERPINA1,ACOT2,CASP8

Table 4.19 continued.

C57Bl6 vs. aP2-SREBP-1c			
Categories	**Disease or Function**	***p*-value**	**Molecules**
Energy Production, Lipid Metabolism, Small Molecule Biochemistry	Oxidation of fatty acid	1.04E-10	PEBP1,ACADVL,FABP4,HPGD,FASN,HADH,BDH2,CYP2E1,ACAA1,ECI1,ACOX1,HSD 17B4,APOA1,FABP2
Lipid Metabolism, Small Molecule Biochemistry	Conversion of fatty acid	3.66E-08	FABP4,ACOX1,HPGD,HSD17B4,FASN,CRAT,CYP2E1
Lipid Metabolism, Molecular Transport, Small Molecule Biochemistry	Concentration of fatty acid	5.76E-08	EGFR,HPGD,FABP4,HINT1,KLKB1,FASN,HADH,CYP2E1,ECI1,THRSP,SIRT3,HSD17B 4,SERPINA1,ACOT2,FABP5
Lipid Metabolism, Small Molecule Biochemistry	Homeostasis of lipid	6.73E-08	APOA4,AMPD2,THRSP,ACADVL,FABP4,SIRT3,HSD17B4,APOA1,NPC2,MAP2K1,Apo c1,FABP2
Lipid Metabolism, Small Molecule Biochemistry	Metabolism of very long chain fatty acid	8.31E-08	ACOX1,ACOT1,HSD17B4,ACOT2,ACAA1
Nucleic Acid Metabolism	Metabolism of nucleic acid component or derivative	2.01E-07	ENTPD5,AMPD2,COMT,PKLR,FASN,THBS1,CYP2E1,GMPPB,PFAS,IDH3A,ACOT1,AP OA1,ACOT2,FBP1,SMPDL3A,Acot1,SUCLG2,APRT,CASP8
Metabolic Disease	Enzymopathy	2.16E-07	CPS1,PSPH,GLUL,ACADVL,COQ7,GNE,CD14,NPC2,HADH,BCHE,HEXA,SUOX,SERP INA1,FBP1
Gastrointestinal Disease, Hepatic System Disease, Metabolic Disease, Organismal Injury and Abnormalities	Hepatic steatosis	3.31E-07	ACADVL,FABP4,H2AFY,CD14,FASN,CYP2E1,ACOX1,ACOT1,SIRT3,HSD17B4,SERPI NA1,FABP5,GSTP1,ERN1
Lipid Metabolism, Molecular Transport, Small Molecule Biochemistry	Export of lipid	6.55E-07	APOA4,APCS,FABP4,CD14,S100A9,APOA1,NPC2,CRAT,APOM
Lipid Metabolism, Molecular Transport, Small Molecule Biochemistry	Flux of lipid	6.55E-07	APOA4,APCS,FABP4,CD14,PKLR,S100A9,APOA1,NPC2,APOM
Lipid Metabolism, Molecular Transport, Small Molecule Biochemistry	Concentration of acylglycerol	7.68E-07	ENTPD5,APOA4,EGFR,FABP4,H2AFY,HINT1,FASN,GSTK1,Apoc1,APOM,ECI1,THRS P,SIRT3,APOA1,FABP5

Table 4.19 continued.

C57Bl6 vs. aP2-SREBP-1c			
Categories	**Disease or Function**	***p*-value**	**Molecules**
Cancer, Organismal Injury and Abnormalities, Respiratory Disease	Lung cancer	1.66E-06	CPS1,GSTA5,TUBB3,LGALS1,FASN,THBS1,TUBA1C,MAP2K1,C8B,PFAS,HIST2H2AC,MYH9,HIST1H1C,RPS19,ACOX1,FBP1,SRM,GSTP1,EGFR,HPGD,H2AFY,FABP4,TUBB,NUCKS1,EIF3A,IGFBP2,BCHE,NME1,LIFR,SND1,IDH3A,ACOT1,HSD17B4,APOA1,CPE,ACOT2,SELENBP1,H1F0,CASP8
Metabolic Disease	Glucose metabolism disorder	1.75E-06	FASN,THBS1,CYP2E1,TUBA1C,Mup1 (includes others),APOM,ENPEP,C2,ACOX1,FBP1,FABP5,GSTP1,FABP2,ENTPD5,EGFR,ACADVL,HPGD,FABP4,TUBB,PKLR,GBE1,INSRR,IGFBP2,HADH,ACAA1,SIRT3,APOA1,CPE,PIN4,ERN1,CASP8
Endocrine System Disorders, Metabolic Disease	Metabolic syndrome X	1.76E-06	FABP4,ACOX1,SIRT3,GBE1,APOA1,FASN,FABP5,THBS1,CYP2E1
Cancer, Organismal Injury and Abnormalities	Adenoma	1.80E-06	ENTPD5,EGFR,GLUL,FABP4,HINT1,LGALS1,TUBB3,IGFBP2,THBS1,TUBA1C,MAP2K1,LIFR,HIST1H1C,ENPEP,APCS,UBE2I,APOA1,GSTP1,SMPDL3A
Metabolic Disease	Amyloidosis	2.13E-06	APOA4,TUBB,CD14,LGALS1,HNRNPU,S100A9,IGFBP2,RAB14,CTGF,BCHE,APCS,CLUH,CAST,APOA1,SERPINA1,SELENBP1,FAM3C,CASP8,ITM2B
Organismal Injury and Abnormalities, Renal and Urological Disease	Proximal tubular toxicity	2.71E-06	FABP4,LGALS1,FASN,HADH,CYP2E1,GSTP1,ACAA1
Cancer, Organismal Injury and Abnormalities	Development of benign tumor	3.59E-06	ENTPD5,EGFR,GLUL,FABP4,HINT1,LGALS1,TUBB3,S100A9,IGFBP2,THBS1,TUBA1C,MAP2K1,LIFR,HIST1H1C,ENPEP,APCS,UBE2I,APOA1,GSTP1,SMPDL3A
Lipid Metabolism, Molecular Transport, Small Molecule Biochemistry	Accumulation of lipid	4.45E-06	ACADVL,FABP4,NPC2,FASN,HEXA,Mup1 (includes others),MYH9,ECI1,Ces1e,ACOX1,SIRT3,APOA1,ERN1
Lipid Metabolism, Molecular Transport, Small Molecule Biochemistry	Efflux of lipid	4.62E-06	APOA4,APCS,FABP4,CD14,S100A9,APOA1,NPC2,APOM
Inflammatory Response, Organismal Injury and Abnormalities	Inflammation of organ	5.50E-06	APOA4,TUBB3,LGALS1,FASN,THBS1,CYP2E1,TUBA1C,MAP2K1,MYH9,ACOX1,FABP5,GSTP1,ENTPD5,EGFR,ACADVL,HPGD,FABP4,TUBB,CD14,S100A9,GSTK1,APCS,ACOT1,SIRT3,UBE2I,APOA1,SELENBP1,APRT,ITM2B
Lipid Metabolism, Molecular Transport, Small Molecule Biochemistry	Transport of lipid	5.65E-06	APOA4,APCS,FABP4,CD14,S100A9,APOA1,NPC2,FABP5,CRAT,APOM,FABP2

Table 4.19 continued.

C57Bl6 vs. aP2-SREBP-1c			
Categories	**Disease or Function**	***p*-value**	**Molecules**
Lipid Metabolism, Nucleic Acid Metabolism, Small Molecule Biochemistry	Metabolism of acyl-coenzyme A	6.00E-06	ACOT1,FASN,ACOT2,Acot1,SUCLG2
Neurological Disease, Organismal Injury and Abnormalities, Psychological Disorders	Tauopathy	6.74E-06	APOA4,TUBB,CD14,LGALS1,TUBB3,HNRNPU,S100A9,IGFBP2,RAB14,CTGF,BCHE,TUBA1C,CLUH,APOA1,SERPINA1,SELENBP1,FAM3C,CASP8
Cell Death and Survival	Cell death of tumor cell lines	7.11E-06	PEBP1,EIF3G,BCL2L13,HINT1,Cdc42,TUBB3,LGALS1,GNE,NPC2,FASN,CTGF,THBS1,CYP2E1,MAP2K1,RPS19,EIF2S2,PA2G4,GSTP1,ENTPD5,EGFR,PUF60,MRPL49,CD14,GBE1,S100A9,IGFBP2,BCHE,NME1,SND1,SIRT3,UBE2I,CAST,ERN1,CASP8
Cellular Movement	Cellular infiltration	7.16E-06	EGFR,FABP4,LGALS1,Cdc42,TUBB,CD14,S100A9,CTGF,THBS1,MYH9,C2,APCS,APOA1,CAST,SERPINA1,SELENBP1
Lipid Metabolism, Molecular Transport, Small Molecule Biochemistry	Concentration of triacylglycerol	7.68E-06	ENTPD5,APOA4,FABP4,H2AFY,FASN,GSTK1,Apoc1,APOM,ECI1,THRSP,SIRT3,APOA1,FABP5
Organismal Survival	Morbidity or mortality	7.88E-06	CPS1,Cdc42,GNE,Hist1h1e,NPC2,FASN,CTGF,THBS1,CYP2E1,MAP2K1,HEXA,CNPY3,MYH9,RPS19,HIST1H1C,LIMA1,GSTP1,EGFR,ACADVL,HPGD,H2AFY,COQ7,CD14,GFRA1,GBE1,INSRR,S100A9,IGFBP2,UROD,BCHE,GSTK1,LIFR,IDH3A,EIF3D,APCS,SIRT3,UBE2I,HSD17B4,CAST,APOA1,SERPINA1,SELENBP1,ERN1,NEDD8,H1F0,APRT,CASP8
alb-SREBP-1c vs. aP2-SREBP-1c			
Categories	**Disease or Function**	***p*-value**	**Molecules**
Developmental Disorder, Hereditary Disorder, Metabolic Disease, Organismal Injury and Abnormalities	Fatty acid oxidation disorder	2.55E-10	MLYCD,ACADS,ETFB,ETFA,CPT2,ETFDH
Developmental Disorder, Hereditary Disorder, Metabolic Disease, Organismal Injury and Abnormalities, Renal and Urological Disease	Glutaric aciduria type 2	1.02E-07	ETFB,ETFA,ETFDH
Metabolic Disease	Enzymopathy	1.15E-07	UPB1,SARDH,ETFB,CPT2,ETFA,NDUFS6,NDUFV2,TPP1,MAN2B1,ETFDH

Table 4.19 continued.

alb-SREBP-1c vs. aP2-SREBP-1c			
Categories	**Disease or Function**	***p*-value**	**Molecules**
Metabolic Disease, Organismal Injury and Abnormalities, Renal and Urological Disease	Organic aciduria	4.33E-07	OAT,MLYCD,ETFB,ETFA,ETFDH
Amino Acid Metabolism, Small Molecule Biochemistry	Synthesis of amino acids	3.66E-06	UPB1,SHMT2,SARDH,GLS2,CTH
Lipid Metabolism, Small Molecule Biochemistry	Fatty acid metabolism	4.96E-06	PON1,MLYCD,MAPK14,FN1,VTN,STARD5,CROT,CLU,ACSM1,MMP12,CPT2,NDUFS6
Developmental Disorder, Hereditary Disorder, Metabolic Disease, Organismal Injury and Abnormalities	Mitochondrial respiratory chain deficiency	5.59E-06	ETFB,ETFA,NDUFS6,NDUFV2,ETFDH
Amino Acid Metabolism, Small Molecule Biochemistry	Synthesis of serine family amino acid	7.16E-06	SHMT2,SARDH,CTH
Cellular Development, Cellular Growth and Proliferation	Re-entry into growth of leukemia cell lines	8.82E-06	FTL,FTH1
Amino Acid Metabolism, Small Molecule Biochemistry	Synthesis of alpha-amino acid	9.92E-06	SHMT2,SARDH,GLS2,CTH
Metabolic Disease	Abnormal activity of enzyme	1.02E-05	PON1,HINT2,CTSC,ALDH2,PPME1
Drug Metabolism, Molecular Transport, Small Molecule Biochemistry	Concentration of glutathione	1.07E-05	CAT,ALDH2,GLS2,CTH,FTH1
Cardiovascular Disease, Organismal Injury and Abnormalities	Abdominal aortic aneurysm	1.08E-05	FTL,CXCL10,MMP12,CTSC
Energy Production, Lipid Metabolism, Small Molecule Biochemistry	Oxidation of lipid	1.10E-05	PON1,MLYCD,MAPK14,ACADS,CROT,CAT,CPT2
Amino Acid Metabolism, Small Molecule Biochemistry	Synthesis of sulfur amino acid	1.13E-05	SHMT2,SARDH,CTH
Cell-To-Cell Signaling and Interaction	Binding of lung cell lines	1.39E-05	VTN,FN1,CXCL10

Table 4.19 continued.

alb-SREBP-1c vs. aP2-SREBP-1c			
Categories	**Disease or Function**	***p*-value**	**Molecules**
Cardiovascular System Development and Function	Morphology of cardiovascular system	1.91E-05	MAPK14,CXCL10,PLEC,FN1,VTN,CLU,CAT,CTSC,EEF1D,CPT2,EFNA1,NDUFS6,MAN2B1
Neurological Disease	Sporadic amyotrophic lateral sclerosis	2.02E-05	PON1,CLU,ANG
Amino Acid Metabolism, Small Molecule Biochemistry	Metabolism of amino acids	2.22E-05	OAT,UPB1,SHMT2,SARDH,GLS2,CTH
Molecular Transport	Transport of molecule	2.28E-05	PON1,MAPK14,FTL,ACADS,CXCL10,MMP12,ANG,S100A13,ATP5F1D,SEPT2,PPME1,FN1,STARD5,CROT,CLU,CAT,CPT2,FTH1,MTDH
Cell-To-Cell Signaling and Interaction, Cellular Compromise, Tumor Morphology	Adhesion of glioma cells	2.64E-05	FN1,VTN
Cell Morphology, Cellular Movement	Cell spreading of lung cell lines	2.64E-05	VTN,FN1
Carbohydrate Metabolism, Small Molecule Biochemistry	Metabolism of mannose	2.64E-05	MAN2B2,MAN2B1
Developmental Disorder, Hereditary Disorder, Metabolic Disease, Organismal Injury and Abnormalities	Inborn error of amino acid metabolism	4.40E-05	SARDH,ETFB,ETFA,CTH,ETFDH
Cell-To-Cell Signaling and Interaction, Nervous System Development and Function	Adhesion of astrocytes	5.27E-05	VTN,FN1
Cellular Movement	Haptotaxis of neuroblastoma cell lines	5.27E-05	FN1,VTN
Metabolic Disease	Disorder of lipid metabolism	6.17E-05	PON1,MLYCD,ACADS,ETFB,CPT2,ETFA,ETFDH
Cell-To-Cell Signaling and Interaction, Cellular Function and Maintenance, Hematological System Development and Function, Inflammatory Response	Phagocytosis by peritoneal macrophages	7.94E-05	MAPK14,VTN,LECT2

Table 4.19 continued.

alb-SREBP-1c vs. aP2-SREBP-1c			
Categories	**Disease or Function**	***p*-value**	**Molecules**
Cellular Compromise, Lipid Metabolism, Small Molecule Biochemistry	Peroxidation of phospholipid	8.77E-05	PON1,CAT
Amino Acid Metabolism, Small Molecule Biochemistry	Synthesis of glycine	8.77E-05	SHMT2,SARDH
Cardiovascular System Development and Function, Organismal Development, Tissue Morphology	Vasodilation of artery	1.02E-04	CXCL10,CAT,ALDH2,CTH
Post-Translational Modification, Protein Synthesis, Protein Trafficking	Homotetramerization of protein	1.02E-04	SHMT2,ACADS,CAT,CTH

4.6 Insulin-like growth factor 2 (IGFBP2) in the pathology of fatty liver

Analysis of liver tissue transcriptome revealed that in comparison of the two different fatty liver models alb-SREBP-1c and aP2-SREBP-1c IGFBP2 was the top regulator effect network with a consistency score of 10.44 (table 4.11). The IGFBP2 regulator effect is caused by an overall differential regulation of components of the canonical signaling pathway of IGF as depicted in figure 4.20. In C57Bl6 versus alb-SREBP-1c only one downstream signaling molecule shows differential regulation, whereas in the metabolic model compared to C57Bl6 and even more pronounced if compared to alb-SREBP-1c almost all known IGF signaling downstream molecules of the canonical pathway show differential abundance.

Further, the analysis of primary hepatocyte secretome also showed that IGFBP2 protein was included in the top score lists of differential protein secretion with 2- to 3-fold lower amounts of IGFBP2 in the supernatant of aP2-SREBP-1c primary hepatocytes compared to either C57Bl6 or alb-SREBP-1c (see section 4.5.2) indicating IGFBP2 regulation involved in cause or consequence of fatty liver phenotype. Investigation of differential protein secretion from the different phenotypes for potential biomarkers in hepatocyte secretome also determined IGFBP2 as a potential biomarker of fatty liver (C57Bl6 vs. aP2-SREBP-1c: *q*-value 0.001, alb-SREBP-1c vs. aP2-SREBP-1c: 0.04). IGFBP2 levels were therefore analyzed in C57Bl6, alb-SREBP-1c and aP2-SREBP-1c animals as well as functionally investigated in primary hepatocytes to gain further insight in the role of IGFBP2 in fatty liver.

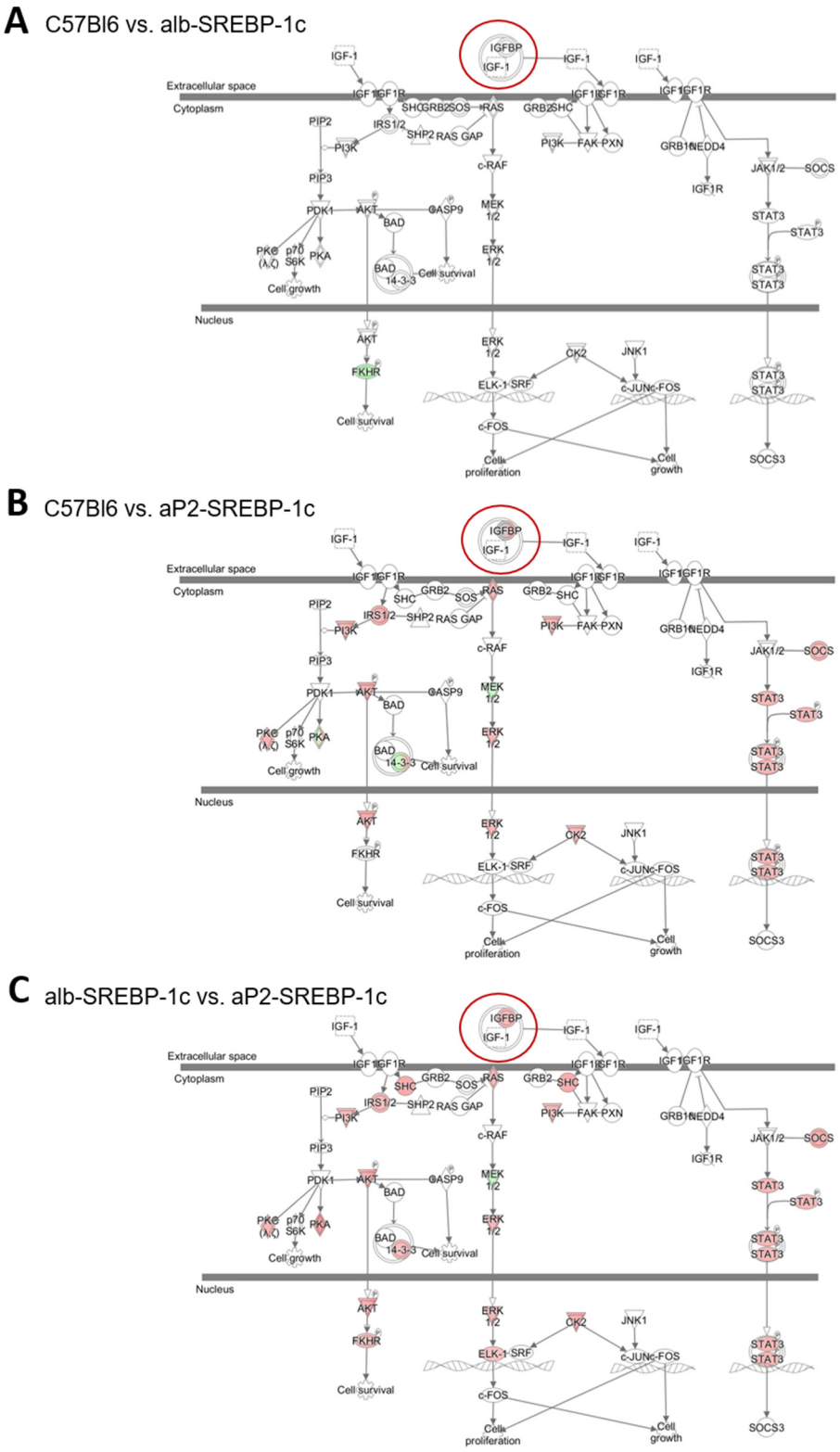

Figure 4.20: Differential activation of downstream molecules of the insulin-like growth factor (IGF) signaling network. Genes with differential gene expression (1.5-fold, p-value < 0.05) were used for IPA core analyses. Different abundance of genes in comparison of hepatic gene expression of (A) C57Bl6 vs. alb-SREBP-1c, (B) C57Bl6 vs. aP2-SREBP-1c and (C) alb-SREBP-1c vs. aP2-SREBP-1c liver tissue were overlaid to the canonical IGF signaling pathway (Ingenuity knowledge database). Color code: red - increase in condition 1, green - decrease in condition 1 based on measured expression differences. Red circles highlight IGFBP2.

4.6.1 Igfbp2 levels in C57Bl6, alb-SREBP-1c and aP2-SREBP-1c mice

In the presented study Igfbp2 concentration in plasma of mice with different fatty liver phenotypes was significantly reduced in aP2-SREBP-1c animals compared to either C57Bl6 or alb-SREBP-1c (figure 4.21 A). Similar results were detected when primary hepatocytes isolated from the different fatty liver phenotypes were investigated. Secretion of Igfbp2 from primary hepatocytes showed a 50 to 65% reduction of the protein in aP2-SREBP-1c culture medium compared to C57Bl6 or alb-SREBP-1c (figure 4.21 B). Also protein content in lysates from primary hepatocytes showed the lowest quantity of Igfbp2 in aP2-SREBP-1c while there were no differences between the two other investigated groups (figure 4.21 C). Further, Igfbp2 gene expression was analyzed from primary hepatocytes and again the results show no differences between alb-SREBP-1c and C57Bl6 but a significant reduction of Igfbp2 expression in aP2-SREBP-1c cells (figure 4.21 D).

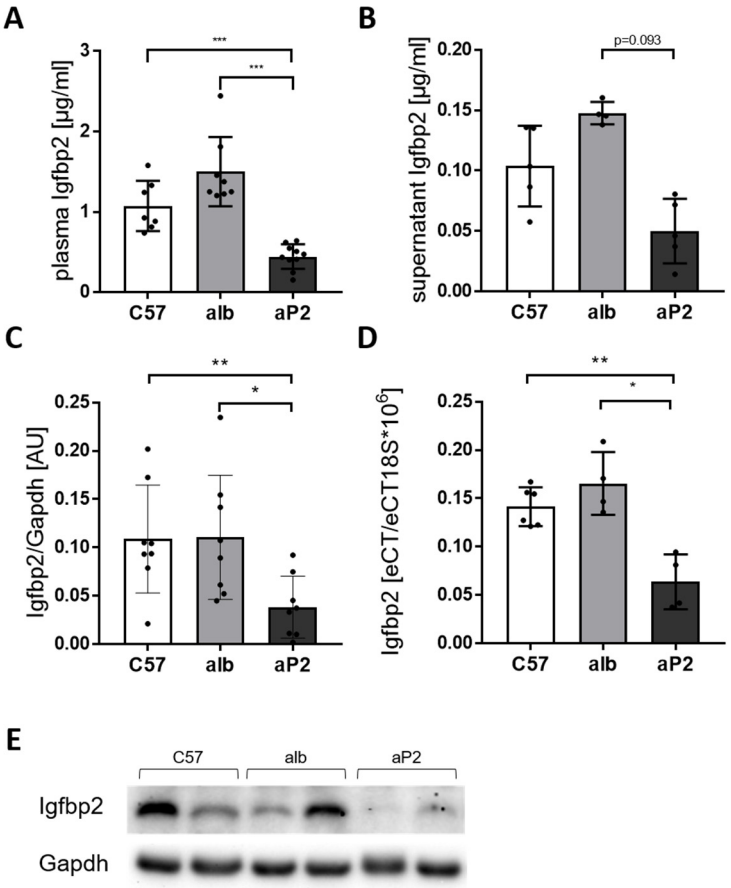

Figure 4.21: Igfbp2 levels in animal models of fatty liver *in vivo* and *ex vivo*. (A) EDTA-plasma from C57Bl6 (C57), alb-SREBP-1c (alb) and aP2-SREBP1c (aP2) mice was analyzed with ELISA to measure Igfbp2 concentration in representatives groups. (B) Secretion of Igfbp2 was measured in supernatants of hepatocyte cultures after overnight culture of the cells. (C) Igfbp2 protein content and (D) Igfbp2 gene expression was measured in primary hepatocytes isolated from the different fatty liver phenotypes. (E) Representative western blot pictures are shown. Bar graphs represent the mean ±SD of 10 animals per group for serum analysis and 4 to 8 independent experiments for analysis of primary hepatocytes. Differences between two groups were calculated using Mann-Whitney-U test. * $p < 0.05$ or ** $p < 0.01$ or *** $p < 0.001$ as indicated.

Igf-I and Igfbp3 levels were also measured in animal plasma, primary hepatocyte culture supernatant as well as their expression level in primary hepatocytes from the different phenotypes used in the study. Igfbp3 plasma levels were not different between the investigated phenotypes (figure 4.22 A) while Igf-I was increased in both fatty liver model systems (alb-SREBP-1c 366.9 ± 60,62 ng/ml; aP2-SREBP-1c 354.9 ± 67.24 ng/ml) compared to C57Bl6 plasma level (265.1 ± 73.12 ng/ml, figure 4.22 D). Secreted Igf-I from primary hepatocytes in culture was not different between the groups (figure 4.22 E). Igfbp3 abundance in culture supernatant from alb-SREBP-1c was significantly lower ($p < 0.05$) compared to the two other phenotypes and highest in aP2-SREBP-1c which was significantly different from the other two groups ($p < 0.05$). Relative gene expression from Igfbp3 and Igf-I (figure 4.22 C and F) were significantly increased in aP2-SREBP-1c animals. There was decreased expression measured for Igfbp3 gene in alb-SREBP-1c compared to C57Bl6 (p-values < 0.05) while Igf-I gene expression was not different between C57Bl6 and alb-SREBP-1c.

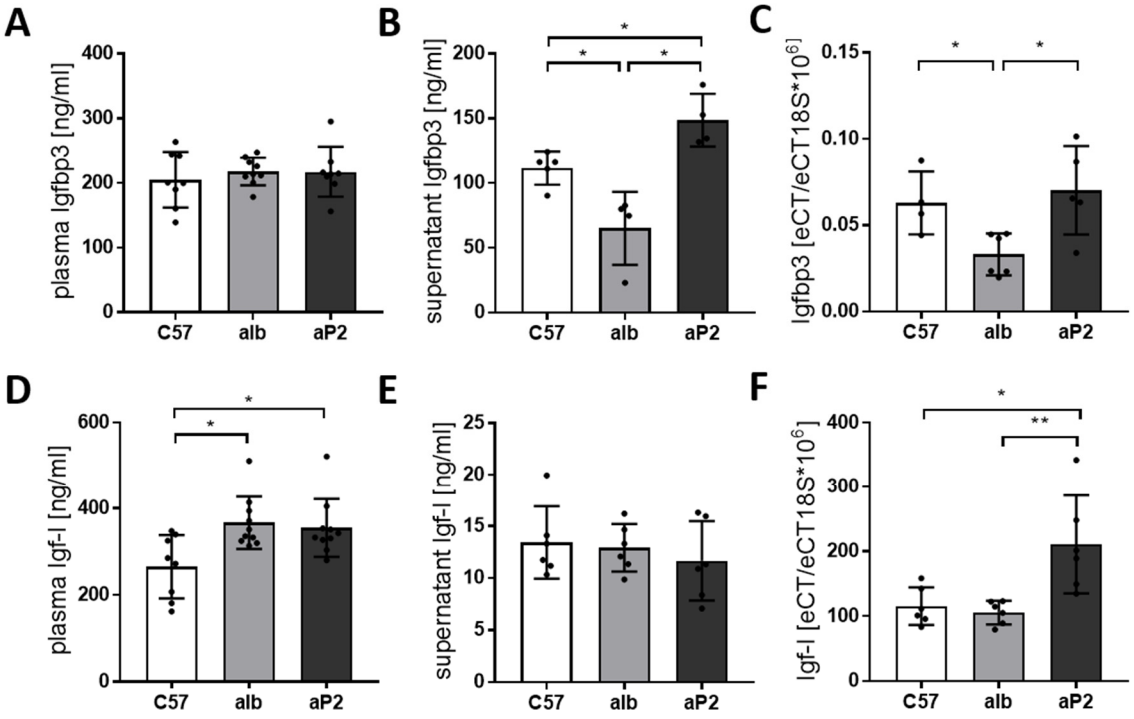

Figure 4.22: Igfbp3 and Igf-I levels in animal models of fatty liver *in vivo* and *ex vivo*. (A, D) Igfbp3 and Igf-I EDTA-plasma concentration was measured via ELISA in representative groups of C57Bl6 (C57), alb-SREBP-1c (alb) and aP2-SREBP-1c (aP2) animals. (B, E) Primary hepatocyte supernatant from overnight culture was analyzed for Igfbp3 and Igf-I concentration. (C, F) Primary hepatocytes were analyzed for relative gene expression of Igfbp3 and Igf-I. Bar graphs represent the mean ±SD of 10 animals per group for serum analysis and 4 to 6 independent experiments for analysis of primary hepatocytes. Differences between two groups were calculated using Mann-Whitney-U test. * $p < 0.05$ or ** $p < 0.01$ as indicated.

4.6.2 Methylation analysis of Igfbp2 gene promotor

DNA methylation status as a potential mechanism of gene expression regulation for the Igfbp2 gene promotor was analyzed in hepatocytes from the fatty liver phenotypes. In figure 4.23 A representative pyrograms for the analysis of C57Bl6, alb-SREBP-1c and aP2-SREBP-1c Igfbp2 promotor region were illustrated. The calculated differences in cytosine methylation showed that aP2-SREBP-1c Igfbp2 promotor had significantly increased methylation compared to either C57Bl6 or alb-SREBP-1c (figure 4.23 B).

Further, methyltransferase activity was assessed in protein lysates from primary hepatocytes isolated from fatty liver mouse models. The activity of methyltransferases was found to be similar in C57Bl6 and alb-SREBP-1c protein lysates but increased 60 to 70% in aP2-SREBP-1c (figure 4.23 C).

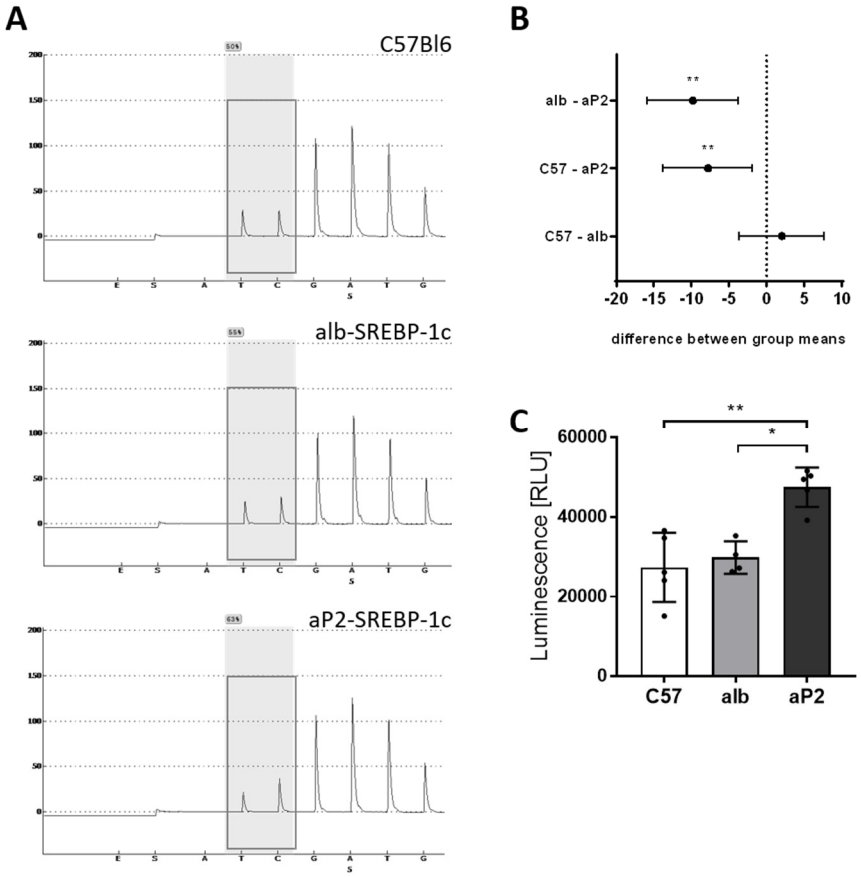

Figure 4.23: Methylation analysis of Igfbp2 gene promotor. Igfbp2 gene promotor region was analyzed for methylation of DNA using pyrosequencing. (A) Representative pyrograms for the analysis of primary hepatocytes isolated from C57Bl6 (C57), alb-SREBP-1c (alb) and aP2-SREBP1c (aP2) animals are shown. (B) Differences between mean methylation of pairwise analysis of C57 vs. alb, C57 vs. aP2 and alb vs. aP2. (C) Methyltransferase activity measured as luminescence signal proportional to catalyzing of S-adenosyl methionine to S-adenosyl homocysteine by methyltransferase present in primary hepatocytes protein lysates. Methylation analysis was performed for 6 to 8 DNA samples per group. Bar graphs represent the mean ±SD of 4 to 5 independent experiments per group. Differences between groups were calculated using (B) one-way ANOVA or (C) Mann-Whitney-U test. * $p < 0.05$ or ** $p < 0.01$ as indicated.

4.6.3 Effects of free fatty acids on Igfbp2 secretion

Primary hepatocytes isolated from C57Bl6 animals were treated either with the saturated fatty acid palmitate (C16:0) or the monounsaturated fatty acid oleate (C18:1) followed by 24 or 48 h incubation. In the supernatants of the hepatocyte cultures Igfbp2, Igfbp3 and Igf-I were measured by ELISA to investigate direct effects of fatty acids on cells from normal liver tissue. After 24 h of incubation none of the investigated molecules showed altered abundance between the supernatant of cells treated with either palmitate nor oleate compared to the respective BSA control condition (figure 4.24 A, C, E, G, I, K). In contrast, palmitate treatment of C57Bl6 cells for 48 h resulted in the reduction of Igfbp2, Igfbp3 and Igf-I in culture supernatants. Igfbp2 was reduced from 84.8 ± 6.12 µg/ml to 73.4 ± 6.12 µg/ml (figure 4.24 B) while the reduction of Igfbp3 was more pronounced with 70 % lower Igfbp3 content in palmitate supernatant (305.3 ± 56.52 pg/ml vs. 183.6 ± 56.52 pg/ml, figure 4.24 F). Igf-I secretion was reduced to 6.5 ± 0.79 ng/ml in palmitate treated cells which was 40% lower compared to the control condition (10.1 ± 0.79 ng/ml, figure 4.24 J). In oleate treated cultures 48 h incubation induced no changes of Igfbp2 or Igfbp3 secretion but showed a small though statistically significant decrease of Igf-I content in culture supernatant compared to the BSA treated control condition.

Further, in these cells marker for endoplasmic reticulum (ER) stress were analyzed at transcriptional level. Binding of immunoglobin protein (BiP) and CAAT/ enhancer-binding protein protein homologous protein (CHOP) are well known to be transcriptionally activated when cells face ER stress (Malhi and Kaufman 2011). The results of RNA analysis showed that oleate treatment had no impact on BiP and CHOP expression in C57Bl6 hepatocytes (figure 4.25 A and B). In contrast, 48 h incubation of C57Bl6 hepatocytes with 500 µM palmitate significantly induced expression of both tested ER stress marker (figure 4.25 C and D) indicating that palmitate treatment confronted the cells with ER stress.

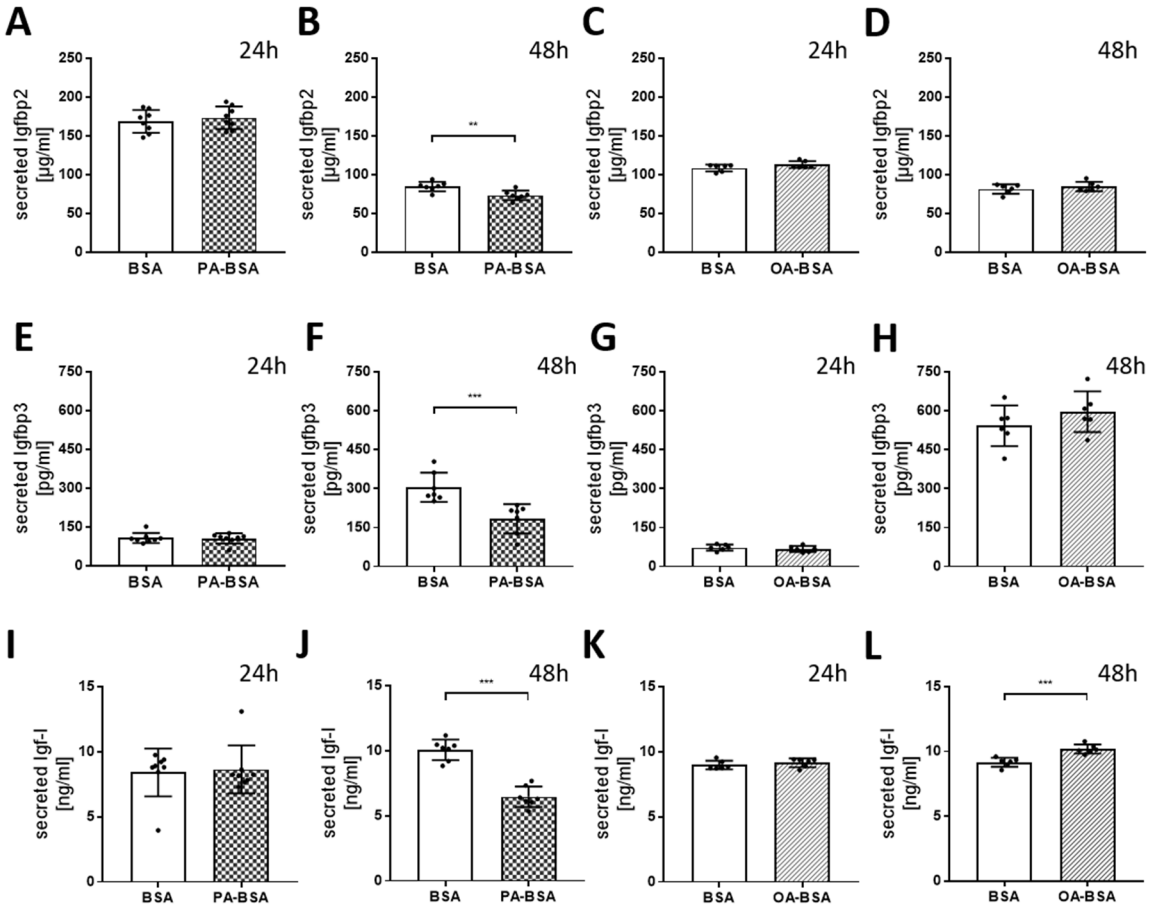

Figure 4.24: Effects of free fatty acids on Igfbp2, Igfbp3 and Igf-I secretion. Primary hepatocytes isolated from C57Bl6 animals were treated with 500 µM palmitate or oleate for 24 or 48 h. Supernatant of hepatocyte culture was investigated for (A - D) Igfbp2, (E - H) Igfbp3 and (I - L) Igf-I concentration using ELISA. Bar graphs represent mean ±SD of 6 to 8 independent experiments. Differences between groups were calculated using Mann-Whitney-U test. ** $p < 0.01$ or *** $p < 0.001$ as indicated.

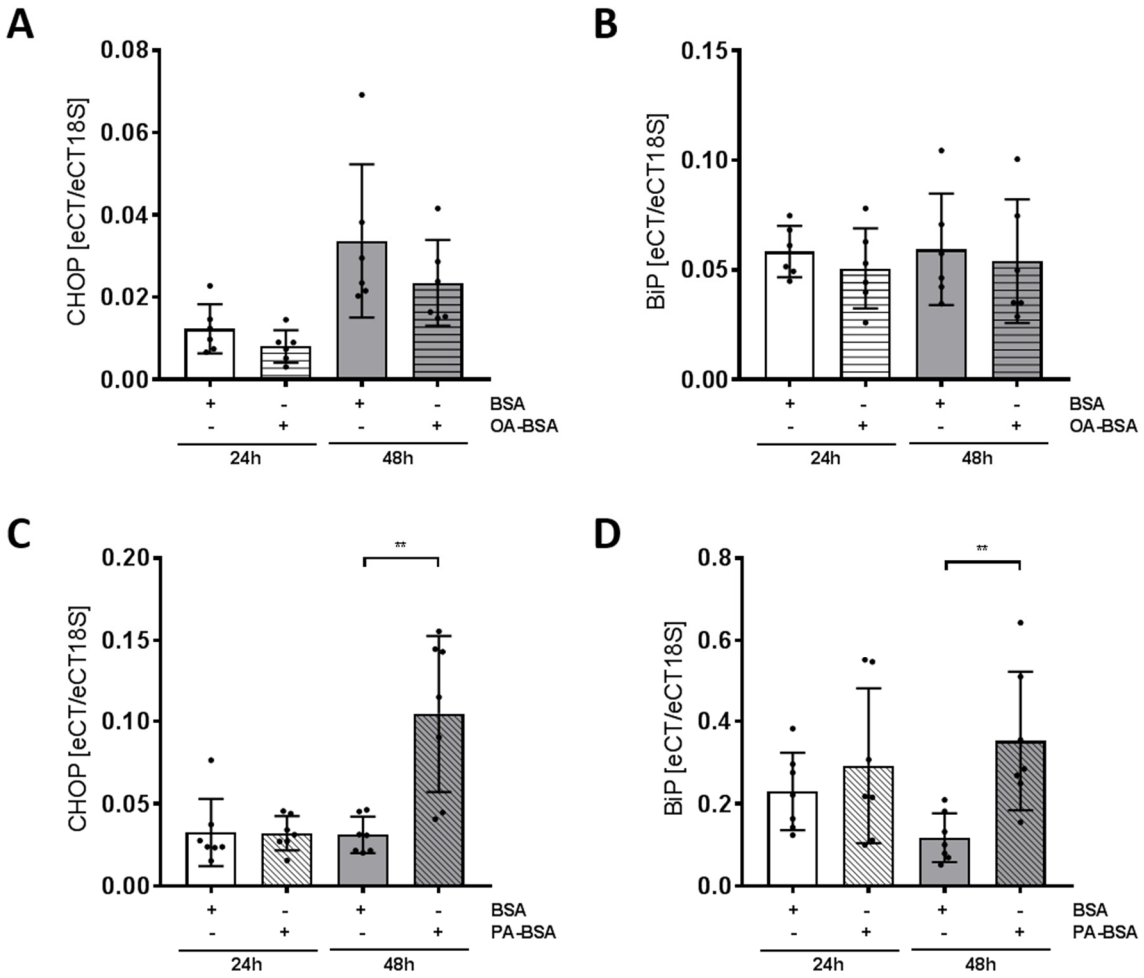

Figure 4.25: Expression of endoplasmic reticulum (ER) stress marker in primary hepatocytes treated with free fatty acids. RNA isolated from primary hepatocytes treated with 500 µM palmitate or oleate for 24 or 48 h was subjected to gene expression analysis of binding of immunoglobin protein (BiP) and CCAAT/ enhancer-binding protein homologous protein (CHOP). Bar graphs represent the mean ±SD of 6 to 7 independent experiments. Differences between two groups were calculated using Mann-Whitney-U test. ** $p < 0.01$.

4.6.4 IGFBP2 signaling and function in primary hepatocytes from fatty liver

The interaction of IGF-I and IGFBP2 in primary hepatocytes isolated from different liver tissues was investigated. At first, IGF-I-stimulated phosphorylation of Akt was analyzed at Ser 473 and Thr 308 as a downstream target of IGF-I signaling cascade in C57Bl6 primary hepatocytes. The cells were treated with either IGF-I or IGFBP2 alone or at equimolar combination before cell lysates were subjected to western blot analysis. IGF-I increased the phosphorylation of both Akt phosphorylation sites up to 65% (figure 4.26 A and B). IGFBP2 alone lead to no changes of IGF-I-mediated Akt phosphorylation. When the cells were incubated with equimolar concentrations of both recombinant proteins IGF-I-mediated increase of Akt Ser 473 and Thr 308 phosphorylation was inhibited by the presence of

IGFBP2 as the level of phosphorylation was equal to Akt phosphorylation in untreated cells (figure 4.26 A and B).

Further, effects of IGF-I and IGFBP2 on hepatic lipid metabolism were investigated in primary hepatocytes isolated from different fatty liver phenotypes. Cells were treated overnight with recombinant proteins prior to the performance of DNL, FAU or FAO experiments. In C57Bl6 primary hepatocytes IGF-I significantly increased DNL while no other condition was different from untreated cells (figure 4.26 C). Also in both fatty liver models DNL was markedly increased in primary hepatocytes when cells were incubated with IGF-I and this effect was not present in cells treated with a combination of IGF-I and IGFBP2. In alb-SREBP-1c hepatocytes IGFBP2 alone also lead to a statistically significant increase in DNL compared to the untreated condition of these cells. In sum, IGF-I increased DNL in all phenotypes 25 to 30% compared to basal condition which was inhibited in presence of IGFBP2 in C57Bl6 and alb-SREBP-1c but not in aP2-SREBP-1c hepatocytes. Investigation of IGF-I and IGFBP2 effects on FAU or FAO (figure 4.26 D or E) resulted in no significant differences between all conditions tested independent from hepatocyte phenotype.

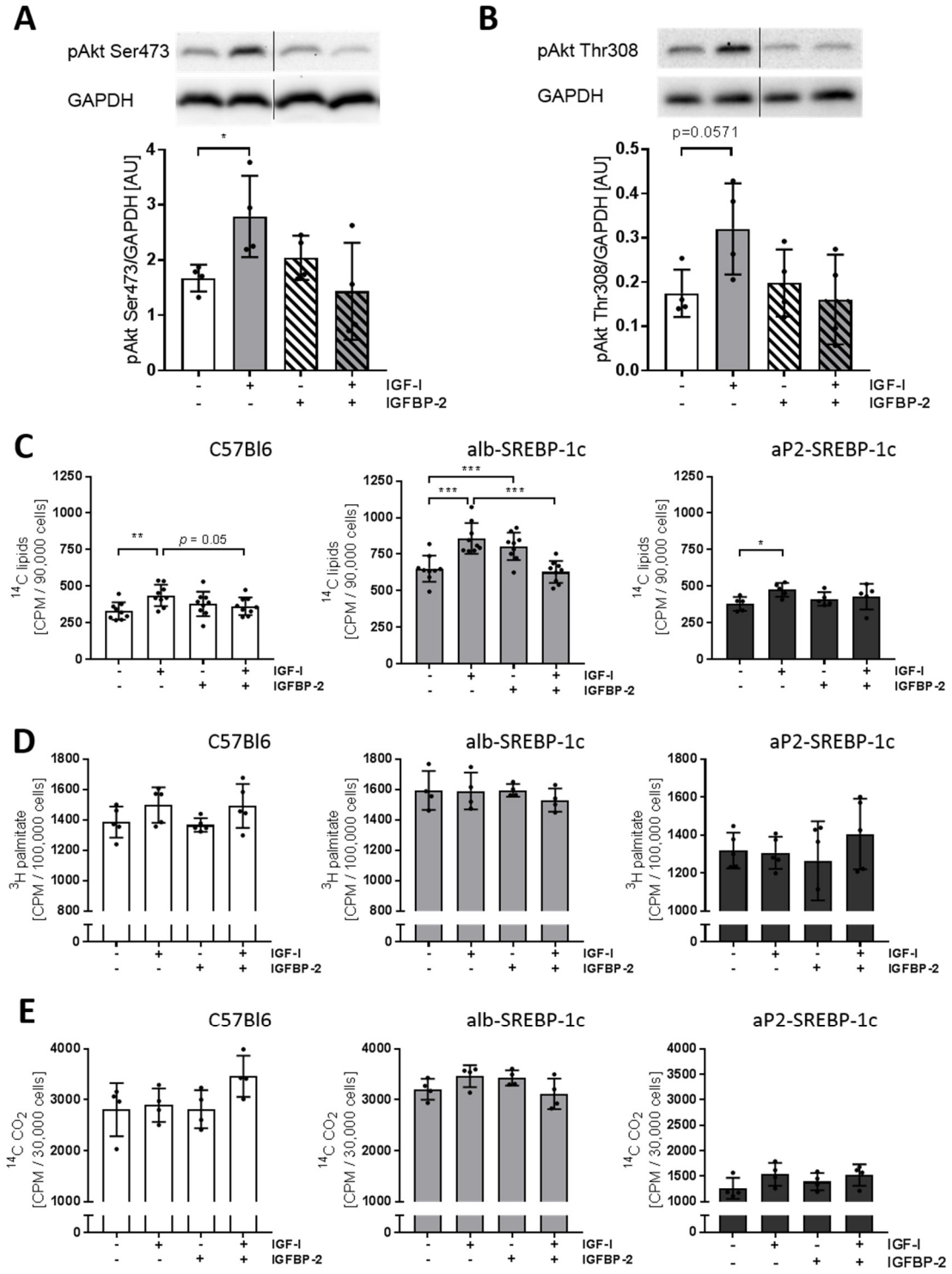

Figure 4.26: IGF-I and IGFBP2 in hepatic lipid metabolism. (A – B) Primary hepatocytes isolated from C57Bl6 animals were treated with 10 nM IGF-I or 10 nM IGFBP2 either alone or in combination for 10 min of incubation. Protein lysates of the cells were analyzed for IGF-I-mediated phosphorylation of Akt at (A) Ser473 or (B) Thr308. Representative western blot pictures are shown. (C – E) Primary hepatocytes isolated from C57Bl6 (C57), alb-SREBP-1c (alb) or aP2-SREBP1c (aP2) animals were treated with 10 nM IGF-I or 10 nM IGFBP2 either alone or in combination and incubated for assay dependent time periods. Cells were subjected to analysis of (C) *de novo* lipogenesis, (D) fatty acid uptake and (E) fatty acid β-oxidation. Bar graphs represent means ±SD of 4 to 9 independent experiments. Differences between two groups were calculated using Mann-Whitney-U test. * $p < 0.05$ or ** $p < 0.01$ or *** $p < 0.001$ as indicated.

4.6.5 IGFBP2 and fatty liver in humans

In a cohort of obese men before and two years after bariatric surgery (Ruige et al. 2012, Bekaert et al. 2015) IGFBP2 serum concentration was measured and an index for the prediction of hepatic steatosis (FLI according to Bedogni et al. 2006) was calculated. Patients with FLI < 30 can be ruled out while patients with FLI ≥ 60 have high probability to suffer from hepatic steatosis.

Patients included in this study had significant reduction in body fat and showed improved homeostatic model assessment of insulin resistance (HOMA-IR) between pre- and post-surgery analysis (table 3.15). In the pre-group mean IGFBP2 concentration of 146 ± 56.36 ng/ml was measured and showed a markedly increase to 395 ± 252.3 ng/ml ($p < 0.001$) in serum of patients 2 years after intervention (figure 4.27 A). The calculated FLI for each patient showed that the prediction for hepatic steatosis was reduced from 98 ± 4 to 72 ± 32 on average which included patients in the post-group who reduced FLI down to 7 (figure 4.27 B). Correlation of FLI difference between each pre- and post-data set and IGFBP2 serum concentration difference showed a significant relation of restored IGFBP2 serum levels and the reduction in hepatic steatosis prediction (Spearman analysis: r = -0.614, *p*-value = 0.0169, figure 4.27 C).

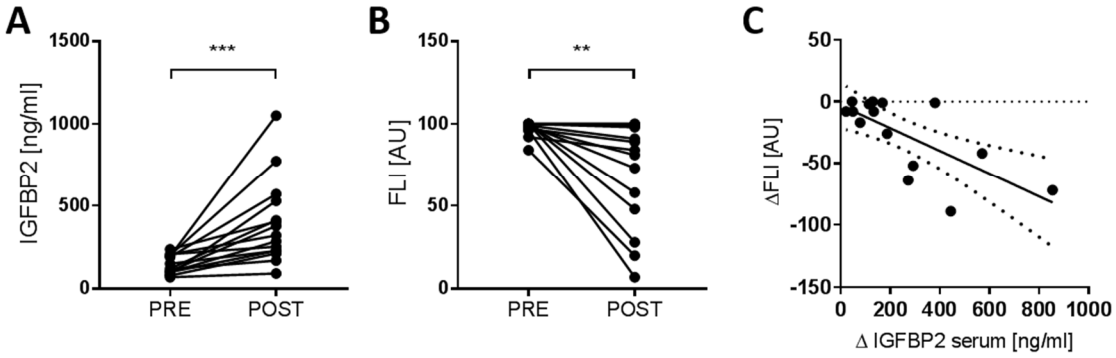

Figure 4.27: IGFBP2 and fatty liver in humans. (A) Serum concentration of IGFBP2 was measured in a cohort of obese men undergoing bariatric surgery. Serum samples were taken before (pre) and two years after (post) bariatric intervention. (B) Fatty liver index (FLI) was calculated for each patient. (C) The differences between pre and post FLI were plotted against the difference between pre and post IGFBP2 serum concentration. (A – B) Data were obtained from 15 individuals per group. Differences between groups were calculated using Mann-Whitney-U test. ** $p < 0.01$ or *** $p < 0.001$ as indicated. (C) Linear regression and 95 % confidence bands (dotted lines) are indicated.

5 Discussion

Today, NAFLD is the leading cause of chronic liver diseases with severe concomitant metabolic conditions like obesity, metabolic syndrome or diabetes. Excess accumulation of hepatic lipids, the major characteristic of NAFLD, is usually benign in the majority of patients while a small proportion develops progressive forms of the disease with inflammation, necrosis cirrhosis or even HCC. The underlying molecular mechanisms of disease development and progression still remain largely unknown although it is commonly accepted that it is a multifactorial disease where the interwoven network of carbohydrate and lipid metabolism gets imbalanced and consequently affects not only liver but also whole body energy homeostasis.

In this thesis, a holistic approach was applied to gain further insight in the molecular nature of the disease using two different mouse models with distinct stages of fatty liver phenotype i.e. a mild and a progressive form. The investigation focused on nodal points of carbohydrate and lipid metabolism and aimed to identify potential biomarker specific for pathophysiology. The novelty of the thesis is given, as the experimental approach allows the differentiation of pathophysiological mechanisms of hepatic lipid accumulation that were specifically caused by increased hepatic *de novo* lipogenesis (DNL) or increased systemic flow of lipids. In detail, results of this thesis indicate that i) differences in hepatic gene expression can be verified in *ex vivo* primary hepatocytes, ii) hepatokine secretion from isolated metabolic active hepatocytes monitors the physiological alteration of the liver which iii) allows the identification and verification of hepatocyte derived biomarker for liver function, e.g. IGFBP2.

5.1 Mouse models of fatty liver

In this study two different mouse models with a phenotype of fatty liver were used. Both models were generated by tissue specific overexpression of the human transcription factor sterol regulatory element-binding protein (SREBP)-1c. The first model develops fatty liver due to constantly active intra-hepatic *de novo* lipid production (alb-SREBP-1c) and represents a genetically lipogenic phenotype. The accumulation of hepatic lipids in the second model (aP2-SREBP-1c) is associated with increased lipid flux due to lipodystrophy and resembles a metabolic form of fatty liver (Shimomura et al. 1998, Knebel et al. 2012).

5.1.1 Genetic versus metabolic induction of hepatic lipid accumulation

In human NAFLD 26% of liver lipid content were found to be derived from intrahepatic DNL (Donnelly et al. 2005). DNL in the liver is predominantly regulated through the transcription factor SREBP-1c which selectively targets genes involved in glucose and lipid homeostasis

(Kawano and Cohen 2013). SREBP-1c, a member of the family of SREBFs, i.e. SREBP-1a, -1c and SREBP-2, is one of the central transcription factors in the regulation of lipid metabolism, (Brown and Goldstein 1997, 1999, 2009; Goldstein et al. 2006). As shown SREBPs regulate central lipid-relevant genes as LDL receptor, acetyl-CoA carboxylase, fatty acid synthase, hydroxymethylglutaryl (HMG)-CoA synthase and HMG-CoA reductase. One potent activator of SREBP-1c is insulin (Kotzka et al. 1998). As initially postulated by Brown and Goldstein 2008, SREBP-1c still remains responsive to insulin-stimulation in states of insulin resistance, which is a metabolically paradox (Brown and Goldstein 2008, Haas et al. 2012, Softic et al. 2016). In contrast, selective hepatic inactivation of the insulin receptor in mice was found to significantly decrease SREBP-1c and its target gene expression (Biddinger et al. 2005 and 2008a). However, SREBP-1c is reduced in states of insulin depletion but insulin resistance increases SREPB-1c. This is due to the complex regulation of the transcription factors of the SREBP family, i.e. a direct transcriptional activation due to e.g. insulin, an alteration of the posttranscriptional release of the transcriptional active N-terminal domain from membrane embedded SREBP precursors, and last not least, insulin induced phosphorylation of the transcriptional active domain to increase transactivity (Streicher et al. 1996, Korn et al. 1998, Kotzka et al. 1998, 2004, 2010 and 2012, Roth et al. 2000 and 2008, Biddinger 2005, Knebel et al. 2012, 2014 and 2018b). Further, increased hepatic DNL was identified to be a major contributor to hepatic steatosis with significantly increased SREPB-1c expression in human liver (Musso et al. 2009, Strable and Ntambi 2010, Saponaro et al. 2015). Hence, the alb-SREBP-1c mouse used in this study represents an appropriate genetic model for investigation of fatty liver with hepatic insulin resistance as consequence of constitutively activated hepatic DNL (Knebel et al. 2012, Jelenik et al. 2017). In contrast, the lypodystrophic animal model (aP2-SREBP-1c) has a phenotype of severe systemic hyperlipidemia, systemic insulin resistance and hepatic steatosis (figure 4.1 and 4.2, Shimomura et al. 1998, Jelenik et al. 2017) presenting a reliable model for the study of metabolically induced fatty liver.

In humans, impaired adipose tissue function is thought to be the main contributor to systemic lipid load. Under healthy conditions the adipose tissue releases fatty acids (FA) in a tightly regulated manner dependent on energy needs of different tissues (Langin 2006). Increased adipose tissue lipolysis due to insufficient suppression by insulin is present in insulin resistant conditions associated with metabolic diseases like obesity, diabetes and NAFLD (DeFronzo 2004, Blaak 2005, Kovacs and Stumvoll 2005, Saprano et al. 2015). In a study by Donnelly and colleagues (2005) investigation of the source of hepatic lipids in patients with NAFLD identified FA flux from the adipose tissue to account for 60-80% of the circulating FA, which in turn contributes to the major proportion of lipids accumulated in fatty liver. Further studies found that whole body free FA flux is affected by lipolysis not only from

visceral but also the subcutaneous adipose depot (Delarue and Magnan 2007). The role of the adipose tissue in NAFLD is further supported by the excessive ectopic accumulation of lipids in the liver of mice and men with lipodystrophy characterized by the selective loss of adipose tissue (Shimomura et al. 1998, Kim et al. 2000, Agarwal and Garg 2006, Cortés et al. 2009). In humans this rare abnormality is also associated with severe systemic insulin resistance, hepatic steatosis as well as hyperlipidemia (Petersen et al. 2002, Gandotra et al. 2011, Knebel et al. 2013) suggesting the absence of adipose tissue to mimic systemic lipid overflow present in conditions of insufficient regulation of adipose tissue lipolysis.

Physiological data obtained in this study showed that the type of fatty liver differs between the two models. Liver weight was markedly increased in the lipodystrophic model accounting for up to 10% of bodyweight while in the genetic phenotype liver weight was equal or moderately increased compared to the control animals accounting for 5% of the bodyweight. Further circulating lipid load and enzymes of liver function had highest levels in aP2-SREBP-1c animals while alb-SREBP-1c mice had modest increased serum levels suggesting the aP2-SREBP-1c a more progressive phenotype of fatty liver. This observation is further supported by recent *in vivo* studies in the two model systems which revealed that the genetic induction of fatty liver is associated with hepatic while the metabolic phenotype associates with systemic insulin resistance (Knebel et al. 2012, Jelenik et al. 2017). In addition, analysis of cellular function in primary hepatocytes isolated from the different mouse models revealed that the effects on fatty liver pathology in each phenotype were triggered by different underlying molecular mechanisms. Investigated pathways in alb-SREBP-1c primary hepatocytes showed minor or no changes compared to the C57Bl6 controls or even improved potential for example in lipogenesis, glycolysis and mitochondrial stress tests. In contrast aP2-SREBP-1c *ex vivo* analysis showed severe impairment in glycolysis, mitochondrial β-oxidation and DNL further supporting that the fatty liver models display different stages of fatty liver progression.

The outstanding feature of these animal models is the development of the fatty liver phenotype without the necessity of any dietary or medical intervention. Diet induced phenotypes are often challenging as already the composition of diet has a high variability of metabolic effects on liver metabolism in mice and men making it difficult to identify the appropriate diet to induce a specific phenotype. Further, not only the composition but also the type of fat or/and sugar is of vital importance as it influences metabolic manifestation (Listenberger et al. 2003, Malhi et al. 2006, Li et al. 2009). Also the amount of food intake has to be tightly controlled as animals often dislike diets resulting in huge differences in dietary intake of animals within one group. Animals on standard chow often serve as reference group although nutrient composition is different between chow and the specific experimental diet for phenotype induction (Ordovas 2008, Lai et al. 2014, Heydemann

2016). Moreover duration of diet and time of analysis are often crucial for experimental outcome and are likely to cause great variances. On the other hand, models with fatty liver induced by hyperphagia like mice with genetic alteration in the leptin system i.e. db/db or ob/ob, or the polygenic NZO model also bare bias as model of hepatic lipid accumulation. Although these models still have lipid storage capacity in the adipose tissue and a counter regulation of the metabolic phenotype e.g. shifting the lipid degradation more to the unregulated peroxisomal degradation was observed (Leiter et al. 1981, Wang et al. 2014, Knebel et al. 2015 and 2018a). Furthermore the genetic background of the mice is crucial e.g. C57Bl6 or C57BlKS, one develops diabetes and the other is prone to develop diabetes (Clee and Attie 2007). Another aspect of diet induced phenotypes is the addition of one more factor influencing the development of the anticipated phenotype as factors like age, sex or physical activity are already affecting parameters (Ordovas 2008, Lai et al. 2014, Heydemann 2016). All animals used in this study were housed on regular, normocaloric chow to circumvent potential bias of diet induced phenotypes. Further, all animals used in this study shared the same background as the transgenic mouse lines were continuously bred with the C57Bl6 line from the control mice used for *ex vivo* analysis.

5.1.2 *In vivo* versus *ex vivo* – persistence of phenotype

The functional analysis of carbohydrate and lipid metabolism was conducted in *ex vivo* experiments using primary hepatocytes isolated from the different fatty liver mouse models. The analysis in primary culture allowed investigation of single aspects of carbohydrate and lipid metabolism in different functional assays under standardized conditions. Key features of *ex vivo* experiments are the reduction of ethical issues as animals are not exposed to distress and reduced animal numbers are needed. Further, controlled culture conditions minimize the variability between samples. Finally, the use of isolated hepatocytes is the only experimental approach to prove that the molecular alterations observed are not a secondary systemic effect, but primary account on the cells itself. Focus on metabolically active hepatocytes as a pure culture together with metabolic characterization of differential gene expression in the fatty liver models was therefore chosen as technical prerequisite to elaborate the primary aim of the thesis, i.e. the identification of mechanistical differences in pathogenesis and progression of fatty liver phenotypes and the identification of biomarkers associated with different disease stages.

Lipid staining in isolated primary hepatocytes showed that the fatty phenotype still persists in culture as illustrated in figure 4.5. The cells show the typical hepatocyte characteristics including hexagonal shape and the presence of two nuclei. The distribution of stained lipids further supports that the underlying mechanisms of the fatty liver phenotypes are different. The genetic increase of DNL, i.e. alb-SREBP-1c, lead to equally distributed small lipid

droplets while cells derived from the aP2-SREBP-1c livers displayed enlarged droplets which were not evenly distributed. Although the phenotype was still persistent in culture, it is important to address that there were differences between the *in vivo* and *ex vivo* situation. In culture, the cells are no longer exposed to surrounding tissue most notably the deprivation of the immune response and environmental body fluids especially systemic lipid load. Experiments with fatty phenotypes were therefore performed within 24 hours after isolation to minimize adaption of the hepatocytes to culture conditions.

Nevertheless, insulin response was observed to improve when cells were investigated in primary culture. *In vivo* study revealed insulin resistance either hepatic or systemic in the animals models (Jelenik et al. 2017) while investigation of the insulin signaling cascade in primary culture (figure 4.12) showed that all phenotypes were responsive to insulin treatment. Cells isolated from the aP2-SREBP-1c phenotype had significantly decreased insulin-stimulated phosphorylation of Akt Ser 473 and Thr 308 residues compared to the other phenotypes, but insulin was still able to significantly induce Akt phosphorylation compared to the untreated aP2-SREBP-1c control condition. Further, alb-SREBP-1c showed no changes in insulin-mediated Akt phosphorylation compared to C57Bl6 controls. These results represent an example for the overall limitation of *ex vivo* models. It is tempting to speculate, that the observations might be related to the ability of the liver to rapidly adapt to environmental changes. This observation might further argue against the use of diet induced metabolic phenotypes. However, it is consistent to the increased metabolic health observed in humans who improved insulin sensitivity after weight loss which lead to reduction of systemic lipid load (Petersen et al. 2005, Al-Jiffri et al. 2013, Schwenger et al. 2018). On the other hand, the epigenetic cellular memory defined by persistent cellular environment of the cell is described to be inheritable and phenotype specific (D'Urso and Brickner 2014, Henikoff and Greally 2016). In methylation analysis the methylation pattern as part of the epigenetic memory was found to be different between the fatty liver phenotypes which was consistent with recent findings in literature (figure 4.23, Kammel et al. 2016), suggesting that the epigenetic status is more robust in primary culture and further defines hepatocyte phenotype.

5.2 Fatty liver metabolism from transcriptional level to functional manifestation

In this study, the holistic liver transcriptome from two different fatty liver phenotypes i.e. lipogenic and metabolic, in comparison to normal liver tissue was investigated. Pairwise comparisons were applied to analyze differences not only between fatty liver and the control group but also to identify specific characteristics of each fatty liver phenotype. Analysis revealed a large data set of differentially expressed genes either phenotype specific or

overlapped between all or certain phenotypes (figure 4.3). Identification of a single gene usually not gives any information about the metabolic or pathogenic consequences of its regulation though standard procedure often includes the selection of a molecule of interest followed by the investigation of its potential function in metabolism as can be seen in a multitude of studies. This approach has its rationale in categorization of molecules, its specific role and assignment to metabolic pathways and also potential consequences of deregulation. However, this concept remains limited to a single molecule and does not allow the integration of its potential role in the complex network of deregulated metabolism underlying the most pathologies. Another conventional approach for data analyses would be co-expression based analyses. In this method statistical procedures, like hierarchical clustering analyses are used to identify molecules with comparable expression signatures over the experimental series. Such methods have high predictive capacity if differences in various stages of the identical condition are of interest e.g. in kinetic, dose response or pairwise matched datasets. However, in regard to metabolic alterations these analyses might not identify relevant pathways as not all molecules necessary for metabolic regulation can be expected to show a comparable expression signature.

Today NAFLD is commonly accepted to be initiated by multiple parallel events which lead to an imbalance in carbohydrate and lipid metabolism and consequently the accumulation of hepatic lipids and progression of NAFLD (Tilg and Moschen 2010, Buzzetti et al. 2016, Fang et al. 2018) pointing out that single molecule-based analyses do not take the complexity of the disease into account. Therefore, this study aimed to annotate differential gene expression to regulatory networks to identify the driving pathways underlying different phenotypes and stages of fatty liver diseases. In order to achieve this, bioinformatics analysis was conducted using the commercial available *Ingenuity® Pathway Analysis* (IPA). The software is a knowledge based tool to identify causal relationships between upstream regulators and their regulatory networks which determine pathology and progression of fatty liver in the two different phenotypes. IPA analyses represents a state of the art method for annotation of statistically pre-analyzed datasets to database entries. Although databases are constantly curated, one limitation of the use of IPA is that entries might be misleading. This can occur in regard to tissue specificity of expression, screwed overrepresentation of certain diseases and pathways due to forced research in the field (e.g. cancer or dementia related diseases). Further, the enrichment of pathways/downstream actions in the bioinformatics results might be simply based on the ratio of molecules identified in a certain pathway which does not estimate the actual impact e.g. if rate limiting molecules were enriched or negligible modifiers.

The results obtained by bioinformatics analysis were therefore further verified in *ex vivo* experiments using primary hepatocytes from each individual phenotype. Nodal points of

carbohydrate and lipid metabolism as well as signal transduction and cell communication aspects were investigated and compared between the control and fatty liver models to identify specific characteristics of liver homeostasis for each phenotype.

5.2.1 Etiology and disease progression of fatty liver specific altered hepatic gene expression.

The novel observation of this study is that the lipogenic and metabolic fatty liver models from different etiology, show selective differential activation of common molecules in the identical pathways or target molecules in a specific fashion. With these observations the datasets generated by bioinformatic analysis allowed the differentiation of various aspects of hepatic lipid accumulation. From the models used, it is somehow system immanent that genes in metabolic relevant pathways were on top scores. The gene expression analyses revealed common upstream regulators like HNF4A, PPARA or MYC to be affected in comparison of all phenotypes. The hepatocyte nuclear factor 4 α (HNF4A) was the top score upstream regulator identified in comparison of hepatic gene expression of controls with either fatty liver phenotype. HNF4A is highly expressed in liver and was found to be crucial in hepatic triglyceride and cholesterol metabolism. Depletion of HNF4A was found to induce hypotriglyceridemia and fatty liver development in mice due to reduction of VLDL secretion, increased bile acid biosynthesis and decreased plasma triglycerides as well as cholesterol (Hayhurst et al. 2001, Inoue et al. 2006, Yin et al. 2011). In a liver-specific mouse knock-out model the loss of HNF4A was suggested to directly contribute to the development of HCC (Bonzo et al. 2012). Further, hepatic overexpression lead to reduction of hepatic triglyceride content and plasma cholesterol (Yin et al. 2011). In humans mutations in HNF4A were associated with β-cell dysfunction and T2D (Yamagata et al. 1996, Fajans et al. 2001). Further, upstream regulatory functions of peroxisome proliferator-activator receptor α (PPARA) are described to regulated FA transport and oxidation (Pawlak et al. 2015). Hepatocyte-specific knock-out of PPARA in mice impaired FA metabolism leading to hepatic lipid accumulation and increased circulating free FA in fasting conditions (Montagner et al. 2016). Further, FA acids promote PPARA activation and concomitant activation of gluconeogenesis related genes, including G6PC, PEPCK and FGF21 in adaptive response to fasting which attributes PPARA to have major impact also on glucose homeostasis (Kersten 2014, Goldstein and Hager 2015). Deletion of PPARA causes severe fasting-induced hypoglycemia and reduces intrahepatic glucose levels (Kersten et al. 1999, Leone et al. 1999, Xu et al. 2002, De Souza et al. 2006). The proto-oncogene MYC is well described as master regulator of cell proliferation and growth and is further involved in regulation of glucose metabolism and mitochondrial biogenesis (Dang 2013, Morrish and

Hockenbery 2014). Induction of MYC in mice was found to promote the pathogenesis of HCC (Beer et al. 2004).

Beside upstream regulators found regulated in both fatty liver phenotypes compared to control or within each other, analysis revealed transcriptional regulators specific for a certain condition. Among differentially expressed genes with high score fold changes between controls and the lipogenic fatty liver phenotype, X-box binding protein 1 (XBP1) is one example which was not included in top-lists of comparisons with the metabolic fatty liver phenotype. XBP1 is well described to be activated by IRE1α during unfolded protein response initiated by cellular ER stress targeting activation of ER genes (Yoshida et al. 2001, Uemura et al. 2009). Further XBP1 function was found attributed to immune response (Martinon et al. 2010), carbohydrate and lipid homeostasis as well as associated with insulin resistance (Wu et al. 2015, Piperi et al. 2016). On the other hand, the nuclear receptor (NR) 1I3 also known as constitutive androstane receptor (CAR), a sensor for xenobiotic stress targeting gene expression after dimerization with the retinoid-X receptor (RXR) was identified with high and specific rate of differential expression in the metabolic fatty liver phenotype compared to controls or the lipogenic fatty liver, but not in comparison of the two latter. A role in hepatic energy metabolism, lipogenesis and also tumor formation is suggested for CAR which was observed to interact with other nuclear receptors like liver X receptor (LXR) and PPARs as well as PPARγ coactivator (PGC) 1α (Xiao et al. 2010, Lake 2018). Exemplary upstream regulators specific for the comparison of the two fatty liver models were INSIG 1 and 2. INSIG proteins regulate cholesterol and lipid metabolism by mediation of SCAP and HMG-CoA function (Dong et al. 2010 and 2012). Specific regulation of gene expression therefore suggests the lipogenic hepatic phenotype responding to overcome cellular stress e.g. by mediation of unfolded protein response due to ER stress while the metabolic phenotype suggests advanced changes in metabolism e.g. by a shift in lipid clearance.

5.2.2 Phenotype-specific changes in lipid metabolism

Given the analytical limitations of knowledge-based analyses, much effort was spent on the physiological validation of the expression differences *ex vivo* using primary hepatocytes from the identical mouse models as for holistic gene expression experiments. The liver as an organ consists of many cell types including metabolic active hepatocytes more immunological relevant Kupffer and stellate cells as well as endothelial cells from the organ's vasculature. Infiltration of macrophages or further immune relevant cells additionally complex the system. The verification analyses solely in the metabolic active cells of the liver bared the advantage that the expression differences observed can be directly broken down to central metabolic pathways. Furthermore, this is an essential prerequisite to functionally

characterize the cell models according to the key goal of the thesis i.e. the identification of biomarkers for hepatic lipid accumulation with special emphasis on the degree of disease progression. Effects that directly derived from hepatocytes are more predictive in regard to the metabolic alterations than secondary effects e.g. from immune active cells.

Increased DNL enables the cell to reduce the load of metabolic intermediates such as acetyl-CoA by conversion into ‘restorable' lipids which can be paced to lipoprotein particles and released from the hepatocyte. As expected, lipogenic primary hepatocytes showed the highest rate of DNL, probably due to hepatic SREBP-1c over-representation and activation of this pathway in these animals. Interestingly, the rate of DNL was also significantly higher in the metabolic fatty liver phenotype with increased hepatic lipid accumulation due to lipodystrophy compared to control hepatocytes although these cells already exhibit a massive lipid load. This paradox was also observed in patients with NAFLD which showed increased DNL, which still remains elevated during fasting (Diraison et al. 2003, Lambert et al. 2014, Stanhope 2016, Chiu et al. 2018). Another pathway to reduce acetyl-CoA is cholesterol synthesis which in the follow is to be secreted as bile acid (Biddinger et al. 2008b). In the models investigated here, genes related to cholesterol as well as bile acid synthesis were altered predominantly in comparisons involving metabolic fatty liver (figure 4.17).

This phenotype specific alterations were reflected in gene expression analysis. Lipid metabolic genes like FASN encoding for fatty acid synthase which catalyzes the last step in fatty acid biosynthesis or ELOVL6 which catalyzes the rate-limiting reaction to constitute the long-chain fatty acids elongation cycle mainly to C16:0 acetyl-CoAs were found to be linked to the metabolic fatty liver phenotype compared to controls (table 4.11). The latter was further included in consistency analysis as target of the regulator effect networks of phosphatidylethanolamine binding protein (PEBP) 1 and SIRT6 annotated to fatty acid and cholesterol metabolism in the metabolic fatty liver phenotype.

As another example SREBF protein family member SREBP-2 is solely differentially regulated in comparisons with the metabolic fatty liver phenotype. SREBP-2 is rather responsible of cholesterol than lipid metabolism regulation. The SREBP-2 regulation is accompanied in the same pattern by cytochrome (Cyb) 5 type A. This cofactor of the rate limiting enzyme of androgen and cortisol synthesis from cholesterol precursors i.e. Cyp17A, is depending on the presence of P450 (cytochrome) oxidoreductase (POR) and CYB5A (Auchus et al. 1998, Miller and Auchus 2011). Also Cyp7a1, the rate limiting gene in cholesterol biosynthesis is regulated this way (Horton et al. 1995, Gupta et al. 2001). This might indicate a metabolic shift forced by increased cholesterol levels in the metabolic fatty liver model.

Taken together the separate consideration of the fatty liver models indicate that different aspects of lipid metabolism enrich specifically (figure 4.16). However, fatty acid uptake was not altered in the compared phenotypes which indicates that differences in lipid metabolism were not simply based on increased substrate availability. Whereas the specific alterations due to genetically increased DNL focused alterations in lipid homeostasis or general lipid metabolism to the lipodystrophic model, specifically accumulated targets associated to intracellular lipid accumulation, lipid droplet formation or further synthesis products, such as phospholipid synthesis. Especially genes which differ within both models but are not regulated in comparison to controls are of interest for the analyses of disease progression. Those targets cover almost all aspects of lipid metabolism. Of note, specific differences in the models concentrate on lipid removal but also on lipidation of proteins. Such covalent addition of lipid species alters the polarity and solubility of proteins. As consequence it interferes with protein functionality, alter membrane permeability and favors translocation within intracellular compartments (Chen et al. 2018).

5.2.3 Phenotype-specific changes in glucose metabolism

Carbohydrate metabolism was less pronounced in bioinformatic annotation of differential gene expression to biological functions suggesting a more FA metabolism centered view in regard of transcriptional differences between the two fatty liver models and the control animals. Nevertheless, targeted analysis found significant differences in carbohydrate metabolism involving markedly higher numbers of differentially expressed genes in the comparisons including metabolic rather than lipogenic fatty liver phenotype (figure 4.4).

Here, e.g. the hepatic expression of G6PC, was altered compared to either hepatic expression in controls or the lipogenic fatty liver phenotype (table 4.6). This was annotated to changes in FXR or PXR activation in the metabolic form of fatty liver by knowledge-based analysis. The nuclear factor FXR was identified to regulate hepatic lipid and glucose homeostasis by transcriptional regulation of genes involved in metabolism of carbohydrates (Sinal et al. 2000, Duran-Sandoval et al. 2005, Cariou et al. 2006, Ma et al. 2006, Zhang et al. 2006, Cipriani et al. 2010). Further, hepatic transcriptome consistency analysis or analyses of specific biological functions showed one potential regulatory network under upstream regulation by Max-like protein X interacting protein like (MLXIPL) also known as carbohydrate response element-binding protein (ChREBP) in the comparison of metabolic fatty liver phenotype to controls (table 4.11). MLXIPL is a glucose sensitive transcription regulator suggested to be the primary factor regulating glucose responsive genes in the liver (Filhouland et al. 2013, Jois and Sleeman 2017) suggesting a rather super-ordinated regulation of carbohydrate metabolism in the metabolic fatty liver phenotype. In accordance, the glycolytic capacity of primary hepatocytes was increased solely in lipogenic fatty liver

while hepatocytes with metabolic phenotype showed the lowest glycolysis profile (figure 4.7 A). Also glycolysis rate was significantly higher solely in the lipogenic phenotype whereas the controls and the metabolic form did not differ with statistical significance. This is accompanied with significantly lower non-glycolytic acidification in the metabolic fatty liver phenotype. The results indicate a markedly higher glycolytic potential in hepatocytes derived from lipogenic fatty liver. In combination to the gene expression analyses, the increase in glucose metabolism relevant genes might indicate an active counter regulation to achieve the status quo observed in the functional metabolic assays in hepatocytes derived from metabolic fatty liver, whilst in the lipogenic form increasing metabolic rates is still possible to cope with the metabolic burden.

Glycolysis can be considered as part of DNL as it converts glucose to acetyl-CoA provided for FA synthesis (Munday 2002, Abu-Elheiga et al. 2005, Kawano and Cohen 2013). In regard to the model system itself it seems plausible that glycolysis is highest in the lipogenic form of fatty liver as sort of adaptive mechanism to provide substrate for the constantly active DNL. This may not hold true for the metabolic phenotype which also showed slightly increased DNL but had an overall lower profile of glycolysis compared to the other phenotypes but without changes in glycolysis rate compared to normal liver physiology.

Experimental analysis of glycogen synthesis revealed significantly lower glycogen production in the metabolic fatty liver phenotype, while the lipogenic form was intermediate, and insulin further gradually increased glycogen synthesis to the respective basal glycogen synthesis. However, both fatty liver phenotypes had significantly lower glycogen synthesis in the insulin-stimulated condition compared to controls especially in the metabolic fatty liver phenotype.

Glycogen synthase activity is regulated by phosphorylation through GSK3 (Sung et al. 1998, Summers et al. 1999) which showed decreased basal phosphorylation possibly linked to decreased glycogen synthesis in metabolic fatty liver. Insulin-stimulated GSK3 phosphorylation was not calculated as significantly different in the metabolic compared to the other phenotypes although it was also lower. Reduced phosphorylation of GSK3 might contribute to reduction of glycogen synthesis in the metabolic fatty liver phenotype but might not be responsible as in the lipogenic condition GSK3 phosphorylation remained unchanged compared to control although glycogen synthesis is reduced between the two phenotypes.

Basal substrate stimulated glucose production indicated no differences between primary hepatocytes from controls and lipogenic fatty liver, while basal glucose production was reduced in hepatocytes derived from the metabolic phenotype. Regulation of gluconeogenesis showed strong relations to hepatic steatosis or NAFLD in humans (Konopelska et al. 2011, Sunny et al. 2011, Honma et al. 2018, Jin et al. 2018) and rodent

models (Massillon et al.1997, Samuel et al. 2004). It must be noted that measurement of glucose production was based on release from the hepatocytes into culture medium and took not into account produced glucose metabolized inside the cells. Hence, intrahepatic production may differ from the released amount of glucose. Taken together, these results are in line with the bioinformatic analysis which already indicated more pronounced changes in glucose metabolism in the metabolic compared to the lipogenic phenotype.

5.2.4 Mitochondrial function in fatty liver

Bioinformatic analysis demonstrated differential gene expression functionally associated with mitochondrial function. Mitochondrial ß-oxidation protruded as differentially regulated according to the etiology of the fatty liver and was further supported by physiological verification in primary hepatocytes. Oxidation of lipids was found significantly decreased in the metabolic fatty liver phenotype suggesting a severe imbalance in hepatic metabolism as lipid production by DNL was increased in these animals. In contrast, the lipogenic form of fatty liver showed no alterations in lipid oxidation compared to the control group, yet (figure 4.6).

As one example for mitochondrial β-oxidation and FA disposal in the liver the rate limiting enzyme in long chain fatty acid oxidation, CPT2 was identified to be transcriptionally regulated specifically to the metabolic fatty liver phenotype. CPT2 is located on the inner mitochondrial membrane and converts long chain acyl-carnitines back to acyl-CoA for full oxidation (McGarry and Brown 1997, Kerner and Hoppel 2000). In mice lacking CPT2 liver TG were reduced and animals were protected from diet induced obesity and glucose intolerance. In contrast the CPT2 deficient mice showed increased hepatic oxidative stress and systemic carnitine deficiency (Lee et al. 2017). In humans CPT2 downregulation was associated with HCC and was further identified to promote tumor progression (Lin et al. 2018) suggesting CPT2 regulation associated with metabolic forms of NAFLD. CPT2 was annotated to several biological functions like energy production, small molecule biochemistry or molecular transport already pointing towards alterations in mitochondrial oxidation.

Transcriptional regulation of hepatic genes identified several members of the SIRT family specific to the metabolic fatty liver phenotype. SIRTs belong to the NAD+-dependent histone deacetylase class III enzymes and this family comprises 7 proteins SIRT1 to 7. Several sirtuins were studied in the context of fatty liver in mice and men. SIRT1 was found to be beneficial in hepatic steatosis by inhibition of DNL and promoting FA oxidation (Ding et al 2017). Murine SIRT1 null mutation lead to the development in fatty liver and was found to be associated with decreased mitochondrial β-oxidation (Wang et al. 2010, Purushotham et al. 2009). SIRT3 regulates mitochondrial protein acetylation and in murine knock-out

studies the loss of SIRT3 was associated with steatosis, several abnormalities in lipid metabolism and the accumulation of acyl-carnitines, intermediate products of FA oxidation (Hirschey at al. 2010 and 2011). Also liver specific deletion of SIRT6 was found to reduce mitochondrial β-oxidation in mice (Kim et al. 2010). Here, investigations of SIRT activity confirmed a significant increase only in hepatocytes of metabolic fatty liver, but not in the lipogenic phenotype compared to controls. Furthermore, SIRT activity was found opposed to the direction of mitochondrial β-oxidation. However, SIRT activity tended to be higher already in the lipogenic form than controls, thus implicating a gradual increase according to the severity of lipid accumulation or stage of disease progression. In context of current knowledge, these findings suggest a compensatory rather than causal role of increased SIRT activity in regard to decreased oxidation in metabolic fatty liver, but not in the lipogenic form. The assay performed does not allow a discrimination of the sirtuins that it remains debatable which precise mechanisms were triggered by increased SIRT activity and remains to be elucidated in detail.

It was previously described, that mitochondria have the ability to adapt to increased cellular lipid load though this is associated with increased generation of cellular stress (Pessayre et al. 2002, Begriche et al. 2006, Ciapaite et al. 2011, Shabalina et al. 2014). Further, in NASH patients ATP levels were found to be decreased (Cortez-Pinto et al. 1999, Serviddio et al. 2008) which might be due to uncoupling of the electron transport chain to prevent further accumulation of reactive oxygen species (ROS) during increased mitochondrial activity (Jiang et al. 2008). Detailed analyses of specific mitochondrial functions in hepatocytes from the different phenotypes revealed that basal respiration was gradually decreased in both fatty liver phenotypes, but only statistically significant in the metabolic form. In contrast, the potential bioenergetic reserve in response to cellular stress as indicator for mitochondrial potential is markedly increased solely in the lipogenic fatty liver. This was in line with increased ATP production. Cells of the metabolic fatty liver do not exhibit this activation potential of mitochondrial function, indicating a decline in the response to altered cellular environment by increasing mitochondrial function in the metabolic form of fatty liver. Taken together, these findings suggest that the lipogenic fatty liver hepatocytes were able to compensate for the increased lipid load with increased mitochondrial function while this sort of rescue mechanism seems to be exhausted in the aggravated fatty liver phenotype.

Transcriptional analysis showed that several PPARs and co-activators (PGC1α) as well as peroxisomal genes (PEX) were regulated specific to the metabolic fatty liver phenotype potentially pointing towards peroxisomal biosynthesis, proliferation and maintenance in these livers. Peroxisomes not only play a role in hepatic lipid metabolism e.g. providing acetyl-CoA for further degradation in the mitochondria (Kohlwein et al. 2013, Schrader et al. 2013) but also play a key role in the maintenance of cellular ROS (Nordgren and Fransen

2014). In patients with NASH increased peroxisome proliferation in response to mitochondrial dysfunction was observed (Pirola et al. 2013) and agonizing PPAR was shown to improve insulin sensitivity and fatty liver phenotype (Shyangdan et al. 2011, Del Ben et al 2014). In this study the activation of peroxisomal genes in the metabolic phenotype suggests the activation of rescue mechanisms to maintain cellular function, prevent severe ROS induced cell damage and support lipid clearance again pointing towards a metabolic shift in this phenotype.

Today, NAFLD is also referred to as mitochondrial disease (García-Ruiz et al. 2013, Koliaki and Roden 2013, Gusdon et al. 2014, Nassir and Ibdah 2014) which is further supported by the findings in this study. The hepatic steatosis in the lipogenic model already has an impact on mitochondrial function potentially to overcome the excessive lipid load primarily by intrahepatic production in this model. In metabolic fatty liver, this compensatory mechanism begins to fail accompanied with the activation of rescue mechanisms to maintain cellular function. The reduced lipid clearance in these hepatocytes contributes to increased accumulation of intrahepatic lipids and further supports this mouse as suitable model for progressive fatty liver.

Taken together, the lipogenic model presents a model of mild steatosis with increased DNL by transgene-mediated overrepresentation of SREBP-1c and increased glycolysis providing increased substrate demand. In the lipogenic cells mitochondrial potential was increased suggesting compensatory bioenergetic response to the increased lipid load (figure 5.1). In contrast, the metabolic phenotype displays progressive fatty liver which was accompanied on functional level with a reduction of the mitochondrial potential and β-oxidation although DNL was increased. The hepatocytes from this phenotype face a severe imbalance in lipid production versus lipid clearance and concomitant cellular stress (figure 5.1). Transcriptional analysis suggests a shift of lipid metabolism in the metabolic phenotype to increased cholesterol homeostasis and peroxisomal activation to overcome the increased metabolic challenge. Further carbohydrate metabolism was not considerably changed in the lipogenic phenotype while analysis indicated a rather super-ordinated transcriptional regulation primarily by changed expression of ChREBP and regulation of glucose relevant genes in the metabolic phenotype.

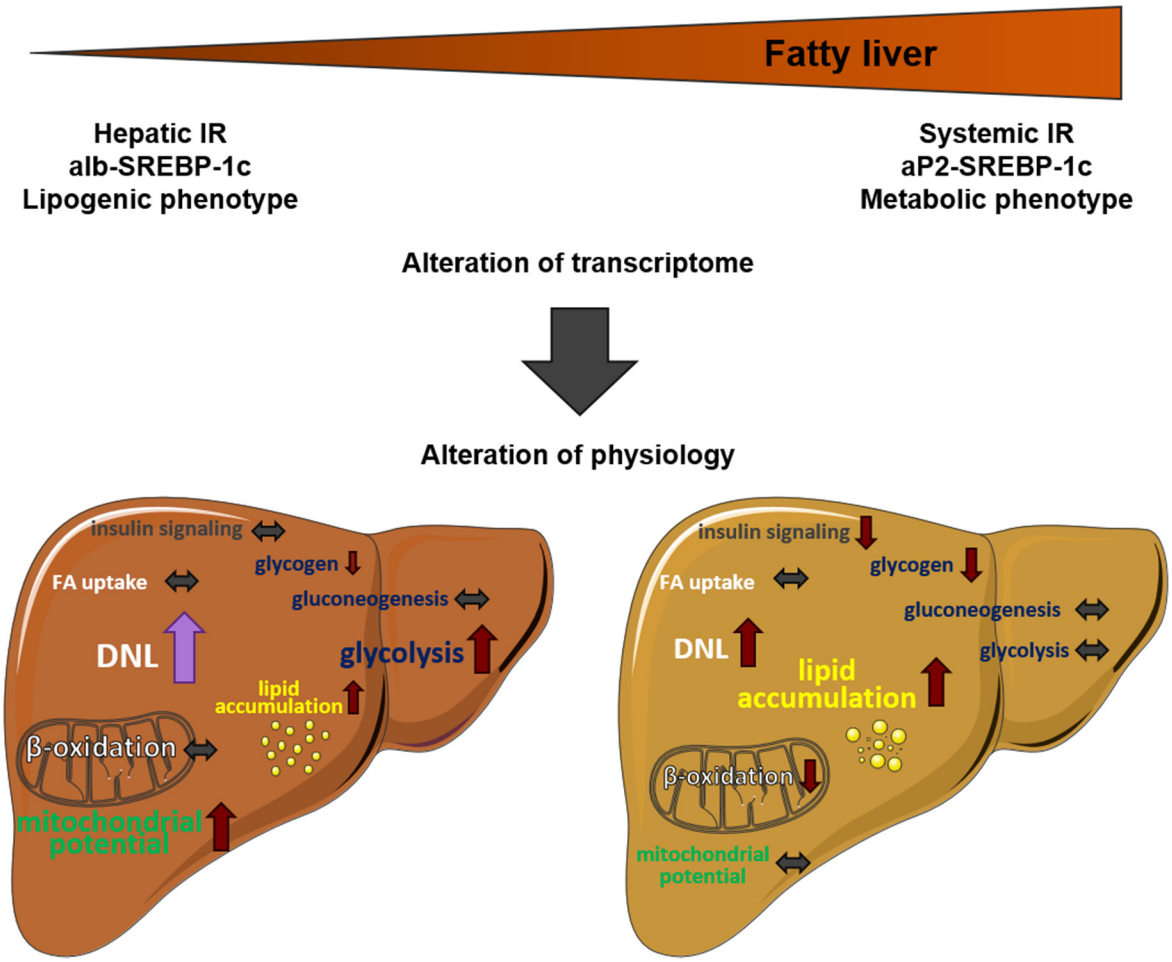

Figure 5.1: Schematic illustration of fatty liver progression from lipogenic to metabolic phenotype. The genetic phenotype associated *in vivo* with hepatic insulin resistance (IR) and mild hepatic lipid accumulation while the metabolic phenotype showed systemic IR *in vivo* and progressed accumulation of lipid in the liver. Differences in hepatic physiology as assayed in primary hepatocytes from the respective models are indicated as arrows, direction in comparison to control hepatocytes. FA: fatty acid, DNL: *de novo* lipogenesis.

5.3 Reflection of metabolic phenotype in hepatocyte secretome

The translational aspect of the thesis focused not only on the verification of transcriptional changes on functional level in the respective hepatocyte at different stages of fatty liver, but also on the identification of secreted factors characterizing each pathological stage, that may be of value as predictive biomarkers.

In fatty liver pathogenesis impaired lipid transport mechanisms provide one potential cause of hepatic lipid accumulation. Proteins involved in lipid transport including the apolipoproteins (Apo) A1, ApoA5, ApoC3, ApoC4 and ApoF, however, no FABPs were found increased in the lipogenic model compared to controls. Apolipoproteins are mainly part of HDL containing particles and chylomicrons. ApoA2 is implemented in the induction of hepatic lipase, whereas ApoC3 is acting as an inhibitor of hepatic lipase thus

downregulating lipolysis (Dominiczak and Caslake 2011). ApoF inhibits cholesteryl ester transfer protein (CETP) the rate-limiting enzyme involved in the generation of HDL particles from smaller lipoprotein particle fractions (Morton and Greene 1994, Serdyuk and Morton 1999). This indicates a regular hunger DNL muting process to be active and functional in the lipogenic model.

In contrast, the metabolic model had decreased ApoA1, ApoC1 ApoM and FABP5 and increased ApoA4, FABP2 and FABP4 compared to controls. This lipoprotein pattern indicates a reduction in lecithin-cholesterol acyltransferase (LCAT) activation thus the rate limiting enzyme for cholesterol ester synthesis and therefore the transporting form of cholesterol esters will be reduced. Furthermore LCAT is essential for the reverse cholesterol transport mechanisms to transport cholesterol from extrahepatic tissues to the liver. This might indicate a kind of stop signal of the metabolic fatty liver to reduce additional cholesterol/lipid influx (Levinson and Wagner 2015). On the other hand ApoA4, also an activator of LCAT which might also regulate lipolysis is still increased. Of FABP proteins FABP2 indicates increased saturated long chain-FA transport. However, increased FABP4, initially expressed in adipose tissue can serve as indicator for the expression profile changes reported in fatty liver towards an adipocyte specific gene expression due to increased PPARγ and PPARα activation by hepatic fatty acids (Tan et al. 2002, Hughes et al. 2015).

Consistent to the comparisons to controls, comparison of the fatty liver models showed an increase in ApoA4 and FABP4 in aP2-SREBP-1c animals whereas ApoA1, ApoA2, ApoC1, ApoC4, lipocalin like ApoM and the structural similar PON-1, as well as FABP5 were increased in alb-SREBP-1c animals. FABP1, 4 and 5 also correlated with the percentage of liver fat in patients with NAFLD (Westerbacka et al. 2007, Higuchi et al. 2011).

Further, to overcome the excessive lipid load the liver responds with molecular remodeling to cope with excessive substrate availability to prevent cellular damage while prolonged lipid overload leads to severe alterations in hepatic metabolism and consequently to pathogenesis and progression of NAFLD. The mouse liver and plasma proteome were found to overlap by 25% indicating that the liver directly secrets proteins into the circulation (Lai et al. 2008, Meex and Watt 2017). As in the concept of adipokine secretion, an accepted model for the reflection of pathological changes in adipose tissue function in diseases like obesity, metabolic syndrome or T2D diabetes (Galic et al. 2010, Fasshauer and Blüher 2015), secreted factors from hepatocytes termed hepatokines might come into play. In this study, hepatocytes isolated from each mouse model were used to identify unique hepatokines as potential biomarker for different stages of fatty liver to facilitate new options for non-invasive diagnosis of the disease and its pathological status.

The use of mouse models for the investigation of potential biomarker has considerable advantages over studies in the human system. Investigation of human hepatocyte secretome would necessitate the use of liver biopsies which are usually limited in availability in particular from healthy tissue. In addition, isolation procedures of hepatocytes from human liver tissue usually require a large amount of tissue of more than 50 g per patient. Although new techniques or improved protocols for primary human hepatocyte isolation are constantly provided (e.g. Bhogal et al. 2011, Kegel et al. 2016 Green et al. 2017) yield and viability of the cells for culture remain a difficult subject most notably in experimental reproducibility. Further, biopsies do not represent the organ as a whole potentially leading to controversial data between samples within the investigated groups. The same would hold true for human tissue culture used for secretome analysis which would include all cell types present in the liver biopsy such as Kupffer or stellate cells not allowing the assignment of secreted factors to specific hepatic cell types. The approach applied in this study included isolation of primary hepatocytes from the whole organ from the exact phenotype used providing a great benefit in reproducibility and consistency of the results. The establishment of a protocol for the isolation of the fatty liver hepatocytes provided an *ex vivo* system to investigate protein secretion in the absence of other hepatic cell types present to consider the hepatocyte as the predominant functional unit in fatty liver disease and progression. This approach allows determination of secreted factors by the hepatocytes to set into direct relation with analysis of circulating molecules. Further the use of animal models has the advantage to provide adequate material for analyses with a stable phenotype throughout several generations.

Overall, the analysis of primary hepatocyte secretome reflected genetic changes in the fatty liver phenotypes as identified in analysis of hepatic transcriptome. The main metabolic pathways affected were lipid and carbohydrate metabolism as well as mitochondrial function and were similar in considerable proportions for the comparisons applied to gene and protein analysis. The lipogenic fatty liver phenotype was identified to be less different from the control animals with in parts improved or equal hepatic function. In contrast, transcriptome and secretome analysis of metabolically induced fatty liver showed progressive steatosis with impaired hepatic function and several indications for cell death, necrosis and even cancer related processes present in these animals. Biomarker analysis from hepatocyte secretome provided several potential new biomarkers for the prediction of fatty liver and even allowed a distinction between the genetically induced lipogenic fatty liver and the metabolic form.

5.3.1 Cell communication as monitor of disease progression

In clinical diagnosis markers of inflammatory processes are often used to determine occurrence or progression of fatty liver diseases. Cytokines or hepatokines as factors released in response to inflammatory processes characterizing NAFLD progression to more progressive forms are well described although their regulation in relation to disease state often remains to be debated (Stojsavljević et al. 2014, du Plessis et al. 2016, Lebensztejn et al. 2016). Fatty liver disease is often associated with systemic metabolic pathologies like insulin resistance or adipose tissue inflammation which also contribute to circulating cytokine pattern. In this thesis, standard cytokine patterns were investigated in mouse plasma as well as in hepatocyte secretome to identify cytokines which are released from the diseased cell into circulation and therefore directly reflect liver status. Comparison of circulating cytokine levels to cytokine concentrations released from primary hepatocytes in culture showed opposite directions of cytokine regulation between normal and fatty liver phenotypes. For example, circulating KC/CXCL1 and MCP-1/CCL2 showed increased abundance in fatty liver phenotypes compared to C57Bl6 control mouse serum. In contrast in secretome analyses from hepatocytes, KC/CXCL1 and MCP-1/CCL2 were found as the most abundant cytokines in control mice but with significantly lower concentrations in the secretome from fatty liver derived primary hepatocytes, irrespective of the disease stage. The same was also observed for most of the cytokines found downregulated in secretomes from fatty liver hepatocyte cultures compared to control indicating that cytokine release from the hepatocyte is not reflected in serum cytokine concentration, suggesting other hepatic cell types or systemic processes contribute in higher proportions to circulating concentration which remains to be elucidated. However, the conclusion drawn from the discrepancy of serum to hepatocellular cytokines was, that the investigation of the secretomes from primary hepatocytes of defined stages of fatty liver disease might be more promising for biomarker identification.

Transcriptional analysis already pointed toward significant differences in genes related to cell communication. The gene expression differences in regard to cellular communication processes increased gradually from the lipogenic to the metabolic form of fatty liver. Even between the two fatty liver models were significant changes suggesting that protein secretion not only specifically reflects the metabolic status of hepatocytes but also disease progression.

Secreted proteome from the fatty liver phenotypes showed common changes compared to the control hepatocytes secretome but also revealed unique molecules changed with each phenotype either compared to control or within the comparison of both fatty liver models. As an example, both fatty liver models secrete increased amounts of several keratin types

compared to the control hepatocytes. Keratines are the largest subgroup of intermediate filaments and are expressed in a highly cell type specific manner with Krt 8/18 being predominantly expressed in hepatocytes (Zatloukal et al. 2004, Moll et al. 2008, Yi et al. 2018). In conditions of chronic liver disease reorganization of intermediate filaments lead to cytoplasmatic aggregation and formation of so-called Mallory-Denk bodies (MDB) which are associated with hepatocellular ballooning in NAFLD progression (Nakamichi et al. 2005, Ku et al. 2007, Zatloukal et al.2007, Strnad et al. 2012, Kucukoglu et al. 2014). Changes in Krt 8/18 expression or mutations within these keratins were also linked to hepatocyte injury, hepatitis or serve as tumor markers as they are released into circulation through tissue damage (Karantza 2011, Strnad et al. 2012, Toivola et al. 2015). Krt18 fragments in the circulation are often presented as markers for hepatocyte injury, as Krt18 serves as major caspase substrate during apoptosis and mutation in Krt18 associated with cirrhosis probably due to predisposition of hepatocytes apoptosis (Ku et al. 2003, Strnad et al. 2012, Toivola et al. 2015) however this is controversially discussed (Schlossberger et al. 2018). Among the secreted proteins from hepatocytes of the lipogenic fatty liver phenotype compared to control cells a specific type of Krt8 (UniProt accession P50446) was identified to be a potential unique biomarker for the lipogenic phenotype which remains to be investigated (position 37 top proteins with increased secretion from alb-SREBP-1c vs. C57Bl6). Interestingly the comparison of both fatty liver phenotypes included no keratins in the top score list of differentially secreted proteins.

Proteins specifically released from the metabolic fatty liver phenotype included several ACOTs or several fibrinogen chains as well as IGFBP2. ACOTs catalyze the hydrolysis of acyl-CoAs to free FA and coenzyme A which is essential in hepatic lipid metabolism. These molecules are further suggested to regulate peroxisomal and mitochondrial FA oxidation as well as trafficking of FA (Hunt and Alexson 2002, Tillander et al. 2017) supporting the observed molecular changes between the two fatty liver models. In contrast, fibrinogen is a prothrombotic factor which is found regulated in metabolic diseases incuding NAFLD (Targher et al. 2008 and 2009, Potze et al. 2015) suggesting changes in hepatocyte secretome to contribute to associated cardiovascular complications. IGFBP2 was protruding as it was identified as most consistent network regulated in hepatic gene expression between the two different fatty liver models and was also found markedly regulated in its secretion between aP2-SREBP-1c and the two other models and will be discussed in greater detail in the following.

5.4 Upstream regulation as key indicator for fatty liver disease progression

Beside these direct relations probably leading to alterations in systemic parameters and direct cell communication in regard to autocrine, paracrine or endocrine small molecules the data allow to raise the question for a common or specific upstream regulator as potential main player or indicator for fatty liver disease progression. The key regulator differing between both fatty liver models deduced from the transcriptome data was IGFBP2. This finding was supported by the notion, that IGFBP2 was also differentially secreted from hepatocytes with metabolic fatty liver phenotype as a result of secretome data. Here, two completely different technologies, one based on mRNA profiling performed in whole liver and the other on proteome profiling in isolated hepatocytes came up with the identical candidate. In both cases IGFBP2 was one of the most different proteins with reduced presence in metabolic fatty liver phenotype compared to controls and the lipogenic form of fatty liver.

IGFBP2 is part of the IGF system. IGF has structural homology to insulin and at least in part shares a signaling cascade to regulate cell metabolism and growth with the liver as primary source contributing to 75 to 80% of systemic IGF-I (Le Roith 2003, Murphy 2003, Clemmons 2007, Annunziata et al. 2011). The bioavailability of IGF is mainly regulated through binding proteins (IGFBPs) which exert IGF-dependent and –independent functions (Mohan and Baylink 2002). Accumulating evidence suggests that dysfunctions in this system contribute to the pathogenesis of metabolic dysfunctions like obesity, metabolic syndrome or T2D (Laager et al. 1993, Ruan and Lai 2010, Kim and Lee 2015). IGF is suggested to have effects on fatty acid uptake and lipogenesis *in vitro* (Pratipanawatr et al. 2002, Scavo et al. 2004) and changes in IGF-I levels were found associated with NAFLD in humans (Ichikawa et al. 2007, Cianfarani et al. 2014). As in several other tissues IGFBP2 is expressed in the liver, although it is not the most abundant IGFBP expressed in this organ (Straus and Takemoto 1990, Ahrens et al. 2013, Kang et al. 2015). Low levels of serum IGFBP2 were previously found to associate with impaired insulin sensitivity (Rajpathak et al. 2009, Lewitt et al. 2014, Kim and Lee 2015) and an imbalanced profile of lipoproteins (Hedbacker et al. 2010, Carter et al. 2014) linking this molecule to metabolic dysfunction.

5.4.1 IGFBP2 in fatty liver pathology

In this study specific transcriptional regulation of the IGF signaling pathway was observed in metabolic fatty liver phenotype. Several molecules within the IGF signaling cascade including IGFBPs were differentially expressed in the metabolic phenotype compared to either controls or the lipogenic form of fatty liver. IGFBP2 was down regulated either in

comparison to healthy liver and also compared to the lipogenic phenotype which showed no differential expression of this gene compared to controls.

These differences observed in bioinformatical analysis were confirmed by hepatocyte expression at RNA and protein level with significantly reduced levels of IGFBP2 in primary cells with progressive steatosis while controls and mild steatosis showed no differences. Further, the secretion of IGFBP2 was markedly decreased from progressive steatosis hepatocytes compared to the other groups which was also mirrored in circulating levels of IGFBP2. AP2-SREBP-1c animals had an approximately 60% reduction of plasma IGFBP2 while the two other phenotypes showed similar plasma concentrations of the protein. These data suggest that the reduction in IGFBP2 secretion from the fatty hepatocyte has a direct correlation with the circulating level indicating the secretion of IGFBP2 into circulation to exert potential endocrine effects.

Previous studies found that transcriptional regulation of the IGFBP2 gene associated with a phenotype of fatty liver in mice and men identified to be regulated at least in part through epigenetic changes of the gene promotor. A specific region was found to be hypermethylated in a cohort of NAFLD patients (Ahrens et al. 2013) as well as in a mouse model of diet induced obesity (Kammel et al. 2016). Hypermethylation was further associated with an increased activity of methyltransferases supporting ongoing epigenetic regulation in this phenotype but whether this is cause or consequence of fatty liver pathology and progression cannot be answered. In this study, investigation of the described promotor region also revealed hypermethylation of the specific DNA region solely in the metabolic fatty liver phenotype. However, DNA methylation pattern remained unchanged in the lipogenic form of fatty liver. This observation allows the speculation, that either the prolonged presence of a metabolically risky environment with increased lipids might be involved in the methylation process, or that the lipogenic form with missing methylation are tendentially reversible. This remains to be elucidated. Implicated from this observation, methylation analyses might not be sufficient to determine the early or mild forms of the disease.

Circulating concentration of IGFBP3 remained unchanged between the three mouse models. Further, IGF-I plasma levels were increased in both fatty liver models in comparison to the control group implying that the ratio of binding protein to IGF-I changes during the pathogenesis of fatty liver. The major proportion of circulating IGF-I is bound to IGFBP3 in the circulation which increases IGF-I half-life and stability. Changes in IGF-I to IGFBP3 ratio were found to be related to hepatocellular carcinoma in humans which was mostly based on increased IGF-I levels compared to patients with hepatic cirrhosis while in contrast to this study overall IGF-I and IGFBP3 levels were decreased in patients with liver cirrhosis, with or without HCC compared to healthy controls (Mattera et al. 2003). A more recent meta-

analysis study including several data from literature databases in regard to IGF-I and IGFBP3 levels and HCC found a gradual decrease of either IGF-I or IGFBP3 from healthy liver to cirrhosis to HCC patients with no significant association of IGF-I to IGBP3 ratio to HCC risk (Wang et al. 2017). In this thesis, the circulating and the intrahepatic levels of IGF-I and IGFBP3 in the animal models used were different as IGF-I gene expression was only upregulated in cells of metabolic fatty liver phenotype, but not reflected in hepatocytes secretion while IGFBP3 gene expression and secretion was reduced in the lipogenic fatty liver phenotype showing the same dichotomy observed in humans.

In NAFLD, overnutrition contributes to excessive systemic lipid load. It was previously described that different types of fatty acids exerts different cellular even lipotoxic effects (Listenberger et al. 2003, Wei et al. 2006, Li et al. 2009). In this thesis, the treatment of metabolic healthy hepatocytes with high concentrations of different fatty acids showed that only cells treated with unsaturated palmitic acid had decreased release of IGFBP2 while the saturated oleic acid did not alter the release of IGFBP2. This effect was accompanied with an increase of CHOP and BiP gene expression indicating ER stress (Malhi and Kaufman 2011, Oslowski and Urano 2011, Sano and Reed 2013) in hepatocytes treated with palmitic acid suggesting reduction of hepatic IGFBP2 release to be directly associated with impaired ER function.

Functional investigation showed that incubation of C57Bl6 hepatocytes with IGFBP2 alone had no effect on targeting Akt as one downstream target of the IGF signaling cascade. Investigation of relevant phosphorylation sites of Akt revealed that IGFBP2 modulates transduction of IGF-I signaling rather than exerting individual functions in primary hepatocytes. The same hold true for a role of IGFBP2 in DNL. Incubation of hepatocytes showed that IGF-I was a potent activator of lipogenesis which was blunted when the cells were incubated with equimolar concentrations of IGF-I and IGFBP2. In primary hepatocytes derived from lipogenic fatty liver phenotype, IGFBP2 was also able to inhibit IGF-I-induced induction of DNL while IGFBP2 failed to modulate IGF-I effect in hepatocytes with metabolic fatty liver phenotype. This was an interesting finding because although this experiment was independent from the decreased secretion IGFBP2 was still unable to modulate IGF-I function suggesting an important role of IGFBP2 in IGF-I-stimulated DNL. From this observation it might be suggested that IGFBP2 function is regulated via an unknown mechanism and not only by abundance which still remains to be elucidated. Further the increased IGF-I abundance in the circulation and increased hepatic expression observed in the progressive fatty liver model indicates an imbalance of the IGF-I to IGFBP2 ratio which might contribute to the increase of DNL in this phenotype.

In bioinformatic data of liver transcriptome consistency analysis identified IGFBP2 as upstream regulator annotated to cell viability of tumor cell lines, expression of RNA,

transcription or viral infection pathways also related to tumor formation. Further, among genes under regulation of IGFBP2 several oncogenes like AKT1, MYC or STAT3 were included as well as fibrosis associated genes like fibronectin (FN) 1 and integrin alpha (ITGA) 5 indicating connective tissue formation as responsive mechanism (Friedman 2003, Bataller and Brenner 2005). IGFBP2 as modulator of IGF-I suggest a decrease of the protein to promote IGF-I functions in the liver like its protective effects found in human HCC cell cultures to inhibit HCV infection which is usually associated with cirrhosis and HCC progression (Pivonello et al. 2014). On the other hand IGFBP2 levels were found to be increased in numerous malignancies and identified to promote tumor development and progression (Russo et al. 2015). These findings might suggest that decreased IGFBP2 in fatty liver disease might be a protective mechanism to prevent progression towards cirrhosis or even HCC.

Beside modulation of IGF-I function, IGFBP2 might exert IGF-I-independent actions. In functional analysis IGFBP2 was not observed to have impact on the investigated key mechanisms of lipid metabolism but it is conceivable that IGFBP2 mediates endocrine effects via ablation of hepatic secretion into the circulation. IGFBP2 overexpression in transgenic mice lead to reduced predisposition of obesity and was found to improve insulin resistance under normal and even high fat diet. *In vitro* IGFBP2 exerts individual function on adipocyte differentiation in murine cell culture (Wheatcroft et al. 2007) suggesting loss of IGFBP2 to contribute to manifestation of adipose tissue dysfunction and manifestation of systemic insulin resistance. Another study further supports a role of IGFBP2 in modulating insulin sensitivity as IGFBP2 overexpression in different mouse models reversed insulin resistance and diet induced obesity (Hedbacker et al. 2010). Further, administration of IGFBP2 to the leptin deficient, severely obese mouse model ob/ob, which also represents a fatty liver phenotype resulted in improved hepatic insulin sensitivity (Hedbacker et al. 2010) supporting systemic impact of IGFBP2. Another individual function of IGFBP2 was found in neovascularization *in vitro* where binding of IGFBP2 to integrin promotes the adhesion of endothelial progenitor cells (EPCs) to endothelial cells thus promoting incorporation of EPCs into tubule networks (Feng et al. 2015). The loss of circulating IGFBP2 might suggest impairment of vascular repair and therefore contributing to cardiovascular complication often found associated with metabolic diseases like NAFLD.

Taken together the experiments performed in this study point towards a role of IGFBP2 in modulation of IGF-I activity in hepatocyte metabolism (figure 5.2). Interestingly, even if IGFBP2 and IGF-I are added in equimolar concentrations to a culture of hepatocytes from metabolically induced fatty liver IGFBP2 is not able to repress IGF-I effect on DNL. In contrast, in mild steatosis IGFBP2 is as potent to reduce IGF-I-induced increase of DNL as in the control hepatocytes suggesting that in progressive fatty liver not only the abundance

of IGFBP2 is reduced but also an impaired biological function is present. Reduced levels of IGFBP2 secretion might prevent disease progression while the reduction in circulating IGFBP2 might promote fatty liver associated complications.

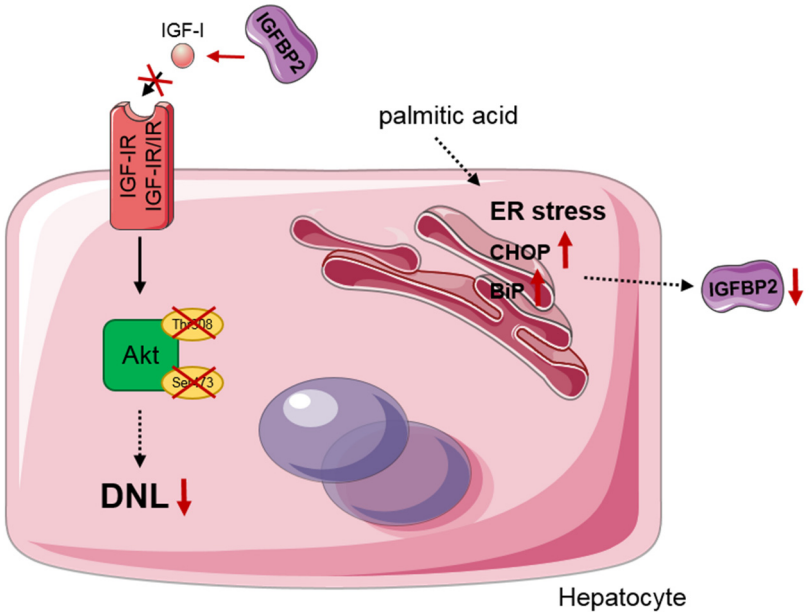

Figure 5.2: IGFBP2 modulates IGF-I signal transduction while reduced secretion is mediated by palmitic acid induced ER stress. In primary hepatocytes the insulin-like growth factor (IGF) binding protein (BP) 2 blunts IGF-I mediated phosphorylation of protein kinase B (Akt) and represses induction of *de novo* lipogenesis (DNL). Palmitic acid treatment of primary hepatocytes is associated with the induction of the endoplasmic reticulum (ER) stress marker genes CAAT/ enhancer-binding protein homologous protein (CHOP) and Binding of immunoglobin (BiP) and decreased hepatic secretion of IGFBP2. IGF-IR: IGF-I receptor, IGF-IR/IR: IGF-I/ Insulin hybrid receptor.

5.4.2 Translational aspects: from mouse to man

IGFBP2 was previously shown to be low in the circulation of patients with metabolic conditions like obesity, metabolic syndrome or type 2 diabetes (Rajpathak et al. 2009, Lewitt et al. 2014, Kim and Lee 2015). Few studies suggest that a state of fatty liver was associated with decreased hepatic expression of the IGFBP2 gene in humans (Ahrens et al. 2013, Kammel et al. 2016). In this thesis, circulating IGFBP2 levels were measured in obese men with predicted presence or absence of hepatic steatosis using the fatty liver index (FLI) according to Bedogni (2006). The protruding feature of this cohort was the possibility to measure IGFBP2 serum concentration prior and 2 years post interventional bariatric surgery. In this cohort most patients showed not only markedly weight loss and improved systemic insulin resistance but also a decrease in fatty liver prediction. The results showed that similar to the fatty liver mouse models IGFBP2 serum levels were low in patients with high prediction of hepatic steatosis and were restored with decreased hepatic steatosis and improved circulating liver enzyme levels.

The results indicate that IGFBP2 is a suitable biomarker for the presence of hepatic steatosis and shows a gradual decrease with severity of lipid accumulation according to FLI in humans. The thesis adds the novel observation, that IGFBP2 is directly secreted from the hepatocytes and hepatocyte transcriptional levels were altered according to the secretion patterns. These results might be promising to establish IGFBP2 as new potential non-invasive biomarker for the diagnosis and graduation of NAFLD. Nevertheless verification needs to be performed in further cohorts as the translational results from this study have some limitations. The cohort was relatively small consisting of 15 patients per group even though individuals were metabolically well characterized hepatic steatosis was based on surrogate parameters and not on imaging techniques or even biopsy-based diagnosis making precise grading of NAFLD progression impossible. Analysis of IGFBP2 in a cohort of patients with classified disease progression would gain further insight whether IGFBP2 is a specific marker for progressed fatty liver.

5.5 Fatty liver: hunger metabolism in food abundance or the burden of optimal adaptation to deficiency supply?

Starvation results in glucose depletion and lipid accumulation in the liver. In periods of starvation the need of glucose is solved by clearance of blood sugars, insulin secretion, repression of glycogen production, increase of hepatic flux of adipose tissue FA and increased gluconeogenesis. In sight of evolution, hepatic DNL is the key to survive hunger periods, as it indicates the ability to produce storable lipids from glucose in times of overnutrition instead of wasting energy by direct oxidation. In starvation, hepatic glucose production and the in parallel insulin-mediated lipolysis via activation of lipoprotein lipase in the adipose tissue provide FA for the liver as additional energy source to counteract this physical condition. The lipogenic and metabolic steatosis models both showed no differences in FA uptake and were both completely dependent on CPT1 mediated mitochondrial FA influx. Increased hepatic lipids act as PPARα activators and PPARα-driven gene regulation increases gluconeogenesis and results in systemic lipid clearance. In parallel, the PPARα target UCP2 increases and results in an ATP decline to form an energy gradient. The metabolic profile of fasting is present in the lipogenic fatty liver model as hepatic glucose output from gluconeogenesis and glycogenolysis, regulation of PPARα nodal gene expression and mitochondrial rates, including the identification of UCP2 generated NAD+ as central upstream activator, usually rate limiting to maintain FA β-oxidation are modulated. If this system runs out of control lipolysis is increased e.g. in obesity and in parallel muscle lipid clearance is reduced. Lipid oxidation, and in the follow overall mitochondrial function were reduced in the metabolic model, putatively because of mitochondrial exhaustion. This was accompanied by the highest SIRT activity in the

metabolic model, a regulator of PGC1α activity and so at least of mitochondrial biogenesis. On the other hand, lipid oxidation and mitochondrial function is increased in the lipogenic model. Markers for cellular maintenance and ER unfolded protein response indicate counteraction to cellular toxification i.e. to ROS products. This completes the mitochondrial metabolic reserve in the lipogenic model, resulting in further excess systemic lipids. The persisting increase of FA in the liver does not only activate PPARα but also PPARγ. With this key transcription factor related to the cascade of adipocyte differentiation, even in the liver an adipocyte-specific transcription pattern is initiated, as indicated in the metabolic steatosis model e.g. with FABP4 expression. Again, this might point to evolution, i.e. the insects FAT body resembles both functions of mammalian liver and visceral adipose tissue and controls the synthesis and utilization of fat as well as glycogen and produces most of circulating metabolites.

However, next to hepatic lipids, hepatic glucose triggers DNL in normal physiological states, the activation of DNL regulators SREBP-1c and ChREBP is due to increased insulin and glucose levels. Insulin action in the lipogenic models is muted on the level of insulin receptor and IRS and indistinguishable on activation of downstream signaling, indicating that the selective hepatic insulin resistance is caused by the non-physiologically systemic environment/ insulin response rather as a molecular impairment of signaling directly. In contrast, in the metabolic model reduced insulin response is not reversible, yet, and is accompanied by hyperinsulinemia. Hyperinsulinemia itself increases SREBP-1c and ChREBP expression acting to increase DNL deactivation, due to prevention of SREBP-1c and ChREBP degradation via FoxO1 inhibition. This results in energy storage in form of triglycerides in starvation. So, SREBP-1c increases FA synthesis and reduces FA oxidation to avoid futile metabolite cycles in the liver. Increased DNL further results in hepatic hypertriglyceridemia and increased levels of saturated fatty acids e.g. palmitate, can cause alterations in the inflammation and apoptosis as seen in the metabolic steatosis model. Lipid efflux from the isolated hepatocytes indicated a differential composition of lipid binding proteins suggesting differential lipoprotein particle formation especially in the metabolic model with forced lipid efflux from the liver and last, not least the reduction of reverse cholesterol transport. This might indicate a facilitated efflux of lipids or lipid subclasses e.g. long chain FA with higher degree of saturation as generated due to insufficient lipid oxidation in mitochondria in the metabolic steatosis model. Furthermore, in the metabolic steatosis model, upregulation of SREBP-2, the SREBP isoform mainly involved in hepatic cholesterol synthesis and accumulation, links DNL to cholesterol metabolism. Here nodal regulation of SREBP-2 and cholesterol metabolism as increased up to the regulation via nuclear receptors FXR, LXR, and RXR to facilitate the cholesterol to bile acid synthesis as the only metabolic pathway for cholesterol clearance. As consequence, this was further

accompanied by an alteration of the secreted lipoprotein species and fatty acid binding proteins shifting from VLDL to HDL featured protein patterns and probably LCAT activation.

Taken together, NAFLD may be the result of a dysregulation of the physiological adaptation to starvation. The evolutionary key to survive turned in a health burden as individuals trap in the loop of DNL dysregulation, either due to genetic susceptibility or massive malnutrition aggravate hepatic lipid accumulation, can only be broken to a certain extent.

Due to the gradual fatty liver phenotype of the models used, the study was able to provide biomarkers, with the potency to differentiate the gradual severity of fatty liver disease. With this unique outcome, the thesis addresses one major clinical issue on the diagnosis and prognosis of NAFLD, i.e. non-invasive marker to support surrogate parameter related prediction. One example is IGFBP2 which is detailed in the thesis. The set of identified biomarkers in the specific diagnosis of early or progressive stages of disease can now be validated in further analyses.

References

Abu-Elheiga L, Matzuk MM, Kordari P, Oh W, Shaikenov T, Gu Z, Wakil SJ. Mutant mice lacking acetyl-CoA carboxylase 1 are embryonically lethal. Proc Natl Acad Sci U S A. 2005 Aug 23;102(34):12011-6. Epub 2005 Aug 15.

Agarwal AK, Garg A. Genetic basis of lipodystrophies and management of metabolic complications. Annu Rev Med. 2006;57:297-311.

Ahrens M, Ammerpohl O, von Schönfels W, Kolarova J, Bens S, Itzel T, Teufel A, Herrmann A, Brosch M, Hinrichsen H, Erhart W, Egberts J, Sipos B, Schreiber S, Häsler R, Stickel F, Becker T, Krawczak M, Röcken C, Siebert R, Schafmayer C, Hampe J. DNA methylation analysis in nonalcoholic fatty liver disease suggests distinct disease-specific and remodeling signatures after bariatric surgery. Cell Metab. 2013 Aug 6;18(2):296-302. doi: 10.1016/j.cmet.2013.07.004.

Akie TE, Cooper MP. Determination of Fatty Acid Oxidation and Lipogenesis in Mouse Primary Hepatocytes. J Vis Exp. 2015 Aug 27;(102):e52982. doi: 10.3791/52982.

Al-Jiffri O, Al-Sharif FM, Abd El-Kader SM, Ashmawy EM. Weight reduction improves markers of hepatic function and insulin resistance in type-2 diabetic patients with non-alcoholic fatty liver. Afr Health Sci. 2013 Sep;13(3):667-72. doi: 10.4314/ahs.v13i3.21.

Alkhouri N, Dixon LJ, Feldstein AE. Lipotoxicity in nonalcoholic fatty liver disease: not all lipids are created equal. Expert Rev Gastroenterol Hepatol. 2009 Aug;3(4):445-51. doi: 10.1586/egh.09.32.

Annunziata M, Granata R, Ghigo E. The IGF system. Acta Diabetol. 2011 Mar;48(1):1-9. doi: 10.1007/s00592-010-0227-z. Epub 2010 Nov 2.

Attar BM, Van Thiel DH. Current concepts and management approaches in nonalcoholic fatty liver disease. ScientificWorldJournal. 2013;2013:481893. doi: 10.1155/2013/481893. Epub 2013 Mar 20.

Auchus RJ, Lee TC, Miller WL. Cytochrome b5 augments the 17,20-lyase activity of human P450c17 without direct electron transfer. J Biol Chem. 1998 Feb 6;273(6):3158-65.

Bataller R, Brenner DA. Liver fibrosis. J Clin Invest. 2005 Feb;115(2):209-18.

Bedogni G, Bellentani S, Miglioli L, Masutti F, Passalacqua M, Castiglione A, Tiribelli C. The Fatty Liver Index: a simple and accurate predictor of hepatic steatosis in the general population. BMC Gastroenterol. 2006 Nov 2;6:33.

Beer S, Zetterberg A, Ihrie RA, McTaggart RA, Yang Q, Bradon N, Arvanitis C, Attardi LD, Feng S, Ruebner B, Cardiff RD, Felsher DW. Developmental context determines latency of MYC-induced tumorigenesis. PLoS Biol. 2004 Nov;2(11):e332. Epub 2004 Sep 28.

Begriche K, Igoudjil A, Pessayre D, Fromenty B. Mitochondrial dysfunction in NASH: causes, consequences and possible means to prevent it. Mitochondrion. 2006 Feb;6(1):1-28. Epub 2006 Jan 5.

Bekaert M, Van Nieuwenhove Y, Calders P, Cuvelier CA, Batens AH, Kaufman JM, Ouwens DM, Ruige JB. Determinants of testosterone levels in human male obesity. Endocrine. 2015 Sep;50(1):202-11. doi: 10.1007/s12020-015-0563-4. Epub 2015 Mar 13.

Bhogal RH, Hodson J, Bartlett DC, Weston CJ, Curbishley SM, Haughton E, Williams KT, Reynolds GM, Newsome PN, Adams DH, Afford SC. Isolation of primary human hepatocytes from normal and diseased liver tissue: a one hundred liver experience. PLoS One. 2011 Mar 29;6(3):e18222. doi: 10.1371/journal.pone.0018222.

Biddinger SB, Almind K, Miyazaki M, Kokkotou E, Ntambi JM, Kahn CR. Effects of diet and genetic background on sterol regulatory element-binding protein-1c, stearoyl-CoA

desaturase 1, and the development of the metabolic syndrome. Diabetes. 2005 May;54(5):1314-23.

Biddinger SB, Haas JT, Yu BB, Bezy O, Jing E, Zhang W, Unterman TG, Carey MC, Kahn CR.Hepatic insulin resistance directly promotes formation of cholesterol gallstones. Nat Med. 2008b Jul;14(7):778-82. doi: 10.1038/nm1785. Epub 2008 Jun 29.

Biddinger SB, Hernandez-Ono A, Rask-Madsen C, Haas JT, Alemán JO, Suzuki R, Scapa EF, Agarwal C, Carey MC, Stephanopoulos G, Cohen DE, King GL, Ginsberg HN, Kahn CR. Hepatic insulin resistance is sufficient to produce dyslipidemia and susceptibility to atherosclerosis. Cell Metab. 2008a Feb;7(2):125-34. doi: 10.1016/j.cmet.2007.11.013.

Blaak EE. Metabolic fluxes in skeletal muscle in relation to obesity and insulin resistance. Best Pract Res Clin Endocrinol Metab. 2005 Sep;19(3):391-403.

Blachier M, Leleu H, Peck-Radosavljevic M, Valla DC, Roudot-Thoraval F. The burden of liver disease in Europe: a review of available epidemiological data. J Hepatol. 2013 Mar;58(3):593-608. doi: 10.1016/j.jhep.2012.12.005.

Blouin CM, Prado C, Takane KK, Lasnier F, Garcia-Ocana A, Ferré P, Dugail I, Hajduch E. Plasma membrane subdomain compartmentalization contributes to distinct mechanisms of ceramide action on insulin signaling. Diabetes. 2010 Mar;59(3):600-10. doi: 10.2337/db09-0897. Epub 2009 Dec 3.

Bonnefont-Rousselot D, Ratziu V, Giral P, Charlotte F, Beucler I, Poynard T; Lido Study Group. Blood oxidative stress markers are unreliable markers of hepatic steatosis. Aliment Pharmacol Ther. 2006 Jan 1;23(1):91-8.

Bonzo JA, Ferry CH, Matsubara T, Kim JH, Gonzalez FJ. Suppression of hepatocyte proliferation by hepatocyte nuclear factor 4α in adult mice. J Biol Chem. 2012 Mar 2;287(10):7345-56. doi: 10.1074/jbc.M111.334599. Epub 2012 Jan 12.

Brown MS, Goldstein JL. A proteolytic pathway that controls the cholesterol content of membranes, cells, and blood. Proc Natl Acad Sci U S A. 1999 Sep 28;96(20):11041-8.

Brown MS, Goldstein JL. Cholesterol feedback: from Schoenheimer's bottle to Scap's MELADL. J Lipid Res. 2009 Apr;50 Suppl:S15-27. doi: 10.1194/jlr.R800054-JLR200. Epub 2008 Oct 29.

Brown MS, Goldstein JL. Selective versus total insulin resistance: a pathogenic paradox. Cell Metab. 2008 Feb;7(2):95-6. doi: 10.1016/j.cmet.2007.12.009.

Brown MS, Goldstein JL. The SREBP pathway: regulation of cholesterol metabolism by proteolysis of a membrane-bound transcription factor. Cell. 1997 May 2;89(3):331-40.

Buzzetti E, Pinzani M, Tsochatzis EA. The multiple-hit pathogenesis of non-alcoholic fatty liver disease (NAFLD). Metabolism. 2016 Aug;65(8):1038-48. doi: 10.1016/j.metabol.2015.12.012. Epub 2016 Jan 4.

Cao J, Dai DL, Yao L, Yu HH, Ning B, Zhang Q, Chen J, Cheng WH, Shen W, Yang ZX. Saturated fatty acid induction of endoplasmic reticulum stress and apoptosis in human liver cells via the PERK/ATF4/CHOP signaling pathway. Mol Cell Biochem. 2012 May;364(1-2):115-29. doi: 10.1007/s11010-011-1211-9. Epub 2012 Jan 15.

Cariou B, van Harmelen K, Duran-Sandoval D, van Dijk TH, Grefhorst A, Abdelkarim M, Caron S, Torpier G, Fruchart JC, Gonzalez FJ, Kuipers F, Staels B. The farnesoid X receptor modulates adiposity and peripheral insulin sensitivity in mice. J Biol Chem. 2006 Apr 21;281(16):11039-49. Epub 2006 Jan 30.

Carter S, Li Z, Lemieux I, Alméras N, Tremblay A, Bergeron J, Poirier P, Deshaies Y, Després JP, Picard F. Circulating IGFBP-2 levels are incrementally linked to correlates of the metabolic syndrome and independently associated with VLDL triglycerides. Atherosclerosis. 2014 Dec;237(2):645-51. doi: 10.1016/j.atherosclerosis.2014.09.022. Epub 2014 Oct 2.

Castera L. Diagnosis of non-alcoholic fatty liver disease/non-alcoholic steatohepatitis: Non-invasive tests are enough. Liver Int. 2018 Feb;38 Suppl 1:67-70. doi: 10.1111/liv.13658.

Chalasani N, Deeg MA, Crabb DW. Systemic levels of lipid peroxidation and its metabolic and dietary correlates in patients with nonalcoholic steatohepatitis. Am J Gastroenterol. 2004 Aug;99(8):1497-502.

Chalasani N, Gorski JC, Asghar MS, Asghar A, Foresman B, Hall SD, Crabb DW. Hepatic cytochrome P450 2E1 activity in nondiabetic patients with nonalcoholic steatohepatitis. Hepatology. 2003 Mar;37(3):544-50.

Chalasani N, Younossi Z, Lavine JE, Diehl AM, Brunt EM, Cusi K, Charlton M, Sanyal AJ. The diagnosis and management of non-alcoholic fatty liver disease: practice Guideline by the American Association for the Study of Liver Diseases, American College of Gastroenterology, and the American Gastroenterological Association. Hepatology. 2012 Jun;55(6):2005-23. doi: 10.1002/hep.25762.

Chan DC, Watts GF, Gan S, Wong AT, Ooi EM, Barrett PH. Nonalcoholic fatty liver disease as the transducer of hepatic oversecretion of very-low-density lipoprotein-apolipoprotein B-100 in obesity. Arterioscler Thromb Vasc Biol. 2010 May;30(5):1043-50. doi: 10.1161/ATVBAHA.109.202275. Epub 2010 Feb 11.

Chen B, Sun Y, Niu J, Jarugumilli GK, Wu X. Protein Lipidation in Cell Signaling and Diseases: Function, Regulation, and Therapeutic Opportunities. Cell Chem Biol. 2018 Jul 19;25(7):817-831. doi: 10.1016/j.chembiol.2018.05.003. Epub 2018 May 31.

Chen G, Liang G, Ou J, Goldstein JL, Brown MS. Central role for liver X receptor in insulin-mediated activation of Srebp-1c transcription and stimulation of fatty acid synthesis in liver. Proc Natl Acad Sci U S A. 2004 Aug 3;101(31):11245-50. Epub 2004 Jul 20.

Chiu S, Mulligan K, Schwarz JM. Dietary carbohydrates and fatty liver disease: de novo lipogenesis. Curr Opin Clin Nutr Metab Care. 2018 Jul;21(4):277-282. doi: 10.1097/MCO.0000000000000469.

Cianfarani S, Inzaghi E, Alisi A, Germani D, Puglianiello A, Nobili V. Insulin-like growth factor-I and -II levels are associated with the progression of nonalcoholic fatty liver disease in obese children. J Pediatr. 2014 Jul;165(1):92-8. doi: 10.1016/j.jpeds.2014.01.052. Epub 2014 Mar 5.

Ciapaite J, van den Broek NM, Te Brinke H, Nicolay K, Jeneson JA, Houten SM, Prompers JJ. Differential effects of short- and long-term high-fat diet feeding on hepatic fatty acid metabolism in rats. Biochim Biophys Acta. 2011 Jul-Aug;1811(7-8):441-51. doi: 10.1016/j.bbalip.2011.05.005. Epub 2011 May 19.

Cipriani S, Mencarelli A, Palladino G, Fiorucci S. FXR activation reverses insulin resistance and lipid abnormalities and protects against liver steatosis in Zucker (fa/fa) obese rats. J Lipid Res. 2010 Apr;51(4):771-84. doi: 10.1194/jlr.M001602. Epub 2009 Sep 25.

Clee SM, Attie AD. The genetic landscape of type 2 diabetes in mice. Endocr Rev. 2007 Feb;28(1):48-83. Epub 2006 Oct 3.

Clemmons DR. Modifying IGF1 activity: an approach to treat endocrine disorders, atherosclerosis and cancer. Nat Rev Drug Discov. 2007 Oct;6(10):821-33.

Cortés VA, Curtis DE, Sukumaran S, Shao X, Parameswara V, Rashid S, Smith AR, Ren J, Esser V, Hammer RE, Agarwal AK, Horton JD, Garg A. Molecular mechanisms of hepatic steatosis and insulin resistance in the AGPAT2-deficient mouse model of congenital generalized lipodystrophy. Cell Metab. 2009 Feb;9(2):165-76. doi: 10.1016/j.cmet.2009.01.002.

Cortez-Pinto H, Chatham J, Chacko VP, Arnold C, Rashid A, Diehl AM. Alterations in liver ATP homeostasis in human nonalcoholic steatohepatitis: a pilot study. JAMA. 1999 Nov 3;282(17):1659-64.

Dang CV. MYC, metabolism, cell growth, and tumorigenesis. Cold Spring Harb Perspect Med. 2013 Aug 1;3(8). pii: a014217. doi: 10.1101/cshperspect.a014217.

Day CP, James OF. Steatohepatitis: a tale of two "hits"? Gastroenterology. 1998 Apr;114(4):842-5.

De Souza AT, Dai X, Spencer AG, Reppen T, Menzie A, Roesch PL, He Y, Caguyong MJ, Bloomer S, Herweijer H, Wolff JA, Hagstrom JE, Lewis DL, Linsley PS, Ulrich RG. Transcriptional and phenotypic comparisons of Ppara knockout and siRNA knockdown mice. Nucleic Acids Res. 2006;34(16):4486-94. Epub 2006 Aug 31.

DeFronzo RA. Dysfunctional fat cells, lipotoxicity and type 2 diabetes. Int J Clin Pract Suppl. 2004 Oct;(143):9-21.

Del Ben M, Polimeni L, Baratta F, Pastori D, Loffredo L, Angelico F. Modern approach to the clinical management of non-alcoholic fatty liver disease. World J Gastroenterol. 2014 Jul 14;20(26):8341-50. doi: 10.3748/wjg.v20.i26.8341.

Delarue J, Magnan C. Free fatty acids and insulin resistance. Curr Opin Clin Nutr Metab Care. 2007 Mar;10(2):142-8.

Di Martino M, Koryukova K, Bezzi M, Catalano C. Imaging Features of Non-Alcoholic Fatty Liver Disease in Children and Adolescents. Children (Basel). 2017 Aug 11;4(8). pii: E73. doi: 10.3390/children4080073.

Diehl AM, Day C. Cause, Pathogenesis, and Treatment of Nonalcoholic Steatohepatitis. N Engl J Med. 2017 Nov 23;377(21):2063-2072. doi: 10.1056/NEJMra1503519.

Ding RB, Bao J, Deng CX. Emerging roles of SIRT1 in fatty liver diseases. Int J Biol Sci. 2017 Jul 6;13(7):852-867. doi: 10.7150/ijbs.19370. eCollection 2017.

Diraison F, Moulin P, Beylot M. Contribution of hepatic de novo lipogenesis and reesterification of plasma non esterified fatty acids to plasma triglyceride synthesis during non-alcoholic fatty liver disease. Diabetes Metab. 2003 Nov;29(5):478-85.

Doege H, Baillie RA, Ortegon AM, Tsang B, Wu Q, Punreddy S, Hirsch D, Watson N, Gimeno RE, Stahl A. Targeted deletion of FATP5 reveals multiple functions in liver metabolism: alterations in hepatic lipid homeostasis. Gastroenterology. 2006 Apr;130(4):1245-58.

Dominiczak MH, Caslake MJ. Apolipoproteins: metabolic role and clinical biochemistry applications. Ann Clin Biochem. 2011 Nov;48(Pt 6):498-515. doi: 10.1258/acb.2011.011111. Epub 2011 Oct 25.

Dong XY, Tang SQ, Chen JD. Dual functions of Insig proteins in cholesterol homeostasis. Lipids Health Dis. 2012 Dec 18;11:173. doi: 10.1186/1476-511X-11-173.

Dong XY, Tang SQ. Insulin-induced gene: a new regulator in lipid metabolism. Peptides. 2010 Nov;31(11):2145-50. doi: 10.1016/j.peptides.2010.07.020. Epub 2010 Sep 15.

Donnelly KL, Smith CI, Schwarzenberg SJ, Jessurun J, Boldt MD, Parks EJ. Sources of fatty acids stored in liver and secreted via lipoproteins in patients with nonalcoholic fatty liver disease. J Clin Invest. 2005 May;115(5):1343-51.

Doulberis M, Kotronis G, Gialamprinou D, Kountouras J, Katsinelos P. Non-alcoholic fatty liver disease: An update with special focus on the role of gut microbiota. Metabolism. 2017 Jun;71:182-197. doi: 10.1016/j.metabol.2017.03.013. Epub 2017 Mar 31.

Dries DR, Gallegos LL, Newton AC. A single residue in the C1 domain sensitizes novel protein kinase C isoforms to cellular diacylglycerol production. J Biol Chem. 2007 Jan 12;282(2):826-30. Epub 2006 Oct 27.

du Plessis J, Korf H, van Pelt J, Windmolders P, Vander Elst I, Verrijken A, Hubens G, Van Gaal L, Cassiman D, Nevens F, Francque S, van der Merwe S. Pro-Inflammatory Cytokines but Not Endotoxin-Related Parameters Associate with Disease Severity in Patients with

NAFLD. PLoS One. 2016 Dec 19;11(12):e0166048. doi: 10.1371/journal.pone.0166048. eCollection 2016.

Duran-Sandoval D, Cariou B, Percevault F, Hennuyer N, Grefhorst A, van Dijk TH, Gonzalez FJ, Fruchart JC, Kuipers F, Staels B. The farnesoid X receptor modulates hepatic carbohydrate metabolism during the fasting-refeeding transition. J Biol Chem. 2005 Aug 19;280(33):29971-9. Epub 2005 May 16.

D'Urso A, Brickner JH. Mechanisms of epigenetic memory. Trends Genet. 2014 Jun;30(6):230-6. doi: 10.1016/j.tig.2014.04.004. Epub 2014 Apr 26.

Emanuelli B, Vienberg SG, Smyth G, Cheng C, Stanford KI, Arumugam M, Michael MD, Adams AC, Kharitonenkov A, Kahn CR. Interplay between FGF21 and insulin action in the liver regulates metabolism. J Clin Invest. 2014 Feb;124(2):515-27. doi: 10.1172/JCI67353. Epub 2014 Jan 9.

Estes C, Anstee QM, Arias-Loste MT, Bantel H, Bellentani S, Caballeria J, Colombo M, Craxi A, Crespo J, Day CP, Eguchi Y, Geier A, Kondili LA, Kroy DC, Lazarus JV, Loomba R, Manns MP, Marchesini G, Nakajima A, Negro F, Petta S, Ratziu V, Romero-Gomez M, Sanyal A, Schattenberg JM, Tacke F, Tanaka J, Trautwein C, Wei L, Zeuzem S, Razavi H. Modeling NAFLD disease burden in China, France, Germany, Italy, Japan, Spain, United Kingdom, and United States for the period 2016-2030. J Hepatol. 2018 Oct;69(4):896-904. doi: 10.1016/j.jhep.2018.05.036. Epub 2018 Jun 8.

European Association for the Study of the Liver (EASL); European Association for the Study of Diabetes (EASD); European Association for the Study of Obesity (EASO). EASL-EASD-EASO Clinical Practice Guidelines for the management of non-alcoholic fatty liver disease. J Hepatol. 2016 Jun;64(6):1388-402. doi: 10.1016/j.jhep.2015.11.004. Epub 2016 Apr 7.

Fabbrini E, Mohammed BS, Magkos F, Korenblat KM, Patterson BW, Klein S. Alterations in adipose tissue and hepatic lipid kinetics in obese men and women with nonalcoholic fatty liver disease. Gastroenterology. 2008 Feb;134(2):424-31. doi: 10.1053/j.gastro.2007.11.038. Epub 2007 Nov 28.

Fabbrini E, Tiemann Luecking C, Love-Gregory L, Okunade AL, Yoshino M, Fraterrigo G, Patterson BW, Klein S. Physiological Mechanisms of Weight Gain-Induced Steatosis in People With Obesity. Gastroenterology. 2016 Jan;150(1):79-81.e2. doi: 10.1053/j.gastro.2015.09.003. Epub 2015 Sep 12.

Fajans SS, Bell GI, Polonsky KS. Molecular mechanisms and clinical pathophysiology of maturity-onset diabetes of the young. N Engl J Med. 2001 Sep 27;345(13):971-80.

Falcon A, Doege H, Fluitt A, Tsang B, Watson N, Kay MA, Stahl A. FATP2 is a hepatic fatty acid transporter and peroxisomal very long-chain acyl-CoA synthetase. Am J Physiol Endocrinol Metab. 2010 Sep;299(3):E384-93. doi: 10.1152/ajpendo.00226.2010. Epub 2010 Jun 8.

Fang YL, Chen H, Wang CL, Liang L. Pathogenesis of non-alcoholic fatty liver disease in children and adolescence: From "two hit theory" to "multiple hit model". World J Gastroenterol. 2018 Jul 21;24(27):2974-2983. doi: 10.3748/wjg.v24.i27.2974.

Fasshauer M, Blüher M. Adipokines in health and disease. Trends Pharmacol Sci. 2015 Jul;36(7):461-70. doi: 10.1016/j.tips.2015.04.014. Epub 2015 May 25.

Feng N, Zhang Z, Wang Z, Zheng H, Qu F, He X, Wang C. Insulin-Like Growth Factor Binding Protein-2 Promotes Adhesion of Endothelial Progenitor Cells to Endothelial Cells via Integrin α5β1. J Mol Neurosci. 2015 Nov;57(3):426-34. doi: 10.1007/s12031-015-0589-3. Epub 2015 Jun 16.

Fierbinteanu-Braticevici C, Dina I, Petrisor A, Tribus L, Negreanu L, Carstoiu C. Noninvasive investigations for non alcoholic fatty liver disease and liver fibrosis. World J Gastroenterol. 2010 Oct 14;16(38):4784-91.

Filhoulaud G, Guilmeau S, Dentin R, Girard J, Postic C. Novel insights into ChREBP regulation and function. Trends Endocrinol Metab. 2013 May;24(5):257-68. doi: 10.1016/j.tem.2013.01.003. Epub 2013 Apr 15.

Fox TE, Houck KL, O'Neill SM, Nagarajan M, Stover TC, Pomianowski PT, Unal O, Yun JK, Naides SJ, Kester M. Ceramide recruits and activates protein kinase C zeta (PKC zeta) within structured membrane microdomains. J Biol Chem. 2007 Apr 27;282(17):12450-7. Epub 2007 Feb 17.

Frangioudakis G, Burchfield JG, Narasimhan S, Cooney GJ, Leitges M, Biden TJ, Schmitz-Peiffer C. Diverse roles for protein kinase C delta and protein kinase C epsilon in the generation of high-fat-diet-induced glucose intolerance in mice: regulation of lipogenesis by protein kinase C delta. Diabetologia. 2009 Dec;52(12):2616-20. doi: 10.1007/s00125-009-1543-0. Epub 2009 Oct 7.

Friedman SL. Liver fibrosis -- from bench to bedside. J Hepatol. 2003;38 Suppl 1:S38-53.

Fu M, Sun T, Bookout AL, Downes M, Yu RT, Evans RM, Mangelsdorf DJ. A Nuclear Receptor Atlas: 3T3-L1 adipogenesis. Mol Endocrinol. 2005 Oct;19(10):2437-50. Epub 2005 Jul 28.

Galic S, Oakhill JS, Steinberg GR. Adipose tissue as an endocrine organ. Mol Cell Endocrinol. 2010 Mar 25;316(2):129-39. doi: 10.1016/j.mce.2009.08.018. Epub 2009 Aug 31.

Gandotra S, Le Dour C, Bottomley W, Cervera P, Giral P, Reznik Y, Charpentier G, Auclair M, Delépine M, Barroso I, Semple RK, Lathrop M, Lascols O, Capeau J, O'Rahilly S, Magré J, Savage DB, Vigouroux C. Perilipin deficiency and autosomal dominant partial lipodystrophy. N Engl J Med. 2011 Feb 24;364(8):740-8. doi: 10.1056/NEJMoa1007487.

Gao D, Nong S, Huang X, Lu Y, Zhao H, Lin Y, Man Y, Wang S, Yang J, Li J. The effects of palmitate on hepatic insulin resistance are mediated by NADPH Oxidase 3-derived reactive oxygen species through JNK and p38MAPK pathways. J Biol Chem. 2010 Sep 24;285(39):29965-73. doi: 10.1074/jbc.M110.128694. Epub 2010 Jul 20.

García-Ruiz C, Baulies A, Mari M, García-Rovés PM, Fernandez-Checa JC. Mitochondrial dysfunction in non-alcoholic fatty liver disease and insulin resistance: cause or consequence? Free Radic Res. 2013 Nov;47(11):854-68. doi: 10.3109/10715762.2013.830717. Epub 2013 Oct 4.

Gastaldelli A, Kozakova M, Højlund K, Flyvbjerg A, Favuzzi A, Mitrakou A, Balkau B; RISC Investigators. Fatty liver is associated with insulin resistance, risk of coronary heart disease, and early atherosclerosis in a large European population. Hepatology. 2009 May;49(5):1537-44. doi: 10.1002/hep.22845.

Goldstein I, Hager GL. Transcriptional and Chromatin Regulation during Fasting - The Genomic Era. Trends Endocrinol Metab. 2015 Dec;26(12):699-710. doi: 10.1016/j.tem.2015.09.005. Epub 2015 Oct 29.

Goldstein JL, DeBose-Boyd RA, Brown MS. Protein sensors for membrane sterols. Cell. 2006 Jan 13;124(1):35-46.

Graif M, Yanuka M, Baraz M, Blank A, Moshkovitz M, Kessler A, Gilat T, Weiss J, Walach E, Amazeen P, Irving CS. Quantitative estimation of attenuation in ultrasound video images: correlation with histology in diffuse liver disease. Invest Radiol. 2000 May;35(5):319-24.

Green CJ, Charlton CA, Wang LM, Silva M, Morten KJ, Hodson L. The isolation of primary hepatocytes from human tissue: optimising the use of small non-encapsulated liver resection surplus. Cell Tissue Bank. 2017 Dec;18(4):597-604. doi: 10.1007/s10561-017-9641-6. Epub 2017 Jul 17.

Gu X, Li K, Laybutt DR, He ML, Zhao HL, Chan JC, Xu G. Bip overexpression, but not CHOP inhibition, attenuates fatty-acid-induced endoplasmic reticulum stress and apoptosis

in HepG2 liver cells. Life Sci. 2010 Dec 18;87(23-26):724-32. doi: 10.1016/j.lfs.2010.10.012. Epub 2010 Oct 21.

Guo Y, Cordes KR, Farese RV Jr, Walther TC. Lipid droplets at a glance. J Cell Sci. 2009 Mar 15;122(Pt 6):749-52. doi: 10.1242/jcs.037630.

Gupta S, Stravitz RT, Dent P, Hylemon PB. Down-regulation of cholesterol 7alpha-hydroxylase (CYP7A1) gene expression by bile acids in primary rat hepatocytes is mediated by the c-Jun N-terminal kinase pathway. J Biol Chem. 2001 May 11;276(19):15816-22. Epub 2001 Feb 13.

Gusdon AM, Song KX, Qu S. Nonalcoholic Fatty liver disease: pathogenesis and therapeutics from a mitochondria-centric perspective. Oxid Med Cell Longev. 2014;2014:637027. doi: 10.1155/2014/637027. Epub 2014 Oct 13.

Gutiérrez-Juárez R, Pocai A, Mulas C, Ono H, Bhanot S, Monia BP, Rossetti L. Critical role of stearoyl-CoA desaturase-1 (SCD1) in the onset of diet-induced hepatic insulin resistance. J Clin Invest. 2006 Jun;116(6):1686-95.

Guy CD, Suzuki A, Burchette JL, Brunt EM, Abdelmalek MF, Cardona D, McCall SJ, Ünalp A, Belt P, Ferrell LD, Diehl AM; Nonalcoholic Steatohepatitis Clinical Research Network. Costaining for keratins 8/18 plus ubiquitin improves detection of hepatocyte injury in nonalcoholic fatty liver disease. Hum Pathol. 2012 Jun;43(6):790-800. doi: 10.1016/j.humpath.2011.07.007. Epub 2011 Oct 28.

Haas JT, Miao J, Chanda D, Wang Y, Zhao E, Haas ME, Hirschey M, Vaitheesvaran B, Farese RV Jr, Kurland IJ, Graham M, Crooke R, Foufelle F, Biddinger SB. Hepatic insulin signaling is required for obesity-dependent expression of SREBP-1c mRNA but not for feeding-dependent expression. Cell Metab. 2012 Jun 6;15(6):873-84. doi: 10.1016/j.cmet.2012.05.002.

Hall RK, Yamasaki T, Kucera T, Waltner-Law M, O'Brien R, Granner DK. Regulation of phosphoenolpyruvate carboxykinase and insulin-like growth factor-binding protein-1 gene expression by insulin. The role of winged helix/forkhead proteins. J Biol Chem. 2000 Sep 29;275(39):30169-75.

Harada N, Oda Z, Hara Y, Fujinami K, Okawa M, Ohbuchi K, Yonemoto M, Ikeda Y, Ohwaki K, Aragane K, Tamai Y, Kusunoki J. Hepatic de novo lipogenesis is present in liver-specific ACC1-deficient mice. Mol Cell Biol. 2007 Mar;27(5):1881-8. Epub 2007 Jan 8.

Hayhurst GP, Lee YH, Lambert G, Ward JM, Gonzalez FJ. Hepatocyte nuclear factor 4alpha (nuclear receptor 2A1) is essential for maintenance of hepatic gene expression and lipid homeostasis. Mol Cell Biol. 2001 Feb;21(4):1393-403.

Hedbacker K, Birsoy K, Wysocki RW, Asilmaz E, Ahima RS, Farooqi IS, Friedman JM. Antidiabetic effects of IGFBP2, a leptin-regulated gene. Cell Metab. 2010 Jan;11(1):11-22. doi: 10.1016/j.cmet.2009.11.007.

Henikoff S, Greally JM. Epigenetics, cellular memory and gene regulation. Curr Biol. 2016 Jul 25;26(14):R644-8. doi: 10.1016/j.cub.2016.06.011.

Heydemann A. An Overview of Murine High Fat Diet as a Model for Type 2 Diabetes Mellitus. J Diabetes Res. 2016;2016:2902351. doi: 10.1155/2016/2902351. Epub 2016 Jul 31.

Higuchi N, Kato M, Tanaka M, Miyazaki M, Takao S, Kohjima M, Kotoh K, Enjoji M, Nakamuta M, Takayanagi R. Effects of insulin resistance and hepatic lipid accumulation on hepatic mRNA expression levels of apoB, MTP and L-FABP in non-alcoholic fatty liver disease. Exp Ther Med. 2011 Nov;2(6):1077-1081. Epub 2011 Aug 9.

Hirosumi J, Tuncman G, Chang L, Görgün CZ, Uysal KT, Maeda K, Karin M, Hotamisligil GS. A central role for JNK in obesity and insulin resistance. Nature. 2002 Nov 21;420(6913):333-6.

Hirschey MD, Shimazu T, Goetzman E, Jing E, Schwer B, Lombard DB, Grueter CA, Harris C, Biddinger S, Ilkayeva OR, Stevens RD, Li Y, Saha AK, Ruderman NB, Bain JR, Newgard CB, Farese RV Jr, Alt FW, Kahn CR, Verdin E. SIRT3 regulates mitochondrial fatty-acid oxidation by reversible enzyme deacetylation. Nature. 2010 Mar 4;464(7285):121-5. doi: 10.1038/nature08778.

Hirschey MD, Shimazu T, Huang JY, Schwer B, Verdin E. SIRT3 regulates mitochondrial protein acetylation and intermediary metabolism. Cold Spring Harb Symp Quant Biol. 2011;76:267-77. doi: 10.1101/sqb.2011.76.010850. Epub 2011 Nov 23.

Honma M, Sawada S, Ueno Y, Murakami K, Yamada T, Gao J, Kodama S, Izumi T, Takahashi K, Tsukita S, Uno K, Imai J, Kakazu E, Kondo Y, Mizuno K, Kawagishi N, Shimosegawa T, Katagiri H. Selective insulin resistance with differential expressions of IRS-1 and IRS-2 in human NAFLD livers. Int J Obes (Lond). 2018 Sep;42(9):1544-1555. doi: 10.1038/s41366-018-0062-9. Epub 2018 May 1.

Horton JD, Bashmakov Y, Shimomura I, Shimano H. Regulation of sterol regulatory element binding proteins in livers of fasted and refed mice. Proc Natl Acad Sci U S A. 1998 May 26;95(11):5987-92.

Horton JD, Cuthbert JA, Spady DK. Regulation of hepatic 7 alpha-hydroxylase expression and response to dietary cholesterol in the rat and hamster. J Biol Chem. 1995 Mar 10;270(10):5381-7.

Horton JD, Shimomura I, Brown MS, Hammer RE, Goldstein JL, Shimano H. Activation of cholesterol synthesis in preference to fatty acid synthesis in liver and adipose tissue of transgenic mice overproducing sterol regulatory element-binding protein-2. J Clin Invest. 1998 Jun 1;101(11):2331-9.

Hotamisligil GS. Inflammation and metabolic disorders. Nature. 2006 Dec 14;444(7121):860-7.

Hughes ML, Liu B, Halls ML, Wagstaff KM, Patil R, Velkov T, Jans DA, Bunnett NW, Scanlon MJ, Porter CJ. Fatty Acid-binding Proteins 1 and 2 Differentially Modulate the Activation of Peroxisome Proliferator-activated Receptor α in a Ligand-selective Manner. J Biol Chem. 2015 May 29;290(22):13895-906. doi: 10.1074/jbc.M114.605998. Epub 2015 Apr 6.

Hunt MC, Alexson SE. The role Acyl-CoA thioesterases play in mediating intracellular lipid metabolism. Prog Lipid Res. 2002 Mar;41(2):99-130.

Ichikawa T, Nakao K, Hamasaki K, Furukawa R, Tsuruta S, Ueda Y, Taura N, Shibata H, Fujimoto M, Toriyama K, Eguchi K. Role of growth hormone, insulin-like growth factor 1 and insulin-like growth factor-binding protein 3 in development of non-alcoholic fatty liver disease. Hepatol Int. 2007 Jun;1(2):287-94. doi: 10.1007/s12072-007-9007-4. Epub 2007 Jun 1.

Inoue Y, Yu AM, Yim SH, Ma X, Krausz KW, Inoue J, Xiang CC, Brownstein MJ, Eggertsen G, Björkhem I, Gonzalez FJ. Regulation of bile acid biosynthesis by hepatocyte nuclear factor 4alpha. J Lipid Res. 2006 Jan;47(1):215-27. Epub 2005 Nov 1.

Jelenik T, Kaul K, Séquaris G, Flögel U, Phielix E, Kotzka J, Knebel B, Fahlbusch P, Hörbelt T, Lehr S, Reinbeck AL, Müller-Wieland D, Esposito I, Shulman GI, Szendroedi J, Roden M. Mechanisms of Insulin Resistance in Primary and Secondary Nonalcoholic Fatty Liver. Diabetes. 2017 Aug;66(8):2241-2253. doi: 10.2337/db16-1147. Epub 2017 May 10.

Ji C, Kaplowitz N. ER stress: can the liver cope? J Hepatol. 2006 Aug;45(2):321-33. Epub 2006 Jun 15.

Jiang Y, Zhang H, Dong LY, Wang D, An W. Increased hepatic UCP2 expression in rats with nonalcoholic steatohepatitis is associated with upregulation of Sp1 binding to its motif within the proximal promoter region. J Cell Biochem. 2008 Sep 1;105(1):277-89. doi: 10.1002/jcb.21827.

Jin ES, Browning JD, Murphy RE, Malloy CR. Fatty liver disrupts glycerol metabolism in gluconeogenic and lipogenic pathways in humans. J Lipid Res. 2018 Sep;59(9):1685-1694. doi: 10.1194/jlr.M086405. Epub 2018 Jul 27.

Jois T, Sleeman MW. The regulation and role of carbohydrate response element-binding protein in metabolic homeostasis and disease. J Neuroendocrinol. 2017 Oct;29(10). doi: 10.1111/jne.12473.

Jump DB. Fatty acid regulation of hepatic lipid metabolism. Curr Opin Clin Nutr Metab Care. 2011 Mar;14(2):115-20. doi: 10.1097/MCO.0b013e328342991c.

Kammel A, Saussenthaler S, Jähnert M, Jonas W, Stirm L, Hoeflich A, Staiger H, Fritsche A, Häring HU, Joost HG, Schürmann A, Schwenk RW. Early hypermethylation of hepatic Igfbp2 results in its reduced expression preceding fatty liver in mice. Hum Mol Genet. 2016 Jun 15;25(12):2588-2599. Epub 2016 Apr 28.

Kang HS, Kim MY, Kim SJ, Lee JH, Kim YD, Seo YK, Bae JH, Oh GT, Song DK, Ahn YH, Im SS. Regulation of IGFBP-2 expression during fasting. Biochem J. 2015 May 1;467(3):453-60. doi: 10.1042/BJ20141248.

Kanuri G, Bergheim I. In vitro and in vivo models of non-alcoholic fatty liver disease (NAFLD). Int J Mol Sci. 2013 Jun 5;14(6):11963-80. doi: 10.3390/ijms140611963.

Karantza V. Keratins in health and cancer: more than mere epithelial cell markers. Oncogene. 2011 Jan 13;30(2):127-38. doi: 10.1038/onc.2010.456. Epub 2010 Oct 4.

Kawano Y, Cohen DE. Mechanisms of hepatic triglyceride accumulation in non-alcoholic fatty liver disease. J Gastroenterol. 2013 Apr;48(4):434-41. doi: 10.1007/s00535-013-0758-5. Epub 2013 Feb 9.

Kegel V, Deharde D, Pfeiffer E, Zeilinger K, Seehofer D, Damm G. Protocol for Isolation of Primary Human Hepatocytes and Corresponding Major Populations of Non-parenchymal Liver Cells. J Vis Exp. 2016 Mar 30;(109):e53069. doi: 10.3791/53069.

Kerner J, Hoppel C. Fatty acid import into mitochondria. Biochim Biophys Acta. 2000 Jun 26;1486(1):1-17.

Kersten S, Seydoux J, Peters JM, Gonzalez FJ, Desvergne B, Wahli W. Peroxisome proliferator-activated receptor alpha mediates the adaptive response to fasting. J Clin Invest. 1999 Jun;103(11):1489-98.

Kersten S. Integrated physiology and systems biology of PPARα. Mol Metab. 2014 Mar 6;3(4):354-71. doi: 10.1016/j.molmet.2014.02.002. eCollection 2014 Jul.

Kim D, Kim WR. Nonobese Fatty Liver Disease. Clin Gastroenterol Hepatol. 2017 Apr;15(4):474-485. doi: 10.1016/j.cgh.2016.08.028. Epub 2016 Aug 28.

Kim HS, Xiao C, Wang RH, Lahusen T, Xu X, Vassilopoulos A, Vazquez-Ortiz G, Jeong WI, Park O, Ki SH, Gao B, Deng CX. Hepatic-specific disruption of SIRT6 in mice results in fatty liver formation due to enhanced glycolysis and triglyceride synthesis. Cell Metab. 2010 Sep 8;12(3):224-36. doi: 10.1016/j.cmet.2010.06.009.

Kim JH, Kwon SY, Lee SW, Lee CH. Validation of fatty liver index and lipid accumulation product for predicting fatty liver in Korean population. Liver Int. 2011 Nov;31(10):1600-1. doi: 10.1111/j.1478-3231.2011.02580.x. Epub 2011 Jul 5.

Kim JK, Fillmore JJ, Chen Y, Yu C, Moore IK, Pypaert M, Lutz EP, Kako Y, Velez-Carrasco W, Goldberg IJ, Breslow JL, Shulman GI. Tissue-specific overexpression of lipoprotein lipase causes tissue-specific insulin resistance. Proc Natl Acad Sci U S A. 2001 Jun 19;98(13):7522-7. Epub 2001 Jun 5.

Kim JK, Gavrilova O, Chen Y, Reitman ML, Shulman GI. Mechanism of insulin resistance in A-ZIP/F-1 fatless mice. J Biol Chem. 2000 Mar 24;275(12):8456-60.

Kim MS, Lee DY. Insulin-like growth factor (IGF)-I and IGF binding proteins axis in diabetes mellitus. Ann Pediatr Endocrinol Metab. 2015 Jun;20(2):69-73. doi: 10.6065/apem.2015.20.2.69. Epub 2015 Jun 30.

Klaunig JE, Kamendulis LM, Hocevar BA. Oxidative stress and oxidative damage in carcinogenesis. Toxicol Pathol. 2010 Jan;38(1):96-109. doi: 10.1177/0192623309356453. Epub 2009 Dec 17.

Klein I, Cornejo JC, Polakos NK, John B, Wuensch SA, Topham DJ, Pierce RH, Crispe IN. Kupffer cell heterogeneity: functional properties of bone marrow derived and sessile hepatic macrophages. Blood. 2007 Dec 1;110(12):4077-85. Epub 2007 Aug 9.

Kleiner DE, Makhlouf HR. Histology of Nonalcoholic Fatty Liver Disease and Nonalcoholic Steatohepatitis in Adults and Children. Clin Liver Dis. 2016 May;20(2):293-312. doi: 10.1016/j.cld.2015.10.011. Epub 2015 Dec 28.

Knebel B, Göddeke S, Hartwig S, Hörbelt T, Fahlbusch P, Al-Hasani H, Jacob S, Koellmer C, Nitzgen U, Schiller M, Lehr S, Kotzka J. Alteration of Liver Peroxisomal and Mitochondrial Functionality in the NZO Mouse Model of Metabolic Syndrome. Proteomics Clin Appl. 2018a Jan;12(1). doi: 10.1002/prca.201700028. Epub 2017 Dec 11.

Knebel B, Haas J, Hartwig S, Jacob S, Köllmer C, Nitzgen U, Muller-Wieland D, Kotzka J. Liver-specific expression of transcriptionally active SREBP-1c is associated with fatty liver and increased visceral fat mass. PLoS One. 2012;7(2):e31812. doi: 10.1371/journal.pone.0031812. Epub 2012 Feb 21.

Knebel B, Hartwig S, Haas J, Lehr S, Goeddeke S, Susanto F, Bohne L, Jacob S, Koellmer C, Nitzgen U, Müller-Wieland D, Kotzka J. Peroxisomes compensate hepatic lipid overflow in mice with fatty liver. Biochim Biophys Acta. 2015 Jul;1851(7):965-76. doi: 10.1016/j.bbalip.2015.03.003. Epub 2015 Mar 17.

Knebel B, Hartwig S, Jacob S, Kettel U, Schiller M, Passlack W, Koellmer C, Lehr S, Müller-Wieland D, Kotzka J. Inactivation of SREBP-1a Phosphorylation Prevents Fatty Liver Disease in Mice: Identification of Related Signaling Pathways by Gene Expression Profiles in Liver and Proteomes of Peroxisomes. Int J Mol Sci. 2018b Mar 25;19(4). pii: E980. doi: 10.3390/ijms19040980.

Knebel B, Kotzka J, Lehr S, Hartwig S, Avci H, Jacob S, Nitzgen U, Schiller M, März W, Hoffmann MM, Seemanova E, Haas J, Muller-Wieland D. A mutation in the c-fos gene associated with congenital generalized lipodystrophy. Orphanet J Rare Dis. 2013 Aug 7;8:119. doi: 10.1186/1750-1172-8-119.

Knebel B, Lehr S, Hartwig S, Haas J, Kaber G, Dicken HD, Susanto F, Bohne L, Jacob S, Nitzgen U, Passlack W, Muller-Wieland D, Kotzka J. Phosphorylation of sterol regulatory element-binding protein (SREBP)-1c by p38 kinases, ERK and JNK influences lipid metabolism and the secretome of human liver cell line HepG2. Arch Physiol Biochem. 2014 Dec;120(5):216-27. doi: 10.3109/13813455.2014.973418.

Kohlwein SD, Veenhuis M, van der Klei IJ. Lipid droplets and peroxisomes: key players in cellular lipid homeostasis or a matter of fat--store 'em up or burn 'em down. Genetics. 2013 Jan;193(1):1-50. doi: 10.1534/genetics.112.143362.

Koliaki C, Roden M. Hepatic energy metabolism in human diabetes mellitus, obesity and non-alcoholic fatty liver disease. Mol Cell Endocrinol. 2013 Oct 15;379(1-2):35-42. doi: 10.1016/j.mce.2013.06.002. Epub 2013 Jun 12.

Koliwad SK, Streeper RS, Monetti M, Cornelissen I, Chan L, Terayama K, Naylor S, Rao M, Hubbard B, Farese RV Jr. DGAT1-dependent triacylglycerol storage by macrophages protects mice from diet-induced insulin resistance and inflammation. J Clin Invest. 2010 Mar;120(3):756-67. doi: 10.1172/JCI36066.

Konopelska S, Kienitz T, Quinkler M. Downregulation of hepatic glucose-6-phosphatase-α in patients with hepatic steatosis. Obesity (Silver Spring). 2011 Dec;19(12):2322-6. doi: 10.1038/oby.2011.118. Epub 2011 May 19.

Koonen DP, Jacobs RL, Febbraio M, Young ME, Soltys CL, Ong H, Vance DE, Dyck JR. Increased hepatic CD36 expression contributes to dyslipidemia associated with diet-induced obesity. Diabetes. 2007 Dec;56(12):2863-71. Epub 2007 Aug 29.

Korn BS, Shimomura I, Bashmakov Y, Hammer RE, Horton JD, Goldstein JL, Brown MS. Blunted feedback suppression of SREBP processing by dietary cholesterol in transgenic mice expressing sterol-resistant SCAP(D443N). J Clin Invest. 1998 Dec 15;102(12):2050-60.

Kotronen A, Peltonen M, Hakkarainen A, Sevastianova K, Bergholm R, Johansson LM, Lundbom N, Rissanen A, Ridderstråle M, Groop L, Orho-Melander M, Yki-Järvinen H. Prediction of non-alcoholic fatty liver disease and liver fat using metabolic and genetic factors. Gastroenterology. 2009 Sep;137(3):865-72. doi: 10.1053/j.gastro.2009.06.005. Epub 2009 Jun 12.

Kotzka J, Knebel B, Avci H, Jacob S, Nitzgen U, Jockenhovel F, Heeren J, Haas J, Muller-Wieland D. Phosphorylation of sterol regulatory element-binding protein (SREBP)-1a links growth hormone action to lipid metabolism in hepatocytes. Atherosclerosis. 2010 Nov;213(1):156-65. doi: 10.1016/j.atherosclerosis.2010.08.046. Epub 2010 Aug 19.

Kotzka J, Knebel B, Haas J, Kremer L, Jacob S, Hartwig S, Nitzgen U, Muller-Wieland D. Preventing phosphorylation of sterol regulatory element-binding protein 1a by MAP-kinases protects mice from fatty liver and visceral obesity. PLoS One. 2012;7(2):e32609. doi: 10.1371/journal.pone.0032609. Epub 2012 Feb 27.

Kotzka J, Lehr S, Roth G, Avci H, Knebel B, Muller-Wieland D. Insulin-activated Erk-mitogen-activated protein kinases phosphorylate sterol regulatory element-binding Protein-2 at serine residues 432 and 455 in vivo. J Biol Chem. 2004 May 21;279(21):22404-11. Epub 2004 Feb 26.

Kotzka J, Müller-Wieland D, Koponen A, Njamen D, Kremer L, Roth G, Munck M, Knebel B, Krone W. ADD1/SREBP-1c mediates insulin-induced gene expression linked to the MAP kinase pathway. Biochem Biophys Res Commun. 1998 Aug 19;249(2):375-9.

Kovacs P, Stumvoll M. Fatty acids and insulin resistance in muscle and liver. Best Pract Res Clin Endocrinol Metab. 2005 Dec;19(4):625-35.

Ku NO, Soetikno RM, Omary MB. Keratin mutation in transgenic mice predisposes to Fas but not TNF-induced apoptosis and massive liver injury. Hepatology. 2003 May;37(5):1006-14.

Ku NO, Strnad P, Zhong BH, Tao GZ, Omary MB. Keratins let liver live: Mutations predispose to liver disease and crosslinking generates Mallory-Denk bodies. Hepatology. 2007 Nov;46(5):1639-49.

Kucukoglu O, Guldiken N, Chen Y, Usachov V, El-Heliebi A, Haybaeck J, Denk H, Trautwein C, Strnad P. High-fat diet triggers Mallory-Denk body formation through misfolding and crosslinking of excess keratin 8. Hepatology. 2014 Jul;60(1):169-78. doi: 10.1002/hep.27068. Epub 2014 May 27.

Kumashiro N, Erion DM, Zhang D, Kahn M, Beddow SA, Chu X, Still CD, Gerhard GS, Han X, Dziura J, Petersen KF, Samuel VT, Shulman GI. Cellular mechanism of insulin resistance in nonalcoholic fatty liver disease. Proc Natl Acad Sci U S A. 2011 Sep 27;108(39):16381-5. doi: 10.1073/pnas.1113359108. Epub 2011 Sep 19.

Kusminski CM, Shetty S, Orci L, Unger RH, Scherer PE. Diabetes and apoptosis: lipotoxicity. Apoptosis. 2009 Dec;14(12):1484-95. doi: 10.1007/s10495-009-0352-8.

Laager R, Ninnis R, Keller U. Comparison of the effects of recombinant human insulin-like growth factor-I and insulin on glucose and leucine kinetics in humans. J Clin Invest. 1993 Oct;92(4):1903-9.

Lai KK, Kolippakkam D, Beretta L. Comprehensive and quantitative proteome profiling of the mouse liver and plasma. Hepatology. 2008 Mar;47(3):1043-51. doi: 10.1002/hep.22123.

Lai M, Chandrasekera PC, Barnard ND. You are what you eat, or are you? The challenges of translating high-fat-fed rodents to human obesity and diabetes. Nutr Diabetes. 2014 Sep 8;4:e135. doi: 10.1038/nutd.2014.30.

Lake AD, Novak P, Hardwick RN, Flores-Keown B, Zhao F, Klimecki WT, Cherrington NJ. The adaptive endoplasmic reticulum stress response to lipotoxicity in progressive human nonalcoholic fatty liver disease. Toxicol Sci. 2014 Jan;137(1):26-35. doi: 10.1093/toxsci/kft230. Epub 2013 Oct 4.

Lake BG. Human relevance of rodent liver tumour formation by constitutive androstane receptor (CAR) activators. Toxicol Res (Camb). 2018 Mar 12;7(4):697-717. doi: 10.1039/c8tx00008e. eCollection 2018 Jul 1.

Lambert JE, Ramos-Roman MA, Browning JD, Parks EJ. Increased de novo lipogenesis is a distinct characteristic of individuals with nonalcoholic fatty liver disease. Gastroenterology. 2014 Mar;146(3):726-35. doi: 10.1053/j.gastro.2013.11.049. Epub 2013 Dec 4.

Langin D. Control of fatty acid and glycerol release in adipose tissue lipolysis. C R Biol. 2006 Aug;329(8):598-607; discussion 653-5. Epub 2006 Apr 27.

Le Roith D. The insulin-like growth factor system. Exp Diabesity Res. 2003 Oct-Dec;4(4):205-12.

Lebensztejn DM, Flisiak-Jackiewicz M, Białokoz-Kalinowska I, Bobrus-Chociej A, Kowalska I. Hepatokines and non-alcoholic fatty liver disease. Acta Biochim Pol. 2016;63(3):459-67. doi: 10.18388/abp.2016_1252. Epub 2016 Jun 6.

Lee J, Choi J, Selen Alpergin ES, Zhao L, Hartung T, Scafidi S, Riddle RC, Wolfgang MJ. Loss of Hepatic Mitochondrial Long-Chain Fatty Acid Oxidation Confers Resistance to Diet-Induced Obesity and Glucose Intolerance. Cell Rep. 2017 Jul 18;20(3):655-667. doi: 10.1016/j.celrep.2017.06.080.

Leite NC, Salles GF, Araujo AL, Villela-Nogueira CA, Cardoso CR. Prevalence and associated factors of non-alcoholic fatty liver disease in patients with type-2 diabetes mellitus. Liver Int. 2009 Jan;29(1):113-9. doi: 10.1111/j.1478-3231.2008.01718.x. Epub 2008 Apr 1.

Leiter EH, Coleman DL, Hummel KP.The influence of genetic background on the expression of mutations at the diabetes locus in the mouse. III. Effect of H-2 haplotype and sex. Diabetes. 1981 Dec;30(12):1029-34.

Leone TC, Weinheimer CJ, Kelly DP. A critical role for the peroxisome proliferator-activated receptor alpha (PPARalpha) in the cellular fasting response: the PPARalpha-null mouse as a model of fatty acid oxidation disorders. Proc Natl Acad Sci U S A. 1999 Jun 22;96(13):7473-8.

Levinson SS, Wagner SG. Implications of reverse cholesterol transport: recent studies. Clin Chim Acta. 2015 Jan 15;439:154-61. doi: 10.1016/j.cca.2014.10.018. Epub 2014 Oct 22.

Lewitt MS, Dent MS, Hall K. The Insulin-Like Growth Factor System in Obesity, Insulin Resistance and Type 2 Diabetes Mellitus. J Clin Med. 2014 Dec 22;3(4):1561-74. doi: 10.3390/jcm3041561.

Li H, Yu X. Emerging role of JNK in insulin resistance. Curr Diabetes Rev. 2013 Sep;9(5):422-8.

Li Z, Berk M, McIntyre TM, Gores GJ, Feldstein AE. The lysosomal-mitochondrial axis in free fatty acid-induced hepatic lipotoxicity. Hepatology. 2008 May;47(5):1495-503. doi: 10.1002/hep.22183.

Li ZZ, Berk M, McIntyre TM, Feldstein AE. Hepatic lipid partitioning and liver damage in nonalcoholic fatty liver disease: role of stearoyl-CoA desaturase. J Biol Chem. 2009 Feb 27;284(9):5637-44. doi: 10.1074/jbc.M807616200. Epub 2009 Jan 1.

Lin M, Lv D, Zheng Y, Wu M, Xu C, Zhang Q, Wu L. Downregulation of CPT2 promotes tumorigenesis and chemoresistance to cisplatin in hepatocellular carcinoma. Onco Targets Ther. 2018 May 25;11:3101-3110. doi: 10.2147/OTT.S163266. eCollection 2018.

Listenberger LL, Han X, Lewis SE, Cases S, Farese RV Jr, Ory DS, Schaffer JE. Triglyceride accumulation protects against fatty acid-induced lipotoxicity. Proc Natl Acad Sci U S A. 2003 Mar 18;100(6):3077-82. Epub 2003 Mar 10.

Lodhi IJ, Semenkovich CF. Peroxisomes: a nexus for lipid metabolism and cellular signaling. Cell Metab. 2014 Mar 4;19(3):380-92. doi: 10.1016/j.cmet.2014.01.002. Epub 2014 Feb 6.

Loomba R, Sanyal AJ. The global NAFLD epidemic. Nat Rev Gastroenterol Hepatol. 2013 Nov;10(11):686-90. doi: 10.1038/nrgastro.2013.171. Epub 2013 Sep 17.

Ma K, Saha PK, Chan L, Moore DD. Farnesoid X receptor is essential for normal glucose homeostasis. J Clin Invest. 2006 Apr;116(4):1102-9. Epub 2006 Mar 23.

Madan K, Bhardwaj P, Thareja S, Gupta SD, Saraya A. Oxidant stress and antioxidant status among patients with nonalcoholic fatty liver disease (NAFLD). J Clin Gastroenterol. 2006 Nov-Dec;40(10):930-5.

Magkos F, Su X, Bradley D, Fabbrini E, Conte C, Eagon JC, Varela JE, Brunt EM, Patterson BW, Klein S. Intrahepatic diacylglycerol content is associated with hepatic insulin resistance in obese subjects. Gastroenterology. 2012 Jun;142(7):1444-6.e2. doi: 10.1053/j.gastro.2012.03.003. Epub 2012 Mar 13.

Makowski L, Hotamisligil GS. The role of fatty acid binding proteins in metabolic syndrome and atherosclerosis. Curr Opin Lipidol. 2005 Oct;16(5):543-8.

Malhi H, Bronk SF, Werneburg NW, Gores GJ. Free fatty acids induce JNK-dependent hepatocyte lipoapoptosis. J Biol Chem. 2006 Apr 28;281(17):12093-101. Epub 2006 Feb 27.

Malhi H, Gores GJ. Molecular mechanisms of lipotoxicity in nonalcoholic fatty liver disease. Semin Liver Dis. 2008 Nov;28(4):360-9. doi: 10.1055/s-0028-1091980. Epub 2008 Oct 27.

Malhi H, Kaufman RJ. Endoplasmic reticulum stress in liver disease. J Hepatol. 2011 Apr;54(4):795-809. doi: 10.1016/j.jhep.2010.11.005. Epub 2010 Nov 13.

Mao J, DeMayo FJ, Li H, Abu-Elheiga L, Gu Z, Shaikenov TE, Kordari P, Chirala SS, Heird WC, Wakil SJ. Liver-specific deletion of acetyl-CoA carboxylase 1 reduces hepatic triglyceride accumulation without affecting glucose homeostasis. Proc Natl Acad Sci U S A. 2006 May 30;103(22):8552-7. Epub 2006 May 22.

Marrero JA, Fontana RJ, Su GL, Conjeevaram HS, Emick DM, Lok AS. NAFLD may be a common underlying liver disease in patients with hepatocellular carcinoma in the United States. Hepatology. 2002 Dec;36(6):1349-54.

Martinon F, Chen X, Lee AH, Glimcher LH. TLR activation of the transcription factor XBP1 regulates innate immune responses in macrophages. Nat Immunol. 2010 May;11(5):411-8. doi: 10.1038/ni.1857. Epub 2010 Mar 28.

Massillon D, Barzilai N, Hawkins M, Prus-Wertheimer D, Rossetti L. Induction of hepatic glucose-6-phosphatase gene expression by lipid infusion. Diabetes. 1997 Jan;46(1):153-7.

Mattera D, Capuano G, Colao A, Pivonello R, Manguso F, Puzziello A, D'Agostino L. Increased IGF-I : IGFBP-3 ratio in patients with hepatocellular carcinoma. Clin Endocrinol (Oxf). 2003 Dec;59(6):699-706.

McGarry JD, Brown NF. The mitochondrial carnitine palmitoyltransferase system. From concept to molecular analysis. Eur J Biochem. 1997 Feb 15;244(1):1-14.

McGarry JD, Foster DW. Regulation of hepatic fatty acid oxidation and ketone body production. Annu Rev Biochem. 1980;49:395-420.

Meex RCR, Watt MJ. Hepatokines: linking nonalcoholic fatty liver disease and insulin resistance. Nat Rev Endocrinol. 2017 Sep;13(9):509-520. doi: 10.1038/nrendo.2017.56. Epub 2017 Jun 9.

Mehta SR, Thomas EL, Bell JD, Johnston DG, Taylor-Robinson SD. Non-invasive means of measuring hepatic fat content. World J Gastroenterol. 2008 Jun 14;14(22):3476-83.

Michael MD, Kulkarni RN, Postic C, Previs SF, Shulman GI, Magnuson MA, Kahn CR. Loss of insulin signaling in hepatocytes leads to severe insulin resistance and progressive hepatic dysfunction. Mol Cell. 2000 Jul;6(1):87-97.

Miller WL, Auchus RJ. The molecular biology, biochemistry, and physiology of human steroidogenesis and its disorders. Endocr Rev. 2011 Feb;32(1):81-151. doi: 10.1210/er.2010-0013. Epub 2010 Nov 4.

Miyazaki M, Kim YC, Ntambi JM. A lipogenic diet in mice with a disruption of the stearoyl-CoA desaturase 1 gene reveals a stringent requirement of endogenous monounsaturated fatty acids for triglyceride synthesis. J Lipid Res. 2001 Jul;42(7):1018-24.

Mohan S, Baylink DJ. IGF-binding proteins are multifunctional and act via IGF-dependent and -independent mechanisms. J Endocrinol. 2002 Oct;175(1):19-31.

Moitra J, Mason MM, Olive M, Krylov D, Gavrilova O, Marcus-Samuels B, Feigenbaum L, Lee E, Aoyama T, Eckhaus M, Reitman ML, Vinson C. Life without white fat: a transgenic mouse. Genes Dev. 1998 Oct 15;12(20):3168-81.

Moll R, Divo M, Langbein L. The human keratins: biology and pathology. Histochem Cell Biol. 2008 Jun;129(6):705-33. doi: 10.1007/s00418-008-0435-6. Epub 2008 May 7.

Monetti M, Levin MC, Watt MJ, Sajan MP, Marmor S, Hubbard BK, Stevens RD, Bain JR, Newgard CB, Farese RV Sr, Hevener AL, Farese RV Jr. Dissociation of hepatic steatosis and insulin resistance in mice overexpressing DGAT in the liver. Cell Metab. 2007 Jul;6(1):69-78.

Montagner A, Polizzi A, Fouché E, Ducheix S, Lippi Y, Lasserre F, Barquissau V, Régnier M1, Lukowicz C, Benhamed F, Iroz A, Bertrand-Michel J, Al Saati T, Cano P, Mselli-Lakhal L, Mithieux G, Rajas F, Lagarrigue S, Pineau T, Loiseau N, Postic C, Langin D, Wahli W, Guillou H. Liver PPARα is crucial for whole-body fatty acid homeostasis and is protective against NAFLD. Gut. 2016 Jul;65(7):1202-14. doi: 10.1136/gutjnl-2015-310798. Epub 2016 Feb 1.

Morrish F, Hockenbery D. MYC and mitochondrial biogenesis. Cold Spring Harb Perspect Med. 2014 May 1;4(5). pii: a014225. doi: 10.1101/cshperspect.a014225.

Morton RE, Greene DJ. Regulation of lipid transfer between lipoproteins by an endogenous plasma protein: selective inhibition among lipoprotein classes. J Lipid Res. 1994 May;35(5):836-47.

Munday MR. Regulation of mammalian acetyl-CoA carboxylase. Biochem Soc Trans. 2002 Nov;30(Pt 6):1059-64.

Murphy LJ. The role of the insulin-like growth factors and their binding proteins in glucose homeostasis. Exp Diabesity Res. 2003 Oct-Dec;4(4):213-24.

Musso G, Gambino R, Cassader M. Recent insights into hepatic lipid metabolism in non-alcoholic fatty liver disease (NAFLD). Prog Lipid Res. 2009 Jan;48(1):1-26. doi: 10.1016/j.plipres.2008.08.001. Epub 2008 Sep 9.

Nakamichi I, Toivola DM, Strnad P, Michie SA, Oshima RG, Baribault H, Omary MB. Keratin 8 overexpression promotes mouse Mallory body formation. J Cell Biol. 2005 Dec 19;171(6):931-7.

Nakamura S, Takamura T, Matsuzawa-Nagata N, Takayama H, Misu H, Noda H, Nabemoto S, Kurita S, Ota T, Ando H, Miyamoto K, Kaneko S. Palmitate induces insulin resistance in H4IIEC3 hepatocytes through reactive oxygen species produced by mitochondria. J Biol Chem. 2009 May 29;284(22):14809-18. doi: 10.1074/jbc.M901488200. Epub 2009 Mar 30.

Nalbantoglu IL, Brunt EM. Role of liver biopsy in nonalcoholic fatty liver disease. World J Gastroenterol. 2014 Jul 21;20(27):9026-37. doi: 10.3748/wjg.v20.i27.9026.

Nassir F, Ibdah JA. Role of mitochondria in nonalcoholic fatty liver disease. Int J Mol Sci. 2014 May 15;15(5):8713-42. doi: 10.3390/ijms15058713.

Neschen S, Morino K, Hammond LE, Zhang D, Liu ZX, Romanelli AJ, Cline GW, Pongratz RL, Zhang XM, Choi CS, Coleman RA, Shulman GI. Prevention of hepatic steatosis and hepatic insulin resistance in mitochondrial acyl-CoA:glycerol-sn-3-phosphate acyltransferase 1 knockout mice. Cell Metab. 2005 Jul;2(1):55-65.

Newberry EP, Xie Y, Kennedy S, Han X, Buhman KK, Luo J, Gross RW, Davidson NO. Decreased hepatic triglyceride accumulation and altered fatty acid uptake in mice with deletion of the liver fatty acid-binding protein gene. J Biol Chem. 2003 Dec 19;278(51):51664-72. Epub 2003 Oct 8.

Nordgren M, Fransen M. Peroxisomal metabolism and oxidative stress. Biochimie. 2014 Mar;98:56-62. doi: 10.1016/j.biochi.2013.07.026. Epub 2013 Aug 9.

Ordovas JM. Genotype-phenotype associations: modulation by diet and obesity. Obesity (Silver Spring). 2008 Dec;16 Suppl 3:S40-6. doi: 10.1038/oby.2008.515.

Orellana M, Rodrigo R, Varela N, Araya J, Poniachik J, Csendes A, Smok G, Videla LA. Relationship between in vivo chlorzoxazone hydroxylation, hepatic cytochrome P450 2E1 content and liver injury in obese non-alcoholic fatty liver disease patients. Hepatol Res. 2006 Jan;34(1):57-63.

Oslowski CM, Urano F. Measuring ER stress and the unfolded protein response using mammalian tissue culture system. Methods Enzymol. 2011;490:71-92. doi: 10.1016/B978-0-12-385114-7.00004-0.

Ozcan U, Cao Q, Yilmaz E, Lee AH, Iwakoshi NN, Ozdelen E, Tuncman G, Görgün C, Glimcher LH, Hotamisligil GS. Endoplasmic reticulum stress links obesity, insulin action, and type 2 diabetes. Science. 2004 Oct 15;306(5695):457-61.

Pawlak M, Lefebvre P, Staels B. Molecular mechanism of PPARα action and its impact on lipid metabolism, inflammation and fibrosis in non-alcoholic fatty liver disease. J Hepatol. 2015 Mar;62(3):720-33. doi: 10.1016/j.jhep.2014.10.039. Epub 2014 Nov 1.

Perla FM, Prelati M, Lavorato M, Visicchio D, Anania C. The Role of Lipid and Lipoprotein Metabolism in Non-Alcoholic Fatty Liver Disease. Children (Basel). 2017 Jun 6;4(6). pii: E46. doi: 10.3390/children4060046.

Pessayre D, Mansouri A, Fromenty B. Nonalcoholic steatosis and steatohepatitis. V. Mitochondrial dysfunction in steatohepatitis. Am J Physiol Gastrointest Liver Physiol. 2002 Feb;282(2):G193-9.

Petäjä EM, Yki-Järvinen H. Definitions of Normal Liver Fat and the Association of Insulin Sensitivity with Acquired and Genetic NAFLD-A Systematic Review. Int J Mol Sci. 2016 Apr 27;17(5). pii: E633. doi: 10.3390/ijms17050633.

Petersen KF, Dufour S, Befroy D, Lehrke M, Hendler RE, Shulman GI. Reversal of nonalcoholic hepatic steatosis, hepatic insulin resistance, and hyperglycemia by moderate weight reduction in patients with type 2 diabetes. Diabetes. 2005 Mar;54(3):603-8.

Petersen KF, Oral EA, Dufour S, Befroy D, Ariyan C, Yu C, Cline GW, DePaoli AM, Taylor SI, Gorden P, Shulman GI. Leptin reverses insulin resistance and hepatic steatosis in patients with severe lipodystrophy. J Clin Invest. 2002 May;109(10):1345-50.

Piperi C, Adamopoulos C, Papavassiliou AG. XBP1: A Pivotal Transcriptional Regulator of Glucose and Lipid Metabolism. Trends Endocrinol Metab. 2016 Mar;27(3):119-122. doi: 10.1016/j.tem.2016.01.001. Epub 2016 Jan 20.

Pirola CJ, Gianotti TF, Burgueño AL, Rey-Funes M, Loidl CF, Mallardi P, Martino JS, Castaño GO, Sookoian S. Epigenetic modification of liver mitochondrial DNA is associated with histological severity of nonalcoholic fatty liver disease. Gut. 2013 Sep;62(9):1356-63. doi: 10.1136/gutjnl-2012-302962. Epub 2012 Aug 9.

Pivonello C, De Martino MC, Negri M, Cuomo G, Cariati F, Izzo F, Colao A, Pivonello R. The GH-IGF-SST system in hepatocellular carcinoma: biological and molecular pathogenetic mechanisms and therapeutic targets. Infect Agent Cancer. 2014 Aug 20;9:27. doi: 10.1186/1750-9378-9-27. eCollection 2014.

Poeta M, Pierri L, Vajro P. Gut-Liver Axis Derangement in Non-Alcoholic Fatty Liver Disease. Children (Basel). 2017 Aug 2;4(8). pii: E66. doi: 10.3390/children4080066.

Postic C, Girard J. Contribution of de novo fatty acid synthesis to hepatic steatosis and insulin resistance: lessons from genetically engineered mice. J Clin Invest. 2008 Mar;118(3):829-38. doi: 10.1172/JCI34275.

Potze W, Siddiqui MS, Sanyal AJ. Vascular Disease in Patients with Nonalcoholic Fatty Liver Disease. Semin Thromb Hemost. 2015 Jul;41(5):488-93. doi: 10.1055/s-0035-1550433. Epub 2015 Jun 6.

Pratipanawatr T, Pratipanawatr W, Rosen C, Berria R, Bajaj M, Cusi K, Mandarino L, Kashyap S, Belfort R, DeFronzo RA. Effect of IGF-I on FFA and glucose metabolism in control and type 2 diabetic subjects. Am J Physiol Endocrinol Metab. 2002 Jun;282(6):E1360-8.

Puri P, Mirshahi F, Cheung O, Natarajan R, Maher JW, Kellum JM, Sanyal AJ. Activation and dysregulation of the unfolded protein response in nonalcoholic fatty liver disease. Gastroenterology. 2008 Feb;134(2):568-76. Epub 2007 Oct 26.

Purushotham A, Schug TT, Xu Q, Surapureddi S, Guo X, Li X. Hepatocyte-specific deletion of SIRT1 alters fatty acid metabolism and results in hepatic steatosis and inflammation. Cell Metab. 2009 Apr;9(4):327-38. doi: 10.1016/j.cmet.2009.02.006.

Rajpathak SN, Gunter MJ, Wylie-Rosett J, Ho GY, Kaplan RC, Muzumdar R, Rohan TE, Strickler HD. The role of insulin-like growth factor-I and its binding proteins in glucose homeostasis and type 2 diabetes. Diabetes Metab Res Rev. 2009 Jan;25(1):3-12. doi: 10.1002/dmrr.919.

Romeo S, Kozlitina J, Xing C, Pertsemlidis A, Cox D, Pennacchio LA, Boerwinkle E, Cohen JC, Hobbs HH. Genetic variation in PNPLA3 confers susceptibility to nonalcoholic fatty liver disease. Nat Genet. 2008 Dec;40(12):1461-5. doi: 10.1038/ng.257. Epub 2008 Sep 25.

Ron D, Walter P. Signal integration in the endoplasmic reticulum unfolded protein response. Nat Rev Mol Cell Biol. 2007 Jul;8(7):519-29.

Roth A, Looser R, Kaufmann M, Meyer UA. Sterol regulatory element binding protein 1 interacts with pregnane X receptor and constitutive androstane receptor and represses their target genes. Pharmacogenet Genomics. 2008 Apr;18(4):325-37. doi: 10.1097/FPC.0b013e3282f706e0.

Roth G, Kotzka J, Kremer L, Lehr S, Lohaus C, Meyer HE, Krone W, Müller-Wieland D. MAP kinases Erk1/2 phosphorylate sterol regulatory element-binding protein (SREBP)-1a at serine 117 in vitro. J Biol Chem. 2000 Oct 27;275(43):33302-7.

Ruan W, Lai M. Insulin-like growth factor binding protein: a possible marker for the metabolic syndrome? Acta Diabetol. 2010 Mar;47(1):5-14. doi: 10.1007/s00592-009-0142-3. Epub 2009 Sep 22.

Ruige JB, Bekaert M, Lapauw B, Fiers T, Lehr S, Hartwig S, Herzfeld de Wiza D, Schiller M, Passlack W, Van Nieuwenhove Y, Pattyn P, Cuvelier C, Taes YE, Sell H, Eckel J, Kaufman JM, Ouwens DM. Sex steroid-induced changes in circulating monocyte chemoattractant protein-1 levels may contribute to metabolic dysfunction in obese men. J Clin Endocrinol Metab. 2012 Jul;97(7):E1187-91. doi: 10.1210/jc.2011-3069. Epub 2012 Apr 20.

Russo VC, Azar WJ, Yau SW, Sabin MA, Werther GA. IGFBP-2: The dark horse in metabolism and cancer. Cytokine Growth Factor Rev. 2015 Jun;26(3):329-46. doi: 10.1016/j.cytogfr.2014.12.001. Epub 2014 Dec 18.

Saadeh S, Younossi ZM, Remer EM, Gramlich T, Ong JP, Hurley M, Mullen KD, Cooper JN, Sheridan MJ. The utility of radiological imaging in nonalcoholic fatty liver disease. Gastroenterology. 2002 Sep;123(3):745-50.

Sabio G, Cavanagh-Kyros J, Ko HJ, Jung DY, Gray S, Jun JY, Barrett T, Mora A, Kim JK, Davis RJ. Prevention of steatosis by hepatic JNK1. Cell Metab. 2009 Dec;10(6):491-8. doi: 10.1016/j.cmet.2009.09.007.

Saini V. Molecular mechanisms of insulin resistance in type 2 diabetes mellitus. World J Diabetes. 2010 Jul 15;1(3):68-75. doi: 10.4239/wjd.v1.i3.68.

Samuel VT, Liu ZX, Qu X, Elder BD, Bilz S, Befroy D, Romanelli AJ, Shulman GI. Mechanism of hepatic insulin resistance in non-alcoholic fatty liver disease. J Biol Chem. 2004 Jul 30;279(31):32345-53. Epub 2004 May 27.

Samuel VT, Liu ZX, Wang A, Beddow SA, Geisler JG, Kahn M, Zhang XM, Monia BP, Bhanot S, Shulman GI. Inhibition of protein kinase Cepsilon prevents hepatic insulin resistance in nonalcoholic fatty liver disease. J Clin Invest. 2007 Mar;117(3):739-45. Epub 2007 Feb 22.

Sanders FW, Griffin JL. De novo lipogenesis in the liver in health and disease: more than just a shunting yard for glucose. Biol Rev Camb Philos Soc. 2016 May;91(2):452-68. doi: 10.1111/brv.12178. Epub 2015 Mar 4.

Sano R, Reed JC. ER stress-induced cell death mechanisms. Biochim Biophys Acta. 2013 Dec;1833(12):3460-3470. doi: 10.1016/j.bbamcr.2013.06.028. Epub 2013 Jul 10.

Sanyal AJ, Brunt EM, Kleiner DE, Kowdley KV, Chalasani N, Lavine JE, Ratziu V, McCullough A. Endpoints and clinical trial design for nonalcoholic steatohepatitis. Hepatology. 2011 Jul;54(1):344-53. doi: 10.1002/hep.24376.

Sanyal AJ, Campbell-Sargent C, Mirshahi F, Rizzo WB, Contos MJ, Sterling RK, Luketic VA, Shiffman ML, Clore JN. Nonalcoholic steatohepatitis: association of insulin resistance and mitochondrial abnormalities. Gastroenterology. 2001 Apr;120(5):1183-92.

Saponaro C, Gaggini M, Carli F, Gastaldelli A. The Subtle Balance between Lipolysis and Lipogenesis: A Critical Point in Metabolic Homeostasis. Nutrients. 2015 Nov 13;7(11):9453-74. doi: 10.3390/nu7115475.

Satapati S, Sunny NE, Kucejova B, Fu X, He TT, Méndez-Lucas A, Shelton JM, Perales JC, Browning JD, Burgess SC. Elevated TCA cycle function in the pathology of diet-induced hepatic insulin resistance and fatty liver. J Lipid Res. 2012 Jun;53(6):1080-92. doi: 10.1194/jlr.M023382. Epub 2012 Apr 9.

Scavo LM, Karas M, Murray M, Leroith D. Insulin-like growth factor-I stimulates both cell growth and lipogenesis during differentiation of human mesenchymal stem cells into adipocytes. J Clin Endocrinol Metab. 2004 Jul;89(7):3543-53.

Schinner S, Scherbaum WA, Bornstein SR, Barthel A. Molecular mechanisms of insulin resistance. Diabet Med. 2005 Jun;22(6):674-82.

Schlossberger V, Worni M, Kihm C, Montani M, Datz C, Hampe J, Stickel F. Plasma Levels of K18 Fragments Do Not Correlate with Alcoholic Liver Fibrosis. Gut Liver. 2018 Sep 21. doi: 10.5009/gnl18037.

Schmid AI, Szendroedi J, Chmelik M, Krssák M, Moser E, Roden M. Liver ATP synthesis is lower and relates to insulin sensitivity in patients with type 2 diabetes. Diabetes Care. 2011 Feb;34(2):448-53. doi: 10.2337/dc10-1076. Epub 2011 Jan 7.

Schmoll D, Walker KS, Alessi DR, Grempler R, Burchell A, Guo S, Walther R, Unterman TG. Regulation of glucose-6-phosphatase gene expression by protein kinase Balpha and the forkhead transcription factor FKHR. Evidence for insulin response unit-dependent and -independent effects of insulin on promoter activity. J Biol Chem. 2000 Nov 17;275(46):36324-33.

Schrader M, Grille S, Fahimi HD, Islinger M. Peroxisome interactions and cross-talk with other subcellular compartments in animal cells. Subcell Biochem. 2013;69:1-22. doi: 10.1007/978-94-007-6889-5_1.

Schwenger KJP, Fischer SE, Jackson T, Okrainec A, Allard JP. In nonalcoholic fatty liver disease, Roux-en-Y gastric bypass improves liver histology while persistent disease is associated with lower improvements in waist circumference and glycemic control. Surg Obes Relat Dis. 2018 Jul 12. pii: S1550-7289(18)30310-1. doi: 10.1016/j.soard.2018.06.007.

Seki S, Kitada T, Sakaguchi H. Clinicopathological significance of oxidative cellular damage in non-alcoholic fatty liver diseases. Hepatol Res. 2005 Oct;33(2):132-4. Epub 2005 Sep 29.

Serdyuk AP, Morton RE. Lipid transfer inhibitor protein defines the participation of lipoproteins in lipid transfer reactions: CETP has no preference for cholesteryl esters in HDL versus LDL. Arterioscler Thromb Vasc Biol. 1999 Mar;19(3):718-26.

Serviddio G, Bellanti F, Tamborra R, Rollo T, Romano AD, Giudetti AM, Capitanio N, Petrella A, Vendemiale G, Altomare E. Alterations of hepatic ATP homeostasis and respiratory chain during development of non-alcoholic steatohepatitis in a rodent model. Eur J Clin Invest. 2008 Apr;38(4):245-52. doi: 10.1111/j.1365-2362.2008.01936.x.

Shabalina IG, Vrbacký M, Pecinová A, Kalinovich AV, Drahota Z, Houštěk J, Mráček T, Cannon B, Nedergaard J. ROS production in brown adipose tissue mitochondria: the question of UCP1-dependence. Biochim Biophys Acta. 2014 Dec;1837(12):2017-2030. doi: 10.1016/j.bbabio.2014.04.005. Epub 2014 Apr 24.

Shimomura I, Bashmakov Y, Ikemoto S, Horton JD, Brown MS, Goldstein JL. Insulin selectively increases SREBP-1c mRNA in the livers of rats with streptozotocin-induced diabetes. Proc Natl Acad Sci U S A. 1999 Nov 23;96(24):13656-61.

Shimomura I, Hammer RE, Richardson JA, Ikemoto S, Bashmakov Y, Goldstein JL, Brown MS. Insulin resistance and diabetes mellitus in transgenic mice expressing nuclear SREBP-1c in adipose tissue: model for congenital generalized lipodystrophy. Genes Dev. 1998 Oct 15;12(20):3182-94.

Shyangdan D, Clar C, Ghouri N, Henderson R, Gurung T, Preiss D, Sattar N, Fraser A, Waugh N. Insulin sensitisers in the treatment of non-alcoholic fatty liver disease: a systematic review. Health Technol Assess. 2011 Nov;15(38):1-110. doi: 10.3310/hta15380.

Silverstein RL, Febbraio M. CD36, a scavenger receptor involved in immunity, metabolism, angiogenesis, and behavior. Sci Signal. 2009 May 26;2(72):re3. doi: 10.1126/scisignal.272re3.

Sinal CJ, Tohkin M, Miyata M, Ward JM, Lambert G, Gonzalez FJ. Targeted disruption of the nuclear receptor FXR/BAR impairs bile acid and lipid homeostasis. Cell. 2000 Sep 15;102(6):731-44.

So JS, Hur KY, Tarrio M, Ruda V, Frank-Kamenetsky M, Fitzgerald K, Koteliansky V, Lichtman AH, Iwawaki T, Glimcher LH, Lee AH. Silencing of lipid metabolism genes through IRE1α-mediated mRNA decay lowers plasma lipids in mice. Cell Metab. 2012 Oct 3;16(4):487-99. doi: 10.1016/j.cmet.2012.09.004.

Softic S, Cohen DE, Kahn CR. Role of Dietary Fructose and Hepatic De Novo Lipogenesis in Fatty Liver Disease. Dig Dis Sci. 2016 May;61(5):1282-93. doi: 10.1007/s10620-016-4054-0. Epub 2016 Feb 8.

Softic S, Kirby M, Berger NG, Shroyer NF, Woods SC, Kohli R. Insulin concentration modulates hepatic lipid accumulation in mice in part via transcriptional regulation of fatty acid transport proteins. PLoS One. 2012;7(6):e38952. doi: 10.1371/journal.pone.0038952. Epub 2012 Jun 20.

Speliotes EK, Butler JL, Palmer CD, Voight BF; GIANT Consortium; MIGen Consortium; NASH CRN, Hirschhorn JN. PNPLA3 variants specifically confer increased risk for histologic nonalcoholic fatty liver disease but not metabolic disease. Hepatology. 2010 Sep;52(3):904-12. doi: 10.1002/hep.23768.

Stanhope KL. Sugar consumption, metabolic disease and obesity: The state of the controversy. Crit Rev Clin Lab Sci. 2016;53(1):52-67. doi: 10.3109/10408363.2015.1084990. Epub 2015 Sep 17.

Stojsavljević S, Gomerčić Palčić M, Virović Jukić L, Smirčić Duvnjak L, Duvnjak M. Adipokines and proinflammatory cytokines, the key mediators in the pathogenesis of nonalcoholic fatty liver disease. World J Gastroenterol. 2014 Dec 28;20(48):18070-91. doi: 10.3748/wjg.v20.i48.18070.

Strable MS, Ntambi JM. Genetic control of de novo lipogenesis: role in diet-induced obesity. Crit Rev Biochem Mol Biol. 2010 Jun;45(3):199-214. doi: 10.3109/10409231003667500.

Straus DS, Takemoto CD. Effect of dietary protein deprivation on insulin-like growth factor (IGF)-I and -II, IGF binding protein-2, and serum albumin gene expression in rat. Endocrinology. 1990 Oct;127(4):1849-60.

Streicher R, Kotzka J, Müller-Wieland D, Siemeister G, Munck M, Avci H, Krone W. SREBP-1 mediates activation of the low density lipoprotein receptor promoter by insulin and insulin-like growth factor-I. J Biol Chem. 1996 Mar 22;271(12):7128-33.

Strnad P, Paschke S, Jang KH, Ku NO. Keratins: markers and modulators of liver disease. Curr Opin Gastroenterol. 2012 May;28(3):209-16. doi: 10.1097/MOG.0b013e3283525cb8.

Summers SA, Kao AW, Kohn AD, Backus GS, Roth RA, Pessin JE, Birnbaum MJ. The role of glycogen synthase kinase 3beta in insulin-stimulated glucose metabolism. J Biol Chem. 1999 Jun 18;274(25):17934-40.

Sung CK, Choi WS, Scalia P. Insulin-stimulated glycogen synthesis in cultured hepatoma cells: differential effects of inhibitors of insulin signaling molecules. J Recept Signal Transduct Res. 1998 Jul-Nov;18(4-6):243-63.

Sunny NE, Parks EJ, Browning JD, Burgess SC. Excessive hepatic mitochondrial TCA cycle and gluconeogenesis in humans with nonalcoholic fatty liver disease. Cell Metab. 2011 Dec 7;14(6):804-10. doi: 10.1016/j.cmet.2011.11.004.

Tan NS, Shaw NS, Vinckenbosch N, Liu P, Yasmin R, Desvergne B, Wahli W, Noy N. Selective cooperation between fatty acid binding proteins and peroxisome proliferator-activated receptors in regulating transcription. Mol Cell Biol. 2002 Jul;22(14):5114-27.

Targher G, Chonchol M, Miele L, Zoppini G, Pichiri I, Muggeo M. Nonalcoholic fatty liver disease as a contributor to hypercoagulation and thrombophilia in the metabolic syndrome. Semin Thromb Hemost. 2009 Apr;35(3):277-87. doi: 10.1055/s-0029-1222606. Epub 2009 May 18.

Targher G, Marra F, Marchesini G. Increased risk of cardiovascular disease in non-alcoholic fatty liver disease: causal effect or epiphenomenon? Diabetologia. 2008 Nov;51(11):1947-53. doi: 10.1007/s00125-008-1135-4. Epub 2008 Sep 2.

Teruel T, Hernandez R, Lorenzo M. Ceramide mediates insulin resistance by tumor necrosis factor-alpha in brown adipocytes by maintaining Akt in an inactive dephosphorylated state. Diabetes. 2001 Nov;50(11):2563-71.

Tilg H, Moschen AR. Evolution of inflammation in nonalcoholic fatty liver disease: the multiple parallel hits hypothesis. Hepatology. 2010 Nov;52(5):1836-46. doi: 10.1002/hep.24001.

Tillander V, Alexson SEH, Cohen DE. Deactivating Fatty Acids: Acyl-CoA Thioesterase-Mediated Control of Lipid Metabolism. Trends Endocrinol Metab. 2017 Jul;28(7):473-484. doi: 10.1016/j.tem.2017.03.001. Epub 2017 Apr 3.

Tiniakos DG, Vos MB, Brunt EM. Nonalcoholic fatty liver disease: pathology and pathogenesis. Annu Rev Pathol. 2010;5:145-71. doi: 10.1146/annurev-pathol-121808-102132.

Todd DJ, Lee AH, Glimcher LH. The endoplasmic reticulum stress response in immunity and autoimmunity. Nat Rev Immunol. 2008 Sep;8(9):663-74. doi: 10.1038/nri2359.

Toivola DM, Boor P, Alam C, Strnad P. Keratins in health and disease. Curr Opin Cell Biol. 2015 Feb;32:73-81. doi: 10.1016/j.ceb.2014.12.008. Epub 2015 Jan 17.

Uemura A, Oku M, Mori K, Yoshida H. Unconventional splicing of XBP1 mRNA occurs in the cytoplasm during the mammalian unfolded protein response. J Cell Sci. 2009 Aug 15;122(Pt 16):2877-86. doi: 10.1242/jcs.040584. Epub 2009 Jul 21.

Unger RH, Clark GO, Scherer PE, Orci L. Lipid homeostasis, lipotoxicity and the metabolic syndrome. Biochim Biophys Acta. 2010 Mar;1801(3):209-14. doi: 10.1016/j.bbalip.2009.10.006. Epub 2009 Nov 27.

Ursini F, Maiorino M, Forman HJ. Redox homeostasis: The Golden Mean of healthy living. Redox Biol. 2016 Aug;8:205-15. doi: 10.1016/j.redox.2016.01.010. Epub 2016 Jan 19.

Vial G, Dubouchaud H, Couturier K, Cottet-Rousselle C, Taleux N, Athias A, Galinier A, Casteilla L, Leverve XM. Effects of a high-fat diet on energy metabolism and ROS production in rat liver. J Hepatol. 2011 Feb;54(2):348-56. doi: 10.1016/j.jhep.2010.06.044. Epub 2010 Sep 7.

Videla LA, Rodrigo R, Orellana M, Fernandez V, Tapia G, Quiñones L, Varela N, Contreras J, Lazarte R, Csendes A, Rojas J, Maluenda F, Burdiles P, Diaz JC, Smok G, Thielemann L, Poniachik J. Oxidative stress-related parameters in the liver of non-alcoholic fatty liver disease patients. Clin Sci (Lond). 2004 Mar;106(3):261-8.

Wanders RJ. Metabolic functions of peroxisomes in health and disease. Biochimie. 2014 Mar;98:36-44. doi: 10.1016/j.biochi.2013.08.022. Epub 2013 Sep 3.

Wang B, Chandrasekera PC, Pippin JJ. Leptin- and leptin receptor-deficient rodent models: relevance for human type 2 diabetes. Curr Diabetes Rev. 2014 Mar;10(2):131-45.

Wang D, Wei Y, Pagliassotti MJ. Saturated fatty acids promote endoplasmic reticulum stress and liver injury in rats with hepatic steatosis. Endocrinology. 2006 Feb;147(2):943-51. Epub 2005 Nov 3.

Wang J, Li YC, Deng M, Jiang HY, Guo LH, Zhou WJ, Ruan B. Serum insulin-like growth factor-1 and its binding protein 3 as prognostic factors for the incidence, progression, and outcome of hepatocellular carcinoma: a systematic review and meta-analysis. Oncotarget. 2017 Jul 12;8(46):81098-81108. doi: 10.18632/oncotarget.19186. eCollection 2017 Oct 6.

Wang RH, Li C, Deng CX. Liver steatosis and increased ChREBP expression in mice carrying a liver specific SIRT1 null mutation under a normal feeding condition. Int J Biol Sci. 2010 Nov 16;6(7):682-90.

Wei Y, Wang D, Pagliassotti MJ. Saturated fatty acid-mediated endoplasmic reticulum stress and apoptosis are augmented by trans-10, cis-12-conjugated linoleic acid in liver cells. Mol Cell Biochem. 2007 Sep;303(1-2):105-13. Epub 2007 Apr 11.

Wei Y, Wang D, Topczewski F, Pagliassotti MJ. Saturated fatty acids induce endoplasmic reticulum stress and apoptosis independently of ceramide in liver cells. Am J Physiol Endocrinol Metab. 2006 Aug;291(2):E275-81. Epub 2006 Feb 21.

Weltman MD, Farrell GC, Hall P, Ingelman-Sundberg M, Liddle C. Hepatic cytochrome P450 2E1 is increased in patients with nonalcoholic steatohepatitis. Hepatology. 1998 Jan;27(1):128-33.

Westerbacka J, Kolak M, Kiviluoto T, Arkkila P, Sirén J, Hamsten A, Fisher RM, Yki-Järvinen H. Genes involved in fatty acid partitioning and binding, lipolysis, monocyte/macrophage recruitment, and inflammation are overexpressed in the human fatty liver of insulin-resistant subjects. Diabetes. 2007 Nov;56(11):2759-65. Epub 2007 Aug 17.

Wheatcroft SB, Kearney MT, Shah AM, Ezzat VA, Miell JR, Modo M, Williams SC, Cawthorn WP, Medina-Gomez G, Vidal-Puig A, Sethi JK, Crossey PA. IGF-binding protein-2 protects against the development of obesity and insulin resistance. Diabetes. 2007 Feb;56(2):285-94.

Wong RJ, Aguilar M, Cheung R, Perumpail RB, Harrison SA, Younossi ZM, Ahmed A. Nonalcoholic steatohepatitis is the second leading etiology of liver disease among adults awaiting liver transplantation in the United States. Gastroenterology. 2015 Mar;148(3):547-55. doi: 10.1053/j.gastro.2014.11.039. Epub 2014 Nov 25.

Wu R, Zhang QH, Lu YJ, Ren K, Yi GH. Involvement of the IRE1α-XBP1 pathway and XBP1s-dependent transcriptional reprogramming in metabolic diseases. DNA Cell Biol. 2015 Jan;34(1):6-18. doi: 10.1089/dna.2014.2552.

Xiao L, Xie X, Zhai Y. Functional crosstalk of CAR-LXR and ROR-LXR in drug metabolism and lipid metabolism. Adv Drug Deliv Rev. 2010 Oct 30;62(13):1316-21. doi: 10.1016/j.addr.2010.07.006. Epub 2010 Jul 24.

Xu J, Xiao G, Trujillo C, Chang V, Blanco L, Joseph SB, Bassilian S, Saad MF, Tontonoz P, Lee WN, Kurland IJ. Peroxisome proliferator-activated receptor alpha (PPARalpha) influences substrate utilization for hepatic glucose production. J Biol Chem. 2002 Dec 27;277(52):50237-44. Epub 2002 Aug 9.

Xu X, So JS, Park JG, Lee AH. Transcriptional control of hepatic lipid metabolism by SREBP and ChREBP. Semin Liver Dis. 2013 Nov;33(4):301-11. doi: 10.1055/s-0033-1358523. Epub 2013 Nov 12.

Yamagata K, Furuta H, Oda N, Kaisaki PJ, Menzel S, Cox NJ, Fajans SS, Signorini S, Stoffel M, Bell GI. Mutations in the hepatocyte nuclear factor-4alpha gene in maturity-onset diabetes of the young (MODY1). Nature. 1996 Dec 5;384(6608):458-60.

Yamaguchi K, Yang L, McCall S, Huang J, Yu XX, Pandey SK, Bhanot S, Monia BP, Li YX, Diehl AM. Inhibiting triglyceride synthesis improves hepatic steatosis but exacerbates liver

damage and fibrosis in obese mice with nonalcoholic steatohepatitis. Hepatology. 2007 Jun;45(6):1366-74.

Yesilova Z, Yaman H, Oktenli C, Ozcan A, Uygun A, Cakir E, Sanisoglu SY, Erdil A, Ates Y, Aslan M, Musabak U, Erbil MK, Karaeren N, Dagalp K. Systemic markers of lipid peroxidation and antioxidants in patients with nonalcoholic Fatty liver disease. Am J Gastroenterol. 2005 Apr;100(4):850-5.

Yi H, Yoon HN, Kim S, Ku NO. The role of keratins in the digestive system: lessons from transgenic mouse models. Histochem Cell Biol. 2018 Oct;150(4):351-359. doi: 10.1007/s00418-018-1695-4. Epub 2018 Jul 24.

Yin L, Ma H, Ge X, Edwards PA, Zhang Y. Hepatic hepatocyte nuclear factor 4α is essential for maintaining triglyceride and cholesterol homeostasis. Arterioscler Thromb Vasc Biol. 2011 Feb;31(2):328-36. doi: 10.1161/ATVBAHA.110.217828. Epub 2010 Nov 11.

Yoshida H, Matsui T, Yamamoto A, Okada T, Mori K. XBP1 mRNA is induced by ATF6 and spliced by IRE1 in response to ER stress to produce a highly active transcription factor. Cell. 2001 Dec 28;107(7):881-91.

Younossi ZM, Koenig AB, Abdelatif D, Fazel Y, Henry L, Wymer M. Global epidemiology of nonalcoholic fatty liver disease-Meta-analytic assessment of prevalence, incidence, and outcomes. Hepatology. 2016 Jul;64(1):73-84. doi: 10.1002/hep.28431. Epub 2016 Feb 22.

Zatloukal K, French SW, Stumptner C, Strnad P, Harada M, Toivola DM, Cadrin M, Omary MB. From Mallory to Mallory-Denk bodies: what, how and why? Exp Cell Res. 2007 Jun 10;313(10):2033-49. Epub 2007 Apr 27.

Zatloukal K, Stumptner C, Fuchsbichler A, Fickert P, Lackner C, Trauner M, Denk H. The keratin cytoskeleton in liver diseases. J Pathol. 2004 Nov;204(4):367-76.

Zhang X, Xu A, Chung SK, Cresser JH, Sweeney G, Wong RL, Lin A, Lam KS. Selective inactivation of c-Jun NH2-terminal kinase in adipose tissue protects against diet-induced obesity and improves insulin sensitivity in both liver and skeletal muscle in mice. Diabetes. 2011 Feb;60(2):486-95. doi: 10.2337/db10-0650.

Zhang Y, Lee FY, Barrera G, Lee H, Vales C, Gonzalez FJ, Willson TM, Edwards PA. Activation of the nuclear receptor FXR improves hyperglycemia and hyperlipidemia in diabetic mice. Proc Natl Acad Sci U S A. 2006 Jan 24;103(4):1006-11. Epub 2006 Jan 12.

Appendix

List of abbreviations

ACC	Acetyl-CoA Carboxylase
ACOT	Acyl-coenzyme A thioesterase
Akt	Protein kinase B
ALT	Alanine aminotransferase
Apo	Apolipoprotein
APS	Ammonium persulfate
AST	Aspartarte aminotransferase
ATF	Activating transcription factor
ATP	Adenosine triphosphate
BCA	Bicinchoninic acid
BMI	Body mass index
BSA	Bovine serum albumine
CAR	Constitutive androstane receptor
cDNA	Complementary DNA
CETP	Cholesteryl ester transfer protein
CHOP	CCAAT/enhancer-binding protein homologous protein
ChREBP	Carbohydrate response element binding protein
CPM	Counts pre minute
CPT	Carnitine palmitoyl transferase
CRP	C-reactive protein
CV	Coeffizient of variation
CYB5A	Cytochrome b5 type A
DG	Diglycerides
DGAT	Acyl-CoA:diacylglycerol acyltransferase
DMEM	Dulbecco’s modified Eagle’s medium
DNA	Deoxyribonucleic acid
DNL	*De novo* lipogenesis
dNTP	Deoxynucleotide
ECAR	Extracellular acidification rate
EDTA	Ethylenediamine tetraacetic acid
ELISA	Enzyme linked immunosorbent assay
ELOVL6	Long chain fatty acid synthase 6
EPC	Endothelial progenitor cells
ER	Endoplasmic reticulum

ETC	Electron transport chain
FA	Fatty acids
FABP	Fatty acid binding protein
FAO	Fatty acid oxidation
FAS	Fatty acid synthase
FASN	Fatty acid synthase gene
FAT/CD36	Fatty acid translocase
FATP	Fatty acid transport protein
FAU	Fatty acid uptake
FCCP	Carbonyl cyanide 4-(trifluoromethoxy)phenylhydrazone
FCS	Fetal calf serum
FFA	Free fatty acids
FLI	Fatty liver index
FN1	Fibronectin 1
FXR	Farnesyl X receptor
GAPDH	Glyceraldehyde 3-phosphate dehydrogenase
gGT	Gamma glutamyl transferase
GLDH	Glutamate dehydrogenase
GPAT	glycerol-3-phosphate acyltransferase
GSK	Glycogen synthase kinase
h	Hours
HBSS	Hanks' balanced salt solution
HCC	Hepatocellular carcinoma
HDL	High density lipoprotein
HEPES	4-(2-Hydroxyethyl)piperazine-1-ethanesulfonic acid
HMG	hydroxymethylglutaryl
HNF4A	Hepatocyte nuclear factor 4 α
HOMA-IR	Homeostatic model assessment of insulin resistance
HRP	Horseradish peroxidase
IGF	Insulin-like growth factor
IGFBP	Insulin-like growth factor binding protein
IL	Interleukin
INSIG	Insulin induced gene
IR	Insulin receptor
IRE1α	Inositol-requiring enzyme 1 α
IRS	Insulin receptor substrate
ITGA5	Integrin alpha 5 (fibronectin receptor alpha)

IVC	Inferior vena cava
JNK	C-Jun N-terminal kinase
KC/CXCL1	Keratinocyte chemoattractant
kDa	Kilo Dalton
KRH	Krebs-Ringer HEPES
Krt	Keratin
LCAT	Lecitin:cholesterol acyltransferase
LDL	Low density lipoprotein
LXR	Liver-X receptor
M	Molar
mA	Milliampere
MAPK	Mitogen-activated protein kinase
MCP1/CCL2	Monocyte chemoattractant protein 1
MDB	Mallory-Denk Bodies
MEM	Minimal essentiel medium
Min	Minutes
ml	Milliliter
MLXIPL	Max-like protein X interacting protein like
MYC	Myelocytomatosis oncogene
NAFLD	Non-alcoholic liver disease
NASH	Non-alcoholic steatohepatitis
nd	Not determined
nm	Nanometer
nM	Nanomolar
NR1I3	Nuclear receptor 1I3
OCR	Oxygen consumption rate
PAGE	Polyacrylamide gel electrophoresis
PBS	Phosphate buffered saline
PCR	Polymerase chain reaction
PEBP1	Phosphatidylethanolamine binding protein 1
PEX	Peroxisomal biogenesis factor
PGC1α	PPARγ coactivator 1 α
POR	P450 (cytochrome) oxidoreductase
PPAR	Peroxisome proliferator activated receptor
PVDF	Polyvinylidene difluoride
rcf	Relative centrifugal force
RIPA	Radioimmunoprecipitation assay buffer

RLU	Relative luminescence units
RNA	Ribonucleic acid
ROS	Reactive oxygen species
rpm	Rounds per minute
RT	Room temperature
RXR	Retinoid-X receptor
SCAP	SREBP cleavage activating protein
SCD	Stearoyl-CoA desaturase
SD	Standard deviation
SDS	Sodium dodecyl sulfate
sec	Seconds
Ser	Serine
SIRT	Sirtuin
SREBP	Sterol regulatory element-binding protein
STAT3	Signal transducer and activator of transcription 3
T2D	Type 2 diabetes
TBS-T	Tris-buffered saline with Tween20
TCA	Tricarboxylic acid
TEMED	Tetraethylethylenediamin
TFA	Total fatty acids
TG	Triglycerides
Thr	Threonine
U	Units
UCP2	Uncoupling protein 2
UPR	Unfolded protein response
V	Volt
VLDL	Very low density lipoprotein
WC	Waist circumference
XBP1	X-box binding protein 1

List of figures

Figures were illustrated using medical images provided by Servier Medical Art (http://smart.servier.com) under a Creative Commons Attribution 3.0 Unported License or GraphPad Prism software (Version 7.04).

List of tables

Eidesstattliche Erklärung

Ich versichere an Eides Statt, dass die Dissertation von mir selbständig und ohne unzulässige fremde Hilfe unter Beachtung der „Grundsätze zur Sicherung guter wissenschaftlicher Praxis an der Heinrich-Heine-Universität Düsseldorf“ erstellt worden ist. Die Dissertation wurde in der vorgelegten oder in ähnlicher Form noch bei keiner anderen Institution eingereicht. Ich habe bisher keine erfolglosen Promotionsversuche unternommen.

04.12.2018 Pia Fahlbusch

Datum Pia Fahlbusch

Danksagung

An erster Stelle möchte ich mich bei Prof. Dr. Hadi Al-Hasani für die Möglichkeit bedanken, diese Arbeit an seinem Institut anzufertigen und für die Unterstützung das Thema mit viel Freiheit zu gestalten, ebenso für die Begutachtung meiner Doktorarbeit.

Herrn Prof. Dr. Michael Feldbrügge danke ich für die Übernahme des Zweitgutachtens und das Interesse an meiner Arbeit.

Ich danke Frau Prof. Dr. Margriet Ouwens für die Mitbetreuung meiner Arbeit und die Bereitstellung projektbezogener Materialien.

Mein besonderer Dank gilt Dr. Birgit Knebel und Dr. Jörg Kotzka. Es war mir wirklich eine große Freude mit euch zusammenzuarbeiten. Vielen Dank für die vielen produktive Gespräche, angeregten Diskussionen und euer stets konstruktives Feedback gerade in der letzten intensiven Phase dieser Arbeit. Danke für euer unermüdliches Engagement und für eure wissenschaftliche Begeisterung die wirklich ansteckend ist. Ihr habt wesentlich zum Gelingen dieser Arbeit beigetragen und dafür danke ich euch sehr.

Dani, Tina und David, was wäre diese Zeit nur ohne euch gewesen. Danke für eure Unterstützung und euren Beistand immer wenn es nötig war, ebenso für all die schönen Erinnerungen und Erlebnisse. Es war mir eine große Freude diesen Lebensabschnitt mit euch zu teilen. Dani, dir gilt ein besonderer Dank für deine tatkräftige Unterstützung im Labor und zwar nicht nur für die die offensichtlich war, sondern auch für die vielen Handgriffe die unbemerkt blieben.